

**C-H ACTIVATION INVOLVING THREE- AND FOUR-COORDINATE  
IRIDIUM(I) PINCER COMPLEXES**

by

**JASON D. HACKENBERG**

A dissertation submitted to the

Graduate School-New Brunswick

Rutgers, the State University of New Jersey

In partial fulfillment of the requirements for the degree of

Doctor of Philosophy

In

Chemistry and Chemical Biology

Written under the direction of

Alan S. Goldman

and approved by

---

---

---

---

New Brunswick, New Jersey  
May 2014

**ABSTRACT OF THE DISSERTATION**  
**C-H ACTIVATION INVOLVING THREE- AND FOUR-COORDINATE**  
**IRIDIUM(I) PINCER COMPLEXES**

By

Jason D. Hackenberg

Dissertation Director:

Alan S. Goldman

This thesis is organized around two themes: (1) C-H activation catalysis involving *in situ* generated three-coordinate iridium-pincer complexes as applied toward the dehydrogenation and metathesis of alkanes and (2) understanding and expanding the reactivity of four-coordinate (pincer)Ir(CO) complexes toward the oxidative addition of C-H bonds.

In the first half of this thesis, we describe the preparation of a novel class of pincer complex that is comprised of both phosphine and phosphinite moieties, representing a “hybrid” of the previously reported bis-phosphine (PCP) and bis-phosphinite (POCOP) parent species. The catalytic activity of (<sup>t</sup>Bu<sup>4</sup>PCOP)Ir toward the transfer and acceptorless dehydrogenation of linear and cyclic alkanes was examined and compared to the activities of (<sup>t</sup>Bu<sup>4</sup>PCP)Ir and (<sup>t</sup>Bu<sup>4</sup>POCOP)Ir, generally exhibiting intermediate activity. (<sup>t</sup>Bu<sup>4</sup>PCOP)Ir and other hybrid (PCOP)Ir complexes were applied to alkane metathesis using a molybdenum alkylidene co-catalyst and found to exhibit far greater activity toward *n*-hexane metathesis compared to either parent catalyst. The

resting state of (<sup>t</sup>Bu<sup>4</sup>PCOP)Ir in alkane metathesis was found to be mixture of the dissimilar resting states exhibited by the parent catalysts, suggesting an ability to effectively catalyze the respective slow steps associated with the (<sup>t</sup>Bu<sup>4</sup>PCP)Ir and (<sup>t</sup>Bu<sup>4</sup>POCOP)Ir routes.

In the latter half of the thesis, we explore the unprecedented oxidative addition of C-H bonds to four-coordinate (pincer)Ir(CO) complexes. Employing a unique acid-catalyzed route, the net oxidative addition of phenylacetylene to square planar (<sup>t</sup>Bu<sup>4</sup>PCP)Ir(CO) was observed to yield exclusively the *trans* six-coordinate C-H addition product, (<sup>t</sup>Bu<sup>4</sup>PCP)Ir(CO)(H)(CCPh); detailed mechanistic and theoretical studies indicate that this rare transformation occurs by generating a protonated intermediate that undergoes electrophilic attack of PhCCH with subsequent deprotonation of the alkyne C-H bond in the rate-determining step. Although this acid-catalyzed reaction was observed to occur only with alkynes, the reverse reaction (acid-catalyzed reductive elimination) was found to occur for both alkyl and aryl substrates, suggesting that the acid-catalyzed oxidative addition of C<sub>sp3</sub>-H and C<sub>sp2</sub>-H bonds might be kinetically possible but thermodynamically unfavored. Preliminary experimental and theoretical explorations of the factors favoring the thermodynamics of addition support a strategy of utilizing less sterically hindered (pincer)Ir(CO) complexes bearing relatively strong σ-donating ligands *trans* to the carbonyl ligand.

## ACKNOWLEDGMENTS

Foremost I would like to thank my advisor, Alan Goldman, who has given me five years of unyielding support, patient guidance, and fervent encouragement. Alan is the kind of advisor that other graduate students dream about, but that I was lucky enough to work with. Alan has not only helped me to become a better scientist, he has exemplified what it means to be a mentor.

I am also indebted to my committee members, Karsten Krogh-Jespersen and Teddy Asefa. Karsten has provided me with patient instruction and sage advice regarding the finer points of theoretical chemistry throughout my time in graduate school. Teddy has always greeted me with an enthusiasm and excitement that is not commonly found in academia. I am also very grateful to Dr. Tom Emge for his x-ray crystallography expertise and to Dr. Nagarajan Murali for his assistance with NMR studies; both of these men make life as a chemistry graduate student considerably easier.

Going to graduate school would not have been possible without the encouragement and guidance of the terrific professors I had as an undergraduate at Monmouth. In particular, my undergraduate advisor, Carolyn Supplee, introduced me to the field of organometallic chemistry; I acquired many of my lab skills and practices from her tutelage. More than anyone, she pushed me toward graduate school and made me feel that I could accomplish great things. I would also like to thank Robert Topper for not only providing me with an invaluable introduction to computational chemistry, but also for the genuine interest he takes in his students. Lastly I would like to express my gratitude to my undergraduate Physics professor, Louis Kijewski, whose words of encouragement and humor I will forever remember.



These past five years have been made enjoyable by the exceptional colleagues I have been surrounded with in the Goldman group; together we created a happy and supportive work environment that was a pleasure to come to each day. Among these colleagues I would like to thank Drs. Sabuj Kundu, Soumik Biswas, Agnieszka Nawara-Hultzsch, and Benudhar Punji, who helped me greatly when I first joined the lab. I particularly want to thank Drs. David Wang and David Laviska for being both good friends and supportive colleagues. The person from whom I probably learned most in the Goldman group was Dr. Jongwook Choi; I will always remember J-Dub's great sense of humor, his expert advice, the genuine interest he expressed in my progress, and his love of *Lost*. Finally I was very lucky to have gone through these past five years with my fellow Monmouth alum, Katie Field. Clearing the numerous hurdles of graduate school alongside Katie has been both motivating and supportive, and Katie's cheerful personality and good humor have made it all the more pleasant.

Of course none of this would have been possible without the love and support of my family. My parents have always been my biggest supporters and I am lucky to be their son. Without their gentle encouragement and guiding hands I would not be where I am today; any successes I have had are attributable directly to them. My brother Mark has always been there for me, and has encouraged and reassured me throughout my life. Finally I will forever be thankful of my grandparents. In all the world over you would never find another pair who took more pride in their grandson's accomplishments (be it a good report card or a single line in a first-grade play) than my grandparents; I can only imagine what earning a Ph.D. would mean to them.

## **DEDICATION**

*For my mother, father, brother, and grandparents*

## Table of Contents

<b>Abstract.....</b>	<b>ii</b>
<b>Acknowledgments .....</b>	<b>iv</b>
<b>Dedication .....</b>	<b>vi</b>
<b>Table of Contents .....</b>	<b>vii</b>
<b>List of Figures.....</b>	<b>xii</b>
<b>List of Schemes .....</b>	<b>xvii</b>
<b>List of Tables .....</b>	<b>xx</b>

<b>Chapter 1</b>	<b>Introduction</b>	1
1.1	Prominent early examples of small molecule activation by transition-metal catalysts	1
1.2	Brief history of C-H activation chemistry	2
1.3	Small molecule activation by pincer-iridium complexes	4
1.4	Research Themes	11
1.5	References	14
<b>Chapter 2</b>	<b>Synthesis, Characterization, and Catalytic Activity of “Hybrid” (PCOP)Ir Complexes toward Dehydrogenation of Alkanes</b>	17
2.1	Introduction	18
2.2	Results and Discussion	24
2.2.1	<i>Synthesis and characterization of the hybrid ligand, <sup>t</sup>Bu<sup>4</sup>PCOP</i>	25

2.2.2	Synthesis and characterization of ( $t\text{Bu}^4\text{PCOP}$ )Ir(H)(Cl)	26
2.2.3	Synthesis and characterization of the hybrid catalyst, ( $t\text{Bu}^4\text{PCCOP}$ )Ir(H) <sub>2</sub>	29
2.2.4	Synthesis and characterization of ( $t\text{Bu}^4\text{PCOP}$ )Ir(CO)	29
2.2.5	Catalytic dehydrogenation activity	30
2.2.5.1	Transfer dehydrogenation of <i>n</i> -octane	31
2.2.5.2	Transfer dehydrogenation of cyclooctane	34
2.2.5.3	Acceptorless dehydrogenation of <i>n</i> -dodecane	36
2.2.5.4	Acceptorless dehydrogenation of cyclodecane	37
2.3	Summary	39
2.4	Acknowledgments	40
2.5	Experimental	40
2.6	Chapter 2 Appendix	46
2.6.1	NMR Spectra	46
2.6.2	Full crystal data of ( $t\text{Bu}^4\text{PCOP}$ )Ir(H)(Cl)	55
2.7	References	65
<b>Chapter 3</b>	<b>Alkane metathesis co-catalyzed by MoF12 and various iridium-pincer complexes</b>	67
3.1	Introduction	68
3.2	Results and Discussion	73
3.2.1	Comparing the catalytic activity of the hybrid catalyst to its parent complexes in <i>n</i> -hexane alkane metathesis	73
3.2.2	Resting state of ( $t\text{Bu}^4\text{PCOP}$ )Ir in alkane metathesis	75

3.2.3	<i>Alkane metathesis with other hybrid (PCOP)Ir catalysts</i>	76
3.2.4	<i>Comparison of the selectivities of various (pincer)Ir catalysts</i>	79
3.2.5	<i>(<sup>t</sup>Bu<sup>4</sup>PCOP)IrH<sub>2</sub> and Arduengo olefin metathesis catalysts</i>	79
3.3	Summary	80
3.4	Acknowledgments	81
3.5	Experimental	82
3.6	Chapter 3 Appendix	85
3.7	References	87
<b>Chapter 4</b>	<b>Acid-catalyzed Oxidative Addition of PhCCH to (<sup>t</sup>Bu<sup>4</sup>PCP)Ir(CO)</b>	89
4.1	Introduction	90
4.2	Results and Discussion	94
4.2.1	<i>Attempts to add C-H bonds to (<sup>t</sup>Bu<sup>4</sup>PCP)Ir(CO)</i>	94
4.2.2	<i>Early studies involving acid-catalyzed addition of PhCCH to (<sup>t</sup>Bu<sup>4</sup>PCP)Ir(CO)</i>	96
4.2.3	<i>Synthesis and characterization of the putative cationic intermediate, (<sup>t</sup>Bu<sup>4</sup>PCP)Ir(CO)(H)<sup>+</sup></i>	101
4.2.4	<i>Establishing the intermediacy of (<sup>t</sup>Bu<sup>4</sup>PCP)Ir(CO)(H)<sup>+</sup></i>	102
4.2.5	<i>Strategies to minimize the production of double-addition product</i>	104
4.2.6	<i>Kinetics of PhCCH addition</i>	105
4.2.7	<i>Proposed mechanism</i>	107

4.2.8	<i>DFT Calculations</i>	109
4.2.9	<i>Isotope effects</i>	111
4.3	Summary	114
4.4	Acknowledgments	114
4.5	Experimental	114
4.6	Chapter 4 Appendix	120
4.6.1	<i>NMR Spectra</i>	120
4.6.2	<i>Full crystal data of (<sup>t</sup>Bu<sup>4</sup>PCP)Ir(CO)(H)<sup>+</sup> BAr<sup>F-</sup></i>	126
4.7	References	146
<b>Chapter 5</b>	<b>Acid-catalyzed reductive elimination of C-H bonds from six-coordinate (<sup>t</sup>Bu<sup>4</sup>PCP)Ir(CO)(H)(R) complexes</b>	148
5.1	Introduction	149
5.2	Results and Discussion	152
5.2.1	<i>Syntheses of (<sup>t</sup>Bu<sup>4</sup>PCP)Ir(CO)(H)(R) complexes</i>	152
5.2.2	<i>Acid-catalyzed reductive elimination of methane from trans-(<sup>t</sup>Bu<sup>4</sup>PCP)Ir(CO)(Me)(H)</i>	155
5.2.3	<i>Acid-catalyzed reductive elimination of ethane from a mixture of cis/trans-(<sup>t</sup>Bu<sup>4</sup>PCP)Ir(CO)(Et)(H)</i>	156
5.2.4	<i>Elimination of benzene from cis/trans (<sup>t</sup>Bu<sup>4</sup>PCP)Ir(CO)(H)(Ph) complexes</i>	158
5.2.5	<i>Proposed mechanism for elimination of trans-(<sup>t</sup>Bu<sup>4</sup>PCP)Ir(CO)(H)(R) complexes</i>	160

5.2.6	<i>DFT Calculations</i>	161
5.3	Summary	164
5.4	Experimental	164
5.5	Chapter 5 Appendix	169
5.6	References	175
<b>Chapter 6</b>	<b>Further experimental and theoretical explorations of acid-catalyzed oxidative addition and reductive elimination reactions involving (pincer)Ir(CO) complexes</b>	176
6.1	Introduction	177
6.2	Results and Discussion	179
6.2.1	<i>Reactions of (<sup>t</sup>Bu<sup>4</sup>PCP)Ir(CO) with non-alkynyl substrates</i>	179
6.2.2	<i>Reactivity of (<sup>i</sup>Pr<sup>4</sup>PCP)Ir(CO) complexes</i>	181
6.2.3	<i>Theoretical insights into factors favoring oxidative addition to square planar Ir(I) carbonyl complexes</i>	187
6.2.4	<i>Acid-catalyzed addition of H<sub>2</sub> to (<sup>t</sup>Bu<sup>4</sup>PCP)Ir(CO)</i>	193
6.3	Summary	196
6.4	Experimental	196
6.5	Chapter 6 Appendix	201
6.6	References	211

## List of Figures

Figure 1.1	Variables for modification of pincer-metal complexes	6
Figure 1.2	(PCP)Ir-catalyzed activation of C-O and C-F bonds via initial C-H activation	8
Figure 1.3	Alkane metathesis co-catalyzed by (pincer)Ir and olefin metathesis catalysts	9
Figure 2.1	Examples of previously reported pincer-iridium complexes exhibiting high catalytic activity for alkane transfer dehydrogenation	20
Figure 2.2	Thermal ellipsoid plot of ( <sup>t</sup> Bu <sup>4</sup> PCOP)IrHCl	28
Figure 2A.1	<sup>1</sup> H nmr spectrum of <sup>t</sup> Bu <sup>4</sup> PCOP ligand ( <b>2-3</b> )	46
Figure 2A.2	<sup>31</sup> P nmr spectrum of <sup>t</sup> Bu <sup>4</sup> PCOP ligand ( <b>2-3</b> )	47
Figure 2A.3	<sup>13</sup> C nmr spectrum of <sup>t</sup> Bu <sup>4</sup> PCOP ligand ( <b>2-3</b> )	48
Figure 2A.4	<sup>1</sup> H nmr spectrum of ( <sup>t</sup> Bu <sup>4</sup> PCOP)Ir(H)(Cl) ligand ( <b>2-4</b> )	49
Figure 2A.5	<sup>31</sup> P nmr spectrum of ( <sup>t</sup> Bu <sup>4</sup> PCOP)Ir(H)(Cl) ligand ( <b>2-4</b> )	50
Figure 2A.6	<sup>13</sup> C nmr spectrum of ( <sup>t</sup> Bu <sup>4</sup> PCOP)Ir(H)(Cl) ligand ( <b>2-4</b> )	51
Figure 2A.7	<sup>1</sup> H nmr spectrum of ( <sup>t</sup> Bu <sup>4</sup> PCOP)Ir(H) <sub>2</sub> ( <b>2-5</b> )	52
Figure 2A.8	<sup>31</sup> P nmr spectrum of ( <sup>t</sup> Bu <sup>4</sup> PCOP)Ir(H) <sub>2</sub> ( <b>2-5</b> )	53
Figure 2A.9	<sup>13</sup> C nmr spectrum of ( <sup>t</sup> Bu <sup>4</sup> PCOP)Ir(H) <sub>2</sub> ( <b>2-5</b> )	54
Figure 2A.10	Crystal structure of <b>2-4</b>	55
Figure 3.1	Catalysts employed in alkane metathesis reactions	71
Figure 3.2	Resting states of ( <sup>t</sup> Bu <sup>4</sup> PCP)Ir ( <b>3-1</b> ) and ( <sup>t</sup> Bu <sup>4</sup> POCOP)Ir ( <b>3-2</b> ) observed in alkane metathesis.	71



Figure 3.3	Schematic diagram indicating relative overall free energy barriers, under alkane metathesis conditions, for the alkane dehydrogenation and olefin hydrogenation segments of the transfer-dehydrogenation catalytic cycle, for (a) ( <sup>t</sup> Bu <sup>4</sup> PCP)Ir, (b) ( <sup>t</sup> Bu <sup>4</sup> POCOP)Ir, (c) a hypothetical species with properties intermediate between ( <sup>t</sup> Bu <sup>4</sup> PCP)Ir and ( <sup>t</sup> Bu <sup>4</sup> POCOP)Ir	72
Figure 3.4	Total product concentrations formed by <i>n</i> -hexane metathesis catalyzed by <b>MoF12</b> and (pincer)Ir catalysts <b>3-1</b> , <b>3-2</b> , and <b>3-3</b> over the first 24 hours at 125 °C.	74
Figure 3.5	<sup>31</sup> P{ <sup>1</sup> H} NMR spectrum of ( <sup>t</sup> Bu <sup>4</sup> PCOP)Ir during alkane ( <i>n</i> -hexane) metathesis after 1 hour at 90 °C, revealing the catalyst resting state	76
Figure 3.6	Other hybrid (PCOP)Ir catalysts	77
Figure 3.7	Total alkane products formed in the metathesis of <i>n</i> -hexane catalyzed by <b>MoF12</b> and (PCOP)Ir catalysts <b>3-3</b> , <b>3-4</b> , and <b>3-5</b> over the first 24 h of reaction at 125 °C.	78
Figure 3.8	Various Ru-alkylidene complexes attempted as olefin metathesis co-catalysts in alkane metathesis of <i>n</i> -hexane	80
Figure 3A.1	<sup>31</sup> P NMR spectrum of ( <sup>t</sup> Bu <sup>4</sup> PCOP)Ir(1-hexene)	86
Figure 4.1	Hydride signals exhibiting <sup>13</sup> C-splitting in <sup>1</sup> H nmr for (a) <i>trans</i> -( <sup>t</sup> Bu <sup>4</sup> PCP)Ir(CO)(H)( <sup>13</sup> CCPh) and (b) <i>cis</i> -( <sup>t</sup> Bu <sup>4</sup> PCP)Ir(CO)(H)( <sup>13</sup> CCPh)	98

Figure 4.2	Conversion of ( <sup>t</sup> Bu <sup>4</sup> PCP)Ir(CO) to <b>4-2</b> and double-addition byproducts as catalyzed by 1 mM trityl BAr <sup>F</sup> at -30 °C	100
Figure 4.3	Thermal ellipsoid plot of ( <sup>t</sup> Bu <sup>4</sup> PCP)Ir(CO)(H) <sup>+</sup> ( <b>4-3</b> )	102
Figure 4.4	Conversion of ( <sup>t</sup> Bu <sup>4</sup> PCP)Ir(CO) to <b>4-2</b> and double-addition byproducts as catalyzed by <b>4-3</b> at -25 °C.	103
Figure 4.5	Deconvoluted hydride signals in the <sup>1</sup> H nmr spectrum of the products obtained in the cross-labeling experiment	109
Figure 4.6	DFT-calculated pathway for acid-catalyzed addition of PhCCH to <b>4-1</b>	110
Figure 4.7	DFT-calculated transition state for deprotonation of the phenylacetylene adduct	111
Figure 4.8	Kinetic isotope effect observed for the addition of (a) PhCCH (200 mM) or (b) PhCCH- <i>d</i> 1 (200 mM) to ( <sup>t</sup> Bu <sup>4</sup> PCP)Ir(CO)	113
Figure 4.9	Competition kinetic isotope effect experiments for the buffer-catalyzed reaction between 167 mM PhCCH- <i>d</i> 1, 33 mM PhCCH, and 10 mM ( <sup>t</sup> Bu <sup>4</sup> PCP)Ir(CO) ( <b>4-1</b> )	113
Figure 4A.1	<sup>1</sup> H nmr spectrum of <b>4-2</b> ( <sup>13</sup> C-labelled PhC <sup>13</sup> CH product)	120
Figure 4A.2	<sup>31</sup> P nmr spectrum of <b>4-2</b> ( <sup>13</sup> C-labelled PhC <sup>13</sup> CH product)	121
Figure 4A.3	<sup>13</sup> C nmr spectrum of <b>4-2</b> ( <sup>13</sup> C-labelled PhC <sup>13</sup> CH product)	122
Figure 4A.4	<sup>1</sup> H nmr spectrum of <b>4-3</b>	123
Figure 4A.5	<sup>31</sup> P nmr spectrum of <b>4-3</b>	124
Figure 4A.6	<sup>19</sup> F nmr spectrum of <b>4-3</b>	125

Figure 4A.7	Full crystal Structure of <b>4-3</b> (incl. $\text{BAr}^{\text{F}}$ counteranion)	126
Figure 5.1	$^{31}\text{P}$ NMR spectra of acid-catalyzed elimination reaction involving <i>cis</i> - and <i>trans</i> -( $^{\text{tBu}}\text{PCP}$ )Ir(CO)(H)( $\text{C}_2\text{H}_3$ ) over the first 40 minutes of reaction.	157
Figure 5.2	$^{31}\text{P}$ NMR spectra of acid-catalyzed elimination reaction involving <i>cis</i> - and <i>trans</i> -( $^{\text{tBu}}\text{PCP}$ )Ir(CO)(H)( $\text{C}_2\text{H}_3$ ) over the first <i>ca.</i> 13 hours of reaction.	158
Figure 5.3	DFT-calculated pathway for acid-catalyzed elimination of methane from <i>trans</i> -( $^{\text{tBu}}\text{PCP}$ )Ir(CO)( $\text{CH}_3$ )(H)	162
Figure 5.4	DFT-calculated methane intermediate exhibiting an agostic interaction	163
Figure 5A.1	$^1\text{H}$ nmr spectrum of ( $^{\text{tBu}}\text{PCP}$ )Ir(CO)(H)( $\text{CH}_3$ )	169
Figure 5A.2	$^{31}\text{P}$ nmr spectrum of ( $^{\text{tBu}}\text{PCP}$ )Ir(CO)(H)( $\text{CH}_3$ )	170
Figure 5A.3	$^1\text{H}$ nmr spectrum of ( $^{\text{tBu}}\text{PCP}$ )Ir(CO)(H)( $\text{CH}_2\text{CH}_3$ )	171
Figure 5A.4	$^{31}\text{P}$ nmr spectrum of ( $^{\text{tBu}}\text{PCP}$ )Ir(CO)(H)( $\text{CH}_2\text{CH}_3$ )	172
Figure 5A.5	$^1\text{H}$ nmr spectrum of ( $^{\text{tBu}}\text{PCP}$ )Ir(CO)(H)( $\text{C}_6\text{H}_5$ )	173
Figure 5A.6	$^{31}\text{P}$ nmr spectrum of ( $^{\text{tBu}}\text{PCP}$ )Ir(CO)(H)( $\text{C}_6\text{H}_5$ )	174
Figure 6.1	$^{31}\text{P}$ and $^1\text{H}$ NMR spectra of reaction of benzene and ( $^{\text{iPr}}\text{PCP}$ )Ir(CO) in presence of buffer mixture at 125 °C after 96 hours.	184
Figure 6.2	(PSiP)Ir complexes reported by (a) Turculet and (b) Sola	189

Figure 6A.1	$^1\text{H}$ nmr spectrum of the acid-catalyzed (10 mM) reaction of $\text{CH}_3\text{CN}$ and $(^{\text{tBu}}\text{PCP})\text{Ir}(\text{CO})$ at room-temperature after five hours.	201
Figure 6A.2	$^{31}\text{P}$ nmr spectrum of the acid-catalyzed (10 mM) reaction of $\text{CH}_3\text{CN}$ and $(^{\text{tBu}}\text{PCP})\text{Ir}(\text{CO})$ at room-temperature after five hours.	202
Figure 6A.3	$^1\text{H}$ nmr spectrum of products from acid-catalyzed reaction of $(^{\text{iPr}}\text{PCP})\text{Ir}(\text{CO})$ (10 mM) and $\text{PhCCH}$ (300 mM).	203
Figure 6A.4	$^{31}\text{P}$ nmr spectrum of products from acid-catalyzed reaction of $(^{\text{iPr}}\text{PCP})\text{Ir}(\text{CO})$ (10 mM) and $\text{PhCCH}$ (300 mM).	204
Figure 6A.5	$^1\text{H}$ NMR spectrum of independently synthesized $(^{\text{iPr}}\text{PCP})\text{Ir}(\text{CO})(\text{H})(\text{Ph})$	205
Figure 6A.6	$^{31}\text{P}$ NMR spectrum of independently synthesized $(^{\text{iPr}}\text{PCP})\text{Ir}(\text{CO})(\text{H})(\text{Ph})$ .	206
Figure 6A.7	$^1\text{H}$ NMR spectrum of independently synthesized $(^{\text{iPr}}\text{PCP})\text{Ir}(\text{CO})(\text{H})(\text{C}_8\text{H}_3\text{F}_6)$	207
Figure 6A.8	$^{31}\text{P}$ NMR spectrum of independently synthesized $(^{\text{iPr}}\text{PCP})\text{Ir}(\text{CO})(\text{H})(\text{C}_8\text{H}_3\text{F}_6)$	208
Figure 6A.9	$^1\text{H}$ NMR spectrum of products from acid-catalyzed reaction of $(^{\text{tBu}}\text{PCP})\text{Ir}(\text{CO})$ (10 mM) and $\text{H}_2$	209
Figure 6A.10	$^{31}\text{P}$ NMR spectrum of products from acid-catalyzed reaction of $(^{\text{tBu}}\text{PCP})\text{Ir}(\text{CO})$ (10 mM) and $\text{H}_2$	210

## List of Schemes

Scheme 2.1	The “benchmark” transfer dehydrogenation reaction between cyclooctane and TBE, as developed originally by Crabtree	19
Scheme 2.2	Mechanism for the ( <sup>t</sup> Bu <sup>4</sup> PCP)Ir-catalyzed transfer dehydrogenation of <i>n</i> -alkanes	23
Scheme 2.3	Synthetic route for the synthesis of the “hybrid” phosphine-phosphinite ligand (2-3)	25
Scheme 2.4	Synthesis of hybrid phosphine-phosphinite pincer-iridium complexes: ( <sup>t</sup> Bu <sup>4</sup> PCOP)Ir(H)(Cl) (2-4) and ( <sup>t</sup> Bu <sup>4</sup> PCOP)Ir(H) <sub>2</sub> (2-5)	27
Scheme 2.5	Synthesis of ( <sup>t</sup> Bu <sup>4</sup> PCOP)Ir(CO) (2-6)	30
Scheme 2.6	Transfer dehydrogenation of <i>n</i> -octane and TBE catalyzed by (pincer)Ir complexes (2-1, 2-2, and 2-5)	33
Scheme 2.7	Transfer dehydrogenation of cyclooctane and TBE catalyzed by (pincer)Ir complexes (2-1, 2-2, and 2-5)	34
Scheme 2.8	Acceptorless dehydrogenation of <i>n</i> -dodecane catalyzed by (pincer)Ir complexes (2-1, 2-2, and 2-5)	36
Scheme 2.9	Acceptorless dehydrogenation of cyclodecane catalyzed by (pincer)Ir complexes (2-1, 2-2, and 2-5)	37
Scheme 3.1	Alkane metathesis via tandem catalysis	70

Scheme 4.1	No reaction takes place between ( <sup>t</sup> Bu <sup>4</sup> PCP)Ir(CO) and PhCCH at room temperature or 125 °C over the course of six months in the absence of a catalyst	95
Scheme 4.2	4-(trifluoromethyl)benzoic acid-catalyzed oxidative addition of PhCCH to ( <sup>t</sup> Bu <sup>4</sup> PCP)Ir(CO)	96
Scheme 4.3	Phenol-catalyzed oxidative addition of PhCCH to ( <sup>t</sup> Bu <sup>4</sup> PCP)Ir(CO)	97
Scheme 4.4	Synthesis of <i>cis</i> -( <sup>t</sup> Bu <sup>4</sup> PCP)Ir(CO)(H)(CCPh) via CO addition to ( <sup>t</sup> Bu <sup>4</sup> PCP)Ir(H)(CCPh)	97
Scheme 4.5	Lewis-acid (trityl BAr <sup>F</sup> )-catalyzed addition of PhCCH to ( <sup>t</sup> Bu <sup>4</sup> PCP)Ir(CO)	100
Scheme 4.6	Independent synthesis of the putative cationic intermediate <b>4-3</b> via direct protonation of <b>4-1</b>	102
Scheme 4.7	Addition of PhCCH (50 mM) to ( <sup>t</sup> Bu <sup>4</sup> PCP)Ir(CO) (20 mM) catalyzed by <b>4-3</b> (1 mM)	103
Scheme 4.8	Acid-catalyzed addition of PhCCH to ( <sup>t</sup> Bu <sup>4</sup> PCP)Ir(CO) in presence of base	104
Scheme 4.9	Proposed mechanism for the acid-catalyzed oxidative addition of PhCCH to ( <sup>t</sup> Bu <sup>4</sup> PCP)Ir(CO)	108
Scheme 4.10	Cross-labeling experiment involving <i>p</i> -methylphenyl-acetylene (150 mM) and phenylacetylene- <i>d</i> 1 (150 mM)	108
Scheme 5.1	Elimination of R-H bonds from five- and six-coordinate (pincer)Ir complexes	150

Scheme 5.2	Previously reported synthesis of <i>cis/trans</i> - ( <sup>t</sup> Bu <sup>4</sup> PCP)Ir(CO)(R)(H) complexes	153
Scheme 5.3	Synthesis of <i>cis/trans</i> -( <sup>t</sup> Bu <sup>4</sup> PCP)Ir(CO)(H)(C <sub>2</sub> H <sub>5</sub> )	154
Scheme 5.4	Synthesis of <i>cis/trans</i> -( <sup>t</sup> Bu <sup>4</sup> PCP)Ir(CO)(H)(C <sub>6</sub> H <sub>5</sub> )	154
Scheme 5.5	Acid-catalyzed reductive elimination of methane from <i>trans</i> -( <sup>t</sup> Bu <sup>4</sup> PCP)Ir(CO)(H)(CH <sub>3</sub> )	155
Scheme 5.6	Acid-catalyzed reductive elimination of ethane from <i>cis</i> - and <i>trans</i> -( <sup>t</sup> Bu <sup>4</sup> PCP)Ir(CO)(H)(C <sub>2</sub> H <sub>3</sub> )	156
Scheme 5.7	Buffer-catalyzed reductive elimination of benzene from <i>cis</i> - and <i>trans</i> -( <sup>t</sup> Bu <sup>4</sup> PCP)Ir(CO)(H)(Ph)	159
Scheme 5.8	Thermolytic loss of benzene exclusively from <i>cis</i> - ( <sup>t</sup> Bu <sup>4</sup> PCP)Ir(CO)(H)(Ph)	160
Scheme 5.9	Proposed mechanism for acid-catalyzed reductive elim- ination of methane from <i>trans</i> -( <sup>t</sup> Bu <sup>4</sup> PCP)Ir(CO)(H)(CH <sub>3</sub> )	161
Scheme 6.1	Addition of CH <sub>3</sub> CN traps the cationic intermediate	180
Scheme 6.2	Acid-catalyzed addition of PhCCH to ( <sup>i</sup> Pr <sup>4</sup> PCP)Ir(CO)	183
Scheme 6.3	Synthesis of <i>trans</i> -( <sup>i</sup> Pr <sup>4</sup> PCP)Ir(CO)(Ph)(H)	185
Scheme 6.4	Synthesis of <i>trans</i> -( <sup>i</sup> Pr <sup>4</sup> PCP)Ir(CO)(H)(C <sub>8</sub> H <sub>3</sub> F <sub>6</sub> )	187
Scheme 6.5	DFT-calculated pathway for the acid-catalyzed oxidative addition of methane to Turculet-ligand ( <sup>i</sup> Pr <sup>4</sup> PSiP)Ir(CO)	192
Scheme 6.6	Acid-catalyzed addition of H <sub>2</sub> to ( <sup>t</sup> Bu <sup>4</sup> PCP)Ir(CO)	194
Scheme 6.7	DFT-calculated pathways for the direct and acid- catalyzed oxidative addition of H <sub>2</sub> to ( <sup>t</sup> Bu <sup>4</sup> PCP)Ir(CO)	195

## List of Tables

Table 2.1	Selected Bond Distances (Å) and Bond Angles (°) for ( <sup>t</sup> Bu <sup>4</sup> PCOP)IrHCl ( <b>2-4</b> )	28
Table 2.2	Octenes formed from (pincer)Ir-catalyzed (1 mM) transfer dehydrogenation of <i>n</i> -octane and TBE (200 mM) at 150 °C (low [TBE] extreme)	33
Table 2.3	Octenes formed from (pincer)Ir-catalyzed (1 mM) transfer dehydrogenation of <i>n</i> -octane and TBE (1 M) at 150 °C (high [TBE] extreme)	34
Table 2.4	Products formed from (pincer)Ir-catalyzed (1.2 mM) transfer dehydrogenation of cyclooctane (3.72 M) and TBE (3.72 M) at 200 °C	35
Table 2.5	Dodecenes products formed from (pincer)Ir (1 mM) catalyzed acceptorless dehydrogenation of <i>n</i> -dodecane at 230 °C	37
Table 2.6	Products formed from (pincer)Ir-catalyzed (1 mM) acceptorless dehydrogenation of cyclodecane at 230 °C	38
Table 2A.1	Crystal data and structure refinement for <b>2-4</b>	56
Table 2A.2	Atomic coordinates ( $\times 10^4$ ) and equivalent isotropic displacement parameters ( $\text{\AA}^2 \times 10^3$ ) for <b>2-4</b>	57
Table 2A.3	Bond lengths [Å] and angles [°] for <b>2-4</b>	58
Table 2A.4	Anisotropic displacement parameters ( $\text{\AA}^2 \times 10^3$ ) for <b>2-4</b>	60



Table 2A.5	Hydrogen coordinates ( $\times 10^4$ ) and isotropic displacement parameters ( $\text{\AA}^2 \times 10^3$ ) for <b>2-4</b>	61
Table 2A.6	Torsion angles [ $^\circ$ ] for <b>2-4</b>	63
Table 3.1	Concentrations (mM) of products formed by metathesis of <i>n</i> -hexane catalyzed by <b>MoF12</b> (16 mM) and (pincer)Ir catalysts <b>3-1</b> , <b>3-2</b> , and <b>3-3</b> (10 mM) at 125 $^\circ\text{C}$	74
Table 3.2	Concentrations (mM) of products formed by metathesis of <i>n</i> -hexane catalyzed by <b>MoF12</b> (16 mM) and (PCOP)Ir catalysts <b>3-4</b> and <b>3-5</b> (10 mM) at 125 $^\circ\text{C}$	78
Table 4.1	Initial rates of reaction for buffer-catalyzed addition of PhCCH to <b>4-1</b> under various concentration conditions	106
Table 4A.1	Crystal data and structure refinement for <b>4-3</b>	127
Table 4A.2	Atomic coordinates ( $\times 10^4$ ) and equivalent isotropic displacement parameters ( $\text{\AA}^2 \times 10^3$ ) for <b>4-3</b>	128
Table 4A.3	Bond lengths [ $\text{\AA}$ ] and angles [ $^\circ$ ] for <b>4-3</b>	131
Table 4A.4	Anisotropic displacement parameters ( $\text{\AA}^2 \times 10^3$ ) for <b>4-3</b>	138
Table 4A.5	Hydrogen coordinates ( $\times 10^4$ ) and isotropic displacement parameters ( $\text{\AA}^2 \times 10^3$ ) for <b>4-3</b>	141
Table 4A.6	Torsion angles [ $^\circ$ ] for <b>4-3</b>	143
Table 6.1	Calculated energies for <i>trans</i> oxidative addition of methane to ( $\text{R}^4\text{PCP}$ )Ir(CO)	182
Table 6.2	Calculated energies for methane oxidative addition to <i>trans</i> -(X)(PH <sub>3</sub> ) <sub>2</sub> Ir(CO) (X = CH <sub>3</sub> , SiH <sub>3</sub> , or GeH <sub>3</sub> )	188

Table 6.3	Calculated energies for methane addition to Turculet-ligand ( $^{\text{R}4}\text{PSiPIr}(\text{CO})$ )	190
Table 6.4	Calculated energies for methane addition to Sola-ligand ( $^{\text{R}4}\text{PSiP}(\text{Ir}(\text{CO}))$ )	191

## Chapter 1

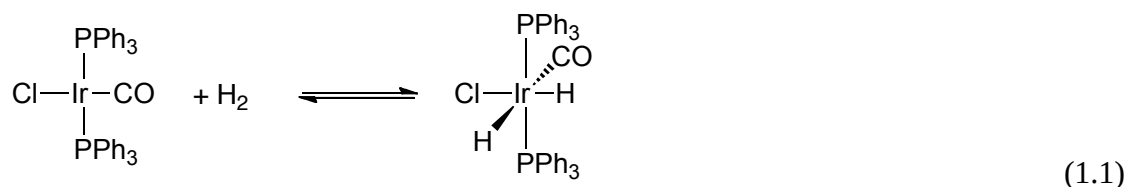
### Introduction

Oxidative addition and its microscopic reverse, reductive elimination, are the two most fundamental transformations in organometallic chemistry. Our understanding of these processes arises in large part from our desire to catalytically transform small molecules; the activation and functionalization of H-H and C-H bonds, in particular, has been the driving force behind rationalizing the factors that influence oxidative addition and reductive elimination. From the earliest examples of H-H and C-H activation, the field of organometallic chemistry, with its applications toward catalytic transformation and reaction development, its potential for sustainable energy, and its continually-evolving intellectual challenges, has blossomed into an indispensable force, breathing new life into stagnant industries and helping to usher in a new modernity enabled by technological advancements. It is with an eye toward future and a nod to the past that we pursue the development of novel catalytic processes.

#### **1.1 Prominent early examples of small molecule activation by transition-metal catalysts**

The development and understanding of C-H activation catalysis rests upon the pioneering discoveries of small molecule activation by transition metal complexes in the mid-twentieth century, which shed light on the two most fundamental processes in organometallic catalysis: oxidative addition and reductive elimination. The earliest example of oxidative addition to an organometallic complex was reported by Vaska, who found relatively facile addition of H<sub>2</sub> to the complex that now bears his name,

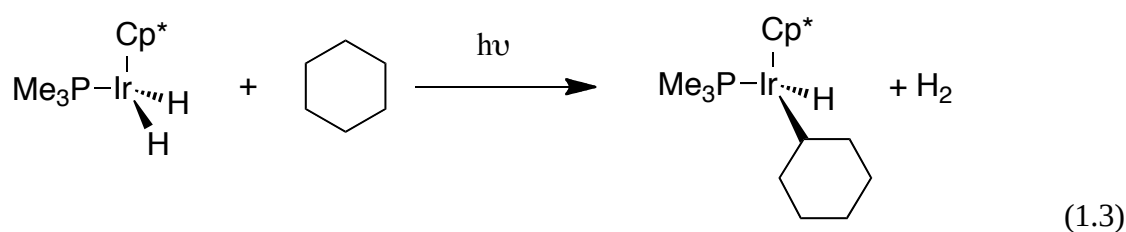
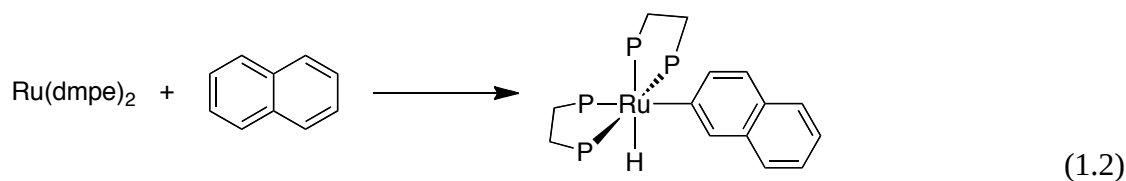
$(\text{PPh}_3)_2\text{Ir}(\text{CO})\text{Cl}$ , to form the corresponding stable dihydride species,  $(\text{PPh}_3)_2\text{Ir}(\text{CO})\text{Cl}(\text{H})_2$  (**eq. 1.1**).<sup>1</sup> Following this, Wilkinson reported his iconic hydrogenation catalyst,  $(\text{PPh}_3)_3\text{RhCl}$ , which could readily add  $\text{H}_2$  upon dissociation of phosphine ligand and subsequently hydrogenate olefins catalytically.<sup>2,3</sup> It was thorough mechanistic investigations of these transformations that contributed to an understanding of oxidative addition and reductive elimination processes, and a recognition that the cleavage of even stronger bonds (particularly C-H or C-C bonds) might possibly be achieved via reaction with organometallic complexes.



## 1.2 Brief history of C-H activation chemistry

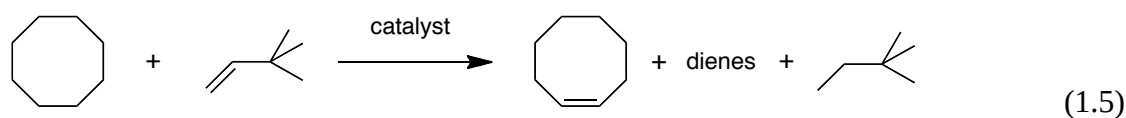
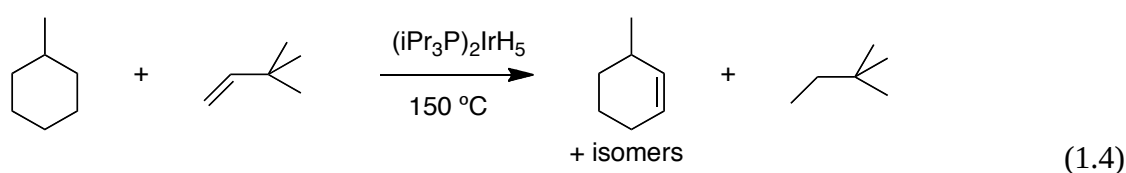
C-H bonds are not only among the most ubiquitous bonds found in nature, they are also among the most difficult to transform chemically, being comprised of relatively strong C-H and C-C bonds and lacking reactive functional groups. This makes the selective and facile activation and subsequent transformation of C-H bonds one of the grand challenges in organometallic catalysis. Despite the relatively short history of the field of organometallic chemistry, the activation of C-H bonds has been a central theme for nearly a half-century. The first generally recognized example of C-H activation by an organometallic complex was discovered by Chatt in the mid-1960s.<sup>4</sup> Chatt had found that treatment of *in situ* generated  $\text{Ru}(\text{dmpe})_2$  with naphthalene resulted in formation of the six-coordinate complex,  $\text{Ru}(\text{dmpe})_2(\text{H})(\text{naphthyl})$  (**eq. 1.2**). This was soon followed by the work of Shilov, who described H/D exchange between methane and  $\text{D}_2\text{O}$ ,

ostensibly occurring following Pt-catalyzed cleavage of the methane C-H bond and subsequent reductive elimination of C-D bonds, though no intermediate could be observed or isolated.<sup>5,6</sup> Shilov followed this a few years later with the first report of selective C-H functionalization, catalyzing the oxidation of methane to methanol and chloromethane.<sup>7,8</sup> It was roughly another 10 years before *direct observation* of alkyl C-H oxidative addition was reported in the early 1980s by Bergman, who reported the activation of cyclohexane C-H bonds and was even able to isolate stable addition products (**eq. 1.3**).<sup>9</sup> Shortly thereafter, Graham isolated the same product upon photolysis of  $\text{Cp}^*\text{Ir}(\text{PMe}_3)(\text{CO})$  in cyclohexane.<sup>10</sup>



Following these initial investigations into basic C-H bond activation, various practical applications were described, particularly with regard to olefin production from alkane starting materials. Felkin described the first catalytic transfer dehydrogenation process, utilizing a  $(i\text{Pr}_3\text{P})_2\text{IrH}_5$  complex to effect transfer dehydrogenation between *tert*-butylethylene (TBE) and methylcyclohexane (**eq. 1.4**).<sup>11</sup> Building off of earlier stoichiometric transformations involving formation of  $\text{L}_2\text{CpIrH}$  complexes from

cyclopentane and an iridium precursor, Crabtree described a useful catalytic process for dehydrogenating cyclooctane using  $trans\text{-}(P(C_6H_5F)_3)_2Ir(H)_2(\kappa^2\text{-TFA})_2$  and a stoichiometric amount of TBE to yield cyclooctenes and *tert*-butylethane, establishing the “benchmark” transformation against which transfer dehydrogenation catalysis has come to be tested (**eq. 1.5**).<sup>12</sup> More recently, a “revived” class of compounds, transition metal-pincer complexes, has been used to great effect to promote alkane dehydrogenation.

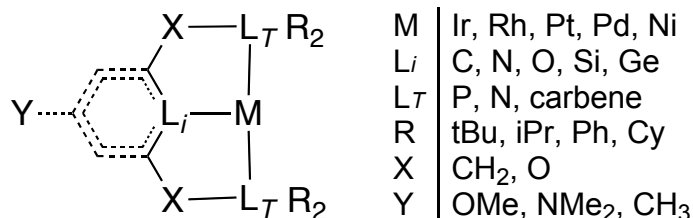


### 1.3 Small-molecule activation by pincer-iridium complexes

#### 1.3.1. Examples of pincer complexes

The first pincer ligands and metal complexes were reported in the mid-1970s by Moulton and Shaw, who coined the term *pincer* to describe the meridionally-coordinating terdentate geometry of their novel ligand,  $\kappa^3\text{-2,6-(}t\text{Bu}_2\text{PCH}_2)_2\text{C}_6\text{H}_3$ .<sup>13</sup> This  $t\text{Bu}^4\text{PCP}$  ligand was ligated to variety of late-transition metals (Ni, Pd, Pt, Rh, and Ir) to yield a series of four-, five-, and six-coordinate complexes (e.g. hydride or carbonyl complexes, hydrido chloride complexes, and hydrido chloride carbonyl complexes, respectively). In the decades since that report, the pincer motif has undergone dramatic expansion while retaining the archetypal terdentate *mer*-coordination geometry, incorporating

modifications that allow for manipulation and tuning of the ligand's stereoelectronic properties (**figure 1.1**). For example, the sterics of the (pincer)M complex, which are known to exert significant effects on reactivity and selectivity, are determined in large extent by the size of the substituents on the *trans*-coordinating atoms (e.g. P in the case of the original PCP ligand); alkyl groups such as *tert*-butyl, *iso*-propyl<sup>14</sup>, adamantyl<sup>15</sup>, cyclohexyl, and phenyl have been commonly employed, with larger, bulkier groups appearing to form more thermally-stable catalysts, preventing both cyclometallation and bimolecular degradation of the complex<sup>15</sup>. The *trans*-coordinating atoms have also been modified beyond phosphines to include functionalities such as carbenes<sup>16-19</sup> or amines<sup>20</sup>, introducing an element of hemilability into (pincer)M-promoted reactions. Further the nature of the central coordinating moiety has been explored, replacing the classical aryl-carbon group with more strongly  $\sigma$ -donating aliphatic-carbon<sup>21</sup> or silicon groups<sup>22,23</sup>, or less donating groups like pyridyl/secondary amines<sup>24,25</sup> and oxygen<sup>26</sup> atoms. The linking groups that connect the central coordinating group to the *trans*-coordinating groups (in the parlance of pincer complexes, the “arms” of the ligand) have also been modified, affecting both steric and electronic properties. Finally, inclusion of a remote functional group in the backbone of the pincer has allowed not only for subtle control of the electronics of the pincer complex (particularly for electron-donating or withdrawing groups *para* to the *ipso*-atom), but has also been used as a tethering point to anchor homogeneous complexes on heterogeneous supports (silica or  $\gamma$ -alumina, for instance), either covalently or via physisorption, which has generally allowed for more robust and recyclable catalysts.<sup>27-29</sup>

**Figure 1.1.** Variables for modification in pincer-metal complexes

### 1.3.2. Reactions involving three-coordinate (pincer)Ir complexes

Although Moulton and Shaw reported ( $t^{Bu}4$ PCP)Ir complexes in the mid-1970s, it was not until nearly twenty years later when pincer-metal complexes began to be exploited for C-H activation chemistry. In the mid-1990s, the research groups of Kaska and Jensen reported an early example of (pincer)M catalyzed C-H activation, demonstrating useful catalytic activity for cyclooctane and *tert*-butylethylene transfer dehydrogenation (*i.e.* Crabtree's benchmark reaction).<sup>30</sup> In the relatively short time since that initial discovery (less than 20 years), the unparalleled activity of these complexes has yielded an embarrassment of riches in terms of small molecule activation, but perhaps the most well-known use of (pincer)Ir complexes continues to be for catalytic alkane dehydrogenation<sup>31</sup>. Following Kaska and Jensen's initial report, Goldman and Jensen subsequently investigated the transfer dehydrogenation of linear alkanes (e.g. *n*-octane) and *tert*-butylethylene using ( $t^{Bu}4$ PCP)Ir and ( $i^{Pr}4$ PCP)Ir catalysts; these catalysts not only produced some of the most active systems for *n*-alkane transfer dehydrogenation ever reported (with significantly higher activity for the less hindered *iso*-propyl-substituted species relative to the *tert*-butyl species), but also displayed surprising and unsurpassed selectivity for terminal olefin formation.<sup>32</sup> Subsequent mechanistic work by Goldman *et al.* elucidated the mechanism of this transformation in detail.<sup>33-37</sup> It was later found that

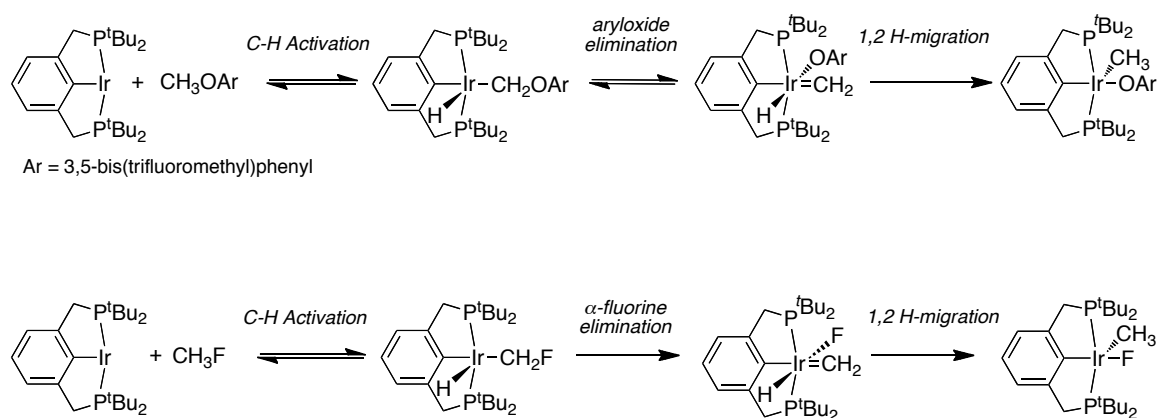


use of an acceptor to remove hydrogen was not necessary with these (PCP)Ir dehydrogenation catalysts, as the rigid *mer*-coordinating pincer ligand imparts high thermal stability to the active catalytic species, allowing for thermal extrusion of H<sub>2</sub> at elevated temperatures and thus avoiding the need for a stoichiometric sacrificial olefin.<sup>38-</sup>

<sup>40</sup> Brookhart later prepared the novel (POCOP)Ir analogue, which displayed much poorer activity for linear alkane transfer dehydrogenation, but yielded some of the highest turnover numbers reported for the benchmark cyclooctane transfer dehydrogenation, apparently owing to the more open metal center produced by the POCOP ligand.<sup>27,41,42</sup>

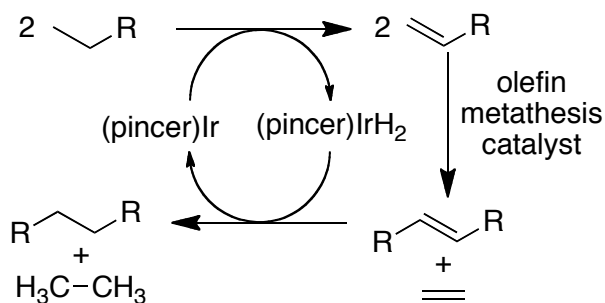
Numerous covalent bonds have been observed to undergo oxidative addition to (pincer)Ir species<sup>43</sup>. A variety of C-H bonds (sp<sup>3</sup>-, sp<sup>2</sup>-, and sp-hybridized) have been found to add to (pincer)Ir complexes, and though these do not necessarily lead to stable or isolable oxidative addition adducts, their reaction with the pincer complex allows for their catalytic transformation into new materials. N-H bonds have not been observed to add to the classical arene-based (PCP)Ir complexes (however, reductive elimination of ammonia from (PCP)Ir(H)(NH<sub>2</sub>) complexes has been observed<sup>44</sup>), but Hartwig and Goldman have observed oxidative addition of N-H bonds of ammonia and aniline to the more strongly  $\sigma$ -donating aliphatic-(PCP)Ir complex.<sup>21</sup> The net oxidative addition of C-O<sup>45</sup> and C-F<sup>46</sup> bonds has also been observed, but interestingly, these transformations do not proceed through direct oxidative addition of the C-X bond; rather, initial activation of the adjacent C-H bond is found to occur, leading to a lower energy pathway ultimately resulting in cleavage of the C-X bond (**figure 1.2**).

**Figure 1.2.** (PCP)Ir-catalyzed activation of C-O and C-F bonds via initial C-H activation.

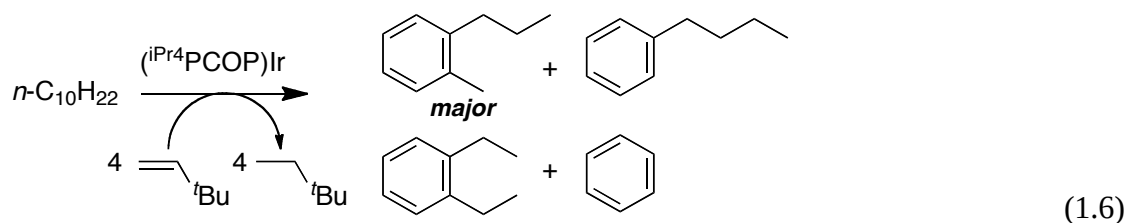


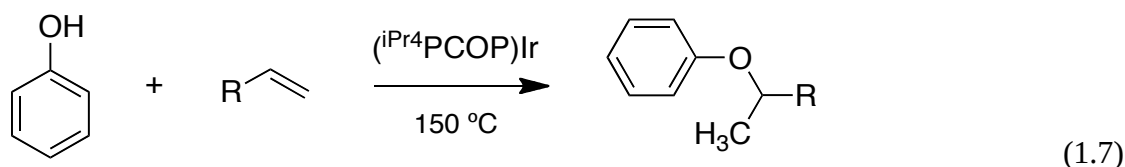
Within the past 10 years, Goldman and Brookhart have described a novel transformation called *alkane metathesis*<sup>47-51</sup>, a tandem catalytic process utilizing pincer-iridium and olefin metathesis co-catalysts to disproportionate alkyl chains into new alkane molecules (for example, converting two *n*-hexane molecules into longer (e.g. *n*-decane) and shorter (e.g. ethane) chains). Alkane metathesis is achieved by first dehydrogenating the *n*-alkane starting material to olefin products utilizing the (pincer)Ir species to remove H<sub>2</sub>, followed by olefin metathesis of these product alkenes, and subsequent hydrogenation of the new (post-metathesis) olefin molecules catalyzed by (pincer)Ir(H)<sub>2</sub>, ultimately affording new (redistributed) *n*-alkane products (**figure 1.3**). To date a variety of (pincer)Ir species and olefin metathesis catalysts have been employed in alkane metathesis. The most active and selective systems typically involve a homogeneous Schrock-type alkylidene olefin metathesis catalysts (which despite their poor thermal stability are compatible with (pincer)Ir species) in conjunction with a (R<sup>4</sup>PCP)Ir catalyst.

**Figure 1.3.** Alkane metathesis co-catalyzed by (pincer)Ir and olefin metathesis catalysts.



More recently, Goldman and Brookhart have reported an interesting and industrially-useful process for converting linear alkanes into alkyl-substituted aromatic compounds utilizing a (PCOP)Ir catalyst. This so-called *dehydroaromatization* process relies on multiple (pincer)Ir-catalyzed dehydrogenations of *n*-alkanes (with carbon chain lengths  $\geq 8$ ) followed by electrocyclization to yield various arene products, including benzene, *o*-xylene, and linear alkyl benzenes (**eq. 1.6**).<sup>52</sup> Further application of this (PCOP)Ir catalyst has recently led to the addition of O-H bonds across unactivated olefins ("hydroaryloxylation") (**eq. 1.7**), which likely occurs via olefin insertion into the Ir-O bond followed by C-H reductive elimination in the rate-determining step (consistent with earlier reports of the reverse reaction: C-O cleavage via initial C-H activation).<sup>53</sup>



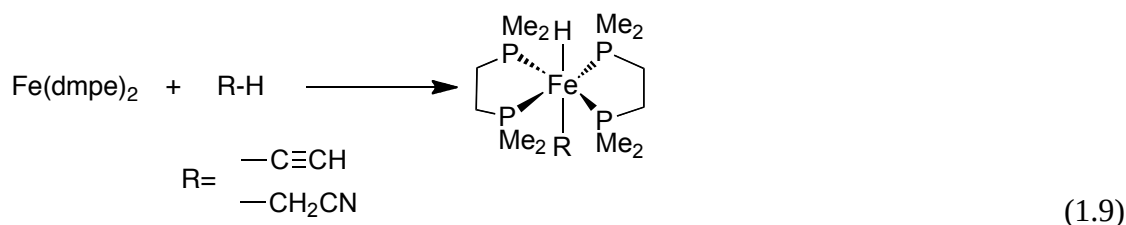


### 1.3.3. Reactions involving four-coordinate (pincer)Ir(CO) and other square-planar complexes

As described earlier, the addition of  $\text{H}_2$  to Vaska's complex is a torch-bearing example of oxidative addition in organometallic chemistry, having lit the fuse for subsequent innovations in organometallic catalysis (e.g. C-H activation), particularly shedding light on fundamental transformations such as oxidative addition and reductive elimination. As a result, the oxidative addition of bonds to square planar carbonyl complexes has become an archetypical transformation, with numerous examples of such complexes adding covalent bonds such as dihydrogen, dihalogen, and C-halogen bonds. Curiously, despite this long and storied history of covalent bond oxidative addition, virtually no examples of *C-H oxidative addition* to such complexes exist. Hoffmann and Saillard examined this aberration in early theoretical work, finding that for oxidative addition of C-H bonds to square planar carbonyl complexes to occur, the complex must distort significantly from square planarity at great energetic costs.<sup>54</sup> This is particularly unfortunate as square planar carbonyls tend to be fairly robust and thermally-stable, but even more so because the lack of reactivity toward C-H bonds prevents simple, economical carbonylation of alkane feedstocks, a highly desirable industrial process.

Although no examples of C-H oxidative addition to *square planar carbonyls* exist, there are a few examples of C-H oxidative addition to other putatively square planar complexes, though these typically involve circuitous means of promoting

oxidative addition involving non-square intermediates. For instance, Sola has reported use of a fifth ligand to promote oxidative addition of a C-H bond by assisting in the formation of distorted (and more reactive) non-square planar intermediates.<sup>55</sup> Earlier, Ittel and Tolman reported oxidative addition of acetylene and acetonitrile C-H bonds to an *in situ* generated  $\text{Fe}(\text{dmpe})_2$  complex (**eq. 1.9**)<sup>56-58</sup>, but this complex was later determined to be a distorted four-coordinate complex based on DFT calculations and spectroscopic analyses<sup>59</sup>. The rarity of C-H oxidative addition to four-coordinate square planar complexes begs further investigation.



## 1.4 Research Themes

This thesis describes our work toward expanding not only the chemistry of pincer-iridium complexes, but also toward pushing the field of organometallic chemistry farther and better understanding the fundamental processes that govern organometallic catalysis. The work presented here can be divided into two main projects: (1) novel (pincer)Ir complexes and their activity toward catalytic C-H bond activation and transformation (Chapters 2 and 3) and (2) acid-catalyzed oxidative addition or reductive elimination of covalent bonds involving square-planar (pincer)Ir(CO) complexes (Chapters 4 to 6).

Chapter 2 presents the synthesis of a novel “hybrid” PCOP pincer ligand and several of its iridium complexes. The novel dihydride species,  $(^{\text{tBu}}\text{PCOP})\text{Ir}(\text{H})_2$ , was found to be catalytically active for transfer and acceptorless dehydrogenation of a variety

of linear and cyclic alkanes. The catalytic activity of this novel catalyst was compared to those of its “parent” complexes, (<sup>t</sup>Bu<sup>4</sup>PCP)Ir and (<sup>t</sup>Bu<sup>4</sup>POCOP)Ir, and found to exhibit catalytic behaviors intermediate to those of its parent species.

Chapter 3 further explores the activity of (<sup>t</sup>Bu<sup>4</sup>PCOP)Ir and several of its less-sterically hindered analogues (specifically (<sup>t</sup>Bu<sup>2</sup>PCOP<sup>i</sup>Pr<sup>2</sup>)Ir and (<sup>i</sup>Pr<sup>4</sup>PCOP)Ir) as co-catalysts (with the Schrock MoF12 catalyst) in alkane metathesis. The activities and selectivities of these novel (PCOP)Ir complexes are compared to those exhibited by (PCP)Ir and (POCOP)Ir. The (<sup>t</sup>Bu<sup>4</sup>PCOP)Ir catalyst was found to be far more active than both (<sup>t</sup>Bu<sup>4</sup>POCOP)Ir and (<sup>t</sup>Bu<sup>4</sup>PCP)Ir (though not as selective for C10 alkanes as the latter). Likewise, the (<sup>t</sup>Bu<sup>2</sup>PCCOP<sup>i</sup>Pr<sup>2</sup>)Ir catalyst was found to be among the most active pincer-iridium catalysts in alkane metathesis reported to date, while the (<sup>i</sup>Pr<sup>4</sup>PCOP)Ir catalyst exhibited high, but short-lived, activity. The resting state of (<sup>t</sup>Bu<sup>4</sup>PCOP)Ir in alkane metathesis was examined and found to be a mixture of dihydride and olefin species (the sole resting states of the parent complexes (<sup>t</sup>Bu<sup>4</sup>PCP)Ir and (<sup>t</sup>Bu<sup>4</sup>POCOP)Ir, respectively).

Chapter 4 presents a unique and unprecedented acid-catalyzed addition of a C-H bond to (<sup>t</sup>Bu<sup>4</sup>PCP)Ir(CO), representing the first direct observation of oxidative addition to a known square planar complex. Phenylacetylene was found to oxidatively add to (<sup>t</sup>Bu<sup>4</sup>PCP)Ir(CO) in the presence of simple Bronsted acids to give the six-coordinate *trans*-(<sup>t</sup>Bu<sup>4</sup>PCP)Ir(CO)(H)(CCPh) complex. The mechanism of this rare transformation was examined in detail via kinetic studies and DFT calculations, and proposed to proceed via a five-coordinate protonated intermediate that undergoes electrophilic addition of phenylacetylene followed by deprotonation of the resulting phenylacetylene-adduct.

Chapter 5, meanwhile, examines the reverse reaction, namely acid-catalyzed *reductive elimination* of C-H bonds from six-coordinate (<sup>t</sup>Bu<sup>4</sup>PCP)Ir(CO)(R)(H) complexes. (<sup>t</sup>Bu<sup>4</sup>PCP)Ir(CO)(R)(H) complexes (R=CH<sub>3</sub>, CH<sub>2</sub>CH<sub>3</sub>, and C<sub>6</sub>H<sub>5</sub>) were independently synthesized and exposed to substoichiometric amounts of Bronsted acid, resulting in elimination of methane, ethane, and benzene. Different rates of reductive elimination were observed for *cis* and *trans* stereoisomers, with acid-catalyzed *trans* elimination occurring much more rapidly. The elimination of methane and ethane occurred readily at room temperature, but reductive elimination of benzene required prolonged heating to elevated temperatures to effect loss of benzene. These results suggest that the microscopic reverse of this reaction, oxidative addition, may be kinetically-feasible for these simple hydrocarbons but formation of isolable six-coordinate products is likely thermodynamically unfavorable.

Chapter 6 further explores the scope of acid-catalyzed addition/elimination involving (pincer)Ir(CO) complexes, particularly with respect to strategies which may promote the thermodynamics of addition. Acid-catalyzed addition of C-H bonds to the less-sterically-hindered (<sup>i</sup>Pr<sup>4</sup>PCP)Ir(CO) were examined in detail. DFT calculations were performed to assess the effects on the thermodynamics of methane addition to a variety of (pincer)Ir(CO) complexes varying in terms of sterics and σ-donating ability of the ligand *trans* to the carbonyl. Finally, addition of H<sub>2</sub> to (<sup>t</sup>Bu<sup>4</sup>PCP)Ir(CO), which has not been previously observed despite the ease of H<sub>2</sub> addition to Vaska's complex, was found to occur only in the presence of a Bronsted acid catalyst to yield the six-coordinate *trans* dihydride species.

## 1.5 References

- (1) Vaska, L.; DiLuzio, J. W. *J. Am. Chem. Soc.* **1962**, *84*, 679.
- (2) Osborn, J. A.; Jardine, F. H.; Young, J. F.; Wilkinson, G. *J. Chem. Soc., A* **1966**, 1711.
- (3) Young, J. F.; Osborn, J. A.; Jardine, F. H.; Wilkinson, G. *Chem. Commun.* **1965**, 131.
- (4) Chatt, J.; Davidson, J. M. *J. Chem. Soc.* **1965**, 843.
- (5) Gol'dshleger, N. F.; Tyabin, M. B.; Shilov, A. E.; Shteinman, A. A. *Zhurnal Fizicheskoi Khimii* **1969**, *43*, 2174.
- (6) Khrushch, A. P.; Tokina, L. A.; Shilov, A. E. *Kinetika i Kataliz* **1966**, *7*, 901.
- (7) Gol'dshleger, N. F.; Es'kova, V. V.; Shilov, A. E.; Shteinman, A. A. *Zhurnal Fizicheskoi Khimii* **1972**, *46*, 1353.
- (8) Kushch, L. A.; Lavrushko, V. V.; Misharin, Y. S.; Moravskii, A. P.; Shilov, A. E. *Nouveau Journal de Chimie* **1983**, *7*, 729.
- (9) Janowicz, A. H.; Bergman, R. G. *J. Am. Chem. Soc.* **1982**, *104*, 352.
- (10) Hoyano, J. K.; Graham, W. A. G. *J. Am. Chem. Soc.* **1982**, *104*, 3723.
- (11) Baudry, D.; Ephritikhine, M.; Felkin, H.; Holmes-Smith, R. *J. Chem. Soc., Chem. Comm.* **1983**, 788.
- (12) Burk, M. J.; Crabtree, R. H. *J. Am. Chem. Soc.* **1987**, *109*, 8025.
- (13) Moulton, C. J.; Shaw, B. L. *J. Chem. Soc., Dalton Trans.* **1976**, 1020.
- (14) Rybtchinski, B.; Ben-David, Y.; Milstein, D. *Organometallics* **1997**, *16*, 3786.
- (15) Punji, B.; Emge, T. J.; Goldman, A. S. *Organometallics* **2010**, *29*, 2702.
- (16) Chianese, A. R.; Mo, A.; Lampland, N. L.; Swartz, R. L.; Bremer, P. T. *Organometallics* **2010**, *29*, 3019.
- (17) Danopoulos, A. A.; Tulloch, A. A. D.; Winston, S.; Eastham, G.; Hursthouse, M. B. *Dalton Trans.* **2003**, 1009.
- (18) Nishiyama, H.; Niwa, E.; Inoue, T.; Ishima, Y.; Aoki, K. *Organometallics* **2002**, *21*, 2572.
- (19) Gruendemann, S.; Albrecht, M.; Loch, J. A.; Faller, J. W.; Crabtree, R. H. *Organometallics* **2001**, *20*, 5485.
- (20) Gandelman, M.; Vigalok, A.; Shimon, L. J. W.; Milstein, D. *Organometallics* **1997**, *16*, 3981.
- (21) Zhao, J.; Goldman, A. S.; Hartwig, J. F. *Science* **2005**, *307*, 1080.
- (22) MacLean, D. F.; McDonald, R.; Ferguson, M. J.; Caddell, A. J.; Turculet, L. *Chem. Commun.* **2008**, 5146.
- (23) MacInnis, M. C.; MacLean, D. F.; Lundgren, R. J.; McDonald, R.; Turculet, L. *Organometallics* **2007**, *26*, 6522.
- (24) Fryzuk, M. D.; MacNeil, P. A. *Organometallics* **1983**, *2*, 355.
- (25) Ozerov, O. V.; Guo, C.; Papkov, V. A.; Foxman, B. M. *J. Am. Chem. Soc.* **2004**, *126*, 4792.
- (26) Haibach, M. C.; Wang, D. Y.; Emge, T. J.; Krogh-Jespersen, K.; Goldman, A. S. *Chem. Sci.* **2013**, *4*, 3683.
- (27) Göttker-Schnetmann, I.; White, P.; Brookhart, M. *J. Am. Chem. Soc.* **2004**, *126*, 1804.



- (28) Kundu, S.; Goldman, A. S.; Huang, Z.; Brookhart, M. In *Abstracts of Papers, 236th ACS National Meeting, Philadelphia, PA, United States, August 17-21, 2008*, INOR 043.
- (29) Huang, Z.; Rolfe, E.; Carson, E. C.; Brookhart, M.; Goldman, A. S.; El-Khalafy, S. H.; MacArthur, A. H. R. *Adv. Synth. Catal.* **2010**, 352, 125.
- (30) Gupta, M.; Hagen, C.; Flesher, R. J.; Kaska, W. C.; Jensen, C. M. *Chem. Commun.* **1996**, 2083.
- (31) Findlater, M.; Choi, J.; Goldman, A. S.; Brookhart, M. In *Alkane C-H Activation by Single-Site Metal Catalysis*; Pérez, P. J., Ed.; Springer: New York, 2012; Vol. 38.
- (32) Liu, F.; Pak, E. B.; Singh, B.; Jensen, C. M.; Goldman, A. S. *J. Am. Chem. Soc.* **1999**, 121, 4086.
- (33) Kanzelberger, M.; Singh, B.; Czerw, M.; Krogh-Jespersen, K.; Goldman, A. S. *J. Am. Chem. Soc.* **2000**, 122, 11017.
- (34) Krogh-Jespersen, K.; Czerw, M.; Zhu, K.; Singh, B.; Kanzelberger, M.; Darji, N.; Achord, P. D.; Renkema, K. B.; Goldman, A. S. *J. Am. Chem. Soc.* **2002**, 124, 10797.
- (35) Krogh-Jespersen, K.; Czerw, M.; Summa, N.; Renkema, K. B.; Achord, P. D.; Goldman, A. S. *J. Am. Chem. Soc.* **2002**, 124, 11404.
- (36) Krogh-Jespersen, K.; Czerw, M.; Goldman, A. S. *J. Mol. Cat., A* **2002**, 189, 95.
- (37) Renkema, K. B.; Kissin, Y. V.; Goldman, A. S. *J. Am. Chem. Soc.* **2003**, 125, 7770.
- (38) Krogh-Jespersen, K.; Czerw, M.; Summa, N.; Goldman, A. S. In *Abstracts of Papers, 223rd ACS National Meeting, Orlando, FL, United States, April 7-11 2002*, INOR 212.
- (39) Liu, F.; Goldman, A. S. *Chem. Commun.* **1999**, 655.
- (40) Xu, W.; Rosini, G. P.; Gupta, M.; Jensen, C. M.; Kaska, W. C.; Krogh-Jespersen, K.; Goldman, A. S. *Chem. Commun.* **1997**, 2273.
- (41) Göttker-Schnetmann, I.; White, P. S.; Brookhart, M. *Organometallics* **2004**, 23, 1766.
- (42) Göttker-Schnetmann, I.; Brookhart, M. *J. Am. Chem. Soc.* **2004**, 126, 9330.
- (43) Choi, J.; MacArthur, A. H. R.; Brookhart, M.; Goldman, A. S. *Chem. Rev.* **2011**, 111, 1761.
- (44) Kanzelberger, M.; Zhang, X.; Emge, T. J.; Goldman, A. S.; Zhao, J.; Incarvito, C.; Hartwig, J. F. *J. Am. Chem. Soc.* **2003**, 125, 13644.
- (45) Choi, J.; Choliy, Y.; Zhang, X.; Emge, T. J.; Krogh-Jespersen, K.; Goldman, A. S. *J. Am. Chem. Soc.* **2009**, 131, 15627.
- (46) Choi, J.; Wang, D. Y.; Kundu, S.; Choliy, Y.; Emge, T. J.; Krogh-Jespersen, K.; Goldman, A. S. *Science* **2011**, 332, 1545.
- (47) Goldman, A. S.; Roy, A. H.; Huang, Z.; Ahuja, R.; Schinski, W.; Brookhart, M. *Science* **2006**, 312, 257.
- (48) Bailey, B. C.; Schrock, R. R.; Kundu, S.; Goldman, A. S.; Huang, Z.; Brookhart, M. *Organometallics* **2009**, 28, 355.
- (49) Ahuja, R.; Kundu, S.; Goldman, A. S.; Brookhart, M.; Vicente, B. C.; Scott, S. L. *Chem. Commun.* **2008**, 253.

- (50) Nawara-Hultzs, A. J.; Hackenberg, J. D.; Punji, B.; Supplee, C.; Emge, T. J.; Bailey, B. C.; Schrock, R. R.; Brookhart, M.; Goldman, A. S. *ACS Catalysis* **2013**, 3, 2505.
- (51) Huang, Z.; Brookhart, M.; Goldman, A. S.; Kundu, S.; Ray, A.; Scott, S. L.; Vicente, B. C. *Adv. Synth. Catal.* **2009**, 351, 188.
- (52) Ahuja, R.; Punji, B.; Findlater, M.; Supplee, C.; Schinski, W.; Brookhart, M.; Goldman, A. S. *Nature Chem.* **2011**, 3, 167.
- (53) Haibach, M. C.; Guan, C.; Wang, D. Y.; Li, B.; Lease, N.; Steffens, A. M.; Krogh-Jespersen, K.; Goldman, A. S. *J. Am. Chem. Soc.* **2013**, 135, 15062.
- (54) Saillard, J.; Hoffmann, R. *J. Am. Chem. Soc.* **1984**, 106, 2006.
- (55) Martín, M.; Torres, O.; Oñate, E.; Sola, E.; Oro, L. A. *J. Am. Chem. Soc.* **2005**, 127, 18074.
- (56) Ittel, S. D.; Tolman, C. A.; English, A. D.; Jesson, J. P. *Adv. Chem. Ser.* **1979**, 173, 67.
- (57) Tolman, C. A.; Ittel, S. D.; English, A. D.; Jesson, J. P. *J. Am. Chem. Soc.* **1979**, 101, 1742.
- (58) Ittel, S. D.; Tolman, C. A.; English, A. D.; Jesson, J. P. *J. Am. Chem. Soc.* **1978**, 100, 7577.
- (59) Macgregor, S. A.; Eisenstein, O.; Whittlesey, M. K.; Perutz, R. N. *J. Chem. Soc., Dalton Trans.* **1998**, 291.

## Chapter 2

### Synthesis, Characterization, and Catalytic Activity of “Hybrid” (PCOP)Ir Complexes toward Dehydrogenation of Alkanes<sup>1</sup>

#### Abstract

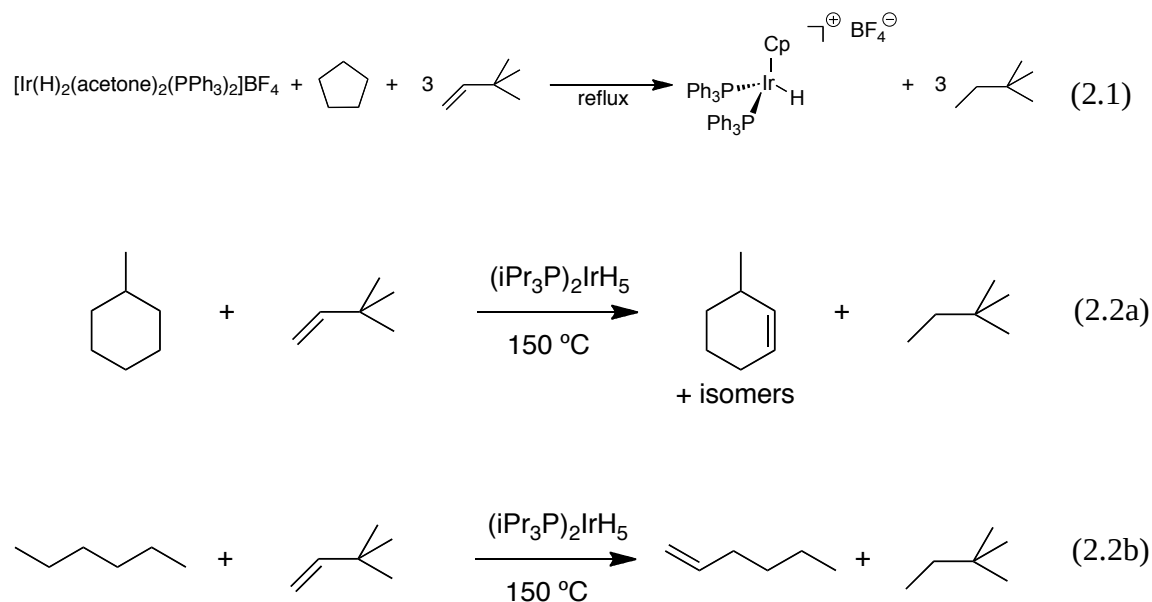
A “hybrid” of the previously reported <sup>t</sup>Bu<sup>4</sup>PCP and <sup>t</sup>Bu<sup>4</sup>POCOP ligands, the novel pincer ligand <sup>t</sup>Bu<sup>4</sup>PCOP (**2-3**) was successfully prepared and metalated with [Ir(COD)Cl]<sub>2</sub> to ultimately yield new pincer complexes (<sup>t</sup>Bu<sup>4</sup>PCOP)Ir(H)(Cl) (**2-4**), (<sup>t</sup>Bu<sup>4</sup>PCOP)Ir(H)<sub>2</sub> (**2-5**), and (<sup>t</sup>Bu<sup>4</sup>PCOP)Ir(CO) (**2-6**). The ligand and subsequent iridium complexes were fully characterized and spectroscopic data is consistent with the notion that the hybrid complex should have intermediate properties with respect to its “parent” complexes. (<sup>t</sup>Bu<sup>4</sup>PCOP)Ir(H)<sub>2</sub> was found to be a suitable pre-catalyst for the transfer and acceptorless dehydrogenation of linear and cyclic alkanes, typically displaying catalytic activity between the extremes exhibited by the parent complexes.

## 2.1 Introduction

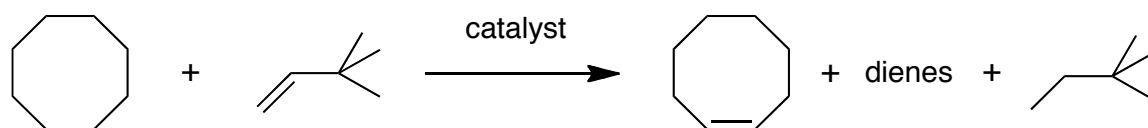
While hydrocarbons are among the most ubiquitous organic molecules found in nature, their use as feedstocks for new materials is hampered by the poor reactivity of their C-H and C-C bonds, particularly in the case of alkanes, thus making subsequent C-H functionalization (especially conversion to alkenes) a critical challenge in catalytic chemistry.<sup>2</sup> The conversion of alkanes to olefins plus H<sub>2</sub> is an entropically favorable process, but is significantly enthalpically disfavored ( $\Delta H_{\text{alkane dehydrogenation}}$  is generally on the order of 28-30 kcal/mol depending upon the alkane substrate).<sup>3</sup> As such, catalytic dehydrogenation often requires fairly high reaction temperatures to overcome the relatively poor thermodynamics of the process and drive loss of the removed H<sub>2</sub> from the active catalyst. The overall thermodynamics of dehydrogenation can be improved, however, by adding a stoichiometric amount of a sacrificial olefin to accept the H<sub>2</sub> removed from the alkane, such that the combination of the enthalpically unfavorable dehydrogenation and the enthalpically favored hydrogenation steps results in a net thermodynamically-favored (or at least thermoneutral) reaction.

Crabtree was the first to report an example of such stoichiometric transfer dehydrogenation, using an iridium dihydride species to effect the hydrogenation of *tert*-butylethylene and subsequent multiple dehydrogenation of cyclopentane to yield a cyclopentadienyl-ligated species (**eq. 2.1**).<sup>4</sup> Felkin performed the first catalytic transfer dehydrogenation reactions utilizing a (*i*Pr<sub>3</sub>P)<sub>2</sub>IrH<sub>5</sub> complex to effect transfer dehydrogenation between TBE and methylcyclohexane (**eq. 2.2a**), as well as reporting a poorly active, but highly regioselective, transfer dehydrogenation between TBE and *n*-hexane to yield the linear  $\alpha$ -olefin product with 90% kinetic selectivity for the terminal

position in the first hour of reaction (**eq. 2.2b**).<sup>5,6</sup> Crabtree then developed a transfer dehydrogenation benchmark reaction between cyclooctane and TBE (**Scheme 2.1**), against which a series of transfer dehydrogenation catalysts have since been tested.<sup>7</sup> Crabtree further developed an acceptorless dehydrogenation reaction, where thermolytic loss of H<sub>2</sub> in an open system drives the reaction forward.<sup>8</sup>



**Scheme 2.1.** The “benchmark” transfer dehydrogenation reaction between cyclooctane and TBE, as developed originally by Crabtree.

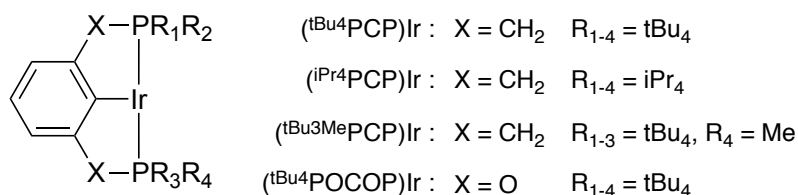


A variety of acceptors have been employed, with marked differences in the resulting productivity. On an industrial scale, the simplest and most-abundant olefin, ethylene, would be an ideal acceptor from an economic standpoint, but the relatively

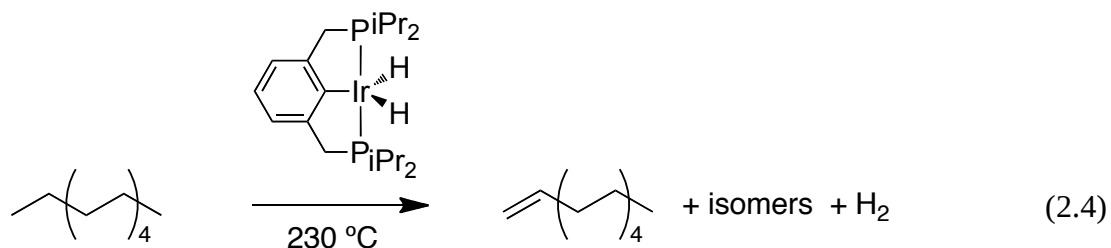
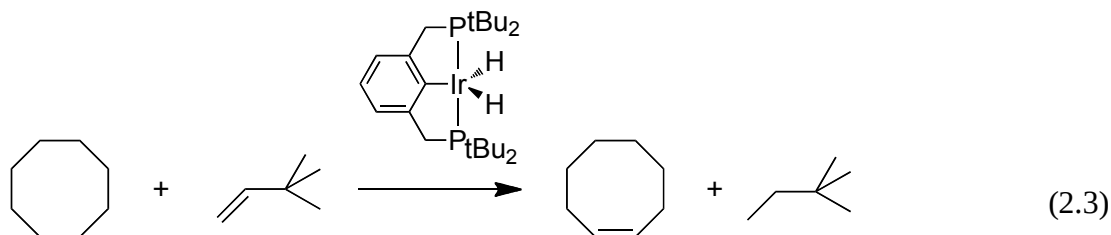
small size of the ethylene molecule typically leads to poor catalytic activity as the strong binding of ethylene in the resulting  $L_nM(\text{ethylene})$  intermediate inhibits further reaction.<sup>9</sup> As such, bulkier acceptors such as *tert*-butylethylene (TBE) or norbornene (NBE) are frequently employed so the resulting  $L_nM(\text{acceptor})$  complexes become less favorable relative to the oxidative addition of the substrate C-H bonds; reaction with a norbornene acceptor has the added benefit of relieving the ring strain imposed by the double bond, further favoring the overall thermodynamics.

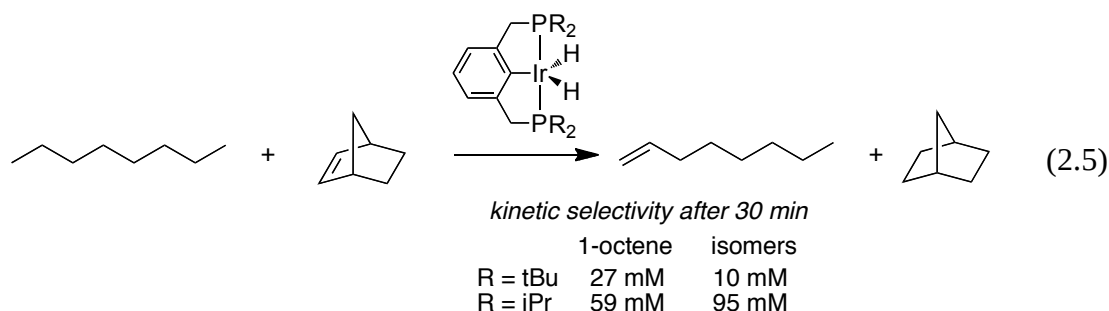
Assuming the thermodynamics of a given dehydrogenation process are favorable, actually converting *n*-alkanes to olefins remains a kinetic challenge. Consequently, recent decades have seen much development of transition-metal catalysts to readily activate C-H bonds and provide a lower energy pathway to olefins or other functionalized products. Transition-metal pincer complexes (**Figure 2.1**), particularly (pincer)Ir complexes, have been chief amongst the multitude of catalyst developed due to their high thermal stabilities, and have been employed to great effect by our group and others for the activation of a range of C-H bonds (e.g.  $sp$ -,  $sp^2$ -, and  $sp^3$ -hybridized C-H bonds), perhaps most impressively activating simple unfunctionalized *n*-alkanes.<sup>3,10,11</sup>

**Figure 2.1.** Examples of previously reported pincer-iridium complexes exhibiting high catalytic activity for alkane transfer dehydrogenation.



The archetypal pincer ligand  $t\text{Bu}^4\text{PCP}$  and its first transition metal complexes were first reported by Moulton and Shaw in the mid-1970s, but it was not until *ca.* twenty years later when Kaska and Jensen reported the first (pincer)M-catalyzed transfer dehydrogenation reactions, utilizing the  $(t\text{Bu}^4\text{PCP})\text{IrH}_2$  complex (**2-1**) in the benchmark reaction earlier established by Crabtree (**eq. 2.3**).<sup>12,13</sup> Goldman and Jensen subsequently extended this work, demonstrating the *acceptorless* dehydrogenation of *n*-undecane to give multiple undecene isomers (largely internal olefins) using a modified ligand where sterics about the metal center were reduced by replacing the *tert*-butyl groups on the phosphine with less bulky *iso*-propyl groups (*i.e.*  $i\text{Pr}^4\text{PCPIr}$ ) (**eq. 2.4**), followed shortly thereafter by the first reported *regioselective* formation of  $\alpha$ -olefins (*i.e.* 1-octene) by  $t\text{Bu}_4$ - and  $i\text{Pr}_4$ -PCPIr-catalyzed transfer dehydrogenation (**eq. 2.5**).<sup>14,15</sup>

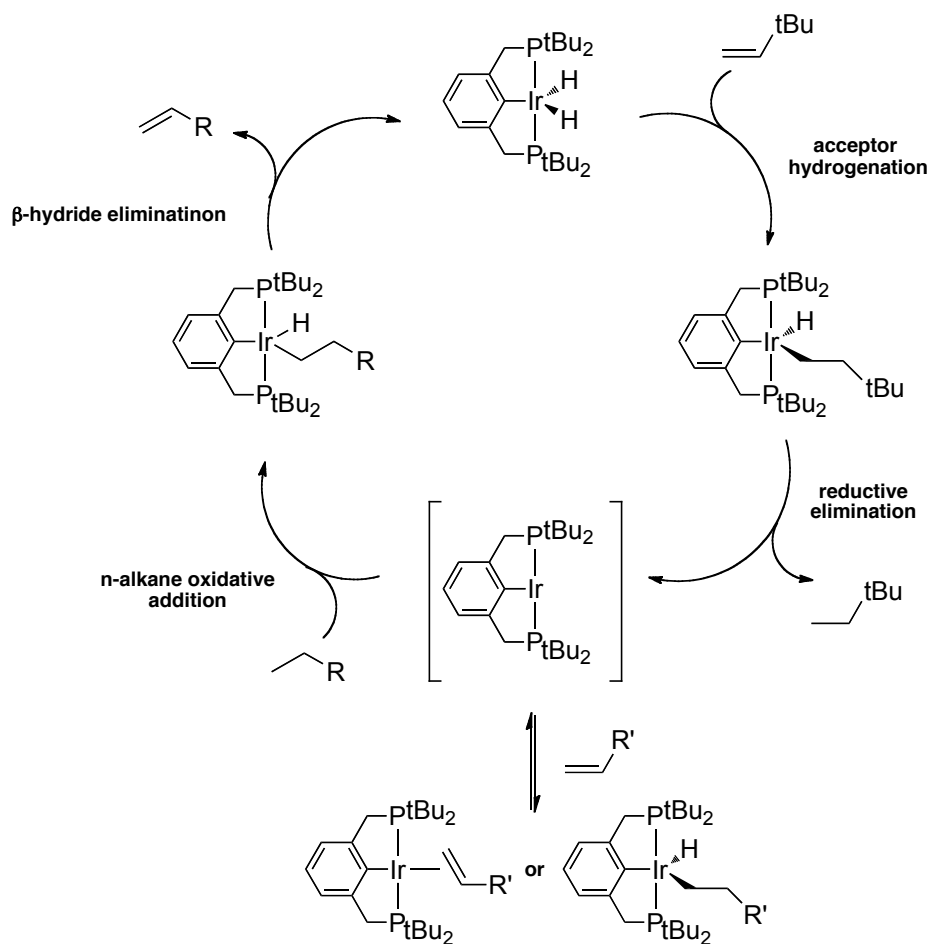




Goldman and Krogh-Jespersen extensively studied the mechanism of (PCP)Ir-catalyzed transfer dehydrogenation, both experimentally and computationally.<sup>16-20</sup> The established mechanism for (pincer)Ir-catalyzed transfer dehydrogenation (**scheme 2.2**) involves insertion of the acceptor into an Ir-H bond and subsequent reductive elimination of the hydrogenated acceptor to generate the key catalytically-active 14-electron intermediate. This intermediate is not isolable, but can react reversibly with excess acceptor or product olefin to give the corresponding (non-productive) adduct. Oxidative addition of a C-H bond to the free 14-electron species occurs to generate a (pincer)Ir(H)(alkyl) intermediate, which can subsequently undergo  $\beta$ -hydride elimination to generate the olefin product and regenerate the starting dihydride complex (**2-1**), starting the catalytic cycle anew. Mechanistic studies have revealed the resting state in (<sup>t</sup>Bu<sup>4</sup>PCP)Ir-catalyzed transfer dehydrogenation of *n*-alkanes to be the (<sup>t</sup>Bu<sup>4</sup>PCP)Ir(olefin) species (except in the presence of high concentration of acceptor, when the (<sup>t</sup>Bu<sup>4</sup>PCP)Ir(acceptor) adduct becomes the resting state), while the dihydride species, (<sup>t</sup>Bu<sup>4</sup>PCP)Ir(H)<sub>2</sub>, is observed to be the resting state for the transfer dehydrogenation of cycloalkanes (e.g. cyclooctane).<sup>20,21</sup>

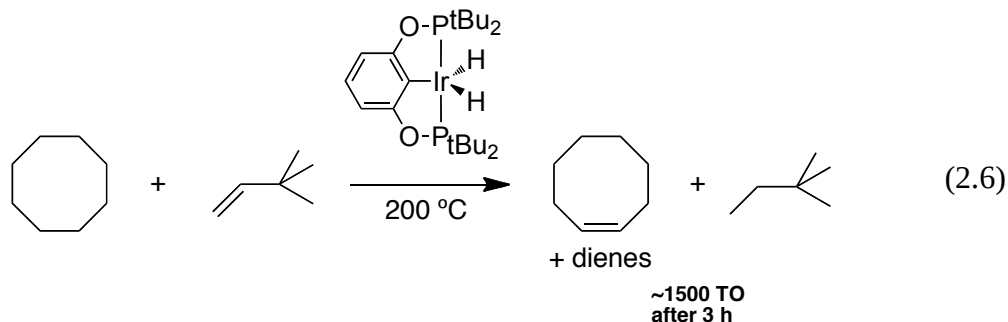


**Scheme 2.2.** Mechanism for the (<sup>t</sup>Bu<sup>4</sup>PCP)Ir-catalyzed transfer dehydrogenation of *n*-alkanes.



Transition-metal catalyzed reactions tend to be sensitive to sterics about the metal center, both in terms of reactivity and selectivity, evidenced with (pincer)Ir-catalyzed processes by the dramatic increase in activity observed for acceptorless and transfer dehydrogenation that occurs when going from sterically-hindered (<sup>t</sup>Bu<sup>4</sup>PCP)Ir to the more open (<sup>i</sup>Pr<sup>4</sup>PCP)Ir analogue. Altering the moieties on the phosphines is one manner in which the sterics around the metal center can be tuned, but even more remote alterations, such as substitution of the methylene -CH<sub>2</sub>- group in the backbone with an oxygen atom,

can have a large effect on reactivity and selectivity. Brookhart first reported the synthesis and catalytic studies of the analogous ( $^{t\text{Bu}}\text{POCOP}$ )Ir catalysts (**2-2**)<sup>22-24</sup>. Interestingly, unlike the ( $^{t\text{Bu}}\text{PCP}$ )Ir-system, Brookhart determined the resting state of the ( $^{t\text{Bu}}\text{POCOP}$ )Ir-system under cyclooctane transfer dehydrogenation conditions to be the olefin-bound species.<sup>24</sup> Brookhart's (POCOP)Ir catalyst was found to be roughly an order of magnitude more active for transfer dehydrogenation of cyclooctane and TBE than the analogous (PCP)Ir catalyst (**eq. 2.6**).<sup>22</sup> In comparison, (POCOP)Ir-catalyzed transfer dehydrogenation of linear *n*-alkanes (*i.e.* *n*-octane) was found to be far poorer than the (PCP)Ir-catalyzed process.<sup>25,26</sup>



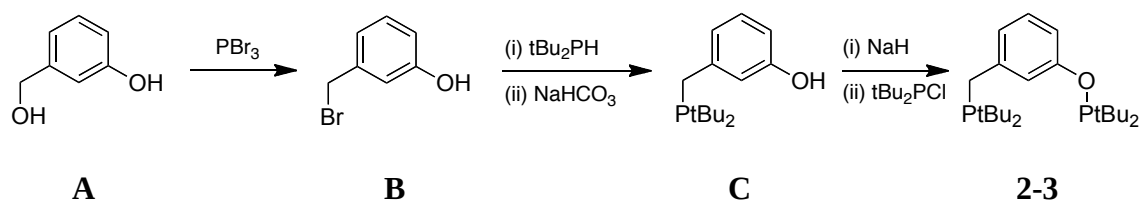
Intrigued by the inverse reactivity behaviors of the (PCP)Ir and (POCOP)Ir catalysts, we set out to create a catalyst that exhibited intermediate behavior, ideally serving as a steric and electronic middle-ground. In this chapter, we describe the synthesis and catalytic activity of “hybrid” unsymmetrical (PCOP)Ir complexes, bearing both phosphine and phosphinite coordinating groups.

## 2.2 Results and discussion

### 2.2.1 Synthesis and characterization of the hybrid ligand, $^{t\text{Bu}}\text{PCOP}$ (**2-3**)

The synthesis of the hybrid phosphine-phosphinite ligand was intended to allow for divergent synthesis of other ligands, specifically to permit variation of the substituents on the phosphine/phosphinite groups to allow for fine-tuning of the sterics in subsequent studies of catalytic activity. As such, as shown in **scheme 2.3**, the synthesis of the ligand began from the commercially available diol, 3-hydroxymethylphenol (**A**). Diol **A** was treated with  $\text{PBr}_3$  to selectively brominate the secondary alcohol, yielding 3-bromomethylphenol (**B**) in 90 % yield.<sup>27</sup> An acetone solution 3-bromomethylphenol was then treated with di-*tert*-butylphosphine to precipitate a white salt from solution, which was subsequently treated with aqueous sodium bicarbonate to afford 3-*tert*-butylphosphinomethylphenol (**C**).<sup>28</sup> Treating **C** with sodium hydride results in deprotonation of the phenol, which can then attack di-*tert*-butylchlorophosphine to afford the hybrid ligand, **2-3**, as a pale yellow viscous oil in 84 % isolated yield after workup and purification.<sup>23</sup> Unlike the previously reported PCP and POCOP ligands, this oil was not found to solidify upon standing, likely as a result of the increased disorder imparted by the asymmetry of the ligand.

**Scheme 2.3.** Synthetic route for the synthesis of the “hybrid” phosphine-phosphinite ligand (**2-3**).



**2-3** was characterized by  $^1\text{H}$ ,  $^{31}\text{P}$ , and  $^{13}\text{C}$  nmr spectroscopy. The  $^{31}\text{P}\{^1\text{H}\}$  NMR spectrum in benzene- $d_6$  displayed a peak at 152.7 ppm corresponding to the O-P(*t*Bu<sub>2</sub>)

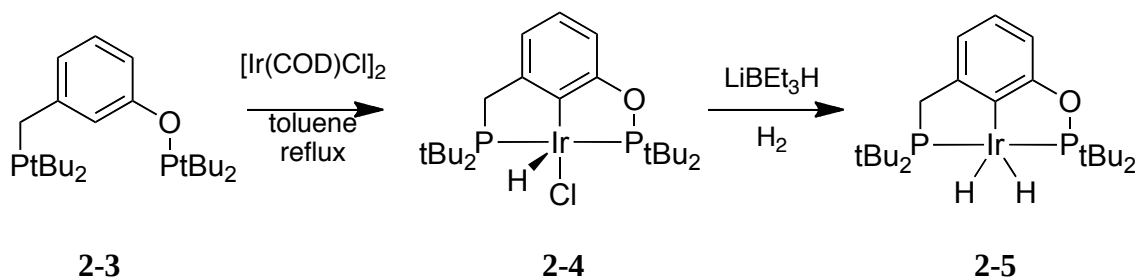
moiety (compare to  $^{t\text{Bu}}\text{POCOP-H}$ : 153.1 ppm) and a peak at 34.1 ppm corresponding to the  $\text{CH}_2\text{-P}(t\text{Bu}_2)$  moiety (compare to  $^{t\text{Bu}}\text{PCP-H}$ : 33.0 ppm). The  $^1\text{H}$  nmr spectrum clearly displayed a doublet of doublets for the *tert*-butyl groups on *each* phosphorus atom, consistent with splitting by the phosphorus atom. A doublet at 2.8 ppm ( $^2J_{\text{PH}} = 2.25$  Hz) is indicative of the diastereotopic methylene ( $-\text{CH}_2-$ ) unit in the pincer arm. The proton located on the *ipso*-carbon of the pincer ligand (that is, the carbon *ortho* to *both* arms of the pincer ligand) presents slightly higher downfield ( $\delta$  7.62 ppm) than the other aromatic protons ( $\delta$  7.10 – 7.20 ppm).

### 2.2.2 Synthesis and characterization of ( $^{t\text{Bu}}\text{PCOP}$ )Ir(H)(Cl) (**2-4**)

Following the previously employed strategies of metallating pincer ligands with iridium, the hybrid ligand was treated with 0.5 equivalents of  $[\text{Ir}(\text{COD})\text{Cl}]_2$  and subjected to reflux in toluene for three days under a hydrogen atmosphere (**scheme 2.4**). The resulting relatively air-stable ( $^{t\text{Bu}}\text{PCCOP}$ )Ir(H)(Cl) complex (**2-4**) can be recrystallized from *n*-pentane to yield red microcrystals in 68 % isolated yield; this complex is very poorly soluble in *n*-pentane, and as such, higher isolated yield can likely be obtained by dissolution in larger volumes of solvent or Soxhlet extraction. The  $^{31}\text{P}$  nmr spectrum of **2-4** displays a doublet of doublets at 168.6 ppm ( $^2J_{\text{PP}} = 345.0$  Hz,  $^2J_{\text{PH}} = 12.3$  Hz) attributable to the O-P( $t\text{Bu}_2$ ) group (*cf.* ( $^{t\text{Bu}}\text{POCOP}$ )IrHCl: 175.8 ppm) and at 70.6 ppm ( $^2J_{\text{PP}} = 345.0$  Hz,  $^2J_{\text{PH}} = 11.0$  Hz) attributable to the  $\text{CH}_2\text{-P}(t\text{Bu}_2)$  group (*cf.* 67.3 ppm,  $^2J_{\text{PH}} = 12.4$  Hz for ( $^{t\text{Bu}}\text{PCP}$ )IrHCl); the large value of  $^2J_{\text{PP}}$  (345.0 Hz) is characteristic of mutually *trans* coordinated inequivalent  $^{31}\text{P}$  nuclei. In the  $^1\text{H}$  nmr spectrum, loss of the  $\text{C}_{\text{ipso}}\text{-H}$  proton ( $\delta$  7.62 ppm) in the ligand is observed along with formation of a hydride signal at -41.4 ppm (dd,  $^2J_{\text{PH}} = 13.3$  Hz,  $^2J_{\text{PH}} = 12.3$  Hz, 1H); this significantly upfield

shift is essentially identical to the corresponding shifts of the parent hydrido chloride species, and is indicative of an apical hydride *trans* to a vacant coordination site in a five-coordinate square pyramidal iridium-pincer complex.<sup>22,29</sup>

**Scheme 2.4.** Synthesis of hybrid phosphine-phosphinite pincer-iridium complexes: (<sup>t</sup>Bu<sup>4</sup>PCOP)Ir(H)(Cl) (**2-4**) and (<sup>t</sup>Bu<sup>4</sup>PCOP)Ir(H)<sub>2</sub> (**2-5**).



Owing to its poor solubility, **2-4** can be conveniently recrystallized in *n*-pentane to yield crystals suitable for x-ray diffraction. **Figure 2.2** shows the thermal ellipsoid plot of the crystallographically-determined species and **table 2.1** highlights selected bond lengths and angles; full crystallographic details are available in the appendix to this chapter. As expected based upon the <sup>1</sup>H NMR spectrum, the coordination geometry is approximately square pyramidal with the hydride located in the apical position. The Ir-P(O) bond length is 2.269 Å, slightly shorter than the Ir-P bond length 2.295(±2) in (<sup>t</sup>Bu<sup>4</sup>POCOP)IrHCl, while the Ir-P(CH<sub>2</sub>) bond length is 2.319 Å, slightly longer than that reported for (<sup>t</sup>Bu<sup>4</sup>PCP)IrHCl (2.305(±1) Å). These values appear generally consistent with a greater *trans* influence exerted by the phosphinite versus the phosphine groups.

The P(1)-Ir-P(2) bond angle of **2-4** (163.6°) is slightly less than that of (<sup>t</sup>Bu<sup>4</sup>PCP)IrHCl (164.3°) and greater than that of (<sup>t</sup>Bu<sup>4</sup>POCOP)IrHCl (160.1°). The C-Ir-

P(CH<sub>2</sub>) bond angles (82.5°) are similar to those reported for (<sup>t</sup>Bu<sup>4</sup>PCP)IrHCl (82.0°, 82.3°) while the C-Ir-P(O) angle (81.3°) is slightly greater than the corresponding angles in (<sup>t</sup>Bu<sup>4</sup>POCOP)IrHCl (80.0°, 80.1°).

**Figure 2.2.** Thermal ellipsoid plot of (<sup>t</sup>Bu<sup>4</sup>PCOP)IrHCl (**2-4**). Hydrogen atoms other than the hydride ligand omitted for clarity.

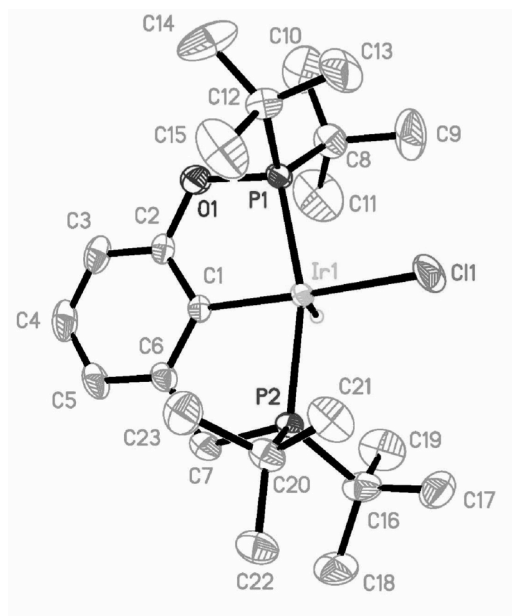


**Table 2.1.** Selected Bond Distances (Å) and Bond Angles (°) for (<sup>t</sup>Bu<sup>4</sup>PCOP)IrHCl (**2-4**).

Bond distances (Å)		Bond angles (°)	
Ir(1)-C(1)	2.016(3)	C(1)-Ir(1)-P(1)	81.27(10)
Ir(1)-P(1)	2.2685(9)	C(1)-Ir(1)-P(2)	82.47(10)
Ir(1)-P(2)	2.3194(8)	P(1)-Ir(1)-P(2)	163.55(3)
Ir(1)-Cl(1)	2.4012(10)	C(1)-Ir(1)-Cl(1)	177.71(9)
P(1)-O(1)	1.662(3)	P(1)-Ir(1)-Cl(1)	97.03(3)
P(1)-C(8)	1.848(4)	P(2)-Ir(1)-Cl(1)	99.16(3)
P(1)-C(12)	1.852(4)	O(1)-P(1)-C(8)	101.01(18)
P(2)-C(7)	1.814(4)	O(1)-P(1)-Ir(1)	104.63(10)
P(2)-C(16)	1.868(4)	C(7)-P(2)-Ir(1)	102.67(13)
P(2)-C(20)	1.865(4)	C(2)-O(1)-P(1)	115.2(2)
		C(6)-C(7)-P(2)	111.0(3)

### 2.2.3 Synthesis and characterization of the hybrid catalyst, (<sup>t</sup>Bu<sup>4</sup>PCCOP)Ir(H)<sub>2</sub> (**2-5**)

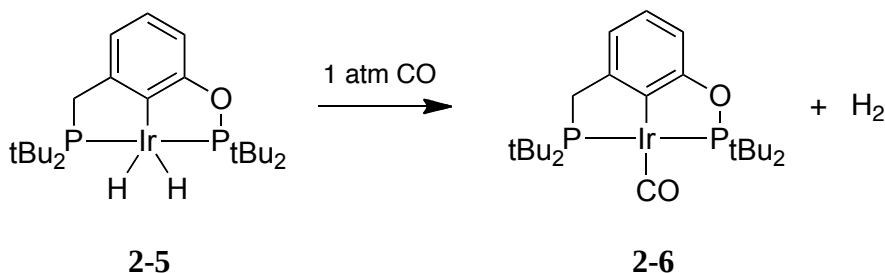
As is the case for both the PCP- and POCOP-ligated parent species, the hybrid hydrido chloride complex is readily reduced under a hydrogen atmosphere by lithium triethylborohydride to the corresponding hydride species (**scheme 2.4**).<sup>30</sup> In the case of (<sup>t</sup>Bu<sup>4</sup>PCP)Ir, the tetrahydride complex is typically the resulting major species, while (<sup>t</sup>Bu<sup>4</sup>POCOP)Ir usually yields only the dihydride complex; for the hybrid species, the dihydride (**2-5**) results as the major species (>99 %), while the tetrahydride is present as a minor species in <1 % yield, after removing volatiles under vacuum. **2-5** displays <sup>31</sup>P{<sup>1</sup>H} NMR signals consistent with those of its parent analogues, exhibiting a doublet at 200.3 ppm (<sup>2</sup>J<sub>PP</sub> = 330 Hz) attributable to the O-P(tBu)<sub>2</sub> group (compare (<sup>t</sup>Bu<sup>4</sup>PCOP)IrH<sub>2</sub>: 204.9 ppm) and a doublet at 87.3 ppm (<sup>2</sup>J<sub>PP</sub> = 330 Hz) due to the CH<sub>2</sub>-P(tBu)<sub>2</sub> group (compare (<sup>t</sup>Bu<sup>4</sup>PCP)IrH<sub>2</sub>: 86.1 ppm). The hydride signal in the <sup>1</sup>H NMR spectrum appears as a triplet at -18.12 ppm with <sup>2</sup>J<sub>PH</sub> = 8.6 Hz; comparison with the corresponding values for the symmetrical analogues supports the assumption that **2-5** should have properties intermediate between (<sup>t</sup>Bu<sup>4</sup>POCOP)IrH<sub>2</sub> (-17.4 ppm, <sup>2</sup>J<sub>PH</sub> = 8.2 Hz) and (<sup>t</sup>Bu<sup>4</sup>PCP)IrH<sub>2</sub> (-19.2 ppm, <sup>2</sup>J<sub>PH</sub> = 8.8 Hz).

### 2.2.4 Synthesis and characterization of (<sup>t</sup>Bu<sup>4</sup>PCOP)Ir(CO) (**2-6**)

The four-coordinate carbonyl complex (<sup>t</sup>Bu<sup>4</sup>PCOP)Ir(CO) (**2-6**) can be readily prepared by introducing **2-5** to an atmosphere of carbon monoxide (**scheme 2.5**), resulting in loss of H<sub>2</sub> and isolation of a bright yellow solid in quantitative yield; a hydrogen acceptor molecule is not needed, presumably as addition of CO to the dihydride species generates a six-coordinate *cis*-dihydride carbonyl species which undergoes rapid H<sub>2</sub> reductive elimination. (<sup>t</sup>Bu<sup>4</sup>PCOP)Ir(CO) (**2-6**) presents as a pair of doublets in the <sup>31</sup>P

nmr at 198.7 ( $J_{\text{PP}} = 288.3$  Hz, O-P( $\text{tBu}_2$ )) and 89.5 ( $J_{\text{PP}} = 288.3$  Hz,  $\text{CH}_2\text{-P}(\text{tBu}_2)$ ) ppm. Carbonyl complex **2-6** exhibits a carbonyl stretching frequency ( $\nu_{\text{CO}}$ ) of  $1938\text{ cm}^{-1}$  via infrared spectroscopy; interestingly, this is exactly the average of the reported  $\nu_{\text{CO}}$  values of the parent species  $(^{\text{tBu}_4}\text{PCP})\text{Ir}(\text{CO})$  ( $\nu_{\text{CO}}=1927\text{ cm}^{-1}$ )<sup>17</sup> and  $(^{\text{tBu}_4}\text{POCOP})\text{Ir}(\text{CO})$  ( $\nu_{\text{CO}}=1949\text{ cm}^{-1}$ )<sup>23</sup>. The intermediacy of the carbonyl stretching frequency of the hybrid complex further supports the notion that PCOP complexes should generally have properties intermediate between the analogous PCP- and POCOP-ligated complexes.

**Scheme 2.5.** Synthesis of  $(^{\text{tBu}_4}\text{PCOP})\text{Ir}(\text{CO})$  (**2-6**).



### 2.2.5 Catalytic dehydrogenation activity

As described earlier, the transfer dehydrogenation of alkanes with a hydrogen acceptor has been widely exploited by our group and others to effectively catalyze the transformation of alkanes to olefins. Such transfer dehydrogenations rely on a stoichiometric amount of a sacrificial olefin to drive the reaction forward. To avoid the expense involved in employing a hydrogen acceptor, so called “acceptorless” transformations have been developed, relying on higher temperatures to drive off  $\text{H}_2$  under a continuous flow of argon. In the remainder of this chapter, we will focus on



pincer-iridium catalyzed dehydrogenation of linear and cyclic alkanes via transfer and acceptorless mechanisms. The activity and selectivity of the novel hybrid complex **2-5** will be compared to those of its parent catalysts, (<sup>t</sup>Bu<sup>4</sup>PCP)IrH<sub>4</sub> (**2-1**) and (<sup>t</sup>Bu<sup>4</sup>POCOP)IrH<sub>2</sub> (**2-2**), in each case.

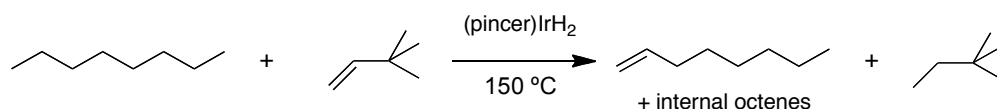
To aid assessment of catalytic activity for both this study and future studies, we have developed “standard” conditions for transfer and acceptorless dehydrogenation. For transfer dehydrogenation, our standard reaction temperature is 150 °C for linear alkanes and 200 °C for cycloalkanes (as the formation of internal olefins is expected to be less favorable kinetically), while acceptorless dehydrogenation necessarily utilizes a higher temperature (230 °C) to thermally drive the loss of H<sub>2</sub> from the (pincer)Ir(H)<sub>2</sub> intermediate. Transfer dehydrogenation catalysis is carried out in a closed system consisting of screw-top Teflon stopcock enclosed 5 mL Pyrex vessels, whereas acceptorless dehydrogenation is carried out in an open-system consisting of custom-built glass vessels featuring a water-cooled condensing column and gas inlet and outlet ports to allow for a continuous flow of argon through the system while retaining the alkane substrate and olefin products.

#### 2.2.5.1 Transfer dehydrogenation of *n*-octane

The transfer dehydrogenation of *n*-octane with *tert*-butylethylene (TBE) (**scheme 2.6**) was carried out using complexes **2-1**, **2-2**, and **2-5** at our standard transfer dehydrogenation temperature of 150 °C using two different limits of TBE concentrations, as the concentration of TBE has been previously observed to affect the rate and mechanism of the reaction: Jensen found that high concentrations of TBE inhibit transfer

dehydrogenation (though subsequent observations suggest that this is likely due to an impurity in TBE, not TBE itself)<sup>13</sup>, while our group has found that under higher concentrations of TBE, the resting state of the active (<sup>t</sup>Bu<sup>4</sup>PCP)Ir catalyst changes from a dihydride species to a TBE-bound complex.<sup>20</sup> **Table 2.2** presents the results of the transfer dehydrogenation of 200 mM TBE with *n*-octane (*ca.* 6.15 M). (<sup>t</sup>Bu<sup>4</sup>PCP)Ir was previously well-known as an efficient catalyst for *n*-octane transfer dehydrogenation, while (<sup>t</sup>Bu<sup>4</sup>POCOP)Ir was known to be significantly less effective. Interestingly, (<sup>t</sup>Bu<sup>4</sup>PCOP)Ir exhibits behavior disproportionately similar to the (<sup>t</sup>Bu<sup>4</sup>POCOP)Ir parent, despite the putative intermediacy that its sterics and electronics suggest. The initial turnover frequency (TOF) of the hybrid catalyst is 1.3 min<sup>-1</sup>, much closer to the initial TOF of (<sup>t</sup>Bu<sup>4</sup>POCOP)Ir (0.9 min<sup>-1</sup>) than to the initial TOF of (<sup>t</sup>Bu<sup>4</sup>PCP)Ir (8.1 min<sup>-1</sup>). After reacting for 1 hour, the total octene products produced by both (<sup>t</sup>Bu<sup>4</sup>PCOP)Ir and (<sup>t</sup>Bu<sup>4</sup>POCOP)Ir are roughly identical (42 and 31 mM, respectively), while (<sup>t</sup>Bu<sup>4</sup>PCP)Ir produces more than three times as much octene products in the same period (131 mM octene products). The activity of (<sup>t</sup>Bu<sup>4</sup>PCOP)Ir peaks after one hour, while (<sup>t</sup>Bu<sup>4</sup>PCOP)Ir and (<sup>t</sup>Bu<sup>4</sup>POCOP)Ir yield slightly more products following an additional hour of reaction: the turnover numbers after two hours for (<sup>t</sup>Bu<sup>4</sup>PCP)Ir is roughly twice than of (<sup>t</sup>Bu<sup>4</sup>PCOP)Ir and slightly more than 2.5 times that of (<sup>t</sup>Bu<sup>4</sup>POCOP)Ir. The selectivity of the hybrid catalyst for terminal olefin formation is essentially as poor as that exhibited by (<sup>t</sup>Bu<sup>4</sup>POCOP)Ir; after the first 10 minutes, practically no 1-octene has formed in either case, while roughly 40 % of the new products formed by (<sup>t</sup>Bu<sup>4</sup>PCP)Ir are terminal olefins.

**Scheme 2.6.** Transfer dehydrogenation of *n*-octane and TBE catalyzed by (pincer)Ir complexes (**2-1**, **2-2**, and **2-5**).

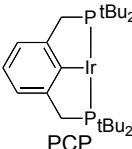
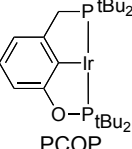
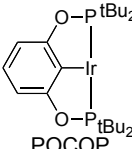


**Table 2.2.** Octenes formed from (pincer)Ir-catalyzed (1 mM) transfer dehydrogenation of *n*-octane and TBE (200 mM) at 150 °C (low [TBE] extreme).

Catalyst	Time (min)	Product Concentrations (mM)				
		1-octene	trans-2-octene	cis-2-octene	others	total octenes
 <b>2-1</b>	10	23	35	17	6	81
	20	19	51	27	13	110
	30	18	58	29	16	121
	60	17	66	33	15	131
	120	12	67	31	22	132
 <b>2-5</b>	10	1	6	1	5	13
	20	2	7	2	6	17
	30	2	10	3	9	24
	60	2	17	6	17	42
	120	2	26	10	29	67
 <b>2-2</b>	10	2	2	2	3	9
	20	2	5	3	3	13
	30	3	7	5	4	19
	60	2	13	7	9	31
	120	2	20	9	18	49
conditions: 1 mM catalyst, 200 mM TBE, oil bath temperature: 150 °C, <i>n</i> -octane b.p.: 125 °C						

At higher TBE concentration (*ca.* 1 M) (**table 2.3**), virtually no difference in catalytic activity is observed for any of these species, in stark contrast to previous observations on related systems;<sup>13</sup> this is potentially explained by the use of a higher purity redistilled TBE reagent (>98 % versus 96 %), where the presence of an inhibitive impurity is likely to have been significantly mitigated.

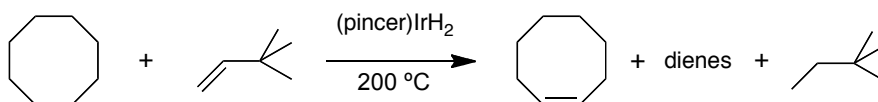
**Table 2.3.** Octenes formed from (pincer)Ir-catalyzed (1 mM) transfer dehydrogenation of *n*-octane and TBE (1 M) at 150 °C (high [TBE] extreme).

Catalyst	Time (min)	Product Concentrations (mM)				
		1-octene	trans-2-octene	cis-2-octene	others	total octenes
 PCP <b>2-1</b>	10	38	30	21	7	96
	30	37	46	25	8	116
	60	34	59	30	8	131
	180	28	65	31	15	139
	360	17	76	34	40	167
 PCOP <b>2-5</b>	10	4	6	1	4	15
	30	5	16	2	9	32
	60	5	23	3	16	47
	180	4	37	5	28	74
	360	2	30	6	28	66
 POCOP <b>2-2</b>	10	3	2	2	1	8
	30	3	6	3	3	15
	60	3	10	5	5	23
	180	4	24	10	14	52
	360	3	27	12	17	59
conditions: 1 mM catalyst, 1000 mM TBE, oil bath temperature: 150 °C, <i>n</i> -octane b.p.: 125 °C						

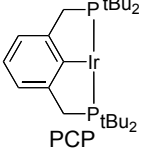
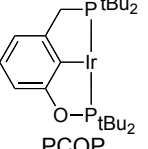
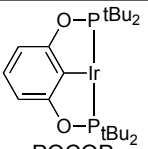
#### 2.2.5.2 Transfer dehydrogenation of cyclooctane

Using 1.2 mM of (pincer)Ir catalyst, the transfer dehydrogenation of cyclooctane and TBE to yield cyclooctene (and TBA) was next examined (**scheme 2.7**). Cyclooctane/cyclooctene is a much more sterically-demanding substrate; unlike the dehydrogenation of *n*-octane, dehydrogenation of cyclooctane can only generate more

**Scheme 2.7.** Transfer dehydrogenation of cyclooctane and TBE catalyzed by (pincer)Ir complexes (**2-1**, **2-2**, and **2-5**).



**Table 2.4.** Products formed from (pincer)Ir-catalyzed (1.2 mM) transfer dehydrogenation of cyclooctane (3.72 M) and TBE (3.72 M) at 200 °C.

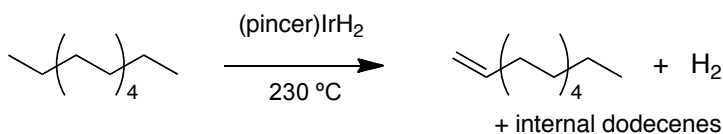
Catalyst	Time (min)	Product Concentrations (mM)			
		cyclooctene	cyclooctadiene	others	total products
 PCP <b>2-1</b>	10	155	0	0	155
	30	164	0	0	164
	60	225	0	0	225
	180	228	0	0	228
	1440	236	0	0	236
 PCOP <b>2-5</b>	10	453	18	1	472
	30	501	20	1	522
	60	542	23	2	567
	180	563	28	2	593
	1440	592	30	2	624
 POCOP <b>2-2</b>	10	947	93	1	1041
	30	1108	146	2	1256
	60	1173	235	2	1410
	180	1256	316	3	1575
	1440	1222	341	3	1566
conditions: 1.2 mM catalyst, 3.72 M TBE, oil bath temperature: 200 °C, COA b.p.: 149 °C					

hindered internal olefins. For this reason, (<sup>t</sup>Bu<sup>4</sup>POCOP)Ir has been observed to be the most effective (pincer)Ir catalyst, presumably as the less hindered/more open (POCOP)Ir complex can more readily yield the bulkier internal olefin product. As **table 2.4** shows, (<sup>t</sup>Bu<sup>4</sup>PCOP)Ir does indeed exhibit intermediate activity, far exceeding (<sup>t</sup>Bu<sup>4</sup>PCP)Ir, while falling short of the unsurpassed activity of (<sup>t</sup>Bu<sup>4</sup>POCOP)Ir. The initial TOF for (<sup>t</sup>Bu<sup>4</sup>PCOP)Ir is roughly 39 min<sup>-1</sup>, a three times rate enhancement compared to (<sup>t</sup>Bu<sup>4</sup>PCP)Ir (12.9 min<sup>-1</sup>); the initial TOF of (<sup>t</sup>Bu<sup>4</sup>POCOP)Ir is about 87 min<sup>-1</sup>, roughly double that of the hybrid catalyst. After 24 hours, the TON for the hybrid catalyst is roughly 2.5 times as much as for the PCP-parent (520 TO versus 197 TO), while (<sup>t</sup>Bu<sup>4</sup>POCOP)Ir exhibits a TON that is 2.5 times that of the hybrid (1305 TO versus 520 TO).

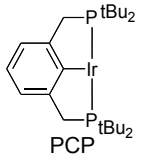
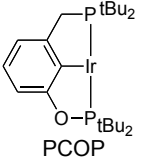
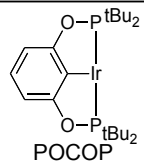
### 2.2.5.3 Acceptorless dehydrogenation of *n*-dodecane

Acceptorless dehydrogenation is envisioned to be the more economical and commercially-viable means of catalytic alkane dehydrogenation, as it obviates the need for (and cost associated with using) a stoichiometric amount of a sacrificial olefin. However, with no means of easily removing H<sub>2</sub>, the thermodynamics of catalytic dehydrogenation become much less favorable. To overcome the poor thermodynamics, higher reaction temperatures are required, which make quantitative analysis of volatile substrates (such as *n*-octane) more difficult (loss of substrate becomes a major concern). As such, we looked at acceptorless dehydrogenation at 230 °C of high-boiling *n*-dodecane (216 °C) (**scheme 2.8**). As shown by **table 2.5**, acceptorless dehydrogenation is a much slower and less productive means of yielding olefin products, regardless of the (pincer)Ir catalyst employed. The hybrid complex exhibits a comparably poor initial TOF (4 hr<sup>-1</sup>) relative to the parent (<sup>t</sup>Bu<sup>4</sup>PCP)Ir complex (35 hr<sup>-1</sup>), making it only marginally superior to (<sup>t</sup>Bu<sup>4</sup>POCOP)Ir (2 hr<sup>-1</sup>). The catalytic activity of all complexes is essentially over after 24 hours, likely as a result of the relatively harsh experimental conditions, with TON after this period staying constant with time. The TON of the hybrid catalyst after 24 hours (28) is roughly two-thirds that of the (<sup>t</sup>Bu<sup>4</sup>PCP)Ir catalyst (42), and roughly three times that of the (<sup>t</sup>Bu<sup>4</sup>POCOP)Ir species (9).

**Scheme 2.8.** Acceptorless dehydrogenation of *n*-dodecane catalyzed by (pincer)Ir complexes (**2-1**, **2-2**, and **2-5**).



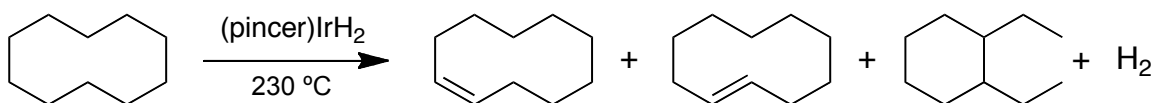
**Table 2.5:** Dodecenes products formed from (pincer)Ir (1 mM) catalyzed acceptorless dehydrogenation of n-dodecane at 230 °C.

Catalyst	Time (h)	Total Dodecenes (mM)
 PCP <b>2-1</b>	1	35
	2	39
	5	40
	24	42
	48	40
 PCOP <b>2-5</b>	1	4
	2	5
	5	8
	24	28
	48	26
 PCOP <b>2-2</b>	1	2
	2	3
	5	5
	24	9
	48	10
conditions: 1 mM catalyst, oil bath: 230 °C, dodecane b.p.: 216 °C		

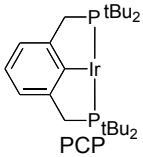
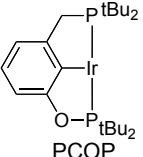
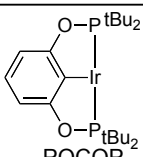
#### 2.2.5.4 Acceptorless dehydrogenation of cyclodecane

Finally, we studied acceptorless dehydrogenation of cyclodecane (**scheme 2.9**). **Table 2.6** shows the results of the dehydrogenation with 1 mM of (pincer)IrH<sub>n</sub> complex at 230 °C (boiling point of cyclodecane is 201 °C). The cyclodecane ring is large enough that the relative ring strain experienced by *cis*- and *trans*-cyclodecene is not as different

**Scheme 2.9.** Acceptorless dehydrogenation of cyclodecane catalyzed by (pincer)Ir complexes (**2-1**, **2-2**, and **2-5**).



**Table 2.6.** Products formed from (pincer)Ir-catalyzed (1 mM) acceptorless dehydrogenation of cyclodecane at 230 °C.

Catalyst	Time (h)	Product Concentrations (mM)			total products
		cis-cyclodecene	trans-cyclodecene	diethylcyclohexane	
 <b>2-1</b>	1	52	47	3	102
	3	156	58	4	218
	24	186	74	7	267
	72	222	72	11	305
	120	241	65	13	319
 <b>2-5</b>	1	93	31	4	128
	3	244	75	14	333
	24	458	101	86	645
	72	1576	441	841	2858
	120	1623	417	856	2896
 <b>2-2</b>	1	272	62	12	346
	3	491	126	49	666
	24	1188	312	439	1939
	72	1540	433	919	2892
	120	1523	448	1377	3348
conditions: 1 mM catalyst, oil bath temperature: 230 °C, cyclodecane b.p.: 201 °C					

as in the case of cyclooctene stereoisomers<sup>31</sup>, and as such, both isomers can be formed in significant yields, though formation of the *cis*-isomer still continues to be more thermodynamically-favored. In addition to multiple stereoisomers, diethylcyclohexane can also be formed as a result of multiple (pincer)Ir-catalyzed dehydrogenations and subsequent Cope rearrangement and re-hydrogenation.<sup>32</sup> The results of cyclodecane acceptorless dehydrogenation are consistent with the general trends observed for cyclooctane/TBE transfer dehydrogenation: the more hindered the metal center, the poorer its catalytic activity. As such, the less sterically-hindered (<sup>t</sup>Bu<sup>4</sup>PCOP)Ir and (<sup>t</sup>Bu<sup>4</sup>POCOP)Ir complexes are far better at dehydrogenation than (<sup>t</sup>Bu<sup>4</sup>PCP)Ir; for example, after reacting for 120 hours, the total amount of new products formed is on the order of 3 M for both the (<sup>t</sup>Bu<sup>4</sup>PCOP)Ir and (<sup>t</sup>Bu<sup>4</sup>POCOP)Ir catalysts (2900 and 3350 turnovers,



respectively), while it is only *ca.* 300 mM for (<sup>t</sup>Bu<sup>4</sup>PCP)Ir (319 turnovers). Interestingly though (<sup>t</sup>Bu<sup>4</sup>PCP)Ir and (<sup>t</sup>Bu<sup>4</sup>PCOP)Ir catalysts exhibit similar initial TOF (100-130 hr<sup>-1</sup>), being roughly a third of that of the (<sup>t</sup>Bu<sup>4</sup>PCOP)Ir catalyst, the (<sup>t</sup>Bu<sup>4</sup>PCOP)Ir species appears to approximately “catch up” to the POCOP species. We must be careful, however, drawing conclusions regarding reaction kinetics of the (pincer)Ir catalysts in the particular case of acceptorless dehydrogenation, since the reaction may take place under both homogeneous and heterogeneous conditions with unknown *in situ* generated active species, potentially giving rise to non-uniform kinetics and induction periods.

### 2.3 Summary

The hybrid ligand <sup>t</sup>Bu<sup>4</sup>PCOP (**2-3**) was successfully prepared and metallated with iridium to generate novel (<sup>t</sup>Bu<sup>4</sup>PCOP)Ir complexes **2-4**, **2-5**, and **2-6**. Spectroscopic (NMR and IR) and crystallographic data indicated that these hybrid complexes should have intermediate properties compared to the parent PCP- and POCOP-ligated species. **2-5** was found to be a useful catalyst for transfer and acceptorless dehydrogenation of linear and cyclic alkanes. In general, the hybrid catalyst **2-5** exhibited activity intermediate to that of the parent catalysts, typically exhibiting initial TOFs between those observed for (<sup>t</sup>Bu<sup>4</sup>PCP)Ir and (<sup>t</sup>Bu<sup>4</sup>POCOP)Ir. For *n*-alkane transfer and acceptorless dehydrogenation, the hybrid complex was observed to fair only slightly better than (<sup>t</sup>Bu<sup>4</sup>POCOP)Ir, but fell quite a bit short of the activity of (<sup>t</sup>Bu<sup>4</sup>PCP)Ir. A similar behavior was observed for cycloalkane dehydrogenation, though (<sup>t</sup>Bu<sup>4</sup>PCOP)Ir generally exhibited significantly improved activity in comparison to (<sup>t</sup>Bu<sup>4</sup>PCP)Ir. Although such behavior may not be ideal for a simple dehydrogenation process, the ability of the hybrid complex to

effectively catalyze multiple steps involving both primary and secondary olefins in a more complex process may be of higher utility, particularly in the context of alkane metathesis.

## 2.4 Acknowledgments

We would like to thank Dr. Thomas Emge for x-ray crystallographic analysis of complex 2-4.

## 2.5 Experimental

**General considerations.** All manipulations were conducted under an argon atmosphere either in a glove box or using standard Schlenk techniques. All anhydrous solvents were purchased from Aldrich, flushed with argon, and stored in an argon atmosphere in glove box. Mesitylene, *n*-hexane (anhydrous, 99%+), *tert*-butylethylene (TBE; 3,3-dimethyl-1-butene, >98%) were purchased from Aldrich and were distilled over Na/benzophenone and stored in a glove box.  $(^t\text{Bu}^4\text{PCP})\text{IrH}_2$ ,<sup>13</sup>  $(^t\text{Bu}^4\text{POCOP})\text{IrH}_2$ ,<sup>23</sup> and 3-(bromomethyl)phenol<sup>27</sup> were prepared as described previously. Di-*tert*-butylphosphine and di-*tert*-butylchlorophosphine were used as purchased from Strem Chemicals, Inc. All other reagents were obtained from commercial sources and used as received. All glassware was dried in an oven at least 24 hours prior to use. NMR spectra were recorded on 400- or 500-MHz Varian VNMRs spectrometers.  $^1\text{H}$  NMR spectra are referenced to residual *protio* signal of the deuterated solvent.  $^{31}\text{P}\{^1\text{H}\}$  NMR chemical shifts are referenced to an external standard consisting of  $\text{PMe}_3$  ( $\delta$  -62.4 ppm) in mesitylene- $d_{12}$  solvent inside a flame-sealed capillary tube. GC analyses were carried out

with a Thermo Focus GC with a flame ionization detector (FID) on the Agilent HP-1 column (100% dimethylpolysiloxane, 30 m length  $\times$  0.32 mm ID  $\times$  0.25  $\mu$ m film thickness) or a Varian 430 gas chromatograph with a Supelco fused silica capillary column, Petrocol<sup>TM</sup>, HD (100 m  $\times$  0.25 mm  $\times$  0.5 $\mu$ m). Elemental analyses were performed by Roberston Microlit Laboratories, Ledgewood, New Jersey.

**Synthesis of 3-(di-*tert*-butylphosphinomethyl)phenol (C).** A mixture of 3-(bromomethyl)phenol (4.003 g, 21.40 mmol) and HP<sup>*t*</sup>Bu<sub>2</sub> (3.161 g, 21.62 mmol) in degassed acetone (30 mL) was heated to reflux for 12 h and then stirred at room temperature overnight. The mother liquor was decanted from the waxy white precipitate that formed and the precipitate was dried under vacuum. The precipitate was treated with saturated solution of aqueous NaHCO<sub>3</sub> (40 mL) and stirred at 80 °C for 6 h. After cooling down to room temperature, the mother liquor was cannulated out and the white precipitate was dried under vacuum. The product was extracted with Et<sub>2</sub>O (30 mL  $\times$  3) and the combined solution was evaporated under vacuum to obtained waxy orange colored products. Yield: 4.807 g, 19.05 mmol, 89%. (NMR  $\delta$ , CDCl<sub>3</sub>): <sup>1</sup>H: 7.01 (t,  $J_{HH}$  = 7.8 Hz, 1H, Ar-H), 6.82 (d,  $J_{HH}$  = 7.5 Hz, 1H, Ar-H), 6.75 (s, 1H, Ar-H), 6.47 (d,  $J_{HH}$  = 8.0 Hz, 1H, Ar-H), 4.66 (s, 1H, OH), 2.71 (d,  $^2J_{PH}$  = 3.5 Hz, 2H, CH<sub>2</sub>), 1.06 (d,  $^3J_{PH}$  = 11.0 Hz, 18H, 2 C(CH<sub>3</sub>)<sub>3</sub>). <sup>13</sup>C{<sup>1</sup>H}: 155.8 (s, Ar-C), 143.8 (d,  $J_{PC}$  = 12.4 Hz, Ar-C), 129.7 (s, Ar-C), 122.3 (d,  $J_{PC}$  = 8.0 Hz, Ar-C), 116.7 (d,  $J_{PC}$  = 9.2 Hz, Ar-C), 112.7 (d,  $J_{PC}$  = 2.1 Hz, Ar-C), 32.1 (d,  $^1J_{PC}$  = 21.7 Hz, CH<sub>2</sub>), 30.1 (d,  $^2J_{PC}$  = 13.1 Hz, 6C, C(CH<sub>3</sub>)<sub>3</sub>), 28.6 (d,  $^1J_{PC}$  = 23.2 Hz, 2C, C(CH<sub>3</sub>)<sub>3</sub>). <sup>31</sup>P{<sup>1</sup>H}: 33.2 (s).

**Synthesis of <sup>t</sup>Bu<sup>4</sup>PCOP ligand (2-3).** A solution of 3-(di-*tert*-butylphosphinomethyl)phenol (**C**) (2.657 g, 10.53 mmol) in THF (40 mL) was added dropwise to the suspension of NaH (0.2779 g, 11.58 mmol) in THF (20 mL) and the reaction mixture was heated to reflux for 1.5 h. After cooling down to room temperature, the solution of di-*tert*-butylchlorophosphine, <sup>t</sup>Bu<sub>2</sub>PCl (2.00 mL, 10.50 mmol) in THF (10 mL) was added dropwise through a cannula and resultant reaction mixture was heated to reflux for 2 h. The solvent was then removed under vacuum and the product was extracted with pentane (20 mL x 2). The combined pentane solution was removed under vacuum to obtain a pale yellow viscous liquid product. Yield: 3.514 g, 8.862 mmol, 84%. (NMR,  $\delta$ , C<sub>6</sub>D<sub>6</sub>) <sup>1</sup>H: 7.62 (s, 1H, Ar-*H*<sub>ipso</sub>), 7.10-7.18 (m, 3 H, Ar-*H*), 2.80 (d, <sup>2</sup>*J*<sub>PH</sub> = 2.25 Hz, 2H, CH<sub>2</sub>), 1.21 (d, <sup>3</sup>*J*<sub>PH</sub> = 11.6 Hz, 18 H, C(CH<sub>3</sub>)<sub>3</sub>), 1.11 (d, <sup>3</sup>*J*<sub>PH</sub> = 10.5 Hz, 18H, C(CH<sub>3</sub>)<sub>3</sub>). <sup>13</sup>C{<sup>1</sup>H}: 160.3 (d, <sup>3</sup>*J*<sub>PC</sub> = 9.4 Hz, Ar-C<sub>ipso</sub>), 143.7 (dd, *J*<sub>PC</sub> = 12.7 Hz, *J*<sub>PC</sub> = 0.7 Hz, Ar-C), 129.5 (s, Ar-C), 123.3 (dd, *J*<sub>PC</sub> = 8.7 Hz, *J*<sub>PC</sub> = 1.2 Hz, Ar-C), 120.1 (dd, *J*<sub>PC</sub> = 11.3 Hz, *J*<sub>PC</sub> = 9.1 Hz, Ar-C), 115.9 (dd, *J*<sub>PC</sub> = 10.5 Hz, *J*<sub>PC</sub> = 1.9 Hz, Ar-C), 35.7 (d, <sup>1</sup>*J*<sub>PC</sub> = 26.8 Hz, CH<sub>2</sub>), 31.8 (d, <sup>1</sup>*J*<sub>PC</sub> = 24.5, C(CH<sub>3</sub>)<sub>3</sub>), 30.0 (d, <sup>2</sup>*J*<sub>PC</sub> = 13.5 Hz, C(CH<sub>3</sub>)<sub>3</sub>), 29.2 (d, <sup>1</sup>*J*<sub>PC</sub> = 25.8 Hz, C(CH<sub>3</sub>)<sub>3</sub>), 27.6 (d, <sup>2</sup>*J*<sub>PC</sub> = 15.8 Hz, C(CH<sub>3</sub>)<sub>3</sub>). <sup>31</sup>P{<sup>1</sup>H}: 152.7 (s, O-P), 34.1 (s, CH<sub>2</sub>-P).

**Synthesis of (<sup>t</sup>Bu<sup>4</sup>PCOP)Ir(H)(Cl) (2-4).** A mixture of the ligand (**2-3**) (3.0 mL of 0.367 M solution in toluene) and [Ir(COD)Cl]<sub>2</sub> (0.335 g, 0.499 mmol) in toluene (15 mL) was heated to reflux for 72 h under H<sub>2</sub> atmosphere. After cooling the reaction mixture to room temperature, the mother liquor was evaporated under vacuum. The product was extracted with pentane (60 mL x 3) and combined pentane solution was evaporated to

obtain orange-red crystalline product, **2-4**. Yield: 0.470 g, 0.753 mmol, 68%. (NMR,  $\delta$ ,  $\text{C}_6\text{D}_6$ )  $^1\text{H}$ : 6.93-6.83 (m, 3H, Ar-H), 3.10 (dd,  $^2J_{\text{HH}} = 17.6$  Hz,  $^2J_{\text{PH}} = 9.5$  Hz, 1H,  $\text{CH}_2$ ), 3.00 (dd,  $^2J_{\text{HH}} = 17.6$  Hz,  $^2J_{\text{PH}} = 8.9$  Hz, 1H,  $\text{CH}_2$ ), 1.34 (d,  $^3J_{\text{PH}} = 14.0$  Hz, 9H,  $\text{C}(\text{CH}_3)_3$ ), 1.29 (d,  $^3J_{\text{PH}} = 14.2$  Hz, 9H,  $\text{C}(\text{CH}_3)_3$ ), 1.22 (d,  $^3J_{\text{PH}} = 13.0$  Hz, 9H,  $\text{C}(\text{CH}_3)_3$ ), 1.19 (d,  $^3J_{\text{PH}} = 13.4$  Hz, 9H,  $\text{C}(\text{CH}_3)_3$ ), -41.38 (dd,  $^2J_{\text{PH}} = 13.3$  Hz,  $^2J_{\text{PH}} = 12.3$  Hz).  $^{13}\text{C}\{^1\text{H}\}$ : 168.1 (apparent t,  $^3J_{\text{PC}} = 6.1$  Hz, Ar- $\text{C}_{\text{ipso}}$ ), 152.0 (dd,  $J_{\text{PC}} = 11.3$  Hz,  $J_{\text{PC}} = 5.5$  Hz, Ar-C), 132.2 (dd,  $J_{\text{PC}} = 5.6$  Hz,  $J_{\text{PC}} = 3.0$  Hz Ar-C), 124.6 (s, Ar-C), 118.1 (d,  $J_{\text{PC}} = 15.5$  Hz, Ar-C), 108.5 (d,  $J_{\text{PC}} = 11.7$  Hz, Ar-C), 43.6 (dd,  $^1J_{\text{PC}} = 19.3$  Hz,  $^3J_{\text{PC}} = 4.9$  Hz,  $\text{C}(\text{CH}_3)_3$ ), 39.4 (dd,  $^1J_{\text{PC}} = 20.9$  Hz,  $^3J_{\text{PC}} = 5.9$  Hz,  $\text{C}(\text{CH}_3)_3$ ), 37.5 (dd,  $^1J_{\text{PC}} = 15.9$  Hz,  $^3J_{\text{PC}} = 3.2$  Hz,  $\text{C}(\text{CH}_3)_3$ ), 35.3 (dd,  $^1J_{\text{PC}} = 29.8$  Hz,  $^3J_{\text{PC}} = 1.0$  Hz,  $\text{CH}_2$ ), 35.0 (dd,  $^1J_{\text{PC}} = 17.7$  Hz,  $^3J_{\text{PC}} = 3.3$  Hz,  $\text{C}(\text{CH}_3)_3$ ), 29.9 (dd,  $^2J_{\text{PC}} = 3.8$  Hz,  $^4J_{\text{PC}} = 1.3$  Hz  $\text{C}(\text{CH}_3)_3$ ), 29.3 (dd,  $^2J_{\text{PC}} = 3.8$  Hz,  $^4J_{\text{PC}} = 1.3$  Hz  $\text{C}(\text{CH}_3)_3$ ), 27.8 (d,  $^2J_{\text{PC}} = 4.9$  Hz,  $\text{C}(\text{CH}_3)_3$ ), 27.7 (dd,  $^2J_{\text{PC}} = 4.9$  Hz,  $^4J_{\text{PC}} = 1.0$  Hz,  $\text{C}(\text{CH}_3)_3$ ).  $^{31}\text{P}\{^1\text{H}\}$ : 168.6 (dd,  $^2J_{\text{PP}} = 345.0$  Hz,  $^2J_{\text{PH}} = 12.3$  Hz O-P), 70.6 (dd,  $^2J_{\text{PP}} = 345.0$  Hz,  $^2J_{\text{PH}} = 11.0$  Hz,  $\text{CH}_2\text{-P}$ ). Anal Calcd. for  $\text{C}_{23}\text{H}_{42}\text{OIrP}_2\text{Cl}$ : C, 44.26; H, 6.78; Cl, 5.68. Found: C, 44.03; H, 6.59; Cl, 5.67.

**Synthesis of ( $^{\text{tBu}}\text{PCOP}$ )Ir(H) $_2$  (2-5).** The (PCOP)IrHCl (**2-4**) (0.150 g, 0.247 mmol) was dissolved in pentane (60 mL) and 1.0 M solution (in THF) of LiBEt $_3$ H (0.25 mL, 0.25 mmol) was added dropwise *via* syringe under hydrogen atmosphere, causing the orange solution to turn a pale yellow and resulting in the precipitation of a white solid. The reaction mixture was stirred for 30 minutes prior to cannula filtration of the solution. The pentane solution was evaporated under vacuum to obtain a red crystalline solid, **2-5**. Yield: 0.136 g, 0.231 mmol, 93%. (NMR,  $\delta$ ,  $\text{C}_6\text{D}_6$ )  $^1\text{H}$ : 7.23 – 7.13 (m, 3H, Ar-H), 3.50

(d,  $^2J_{\text{PH}} = 8.4$  Hz, 2H,  $\text{CH}_2$ ), 1.34 (d,  $^3J_{\text{PH}} = 13.8$  Hz, 18H,  $\text{C}(\text{CH}_3)_3$ ), 1.19 (d,  $^3J_{\text{PH}} = 12.9$  Hz, 18H,  $\text{C}(\text{CH}_3)_3$ ), -18.12 (apparent t,  $^2J_{\text{PH}} = 8.6$  Hz, 2H,  $\text{IrH}_2$ ).  $^{13}\text{C}\{^1\text{H}\}$ : 171.0 (dd,  $^3J_{\text{PC}} = 5.7$  Hz,  $^3J_{\text{PC}} = 3.1$  Hz, Ar- $\text{C}_{\text{ipso}}$ ) 170.7 (dd,  $J_{\text{PC}} = 8.5$  Hz,  $J_{\text{PC}} = 7.0$  Hz, Ar-C), 157.6 (dd,  $J_{\text{PC}} = 14.2$  Hz,  $J_{\text{PC}} = 5.8$  Hz, Ar-C), 129.5 (dd,  $J_{\text{PC}} = 0.6$  Hz, Ar-C), 116.3 (d,  $J_{\text{PC}} = 16.1$  Hz, Ar-C), 107.7 (d,  $J_{\text{PC}} = 12.5$  Hz, Ar-C), 40.3 (d,  $^1J_{\text{PC}} = 28.6$  Hz,  $\text{CH}_2$ ), 40.1 (dd,  $^1J_{\text{PC}} = 20.7$  Hz,  $^3J_{\text{PC}} = 4.6$  Hz,  $\text{C}(\text{CH}_3)_3$ ), 35.1 (dd,  $^1J_{\text{PC}} = 17.6$  Hz,  $^3J_{\text{PC}} = 2.4$  Hz,  $\text{C}(\text{CH}_3)_3$ ), 29.9 (dd,  $^2J_{\text{PC}} = 5.3$  Hz,  $^4J_{\text{PC}} = 0.8$  Hz,  $\text{C}(\text{CH}_3)_3$ ), 29.0 (d,  $^2J_{\text{PC}} = 6.3$  Hz,  $\text{C}(\text{CH}_3)_3$ ).  $^{31}\text{P}\{^1\text{H}\}$ : 200.3 (d,  $^2J_{\text{PP}} = 330$  Hz, O-P), 87.3 (d,  $^2J_{\text{PP}} = 330$  Hz,  $\text{CH}_2$ -P). Anal Calcd. for  $\text{C}_{23}\text{H}_{43}\text{OIrP}_2$ : C, 46.84; H, 7.35. Found: C, 41.89; H, 6.55.

**Synthesis of ( $^t\text{Bu}^4\text{PCOP}$ )Ir(CO) (2-6).** 25 mg of **2-5** (0.04 mmol) was dissolved in 1 mL of n-pentane in a J. Young nmr tube. The homogeneous sample was then frozen in liquid nitrogen and the headspace evacuated on the high-vacuum line. 1 atmosphere of CO was subsequently added and the sample was warmed to room temperature with shaking to promote mixture. Upon warming to room temperature, the color of the solution rapidly changed from red-brown to bright yellow. Removal of solvent and atmosphere under vacuum results in isolation of bright yellow crystals of the product, **2-6**, in quantitative yield. (NMR,  $\delta$ ,  $p$ -xylene- $\text{d}_{10}$ )  $^1\text{H}$ : 6.93 (m, 3H), 3.53 (d,  $J = 8.9$  Hz, 4H), 1.52 (d,  $J = 14.1$  Hz, 18H), 1.38 (d,  $J = 13.2$  Hz, 18H).  $^{31}\text{P}\{^1\text{H}\}$ : 198.7 (d,  $J = 288.3$  Hz, O-P), 89.5 (d,  $J = 288.3$  Hz,  $\text{CH}_2$ -P).

**Transfer dehydrogenation catalytic studies.** For all transfer dehydrogenation studies, stock solutions of the (pincer)Ir catalysts were prepared in an argon-atmosphere glovebox. The vessel was sealed with an inert septum and the Teflon screw-top. The vessel was submerged partially in a 150 °C oil bath and monitored periodically by cooling to room-temperature, bringing the vessel into the glovebox, and using a microliter syringe to withdraw 0.5 microliter samples for GC analysis.

**Acceptorless dehydrogenation catalytic studies.** Stock solutions of the (pincer)Ir complexes were prepared in the argon-atmosphere glovebox. The reaction solution was transferred to the reaction vessel, which was sealed with an inert rubber septum and Teflon stopcocks under argon atmosphere. Outside the glovebox, a flow of argon was established throughout the reaction vessel and the condenser was connected to water flow, prior to the round-bottom portion of the vessel being completely submerged in a 230 °C oil bath. The reaction was periodically monitored by cooling to room temperature and then withdrawing small aliquots of the reaction mixture via the septum-sealed port under positive argon flow.

## 2.6 Chapter 2 Appendix

### 2.6.1 NMR spectra

**Figure 2A.1.**  $^1\text{H}$  nmr spectrum of  $^{\text{tBu}}_4\text{PCOP}$  ligand (2-3).

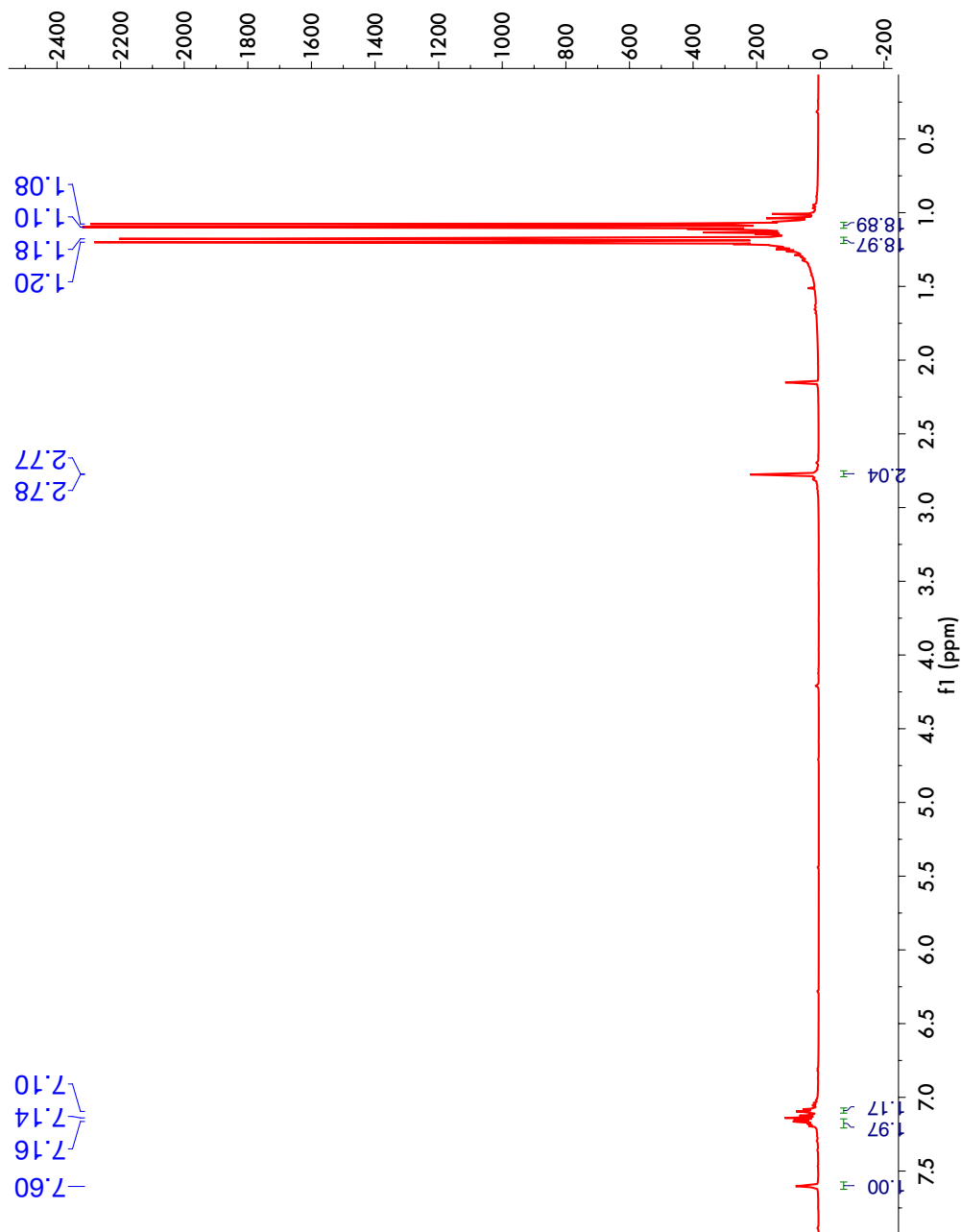




**Figure 2A.2.**  $^{31}\text{P}$  nmr spectrum of  $^{\text{tBu}}\text{PCOP}$  ligand (2-3).

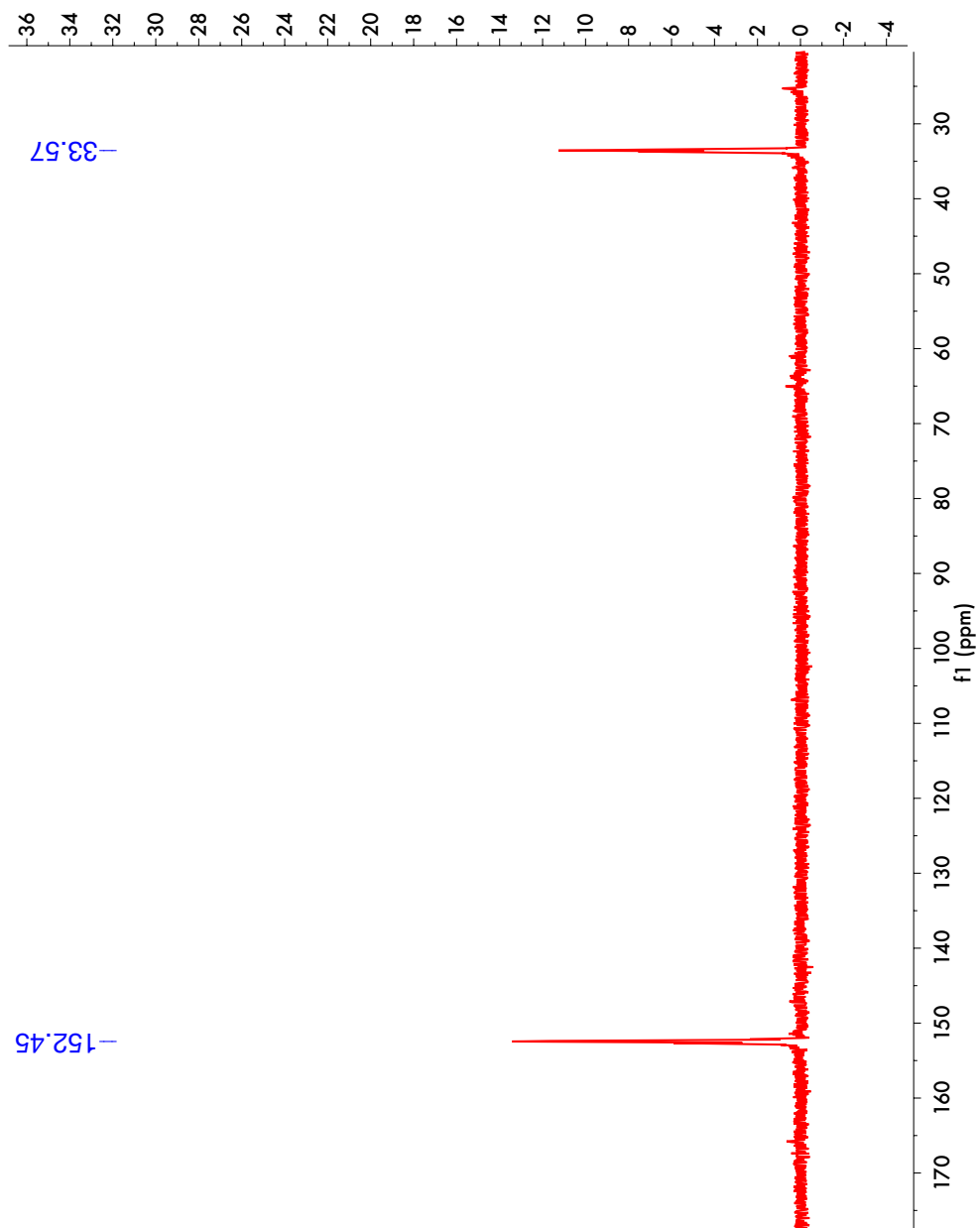


**Figure 2A.3.**  $^{13}\text{C}$  nmr spectrum of  $^{\text{tBu}}_4\text{PCOP}$  ligand (2-3).

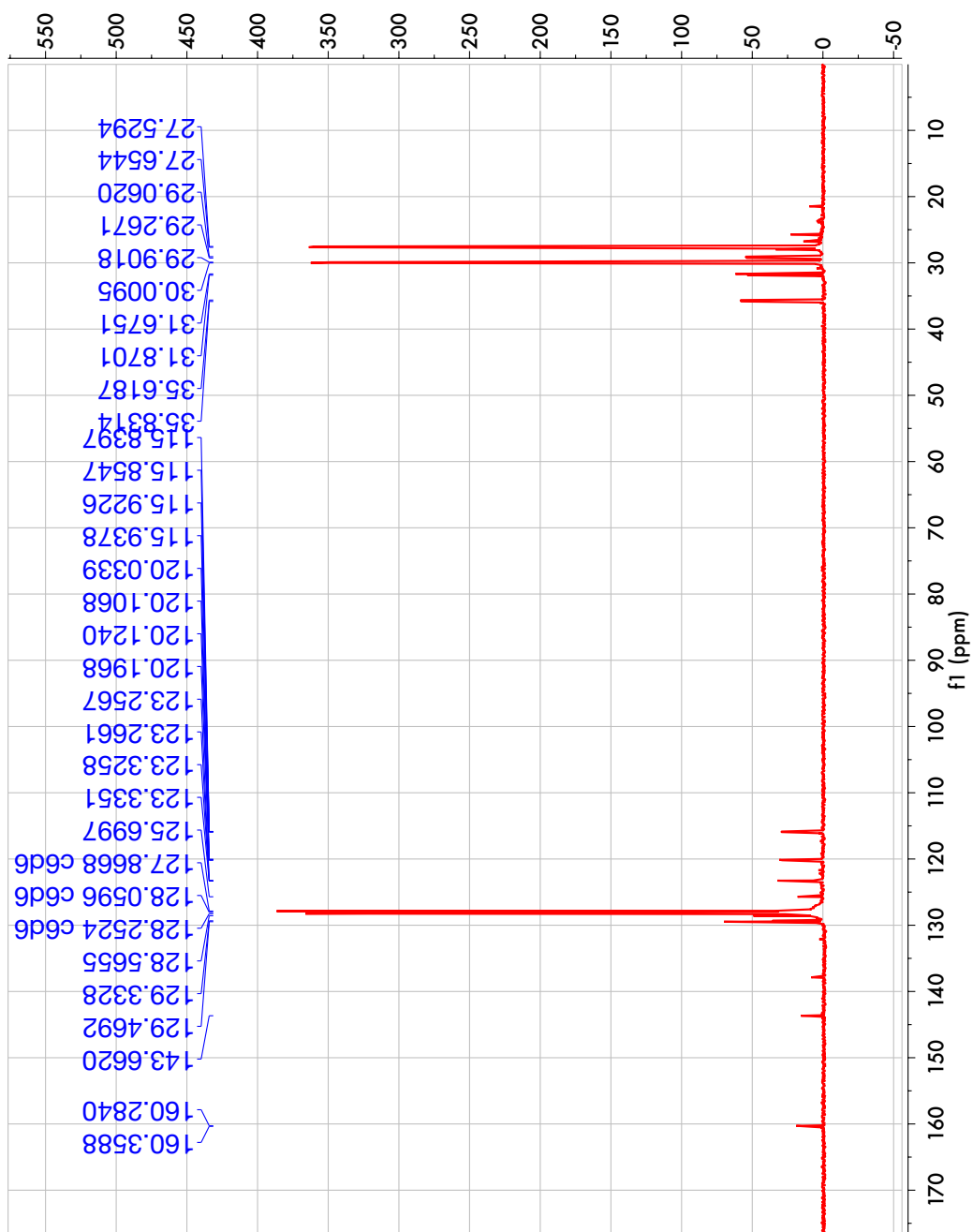


**Figure 2A.4.**  $^1\text{H}$  nmr spectrum of  $(^t\text{Bu}^4\text{PCOP})\text{Ir}(\text{H})(\text{Cl})$  ligand (2-4).

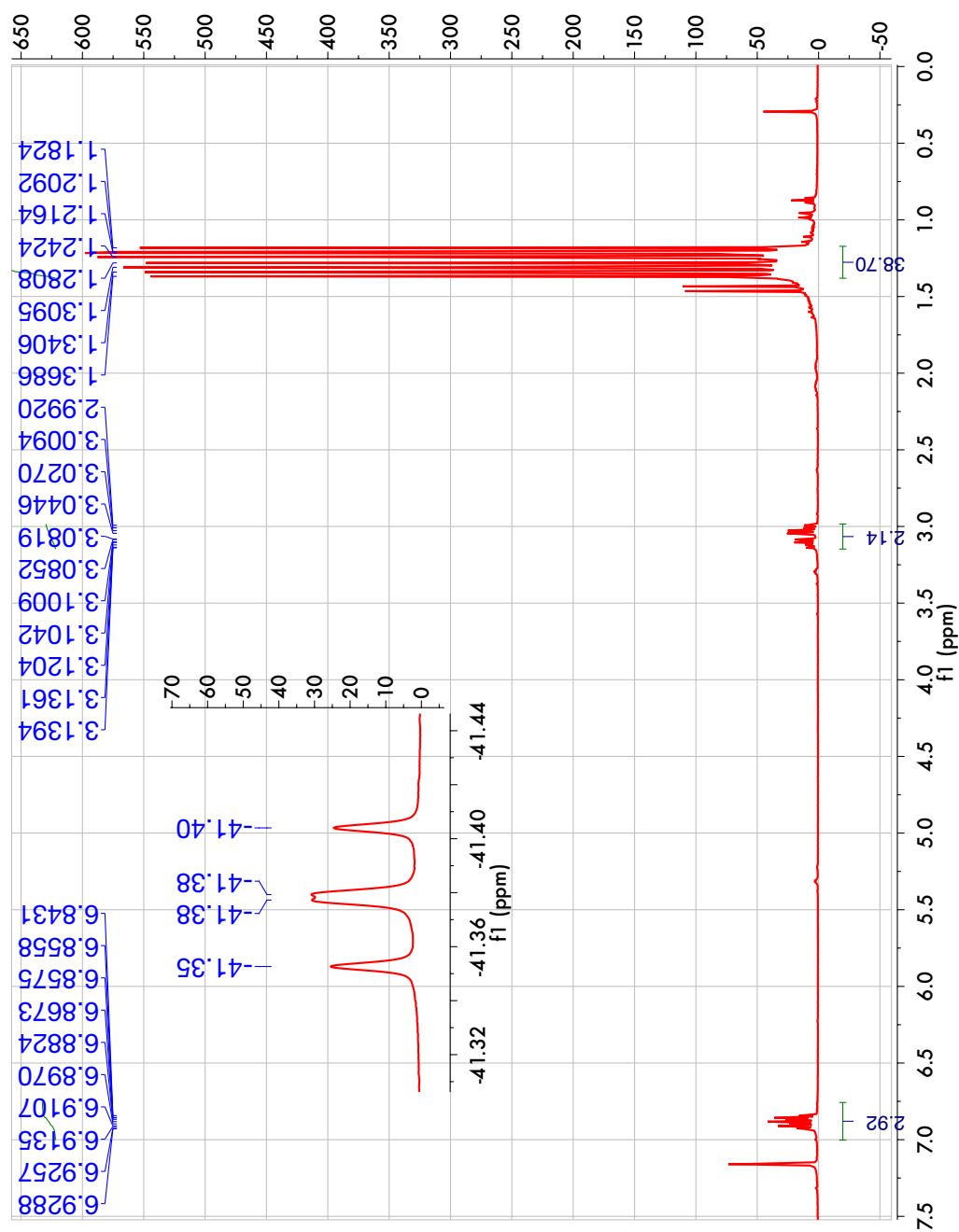


**Figure 2A.5.**  $^{31}\text{P}$  nmr spectrum of  $(^{\text{tBu}}\text{PCOP})\text{Ir}(\text{H})(\text{Cl})$  ligand (2-4).

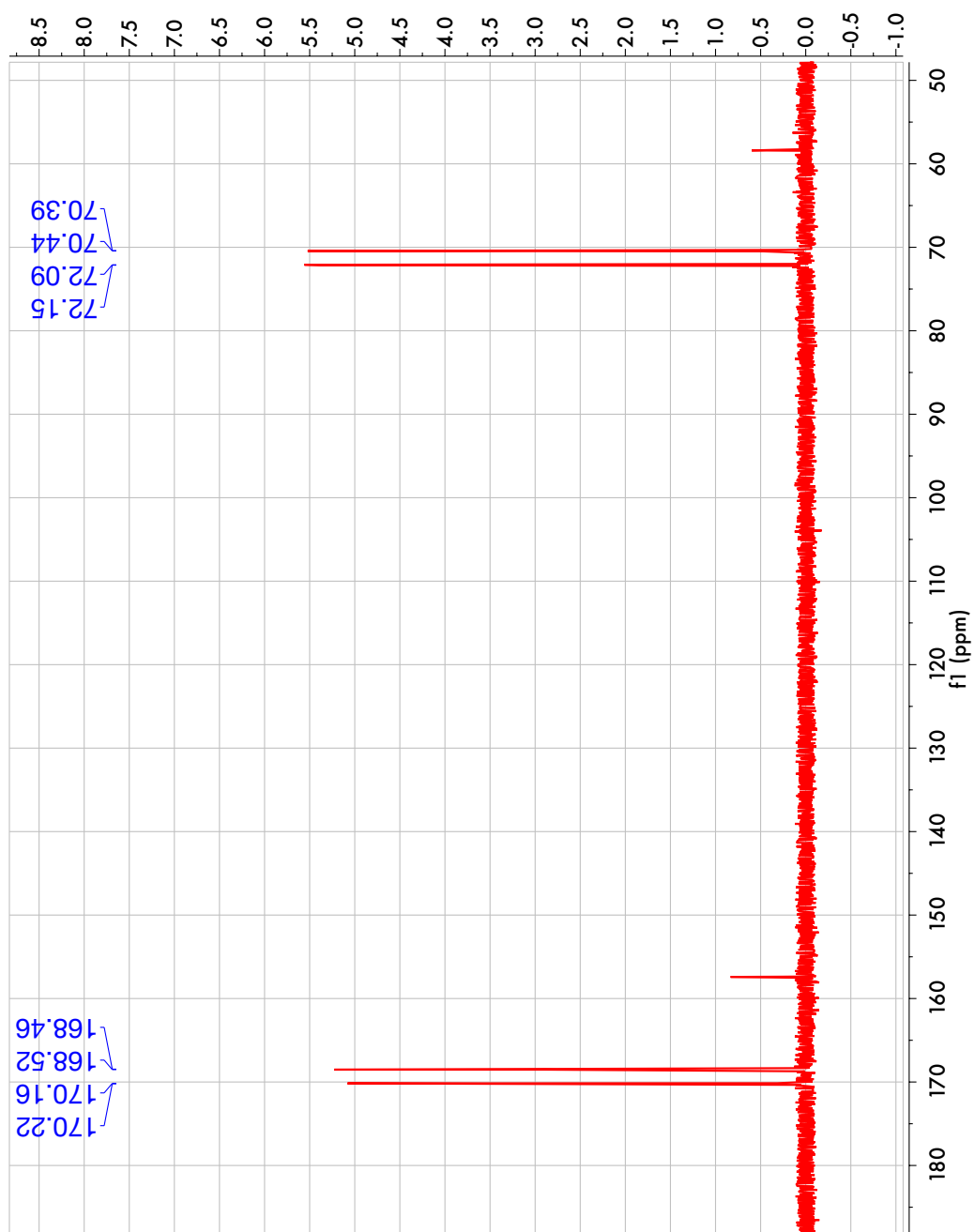


**Figure 2A.6.**  $^{13}\text{C}$  nmr spectrum of  $(^t\text{Bu}^4\text{PCOP})\text{Ir}(\text{H})(\text{Cl})$  ligand (2-4).

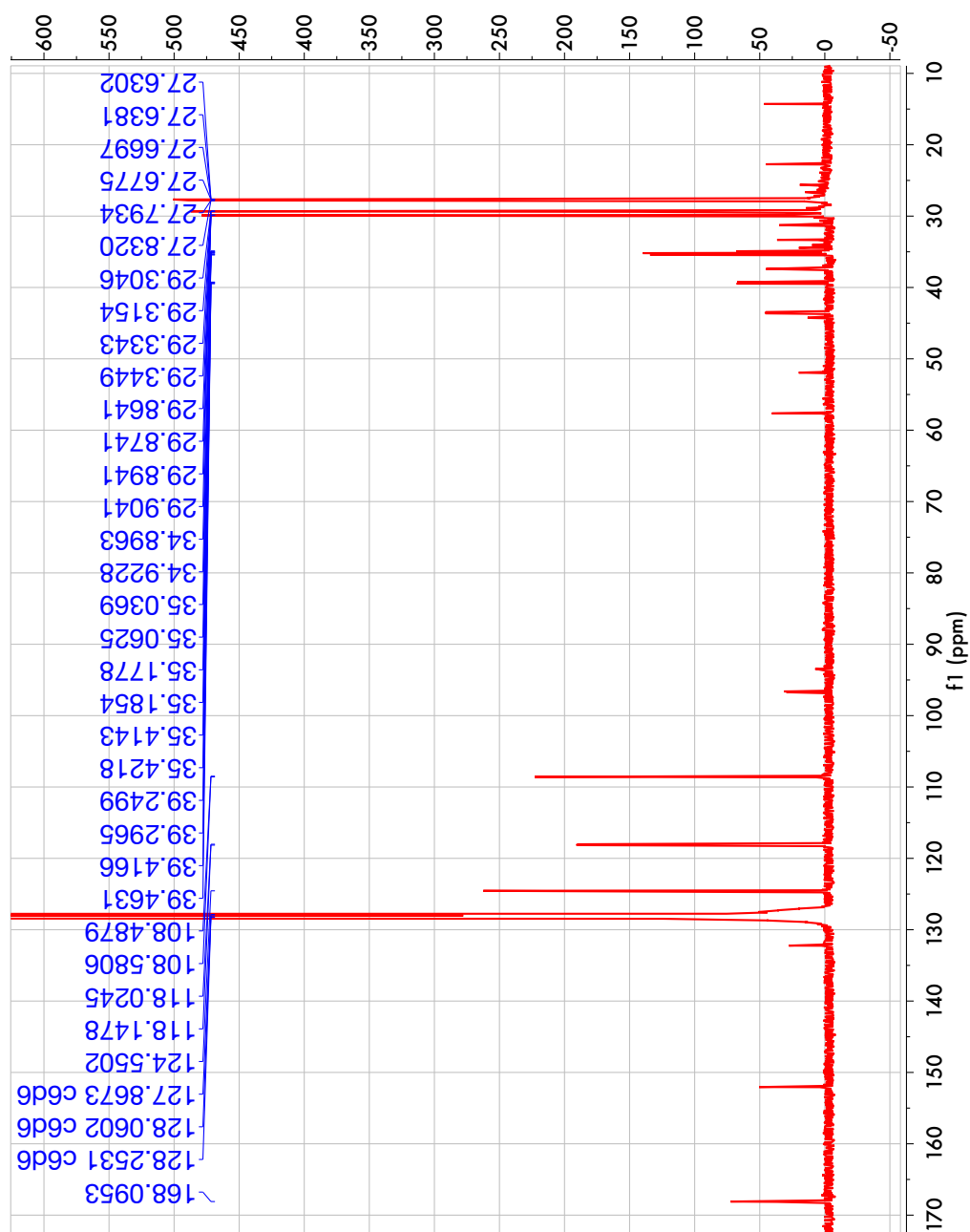


**Figure 2A.7.**  $^1\text{H}$  nmr spectrum of  $(^t\text{Bu}^4\text{PCOP})\text{Ir}(\text{H})_2$  (2-5).

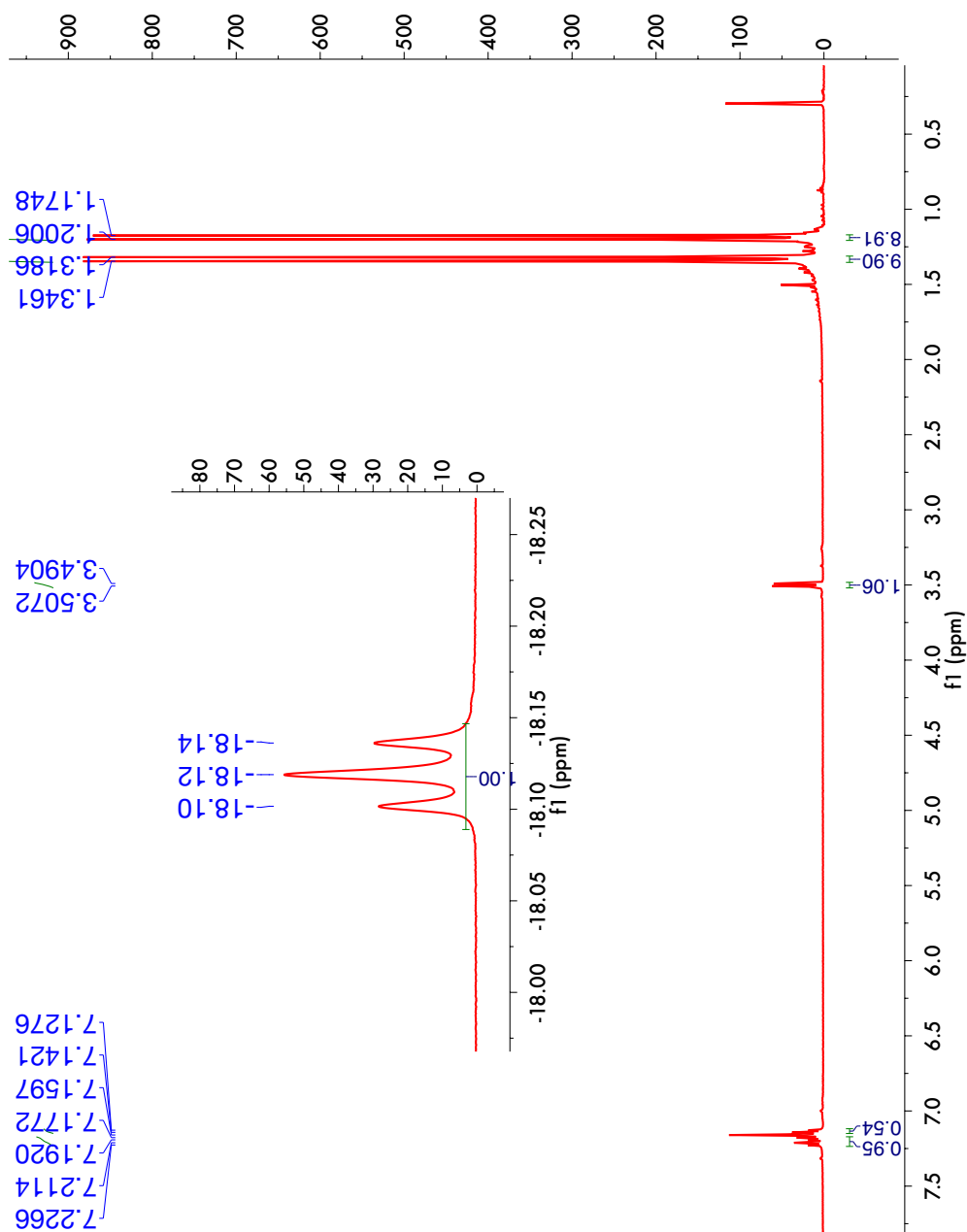


**Figure 2A.8.**  $^{31}\text{P}$  nmr spectrum of  $(^{\text{tBu}}\text{PCOP})\text{Ir}(\text{H})_2$  (2-5).

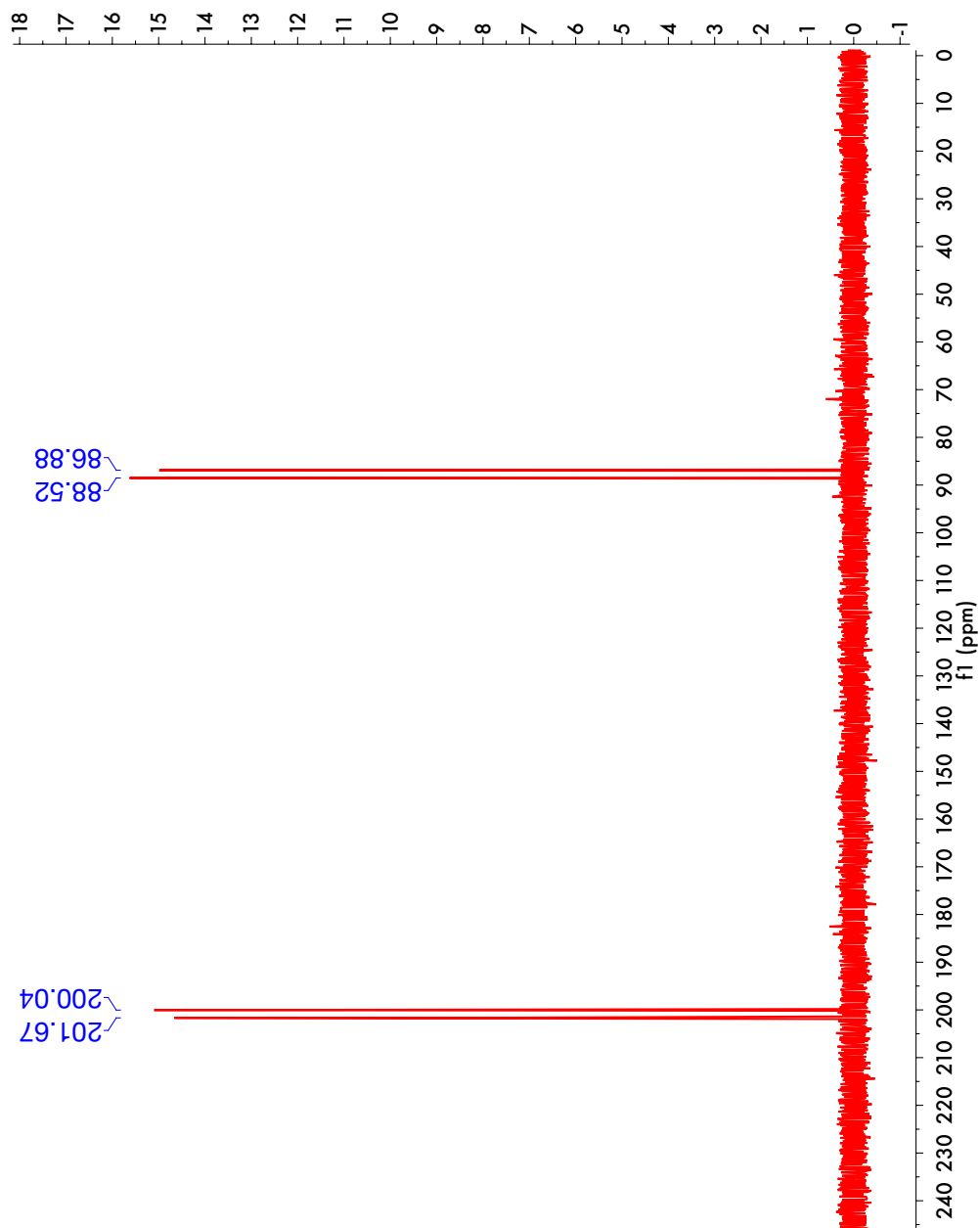
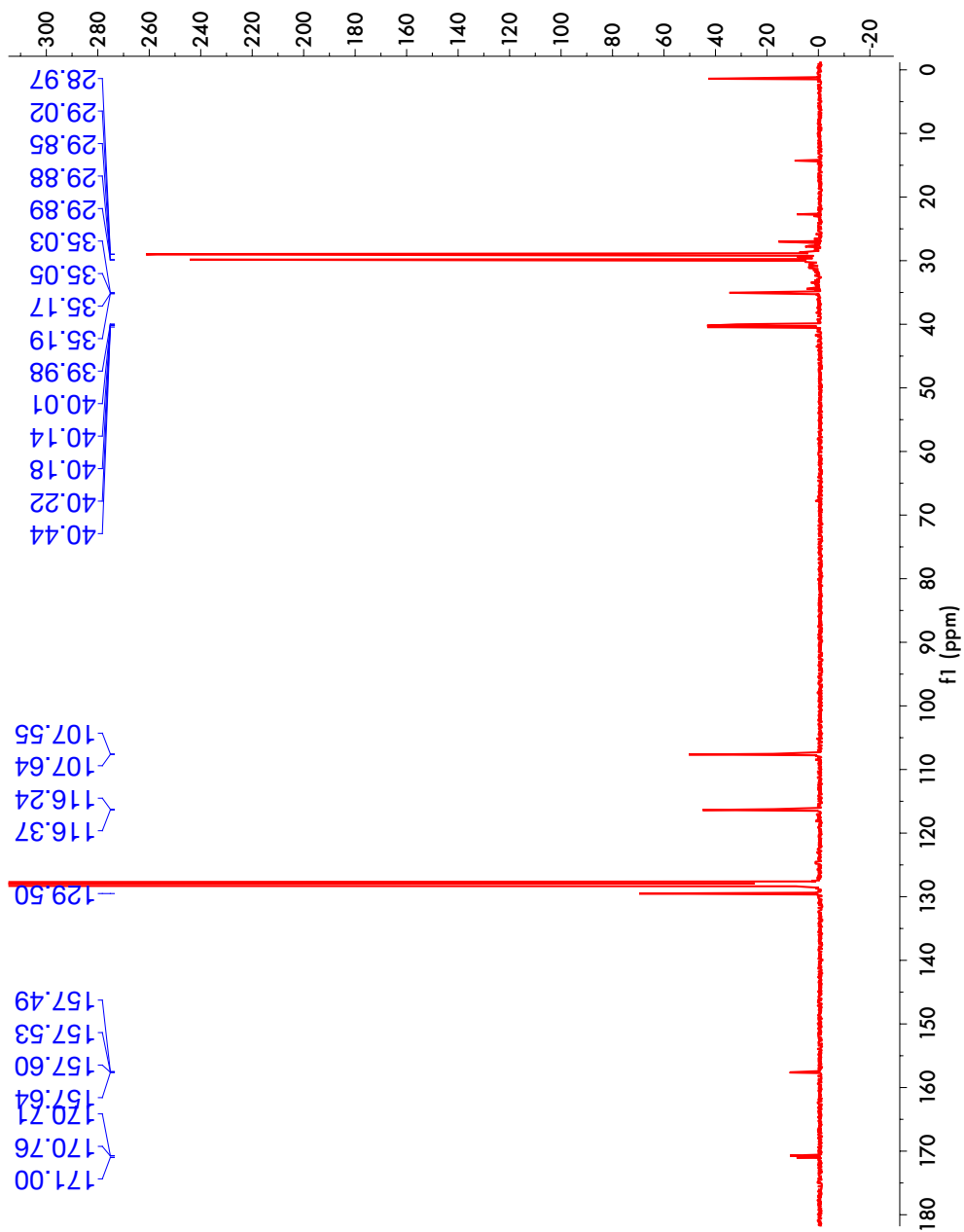


**Figure 2A.9.**  $^{13}\text{C}$  nmr spectrum of  $(^t\text{Bu}^4\text{PCOP})\text{Ir}(\text{H})_2$  (2-5).





### 2.6.2. Full crystal data of (<sup>t</sup>Bu<sup>4</sup>PCOP)Ir(H)(Cl) (2-4).

**X-ray Structure Determination.** X-ray diffraction data were collected on a Bruker Smart APEX CCD diffractometer with graphite monochromatized Mo K $\alpha$  radiation ( $\lambda$  = 0.71073 Å) at 100 K. Crystals were immersed in Paratone oil, placed on a glass needle, and examined at 100 K. The data were corrected for Lorentz effects, polarization, and absorption, the latter by a multi-scan (SADABS) method.<sup>33</sup> The structures were solved by direct methods (SHELXS86).<sup>34</sup> All non-hydrogen atoms were refined (SHELXL97)<sup>35</sup> based upon  $F_{\text{obs}}^2$ . All hydrogen atom coordinates were calculated with idealized geometries (SHELXL97). Scattering factors ( $f_o$ ,  $f'$ ,  $f''$ ) are as described in SHELXL97.

**Figure 2A.10.** Crystal structure of 2-4.

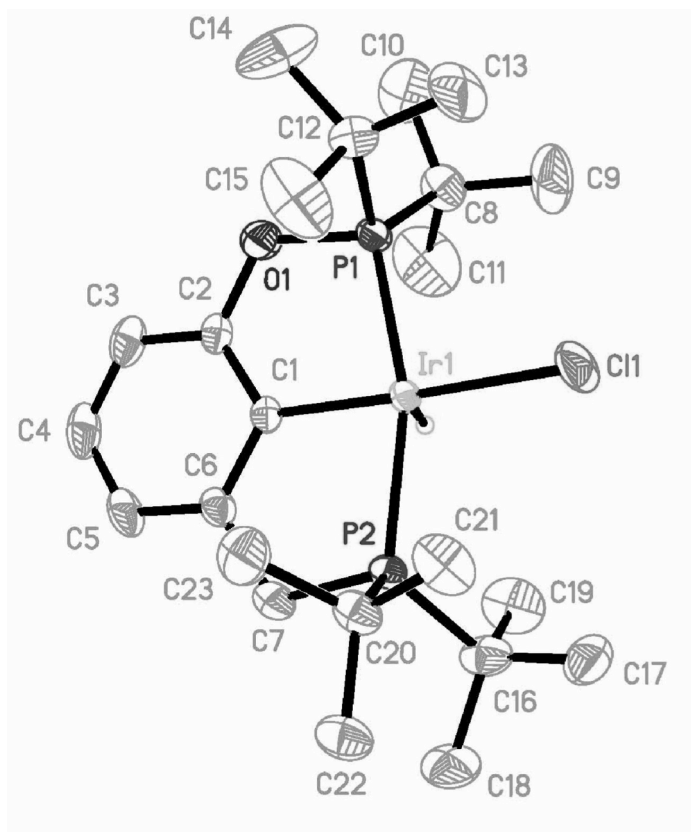


**Table 2A.1.** Crystal data and structure refinement for **2-4**.

Identification code	tBu4pccopIrHCl	
Empirical formula	C <sub>23</sub> H <sub>42</sub> Cl Ir O P <sub>2</sub>	
Formula weight	624.16	
Temperature	100(2) K	
Wavelength	0.71073 Å	
Crystal system	Monoclinic	
Space group	P2(1)/n	
Unit cell dimensions	a = 15.2089(7) Å	a = 90°.
	b = 11.9058(6) Å	b = 112.673(1)°.
	c = 15.6368(8) Å	g = 90°.
Volume	2612.6(2) Å <sup>3</sup>	
Z	4	
Density (calculated)	1.587 Mg/m <sup>3</sup>	
Absorption coefficient	5.347 mm <sup>-1</sup>	
F(000)	1248	
Crystal size	0.34 x 0.16 x 0.12 mm <sup>3</sup>	
Theta range for data collection	2.22 to 31.50°.	
Index ranges	-22 ≤ h ≤ 22, -17 ≤ k ≤ 17, -22 ≤ l ≤ 22	
Reflections collected	32353	
Independent reflections	8682 [R(int) = 0.0250]	
Completeness to theta = 31.50°	99.8 %	
Absorption correction	Semi-empirical from equivalents	
Max. and min. transmission	0.7463 and 0.4517	
Refinement method	Full-matrix least-squares on F <sup>2</sup>	
Data / restraints / parameters	8682 / 0 / 268	
Goodness-of-fit on F <sup>2</sup>	1.005	
Final R indices [I > 2σ(I)]	R1 = 0.0322, wR2 = 0.0742	
R indices (all data)	R1 = 0.0353, wR2 = 0.0756	
Largest diff. peak and hole	2.764 and -2.491 e.Å <sup>-3</sup>	

**Table 2A.2.** Atomic coordinates ( $\times 10^4$ ) and equivalent isotropic displacement parameters ( $\text{\AA}^2 \times 10^3$ ) for **2-4**.  $U(\text{eq})$  is defined as one third of the trace of the orthogonalized  $U^{ij}$  tensor.

	x	y	z	$U(\text{eq})$
Ir(1)	7323(1)	1182(1)	9926(1)	20(1)
Cl(1)	8564(1)	1880(1)	11306(1)	58(1)
P(1)	7447(1)	-652(1)	10350(1)	23(1)
P(2)	6915(1)	2842(1)	9088(1)	22(1)
O(1)	6654(2)	-1309(2)	9443(2)	33(1)
C(1)	6314(2)	544(3)	8769(2)	20(1)
C(2)	6123(2)	-611(3)	8698(2)	23(1)
C(3)	5429(3)	-1108(4)	7933(3)	35(1)
C(4)	4912(3)	-431(4)	7193(3)	41(1)
C(5)	5068(3)	700(4)	7221(3)	36(1)
C(6)	5757(2)	1203(3)	8007(2)	26(1)
C(7)	5853(3)	2452(3)	8100(3)	36(1)
C(8)	7059(3)	-1096(4)	11282(3)	38(1)
C(9)	7679(5)	-557(5)	12198(3)	65(2)
C(10)	7056(5)	-2382(5)	11410(4)	67(2)
C(11)	6024(5)	-688(8)	10980(5)	87(2)
C(12)	8563(3)	-1329(3)	10400(3)	33(1)
C(13)	9367(4)	-1121(6)	11314(4)	64(2)
C(14)	8424(4)	-2584(4)	10141(6)	72(2)
C(15)	8794(4)	-760(7)	9630(4)	70(2)
C(16)	6516(3)	4037(4)	9624(3)	39(1)
C(17)	7407(4)	4633(4)	10342(3)	48(1)
C(18)	5906(4)	4923(4)	8920(4)	54(1)
C(19)	5961(4)	3547(5)	10166(4)	57(1)
C(20)	7791(3)	3304(3)	8592(3)	31(1)
C(21)	8786(3)	3374(5)	9342(3)	46(1)
C(22)	7533(3)	4390(4)	8035(3)	41(1)
C(23)	7799(4)	2333(4)	7918(3)	48(1)

**Table 2A.3.** Bond lengths [Å] and angles [°] for **2-4**.

Ir(1)-C(1)	2.016(3)	C(4)-C(5)	1.366(7)
Ir(1)-P(1)	2.2685(9)	C(5)-C(6)	1.406(5)
Ir(1)-P(2)	2.3194(8)	C(6)-C(7)	1.495(5)
Ir(1)-Cl(1)	2.4012(10)	C(8)-C(9)	1.520(7)
P(1)-O(1)	1.662(3)	C(8)-C(11)	1.536(7)
P(1)-C(8)	1.848(4)	C(8)-C(10)	1.544(7)
P(1)-C(12)	1.852(4)	C(12)-C(13)	1.500(7)
P(2)-C(7)	1.814(4)	C(12)-C(15)	1.535(6)
P(2)-C(20)	1.865(4)	C(12)-C(14)	1.542(7)
P(2)-C(16)	1.868(4)	C(16)-C(19)	1.525(6)
O(1)-C(2)	1.405(4)	C(16)-C(18)	1.548(6)
C(1)-C(2)	1.401(5)	C(16)-C(17)	1.558(7)
C(1)-C(6)	1.405(4)	C(20)-C(21)	1.518(6)
C(2)-C(3)	1.386(5)	C(20)-C(22)	1.523(5)
C(3)-C(4)	1.381(6)	C(20)-C(23)	1.567(6)
C(1)-Ir(1)-P(1)	81.27(10)	C(2)-O(1)-P(1)	115.2(2)
C(1)-Ir(1)-P(2)	82.47(10)	C(2)-C(1)-C(6)	116.3(3)
P(1)-Ir(1)-P(2)	163.55(3)	C(2)-C(1)-Ir(1)	120.3(2)
C(1)-Ir(1)-Cl(1)	177.71(9)	C(6)-C(1)-Ir(1)	123.5(2)
P(1)-Ir(1)-Cl(1)	97.03(3)	C(3)-C(2)-C(1)	123.6(3)
P(2)-Ir(1)-Cl(1)	99.16(3)	C(3)-C(2)-O(1)	117.8(3)
O(1)-P(1)-C(8)	101.01(18)	C(1)-C(2)-O(1)	118.6(3)
O(1)-P(1)-C(12)	100.53(17)	C(4)-C(3)-C(2)	118.2(4)
C(8)-P(1)-C(12)	114.1(2)	C(5)-C(4)-C(3)	120.9(4)
O(1)-P(1)-Ir(1)	104.63(10)	C(4)-C(5)-C(6)	120.7(4)

C(8)-P(1)-Ir(1)	119.32(15)	C(1)-C(6)-C(5)	120.4(3)
C(12)-P(1)-Ir(1)	113.76(13)	C(1)-C(6)-C(7)	118.0(3)
C(7)-P(2)-C(20)	105.43(19)	C(5)-C(6)-C(7)	121.3(3)
C(7)-P(2)-C(16)	103.9(2)	C(6)-C(7)-P(2)	111.0(3)
C(20)-P(2)-C(16)	111.69(19)	C(9)-C(8)-C(11)	110.2(5)
C(7)-P(2)-Ir(1)	102.67(13)	C(9)-C(8)-C(10)	109.2(4)
C(20)-P(2)-Ir(1)	114.11(12)	C(11)-C(8)-C(10)	107.4(5)
C(16)-P(2)-Ir(1)	117.27(13)	C(9)-C(8)-P(1)	110.6(3)
C(11)-C(8)-P(1)	105.5(4)	C(18)-C(16)-C(17)	108.6(4)
C(10)-C(8)-P(1)	113.8(3)	C(19)-C(16)-P(2)	107.7(3)
C(13)-C(12)-C(15)	109.0(4)	C(18)-C(16)-P(2)	114.2(3)
C(13)-C(12)-C(14)	112.9(5)	C(17)-C(16)-P(2)	109.1(3)
C(15)-C(12)-C(14)	105.7(5)	C(21)-C(20)-C(22)	110.8(4)
C(13)-C(12)-P(1)	111.5(3)	C(21)-C(20)-C(23)	107.3(4)
C(15)-C(12)-P(1)	104.9(3)	C(22)-C(20)-C(23)	108.0(3)
C(14)-C(12)-P(1)	112.3(3)	C(21)-C(20)-P(2)	110.7(3)
C(19)-C(16)-C(18)	110.3(4)	C(22)-C(20)-P(2)	114.9(3)
C(19)-C(16)-C(17)	106.7(4)	C(23)-C(20)-P(2)	104.7(3)

**Table 2A.4.** Anisotropic displacement parameters ( $\text{\AA}^2 \times 10^3$ ) for **2-4**. The anisotropic displacement factor exponent takes the form:  $-2\pi^2[h^2 a^{*2}U_{11} + \dots + 2 h k a^* b^* U_{12}]$ .

	$U^{11}$	$U^{22}$	$U^{33}$	$U^{23}$	$U^{13}$	$U^{12}$
Ir(1)	18(1)	20(1)	17(1)	0(1)	1(1)	0(1)
Cl(1)	67(1)	39(1)	34(1)	6(1)	-18(1)	-24(1)
P(1)	23(1)	23(1)	20(1)	3(1)	6(1)	1(1)
P(2)	20(1)	22(1)	23(1)	2(1)	7(1)	3(1)
O(1)	34(1)	26(1)	34(1)	0(1)	7(1)	-4(1)
C(1)	14(1)	26(1)	19(1)	-4(1)	6(1)	2(1)
C(2)	18(1)	29(2)	23(1)	-6(1)	8(1)	-2(1)
C(3)	24(2)	41(2)	38(2)	-18(2)	10(1)	-8(1)
C(4)	24(2)	61(3)	31(2)	-20(2)	3(1)	-3(2)
C(5)	23(2)	57(2)	22(2)	-3(2)	0(1)	9(2)
C(6)	21(1)	33(2)	22(1)	0(1)	5(1)	4(1)
C(7)	38(2)	34(2)	28(2)	5(1)	2(2)	5(2)
C(8)	42(2)	45(2)	33(2)	4(2)	23(2)	-2(2)
C(9)	99(5)	74(4)	31(2)	-9(2)	35(3)	-25(3)
C(10)	106(5)	54(3)	60(3)	5(3)	53(4)	-27(3)
C(11)	58(4)	145(7)	78(4)	9(5)	47(4)	34(4)
C(12)	30(2)	31(2)	41(2)	3(2)	17(2)	1(1)
C(13)	32(2)	89(4)	52(3)	-4(3)	-3(2)	24(3)
C(14)	48(3)	38(3)	138(6)	-8(3)	44(4)	6(2)
C(15)	39(3)	124(6)	54(3)	16(3)	27(2)	-9(3)
C(16)	50(2)	34(2)	45(2)	8(2)	31(2)	14(2)
C(17)	70(3)	34(2)	45(2)	-6(2)	27(2)	0(2)
C(18)	65(3)	44(3)	60(3)	9(2)	30(3)	31(2)
C(19)	52(3)	72(3)	65(3)	10(3)	41(3)	12(3)
C(20)	29(2)	38(2)	29(2)	8(1)	16(1)	6(1)
C(21)	31(2)	64(3)	45(2)	11(2)	16(2)	-5(2)
C(22)	46(2)	40(2)	40(2)	14(2)	21(2)	1(2)
C(23)	53(3)	56(3)	45(2)	-3(2)	29(2)	12(2)

**Table 2A.5.** Hydrogen coordinates ( $\times 10^4$ ) and isotropic displacement parameters ( $\text{\AA}^2 \times 10^3$ ) for **2-4**.

	x	y	z	U(eq)
H(1)	6360(30)	1300(40)	10130(30)	31
H(3)	5316	-1877	7918	42
H(4)	4451	-750	6668	49
H(5)	4714	1143	6715	44
H(7A)	5296	2761	8175	44
H(7B)	5884	2766	7540	44
H(9A)	7690	242	12119	98
H(9B)	8315	-848	12396	98
H(9C)	7423	-724	12657	98
H(10A)	7700	-2656	11642	100
H(10B)	6699	-2730	10824	100
H(10C)	6769	-2559	11842	100
H(11A)	5764	-947	11415	131
H(11B)	5652	-981	10376	131
H(11C)	6010	117	10959	131
H(13A)	9945	-1426	11299	95
H(13B)	9229	-1478	11798	95
H(13C)	9440	-328	11428	95
H(14A)	8951	-2847	10002	109
H(14B)	7843	-2682	9607	109
H(14C)	8390	-3005	10651	109
H(15A)	8921	23	9773	104

H(15B)	8261	-837	9050	104
H(15C)	9344	-1109	9587	104
H(17A)	7207	5171	10688	72
H(17B)	7749	5010	10023	72
H(17C)	7814	4085	10759	72
H(18A)	5365	4562	8461	82
H(18B)	6283	5275	8624	82
H(18C)	5691	5481	9239	82
H(19A)	5752	4144	10456	86
H(19B)	6364	3045	10633	86
H(19C)	5417	3144	9752	86
H(21A)	9243	3463	9061	69
H(21B)	8922	2698	9704	69
H(21C)	8823	4006	9736	69
H(22A)	7617	5013	8448	61
H(22B)	6881	4357	7607	61
H(22C)	7939	4483	7698	61
H(23A)	8262	2496	7657	72
H(23B)	7179	2270	7429	72
H(23C)	7960	1638	8254	72



**Table 2A.6.** Torsion angles [°] for **2-4**.

C(1)-Ir(1)-P(1)-O(1)	0.79(14)	O(1)-C(2)-C(3)-C(4)	-179.2(3)
P(2)-Ir(1)-P(1)-O(1)	-7.90(17)	C(2)-C(3)-C(4)-C(5)	-1.2(6)
Cl(1)-Ir(1)-P(1)-O(1)	-177.66(12)	C(3)-C(4)-C(5)-C(6)	-0.3(6)
C(1)-Ir(1)-P(1)-C(8)	-111.11(19)	C(2)-C(1)-C(6)-C(5)	-1.3(5)
P(2)-Ir(1)-P(1)-C(8)	-119.8(2)	Ir(1)-C(1)-C(6)-C(5)	179.8(3)
Cl(1)-Ir(1)-P(1)-C(8)	70.44(18)	C(2)-C(1)-C(6)-C(7)	172.6(3)
C(1)-Ir(1)-P(1)-C(12)	109.53(17)	Ir(1)-C(1)-C(6)-C(7)	-6.2(5)
P(2)-Ir(1)-P(1)-C(12)	100.84(18)	C(4)-C(5)-C(6)-C(1)	1.6(6)
Cl(1)-Ir(1)-P(1)-C(12)	-68.91(16)	C(4)-C(5)-C(6)-C(7)	-172.1(4)
C(1)-Ir(1)-P(2)-C(7)	10.15(17)	C(1)-C(6)-C(7)-P(2)	15.4(5)
P(1)-Ir(1)-P(2)-C(7)	18.8(2)	C(5)-C(6)-C(7)-P(2)	-170.8(3)
Cl(1)-Ir(1)-P(2)-C(7)	-171.48(16)	C(20)-P(2)-C(7)-C(6)	103.9(3)
C(1)-Ir(1)-P(2)-C(20)	-103.39(16)	C(16)-P(2)-C(7)-C(6)	-138.5(3)
P(1)-Ir(1)-P(2)-C(20)	-94.72(18)	Ir(1)-P(2)-C(7)-C(6)	-15.9(3)
Cl(1)-Ir(1)-P(2)-C(20)	74.98(15)	O(1)-P(1)-C(8)-C(9)	-178.3(4)
C(1)-Ir(1)-P(2)-C(16)	123.3(2)	C(12)-P(1)-C(8)-C(9)	74.8(4)
P(1)-Ir(1)-P(2)-C(16)	131.9(2)	Ir(1)-P(1)-C(8)-C(9)	-64.5(4)
Cl(1)-Ir(1)-P(2)-C(16)	-58.35(19)	O(1)-P(1)-C(8)-C(11)	-59.1(5)
C(8)-P(1)-O(1)-C(2)	123.1(3)	C(12)-P(1)-C(8)-C(11)	-166.0(4)
C(12)-P(1)-O(1)-C(2)	-119.5(3)	Ir(1)-P(1)-C(8)-C(11)	54.7(5)
Ir(1)-P(1)-O(1)-C(2)	-1.4(3)	O(1)-P(1)-C(8)-C(10)	58.4(4)
P(1)-Ir(1)-C(1)-C(2)	-0.2(2)	C(12)-P(1)-C(8)-C(10)	-48.5(5)
P(2)-Ir(1)-C(1)-C(2)	177.3(2)	Ir(1)-P(1)-C(8)-C(10)	172.3(4)
Cl(1)-Ir(1)-C(1)-C(2)	42(3)	O(1)-P(1)-C(12)-C(13)	-164.3(4)
P(1)-Ir(1)-C(1)-C(6)	178.6(3)	C(8)-P(1)-C(12)-C(13)	-57.0(4)

P(2)-Ir(1)-C(1)-C(6)	-3.9(3)	Ir(1)-P(1)-C(12)-C(13)	84.5(4)
Cl(1)-Ir(1)-C(1)-C(6)	-139(2)	O(1)-P(1)-C(12)-C(15)	78.0(4)
C(6)-C(1)-C(2)-C(3)	-0.1(5)	C(8)-P(1)-C(12)-C(15)	-174.8(4)
Ir(1)-C(1)-C(2)-C(3)	178.7(3)	Ir(1)-P(1)-C(12)-C(15)	-33.3(4)
C(6)-C(1)-C(2)-O(1)	-179.5(3)	O(1)-P(1)-C(12)-C(14)	-36.5(4)
Ir(1)-C(1)-C(2)-O(1)	-0.6(4)	C(8)-P(1)-C(12)-C(14)	70.7(5)
P(1)-O(1)-C(2)-C(3)	-178.0(3)	Ir(1)-P(1)-C(12)-C(14)	-147.7(4)
P(1)-O(1)-C(2)-C(1)	1.4(4)	C(7)-P(2)-C(16)-C(19)	77.5(4)
C(1)-C(2)-C(3)-C(4)	1.4(5)	C(20)-P(2)-C(16)-C(19)	-169.3(3)
Ir(1)-P(2)-C(16)-C(19)	-34.9(4)	C(16)-P(2)-C(20)-C(21)	82.1(4)
C(7)-P(2)-C(16)-C(18)	-45.3(4)	Ir(1)-P(2)-C(20)-C(21)	-53.8(3)
C(20)-P(2)-C(16)-C(18)	67.9(4)	C(7)-P(2)-C(20)-C(22)	67.8(4)
Ir(1)-P(2)-C(16)-C(18)	-157.7(3)	C(16)-P(2)-C(20)-C(22)	-44.4(4)
C(7)-P(2)-C(16)-C(17)	-167.0(3)	Ir(1)-P(2)-C(20)-C(22)	179.7(3)
C(20)-P(2)-C(16)-C(17)	-53.9(3)	C(7)-P(2)-C(20)-C(23)	-50.4(3)
Ir(1)-P(2)-C(16)-C(17)	80.5(3)	C(16)-P(2)-C(20)-C(23)	-162.6(3)
C(7)-P(2)-C(20)-C(21)	-165.7(3)	Ir(1)-P(2)-C(20)-C(23)	61.5(3)

## 2.7. References

- (1) This chapter is partially adapted from the following paper: Nawara-Hultzs, A. J.; Hackenberg, J. D.; Punji, B.; Supplee, C.; Emge, T. J.; Bailey, B. C.; Schrock, R. R.; Brookhart, M.; Goldman, A. S. *ACS Catalysis*, **2013**, 3, 2505.
- (2) *Activation and Functionalization of C-H Bonds*; Goldberg, K. I.; Goldman, A. S., Eds.; American Chemical Society: Washington, D.C., 2004.
- (3) Findlater, M.; Choi, J.; Goldman, A. S.; Brookhart, M. In *Alkane C-H Activation by Single-Site Metal Catalysis*; Pérez, P. J., Ed.; Springer: New York, 2012; Vol. 38.
- (4) Crabtree, R. H.; Mihelcic, J. M.; Quirk, J. M. *J. Am. Chem. Soc.* **1979**, 101, 7738.
- (5) Felkin, H.; Fillebeen-Khan, T.; Gault, Y.; Holmes-Smith, R.; Zakrzewski, J. *Tetrahedron Lett.* **1984**, 25, 1279.
- (6) Felkin, H.; Fillebeen-Khan, T.; Holmes-Smith, R.; Lin, Y. *Tetrahedron Lett.* **1985**, 26, 1999.
- (7) Burk, M. J.; Crabtree, R. H. *J. Am. Chem. Soc.* **1987**, 109, 8025.
- (8) Aoki, T.; Crabtree, R. H. *Organometallics* **1993**, 12, 294.
- (9) Haibach, M. C.; Guan, C.; Wang, D. Y.; Li, B.; Lease, N.; Steffens, A. M.; Krogh-Jespersen, K.; Goldman, A. S. *J. Am. Chem. Soc.* **2013**, 135, 15062.
- (10) Choi, J.; MacArthur, A. H. R.; Brookhart, M.; Goldman, A. S. *Chem. Rev.* **2011**, 111, 1761.
- (11) Choi, J.; Goldman, A. S. *Top. Organomet. Chem.* **2011**, 34, 139.
- (12) Moulton, C. J.; Shaw, B. L. *J. Chem. Soc., Dalton Trans.* **1976**, 1020.
- (13) Gupta, M.; Hagen, C.; Flesher, R. J.; Kaska, W. C.; Jensen, C. M. *Chem. Commun.* **1996**, 2083.
- (14) Xu, W.; Rosini, G. P.; Gupta, M.; Jensen, C. M.; Kaska, W. C.; Krogh-Jespersen, K.; Goldman, A. S. *Chem. Commun.* **1997**, 2273.
- (15) Liu, F.; Pak, E. B.; Singh, B.; Jensen, C. M.; Goldman, A. S. *J. Am. Chem. Soc.* **1999**, 121, 4086.
- (16) Kanzelberger, M.; Singh, B.; Czerw, M.; Krogh-Jespersen, K.; Goldman, A. S. *J. Am. Chem. Soc.* **2000**, 122, 11017.
- (17) Krogh-Jespersen, K.; Czerw, M.; Zhu, K.; Singh, B.; Kanzelberger, M.; Darji, N.; Achord, P. D.; Renkema, K. B.; Goldman, A. S. *J. Am. Chem. Soc.* **2002**, 124, 10797.
- (18) Krogh-Jespersen, K.; Czerw, M.; Summa, N.; Renkema, K. B.; Achord, P. D.; Goldman, A. S. *J. Am. Chem. Soc.* **2002**, 124, 11404.
- (19) Krogh-Jespersen, K.; Czerw, M.; Goldman, A. S. *J. Mol. Cat., A* **2002**, 189, 95.
- (20) Renkema, K. B.; Kissin, Y. V.; Goldman, A. S. *J. Am. Chem. Soc.* **2003**, 125, 7770.
- (21) Biswas, S.; Huang, Z.; Choliy, Y.; Wang, D. Y.; Brookhart, M.; Krogh-Jespersen, K.; Goldman, A. S. *J. Am. Chem. Soc.* **2012**, 134, 13276.
- (22) Göttker-Schnetmann, I.; White, P.; Brookhart, M. *J. Am. Chem. Soc.* **2004**, 126, 1804.
- (23) Göttker-Schnetmann, I.; White, P. S.; Brookhart, M. *Organometallics* **2004**, 23, 1766.
- (24) Göttker-Schnetmann, I.; Brookhart, M. *J. Am. Chem. Soc.* **2004**, 126, 9330.

- (25) Biswas, S.; Brookhart, M.; Choliy, Y.; Goldman, A.; Huang, Z.; Krogh-Jespersen, K. In *Abstracts of Papers, 239th ACS National Meeting, San Francisco, CA, United States, March 21-25, 2010*, INOR 670.
- (26) Biswas, S.; Choliy, Y.; Krogh-Jespersen, K.; Brookhart, M.; Goldman, A. S. In *Abstracts of Papers, 238th ACS National Meeting, Washington, DC, United States, August 16-20, 2009*, INOR 479.
- (27) Przybilla, K. J.; Vögtle, F. *Chem. Ber.* **1989**, 122, 347.
- (28) Kennedy, A. R.; Cross, R. J.; Muir, K. W. *Inorg. Chim. Acta* **1995**, 231, 195.
- (29) Gupta, M.; Hagen, C.; Kaska, W. C.; Cramer, R. E.; Jensen, C. M. *J. Am. Chem. Soc.* **1997**, 119, 840.
- (30) Goldman, A. S.; Ghosh, R. In *Handbook of C-H Transformations - Applications in Organic Synthesis*; Dyker, G., Ed.; Wiley-VCH: New York, 2005, p 616.
- (31) Barrows, S. E.; Eberlein, T. H. *J. Chem. Ed.* **2005**, 82, 1334.
- (32) Liu, F.; Goldman, A. S. *Chem. Commun.* **1999**, 655.
- (33) Bruker-AXS. SADABS, Bruker area detector scaling and absorption correction, v2.05, Bruker-AXS Inc., Madison, Wisconsin, 2003; SAINTplus, Bruker area detector data reduction program, v6.45, Bruker-AXS Inc., Madison, Wisconsin, 2003.
- (34) Sheldrick, G. M. SHELX86, Program for the Solution of Crystal Structures, University of Göttingen, Germany, 1986.
- (35) Sheldrick, G. M. SHELXL97, Program for Crystal Structure Refinement, University of Göttingen, Germany, 1997.

## Chapter 3

### Alkane metathesis co-catalyzed by MoF12 and various iridium-pincer complexes<sup>1</sup>

#### Abstract

Both the bis-phosphine and bis-phosphinite pincer complexes (<sup>t</sup>Bu<sup>4</sup>PCP)IrH<sub>2</sub> (**3-1**) and (<sup>t</sup>Bu<sup>4</sup>POCOP)IrH<sub>2</sub> (**3-2**) can co-catalyze alkane metathesis in tandem with olefin metathesis catalysts, but the two complexes have different resting states during catalysis, suggesting that different steps are turnover-limiting in each case. This led to the hypothesis that a complex with intermediate properties would be catalytically more active than either of these two species. Accordingly, “hybrid” phosphine-phosphinite pincer ligands (PCOP') and the corresponding iridium complexes that were described in chapter 2 have been applied toward the metathesis of *n*-hexane. In tandem with olefin-metathesis catalyst **MoF12**, (<sup>t</sup>Bu<sup>4</sup>PCOP)IrH<sub>2</sub> (**3-3**) displays significantly higher activity for the metathesis of *n*-hexane than does (<sup>t</sup>Bu<sup>4</sup>PCP)IrH<sub>2</sub> (**3-1**) or (<sup>t</sup>Bu<sup>4</sup>POCOP)IrH<sub>2</sub> (**3-2**). (<sup>t</sup>Bu<sup>2</sup>PCOP<sup>i</sup>Pr<sup>2</sup>)IrH<sub>4</sub> (**3-4**) is even more active (>30-fold more active than (<sup>t</sup>Bu<sup>4</sup>POCOP)IrH<sub>2</sub>), and affords nearly 4.6 M alkane products after 8 h at 125 °C. The resting state of the (<sup>t</sup>Bu<sup>4</sup>PCCOP)Ir catalyst was studied and found to be a mixture of the resting states exhibited by its parent complexes, (<sup>t</sup>Bu<sup>4</sup>PCP)Ir and (<sup>t</sup>Bu<sup>4</sup>POCOP)Ir.

### 3.1 Introduction

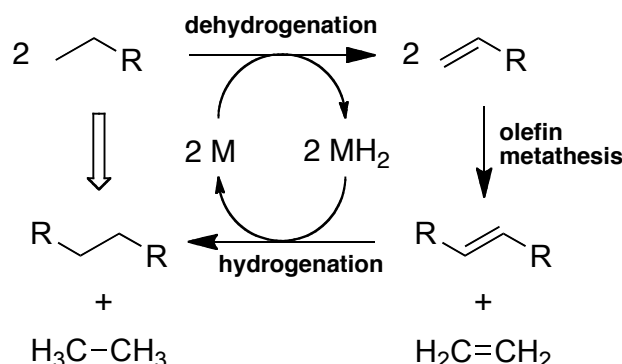
The gap between global consumption of liquid fuels and production of conventional crude oil is expected to widen dramatically over the next several decades.<sup>2-4</sup> While conventional crude is the source of greater than 90% of liquid fuel consumed today, it is estimated that this fraction will decline to roughly 50% by 2050 and perhaps 15% by 2080;<sup>2</sup> regardless of any uncertainty in the rate of decline, the outcome in the absence of new discoveries is inevitable. The gap will be met by large increases in the use of “natural gas liquids” and condensates (low molecular weight hydrocarbons from geologic sources) and, especially, “unconventional liquids” of origin that is yet to be determined.<sup>2,5</sup> Fischer-Tropsch (F-T) catalysis is likely to play an important role in the context of unconventional liquid fuel production.<sup>6-8</sup> The feedstock for F-T may be derived from coal or natural gas (the current sources for commercial reactors), from biomass (for potentially carbon-neutral biofuels),<sup>9-13</sup> or from CO<sub>2</sub>/H<sub>2</sub>O with energy input from carbon-free sources.<sup>14-17</sup>

The increased demand for liquid fuel is driven specifically by increased demand for diesel and jet fuel,<sup>4,18</sup> both of which are generally of high molecular weight (typically *ca.* C<sub>9</sub>-C<sub>19</sub> and C<sub>8</sub>-C<sub>16</sub> respectively). While F-T catalysis followed by hydrocracking of the heavier products can give high yields in this range, lighter *n*-alkanes are still produced in substantial amounts. Further, natural gas liquids and condensates are composed exclusively of alkanes with molecular weights well below this desirable range. Thus, we can anticipate a critical need for the development of practical methods for the large-scale catalytic conversion of lighter alkanes to heavier molecular weight species.

The only general method reported to date for the direct conversion of light alkanes to heavier alkanes is alkane metathesis. Alkane metathesis with heterogeneous catalysts has been reported by Burnett and Hughes,<sup>19</sup> and, more recently, by Basset and Coperet *et al.*<sup>20</sup> Burnett and Hughes had found high-temperature (400 °C) conversion of *n*-hexane to a broad distribution of *n*-alkanes using a mixture two heterogeneous catalysts (Pt/alumina for transfer dehydrogenation and tungsten oxide/silica for olefin metathesis). Several decades later, Basset and Coperet reported another heterogeneous process operating at a much lower temperature (150 °C) that was capable of converting lower molecular weight alkanes to other generally low molecular weight products using tantalum hydride complexes supported on silica. While these systems represent major breakthroughs, they suffer from critical limitations including the need for severe reaction conditions, relatively low reaction rates, and low selectivity with respect to the formation of higher molecular weight and unbranched species.

Our group has previously reported the relatively low temperature (125 °C) catalytic metathesis of *n*-alkanes based on a tandem process that utilizes an iridium-based catalyst for alkane dehydrogenation and an olefin metathesis catalyst to metathesize the alkenes generated *in situ* (**scheme 3.1**).<sup>21-23</sup> The hydrogen removed from the alkanes is then used to hydrogenate the metathesized olefin products. Since the olefin metathesis catalysts afford high reaction rates even at ambient temperatures, whereas alkane metathesis and simple transfer-dehydrogenation require temperatures over 100 °C to achieve even modest rates, it is presumed that the transfer-dehydrogenation component limits the rate of alkane metathesis; however, it is not obvious which segment of the transfer-dehydrogenation cycle (hydrogenation or dehydrogenation) is rate-limiting.

**Scheme 3.1.** Alkane metathesis via tandem catalysis (transfer dehydrogenation and olefin metathesis).



Our previous reports have focused on PCP- and POCOP-ligated iridium catalysts (**figure 3.1: 3-1** and **3-2**, respectively) for dehydrogenation<sup>21,22</sup> in combination with various types of olefin metathesis catalysts, including molecular species, such as  $\text{Mo}(\text{NAr})(\text{CHCMe}_2\text{Ph})[\text{OCMe}(\text{CF}_3)_2]_2$  ( $\text{Ar}=2,6\text{-}i\text{-PrC}_6\text{H}_3$ ) (**MoF12**),<sup>24</sup> as well as traditional heterogeneous olefin metathesis catalysts, like  $\text{Re}_2\text{O}_7$  on  $\gamma$ -alumina.<sup>25</sup> In our initial work we observed that similar rates of alkane metathesis were obtained with PCP and POCOP iridium species (operating in tandem with **MoF12**).<sup>20,21</sup> Interestingly, despite the seemingly similar rates of alkane metathesis, different resting states have been observed for (PCP)Ir- and (POCOP)Ir-catalyzed processes; in the case of (PCP)Ir catalysis, the resting state is the dihydride species, while for (POCOP)Ir, the resting state is an olefin-bound species (**figure 3.2**).<sup>21</sup> The observed difference in resting states therefore implies that although the pathways may be analogous, the respective rate-determining steps in the catalytic cycles are different for the two catalysts. Specifically, the  $(^{\text{tBu}}\text{PCP})\text{IrH}_2$  resting state implies that olefin hydrogenation is rate-determining while the  $(^{\text{tBu}}\text{POCOP})\text{Ir}(\text{olefin})$  resting state implies that the rate-determining step involves



loss of olefin (possibly reversible) followed by alkane dehydrogenation. Moreover, this suggests that the corresponding step for each catalyst that is *not* rate-determining is relatively fast, (e.g. olefin hydrogenation by  $(^t\text{Bu}^4\text{POCOP})\text{IrH}_2$ ).<sup>26</sup> Thus for the  $^t\text{Bu}^4\text{PCPIr}$  catalyst the olefin-hydrogenation segment of the cycle is relatively slow and the alkane-dehydrogenation segment (including dissociation of olefin to give the active fragment, (pincer)Ir)<sup>27</sup> is relatively fast, while the converse is true for the  $^t\text{Bu}^4\text{POCOP}$  catalyst.

**Figure 3.1.** Catalysts employed in alkane metathesis reactions.

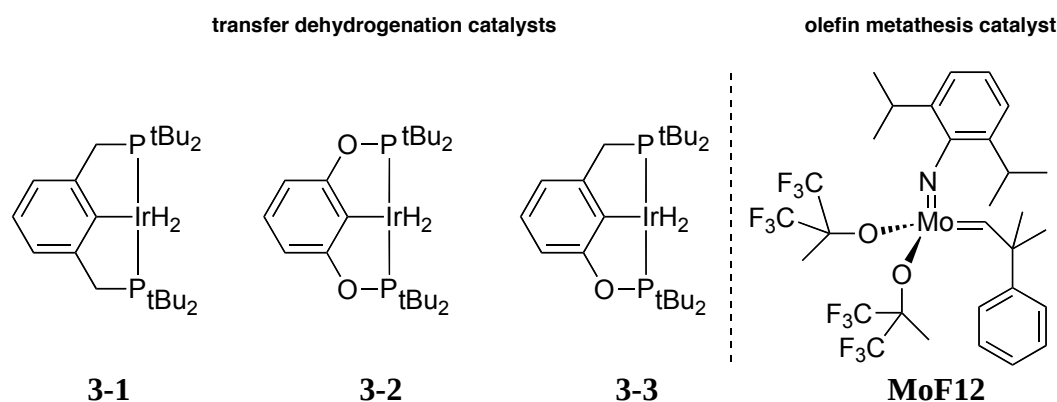
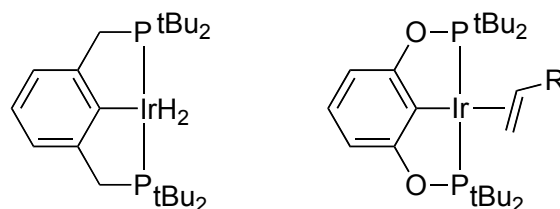


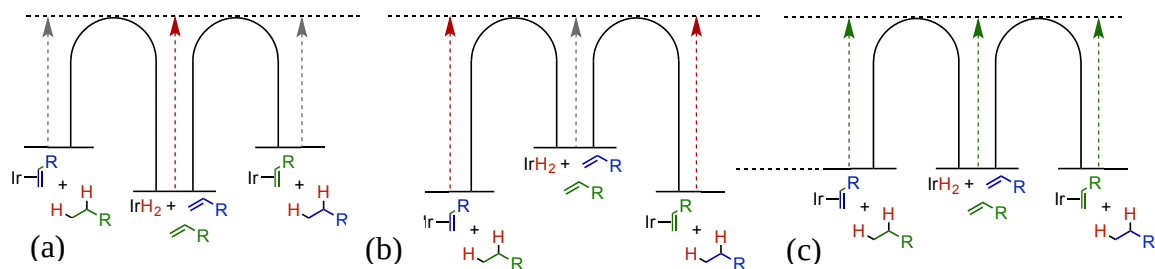
**Figure 3.2.** Resting states of  $(^t\text{Bu}^4\text{PCP})\text{Ir}$  (**3-1**) and  $(^t\text{Bu}^4\text{POCOP})\text{Ir}$  (**3-2**) previously observed in alkane metathesis.



We considered the possibility that if the catalytic cycles of the  $^t\text{Bu}^4\text{PCP}$  and  $^t\text{Bu}^4\text{POCOP}$  catalysts include converse sets of one slow and one fast segment, then the catalytic cycle of a species whose properties are intermediate between  $^t\text{Bu}^4\text{PCP}$  and

$^t\text{Bu}^4\text{POCOP}$  could contain two segments with rates that are each intermediate between the two extremes. If indeed the two segments have intermediate rates, rather than one fast and one slow, the overall catalytic rate of such a species would be *faster* than that of either  $^t\text{Bu}^4\text{PCP}$  or  $^t\text{Bu}^4\text{POCOP}$  catalysts; the energetics of such catalysis is envisioned in the *hypothetical* free energy schematic in **figure 3.3**. The most obvious candidate for a species with intermediate reactivity between that of  $(^t\text{Bu}^4\text{PCP})\text{Ir}$  and  $(^t\text{Bu}^4\text{POCOP})\text{Ir}$  catalysts would be a “hybrid” phosphine-phosphinite species  $(^t\text{Bu}^4\text{PCOP})\text{Ir}$  (**figure 3.1: 3-3**). In this chapter, we report that these hybrid PCOP complexes are indeed found to be highly effective, yielding the highest catalytic activities reported to date for this class of alkane metathesis catalysts.

**Figure 3.3.** Schematic diagram indicating relative overall free energy barriers, under alkane metathesis conditions, for the alkane dehydrogenation and olefin hydrogenation segments of the transfer-dehydrogenation catalytic cycle, for (a)  $(^t\text{Bu}^4\text{PCP})\text{Ir}$ , (b)  $(^t\text{Bu}^4\text{POCOP})\text{Ir}$ , (c) a hypothetical species with properties intermediate between  $(^t\text{Bu}^4\text{PCP})\text{Ir}$  and  $(^t\text{Bu}^4\text{POCOP})\text{Ir}$ .



## 3.2 Results and Discussion

### 3.2.1 Comparing the catalytic activity of the hybrid catalyst, $^{t\text{Bu}}\text{PCOPIr}$ , to its parent complexes, $^{t\text{Bu}}\text{PCPIr}$ and $^{t\text{Bu}}\text{POCOPIr}$ , in *n*-hexane alkane metathesis

Alkane metathesis reactions catalyzed by  $(^{t\text{Bu}}\text{PCOP})\text{IrH}_2$  (**3-3**) as well as the previously reported symmetrical parent complexes  $(^{t\text{Bu}}\text{POCOP})\text{IrH}_2$  (**3-2**) and  $(^{t\text{Bu}}\text{PCP})\text{IrH}_2$  (**3-1**) were performed with 10 mM of the (pincer)Ir catalyst, 16 mM of the olefin metathesis catalyst,  $\text{Mo}(\text{NAr})(\text{CHCMe}_2\text{Ph})[\text{OCMe}(\text{CF}_3)_2]$  ( $\text{Ar} = 2,6\text{-}i\text{-PrC}_6\text{H}_3$ ) (**MoF12**), 30 mM mesitylene (internal GC standard), and *n*-hexane as the solvent/substrate (*ca.* 7.6 M). 20 mM 3,3-dimethyl-1-butene (TBE) was added as a hydrogen acceptor to dehydrogenate the active catalyst and to generate a steady-state concentration of olefin. All experiments were performed under an argon atmosphere. Reactions were conducted at 125 °C in flame-sealed tubes, and the progress of the reaction was monitored by gas chromatography at intervals of 1, 3, 8, and 24 hours, with three tubes analyzed at each time. Reported values are the average of the three samples.

Complex **3-3** is found to be a remarkably active catalyst (**Table 3.1** and **figure 3.4**), strongly supporting the hypothesis that a “hybrid” species with properties intermediate between those of  $(^{t\text{Bu}}\text{POCOP})\text{Ir}$  and  $(^{t\text{Bu}}\text{PCP})\text{Ir}$  would display activity greater than that of either of the symmetrical complexes. For the first 8 hours all three catalysts display roughly constant turnover frequencies. The relative conversions for  $(^{t\text{Bu}}\text{POCOP})\text{Ir}$  (**3-2**),  $(^{t\text{Bu}}\text{PCP})\text{Ir}$  (**3-1**), and  $(^{t\text{Bu}}\text{PCOP})\text{Ir}$  (**3-3**) are approximately 1 : 2.1 : 7.4 after one hour, 1 : 2.2 : 8.4 after three hours, and 1 : 1.8 : 7.0 after eight hours. Since a larger fraction of the hexane has undergone conversion in the  $(^{t\text{Bu}}\text{PCOP})\text{Ir}$ -catalyzed reactions (e.g. 41% after 8 h), the values indicated for this catalyst are somewhat lower

than the actual relative rates due to increased back-reactions that produce hexane as well as the decreased rate of reaction with hexane due to its lowered concentration.

**Table 3.1.** Concentrations (mM) of products formed by metathesis of *n*-hexane catalyzed by **MoF12** (16 mM) and (pincer)Ir catalysts **3-1**, **3-2**, and **3-3** (10 mM) at 125 °C. Values reported are average of three runs.

Catalyst 3-1, ( <sup>t</sup> Bu <sub>2</sub> PCP <sup>t</sup> Bu <sub>2</sub> )IrH <sub>2</sub>												Selectivity
t(h)	C2	C3	C4	C5	C7	C8	C9	<i>trans</i> -5-decene	C10	C11-19	[Total product]	C10/(C7-10)
1	21	14	21	22	11	1	4	11	7	0	113	0.55
3	63	52	30	100	57	6	10	14	38	1	370	0.42
8	165	96	62	200	121	14	19	12	106	10	805	0.43
24	295	158	119	303	167	26	32	7	202	25	1335	0.48

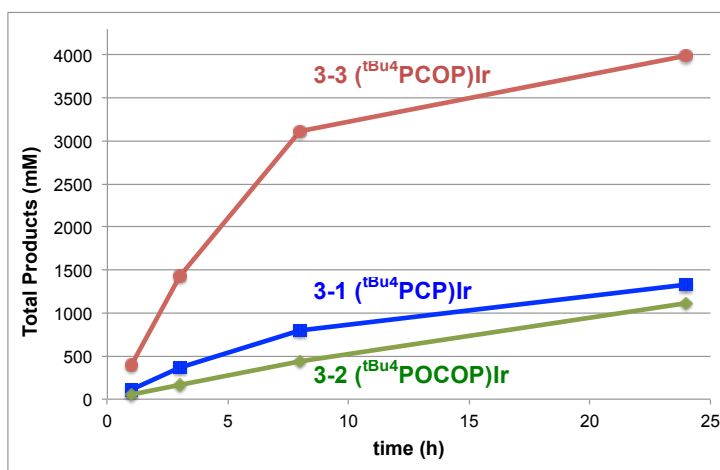
  

Catalyst 3-2, ( <sup>t</sup> Bu <sub>2</sub> POCOP <sup>t</sup> Bu <sub>2</sub> )IrH <sub>2</sub>												Selectivity
t(h)	C2	C3	C4	C5	C7	C8	C9	<i>trans</i> -5-decene	C10	C11-19	[Total product]	C10/(C7-10)
1	2	12	11	10	7	4	3	2	2	1	54	0.22
3	4	38	34	34	22	14	9	2	6	7	171	0.15
8	7	93	81	94	64	40	28	1	19	14	442	0.13
24	15	232	194	249	168	98	76	1	47	33	1111	0.12

Catalyst 3-3, ( <sup>t</sup> Bu <sub>2</sub> PCCOP <sup>t</sup> Bu <sub>2</sub> )IrH <sub>2</sub>												Selectivity
t(h)	C2	C3	C4	C5	C7	C8	C9	<i>trans</i> -5-decene	C10	C11-19	[Total product]	C10/(C7-10)
1	12	82	53	103	67	28	20	2	19	15	401	0.16
3	33	317	215	339	233	115	74	2	55	53	1437	0.12
8	85	708	495	727	477	234	145	2	104	134	3111	0.11
24	156	896	639	948	576	267	183	2	162	168	3997	0.14

**Figure 3.4.** Total product concentrations formed by *n*-hexane metathesis catalyzed by **MoF12** and (pincer)Ir catalysts **3-1**, **3-2**, and **3-3** over the first 24 hours at 125 °C.



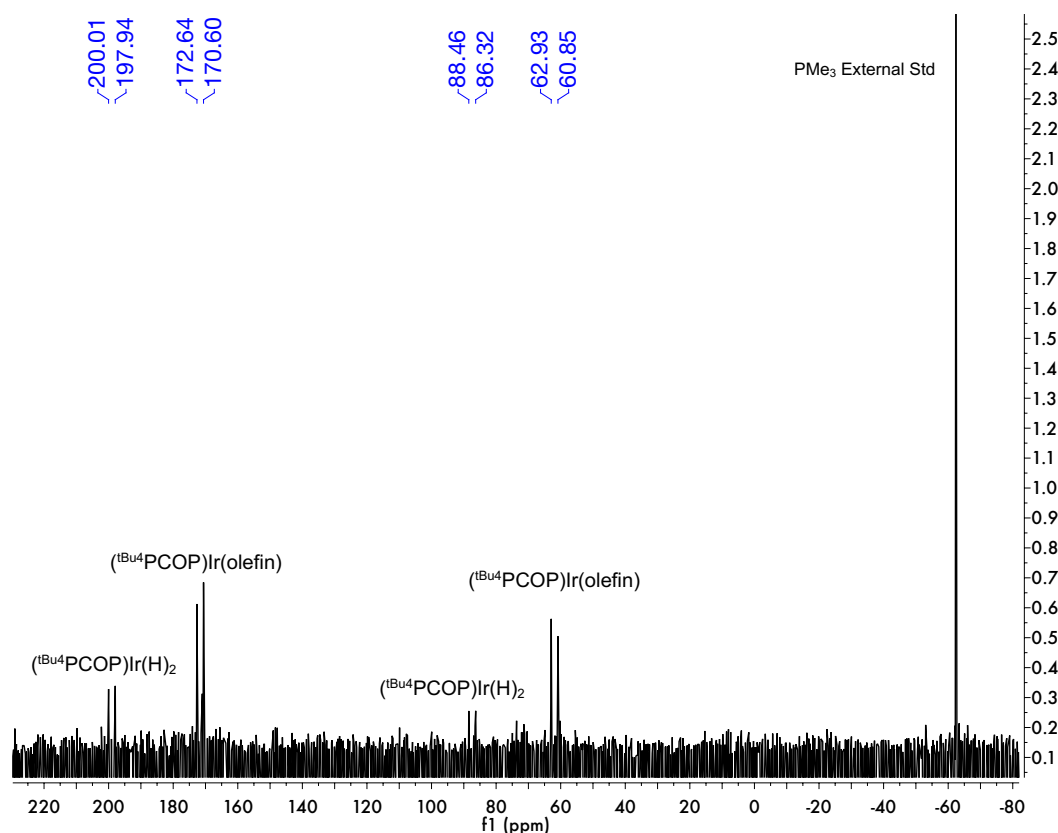
After 8 h, the reaction rates decrease. This presumably reflects decomposition of the **MoF12** catalyst,<sup>21,24,28,29</sup> decreased concentration of hexane (particularly in the case of catalyst **3-3**), and possibly some decomposition of (pincer)Ir. The concentration of total products obtained with **3-3** at 24 h is 4.0 M (*ca.* 52% conversion).

### 3.2.2 Resting State of (<sup>t</sup>Bu<sup>4</sup>PCOP)Ir (**3-3**) in alkane metathesis

Our initial hypothesis was based on the premise that the transfer dehydrogenation cycles of (<sup>t</sup>Bu<sup>4</sup>PCP)Ir and (<sup>t</sup>Bu<sup>4</sup>POCOP)Ir each had one fast segment and one slow segment (for (<sup>t</sup>Bu<sup>4</sup>PCP)Ir alkane dehydrogenation is fast and olefin hydrogenation is slow while the reverse is true for (<sup>t</sup>Bu<sup>4</sup>POCOP)Ir); a hybrid species would approach a limit whereby the rates of the two segments would be intermediate between the two extremes and the overall rate would therefore be greater.

To test the validity of this reasoning we investigated the nature of the resting state in the (<sup>t</sup>Bu<sup>4</sup>PCOP)Ir-catalyzed reaction. A *n*-hexane solution of (<sup>t</sup>Bu<sup>4</sup>PCOP)IrH<sub>2</sub> (**3-3**) (10 mM), **MoF12** (16 mM), TBE (40 mM), was prepared and monitored by <sup>31</sup>P NMR at 90 °C. After 60 min it exhibited two major sets of signals, a smaller set attributable to (<sup>t</sup>Bu<sup>4</sup>PCOP)IrH<sub>2</sub> and a larger set (a doublet at d 171.2 ppm and doublet at d 67.6 ppm) which appeared to be attributable to the olefin-bound complex (**figure 3.5**). In a separate NMR tube, 40 mM 1-hexene was added to a *p*-xylene-*d*<sub>10</sub> solution of 10 mM <sup>t</sup>Bu<sup>4</sup>PCOPIrH<sub>2</sub>; this yielded the doublets at 171.2 and 67.6 ppm in the <sup>31</sup>P NMR spectrum, indicating that the larger set of peaks is indeed attributable to an olefin-bound species. Thus, the mixture of hydride and olefin complex in the alkane solutions confirms that the rates of alkane dehydrogenation and olefin hydrogenation are indeed comparable with this catalyst.

**Figure 3.5.**  $^{31}\text{P}\{^1\text{H}\}$  NMR spectrum of  $(^t\text{Bu}^4\text{PCOP})\text{Ir}$  during alkane (*n*-hexane) metathesis after 1 hour at 90 °C, revealing the mixed catalyst resting state.

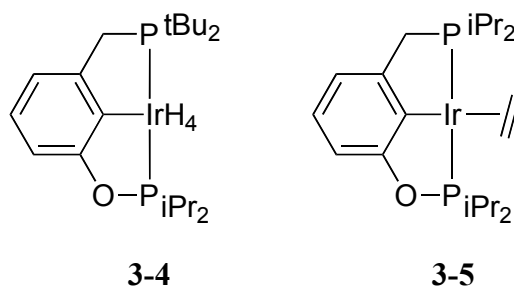


### 3.2.3 Alkane metathesis with other hybrid (PCOP)Ir catalysts

In addition to the differences in sterics introduced by replacing the  $-\text{CH}_2-$  methylene unit in the pincer ligand with an O atom, one may also alter the sterics by varying the substituents on the phosphine moieties. Our group has previously found that even seemingly subtle substitutions on the phosphine can have large effects on reactivity and selectivity.<sup>25</sup> To this end, we sought to examine the effect of varying the substituents on each phosphorus atom. In analogy to the preparation of  $^t\text{Bu}^4\text{PCOP}$ ,  $^t\text{Bu}^2\text{PCOP}^{i\text{Pr}^2}$  and  $^{i\text{Pr}^4}\text{PCOP}$  were prepared by Benudhar Punji<sup>1</sup>; these ligands were then metalated with

$[\text{Ir}(\text{COD})\text{Cl}]_2$  to yield the corresponding hydrido chloride complexes, which were reduced under  $\text{H}_2$  ( $^{\text{tBu}_2}\text{PCOP}^{\text{iPr}_2}$ ) or ethylene ( $^{\text{iPr}_4}\text{PCOP}$ ) atmosphere to yield the tetrahydride (**3-4**) and ethylene (**3-5**) complexes, respectively.

**Figure 3.6.** Other hybrid (PCOP)Ir catalysts.



$(^{\text{tBu}_2}\text{PCOP}^{\text{iPr}_2})\text{IrH}_4$  (**3-4**) afforded catalytic rates even greater than those of  $(^{\text{tBu}_4}\text{PCOP})\text{IrH}_2$  (**3-3**) (**table 3.2** and **figure 3.7**). After 1 hour at 150 °C and under identical reaction conditions as employed for the above studies, 1.75 M metathesis products were obtained, representing a rate 4.4 times that of **3-3** or *ca.* 32 times that of  $(^{\text{tBu}_4}\text{POCOP})\text{IrH}_2$  (**3-2**). After 3 h and 8 h, 3.2 M and 4.6 M product was observed. **3-4** is the most active (pincer)Ir dehydrogenation catalyst for alkane metathesis reported to date.

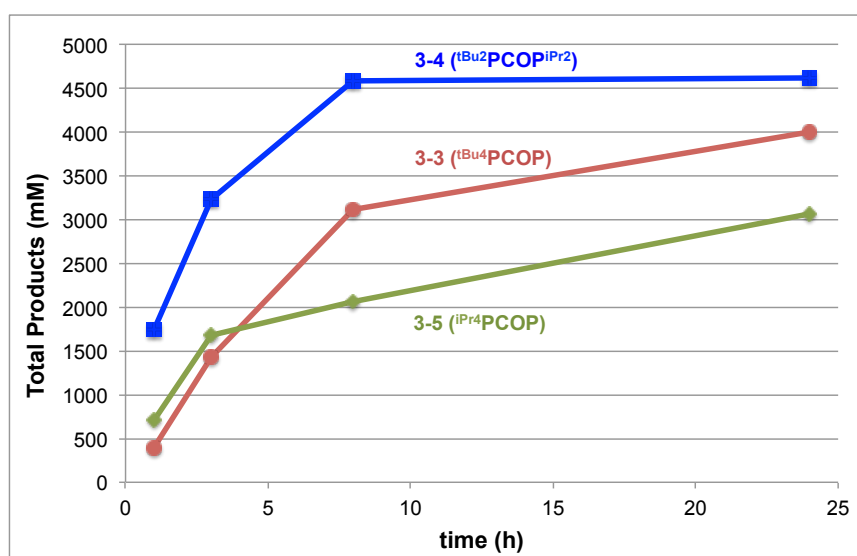
**Table 3.2.** Concentrations (mM) of products formed by metathesis of *n*-hexane catalyzed by **MoF12** (16 mM) and (PCOP)Ir catalysts **3-4** and **3-5** (10 mM) at 125 °C. Values reported are average of three runs.

Catalyst 3-4, ( <sup>t</sup> Bu <sub>2</sub> PCCOP <sup>i</sup> Pr <sub>2</sub> )IrH <sub>n</sub>												
t(h)	C2	C3	C4	C5	C7	C8	C9	<i>trans</i> -5-decene	C10	C11-19	[Total product]	Selectivity C10/(C7-10)
1	133	339	248	385	224	105	120	4	143	48	1750	0.25
3	220	595	509	754	441	218	204	2	193	99	3234	0.18
8	450	986	764	969	535	278	234	1	190	187	4594	0.15
24	344	974	792	1029	572	293	242	1	189	183	4619	0.15

Catalyst 3-5, ( <sup>i</sup> Pr <sub>2</sub> PCCOP <sup>i</sup> Pr <sub>2</sub> )Ir(C <sub>2</sub> H <sub>4</sub> )												
t(h)	C2	C3	C4	C5	C7	C8	C9	<i>trans</i> -5-decene	C10	C11-19	[Total product]	Selectivity C10/(C7-10)
1	25	119	78	179	118	46	69	1	67	10	712	0.23
3	55	307	202	424	256	102	138	3	169	31	1687	0.26
8	70	398	261	521	298	117	153	4	200	44	2066	0.26
24	127	717	463	771	368	146	167	0	197	120	3076	0.22

**Figure 3.7.** Total alkane products formed in the metathesis of *n*-hexane catalyzed by **MoF12** and (PCOP)Ir catalysts **3-3**, **3-4**, and **3-5** over the first 24 h of reaction at 125 °C.





(<sup>i</sup>Pr<sup>4</sup>PCOP)Ir(C<sub>2</sub>H<sub>4</sub>) (**3-5**) was also found to give a higher turnover number after 1 hour than the (<sup>t</sup>Bu<sup>4</sup>PCOP)Ir precursor **3-3**, but not as great as obtained with **3-4**. Moreover, productivity leveled off with **3-5** earlier than with catalysts **3-(1-4)**; it seems likely this is due to bimolecular degradation of the less sterically hindered complex, possibly dimerization or perhaps a reaction with **MoF12** or its degradation products.

### 3.2.4 Comparison of the selectivities of various (pincer)Ir catalysts

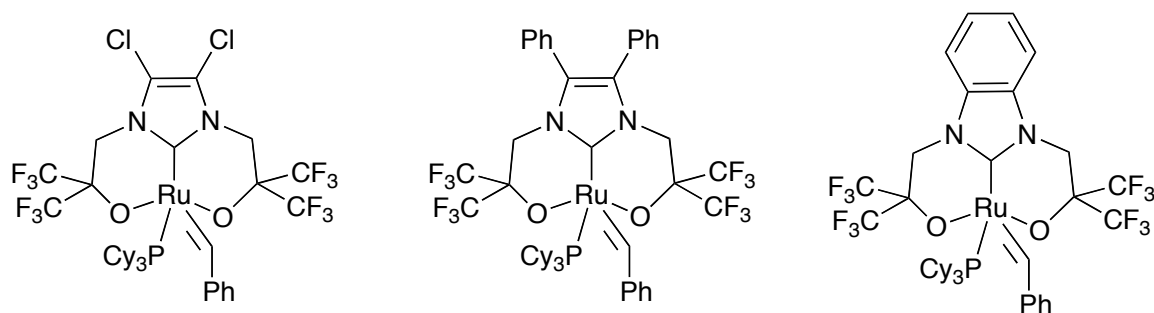
The molecular-weight or chain-length selectivity obtained with all three (PCOP)Ir catalysts was similar to that obtained with (<sup>t</sup>Bu<sup>4</sup>POCOP)Ir and not intermediate between (<sup>t</sup>Bu<sup>4</sup>POCOP)Ir and (<sup>t</sup>Bu<sup>4</sup>PCP)Ir (the latter is much more selective for the formation of C<sub>2n-2</sub> alkanes and ethane from C<sub>n</sub> alkanes, in this case *n*-decane and ethane from *n*-hexane). We believe that the large selectivity difference observed for the (<sup>t</sup>Bu<sup>4</sup>POCOP)Ir and (<sup>t</sup>Bu<sup>4</sup>PCP)Ir-based catalysts in alkane metathesis reflects different regioselectivities of alkane dehydrogenation, which results from the two catalysts having a different rate- and product-determining step (e.g. C-H addition, β-H elimination, or olefin loss) in the overall alkane dehydrogenation.<sup>30</sup> The similar selectivity (or lack thereof) in alkane metathesis observed for the (PCOP)Ir complexes and (<sup>t</sup>Bu<sup>4</sup>POCOP)Ir suggests that these complexes all have the same rate- and product-determining step within the alkane dehydrogenation sequence (or at least that they do not share the same rate- and product-determining step as (<sup>t</sup>Bu<sup>4</sup>PCP)Ir).

### 3.2.5 (<sup>t</sup>Bu<sup>4</sup>PCOP)IrH<sub>2</sub> (**3-3**) and Arduengo olefin metathesis catalysts

Our work with homogeneous alkane metathesis has largely focused the use of “Schrock-type” alkylidene catalysts for olefin metathesis. We have previously found that “Grubbs-type” olefin metathesis catalysts are incompatible with the iridium-pincer

complexes, particularly when the Grubbs catalyst has a chloride bound to it. In the course of our work with hybrid PCOP catalysts, we further attempted to perform alkane metathesis of *n*-hexane with several “Grubbs-like” Ru-alkylidene co-catalysts that did not bear metal-bound chloride ligands (**figure 3.8**). Unfortunately, none of these Ru-alkylidene complexes had any significant activity toward *n*-hexane metathesis; the relatively small amount of initially formed metathesis products did not change over time, likely indicating that decomposition of the olefin metathesis catalyst occurs after relatively few turnovers, perhaps with subsequent degradation of the iridium-pincer catalyst.

**Figure 3.8.** Various Ru-alkylidene complexes attempted as olefin metathesis co-catalysts in alkane metathesis of *n*-hexane.



### 3.3 Summary

Bis-phosphine complex (<sup>t</sup>Bu<sup>4</sup>PCP)Ir (**3-1**) and bis-phosphinite complex (<sup>t</sup>Bu<sup>4</sup>POCOP)Ir (**3-2**), previously reported to catalyze alkane metathesis in tandem with **MoF12**, catalyze transfer dehydrogenation with similar rates under typical alkane metathesis conditions. Different resting states observed for each catalyst, however, indicate that different segments of the transfer dehydrogenation cycle are rate-

determining in each case. This observation led to the hypothesis that for a species with intermediate properties, neither segment of its catalytic cycle would be as slow as the respective rate-determining segments for (<sup>t</sup>Bu<sup>4</sup>PCP)Ir and (<sup>t</sup>Bu<sup>4</sup>POCOP)Ir, and thus the overall rate of catalysis would be faster. Indeed, the “hybrid” phosphine-phosphinite catalyst (<sup>t</sup>Bu<sup>4</sup>PCOP)Ir is found to co-catalyze alkane metathesis ca. 4 and 8 times faster than (<sup>t</sup>Bu<sup>4</sup>PCP)Ir and (<sup>t</sup>Bu<sup>4</sup>POCOP)Ir, respectively, and affords higher total turnover numbers. In accord with the idea that the hybrid catalyst approaches a balance whereby the hydrogenation and dehydrogenation segments of the catalytic cycle are comparably fast under catalytic conditions, the resting state is found to be a mixture of dihydride and dehydrogenated (olefin-bound) complex.

Decreasing the steric bulk of the phosphine-phosphinite pincer led to the synthesis of catalyst precursor (<sup>t</sup>Bu<sup>2</sup>PCOP<sup>i</sup>Pr<sup>2</sup>)IrH<sub>4</sub> (**3-4**) which exhibits rates of catalysis about a factor of four faster than (<sup>t</sup>Bu<sup>4</sup>PCOP)IrH<sub>2</sub>, *i.e.* nearly 32 times faster than (<sup>t</sup>Bu<sup>4</sup>POCOP)Ir. Further decreasing steric crowding led to a (<sup>i</sup>Pr<sup>4</sup>PCOP)Ir precursor (the corresponding ethylene complex) which gave rates faster than (<sup>t</sup>Bu<sup>4</sup>PCOP)Ir but slower than (<sup>t</sup>Bu<sup>2</sup>PCOP<sup>i</sup>Pr<sup>2</sup>)IrH<sub>4</sub>, and appeared to undergo decomposition more readily than the other catalysts studied.

### 3.4 Acknowledgments

We would like to express our gratitude to Drs. Brad Bailey, Jian Yuan, and Richard Schrock for their generous donation of the **MoF12** catalyst. We thank Drs. Jason Runyon and A. J. Arduengo for donation of the Ru-alkylidene complexes.

### 3.5 Experimental

**General Considerations.** All manipulations were conducted under an argon atmosphere either in a glove box or using standard Schlenk techniques. All anhydrous solvents were purchased from Aldrich, flushed with argon, and stored in an argon atmosphere in the glove box. Mesitylene, *n*-hexane (anhydrous, 99%+), *tert*-butylethylene (TBE; 3,3-dimethyl-1-butene, 98%) were purchased from Aldrich and were distilled over Na/benzophenone and stored in the glove box. (<sup>t</sup>Bu<sup>4</sup>PCP)IrH<sub>2</sub> (**3-1**),<sup>31</sup> (<sup>t</sup>Bu<sup>4</sup>POCOP)IrH<sub>2</sub> (**3-2**),<sup>32</sup> and Mo(NAr(CHCMe<sub>2</sub>Ph)(OCMe(CF<sub>3</sub>)<sub>2</sub>) (Ar=2,6-*i*-PrC<sub>6</sub>H<sub>3</sub>) (**MoF12**)<sup>33</sup> were prepared as described previously. <sup>1</sup>Pr<sub>2</sub>PCl and <sup>1</sup>Bu<sub>2</sub>PCl were used as purchased from Strem Chemicals, Inc. All glassware was flame-dried and placed in a vacuum oven at least 24 hours prior to use. NMR spectra were recorded on 400-MHz Varian VNMRS spectrometer. <sup>1</sup>H NMR spectra are referenced to residual *protio* signal in the deuterated solvent. <sup>31</sup>P{<sup>1</sup>H} NMR chemical shifts are referenced to an external standard consisting of PMe<sub>3</sub> (δ -62.4 ppm) in *p*-xylene-d<sub>10</sub> solvent inside a flame-sealed capillary tube.

**Representative Procedure for Alkane Metathesis Experiment.** In an argon-filled glove box, a 20-mL vial was charged with the (pincer)Ir catalysts (0.050 mmol) and the **MoF12** catalyst (0.080 mmol). 5.0 mL of an *n*-hexane solution containing mesitylene (0.162 mmol as an internal standard) and TBE (0.100 mmol for dihydrides, 0.200 mmol for tetrahydride, none for ethylene complex) was added and the solution was thoroughly mixed. Twelve aliquots of this stock solution (0.400 mL each) were then syringed into glass tubes (5 mm x 120 mm). Vacuum adapters were fixed onto the tubes via plastic tubing to allow for flame-sealing. Samples were frozen in liquid nitrogen and the

headspace was evacuated on a high vacuum line, after which the glass tubes were flame-sealed so that the ratio between liquid phase and headspace was approximately 1:1. The samples were placed in a temperature-calibrated GC oven at 125 °C. Tubes were taken from the oven at appropriate intervals and frozen in liquid nitrogen to minimize the escape of volatile alkanes. The seal of each tube was then broken and quickly capped with a 5-mm rubber septum. The sample was then brought back to room temperature and promptly analyzed by GC.

### **GC Separation Method**

Gas chromatography was performed on a Varian 430 gas chromatograph utilizing flame ionization detection with the following parameters:

Column: 30 m × 0.25 mm × 0.5µm Supelco Fused silica capillary column, Petrocol<sup>TM</sup>, HD

Starting temperature: 38 °C

Time at starting temp: 1.4 min

Ramp: 20 °C/min to temperature of 250 °C, hold time 3 min

Ramp 280 °C at 30 °C/min, hold time 35 min

Flow rate: 1 mL/min (He)

Split ratio: 90

Ending temp: 280 °C

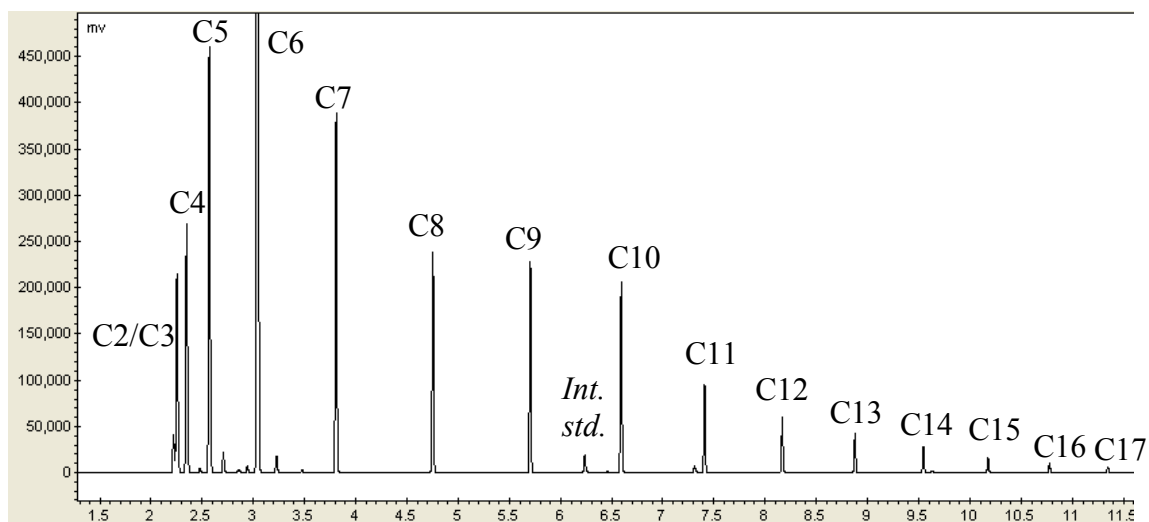
Injector temp: 300 °C

Detector temp: 310 °C.

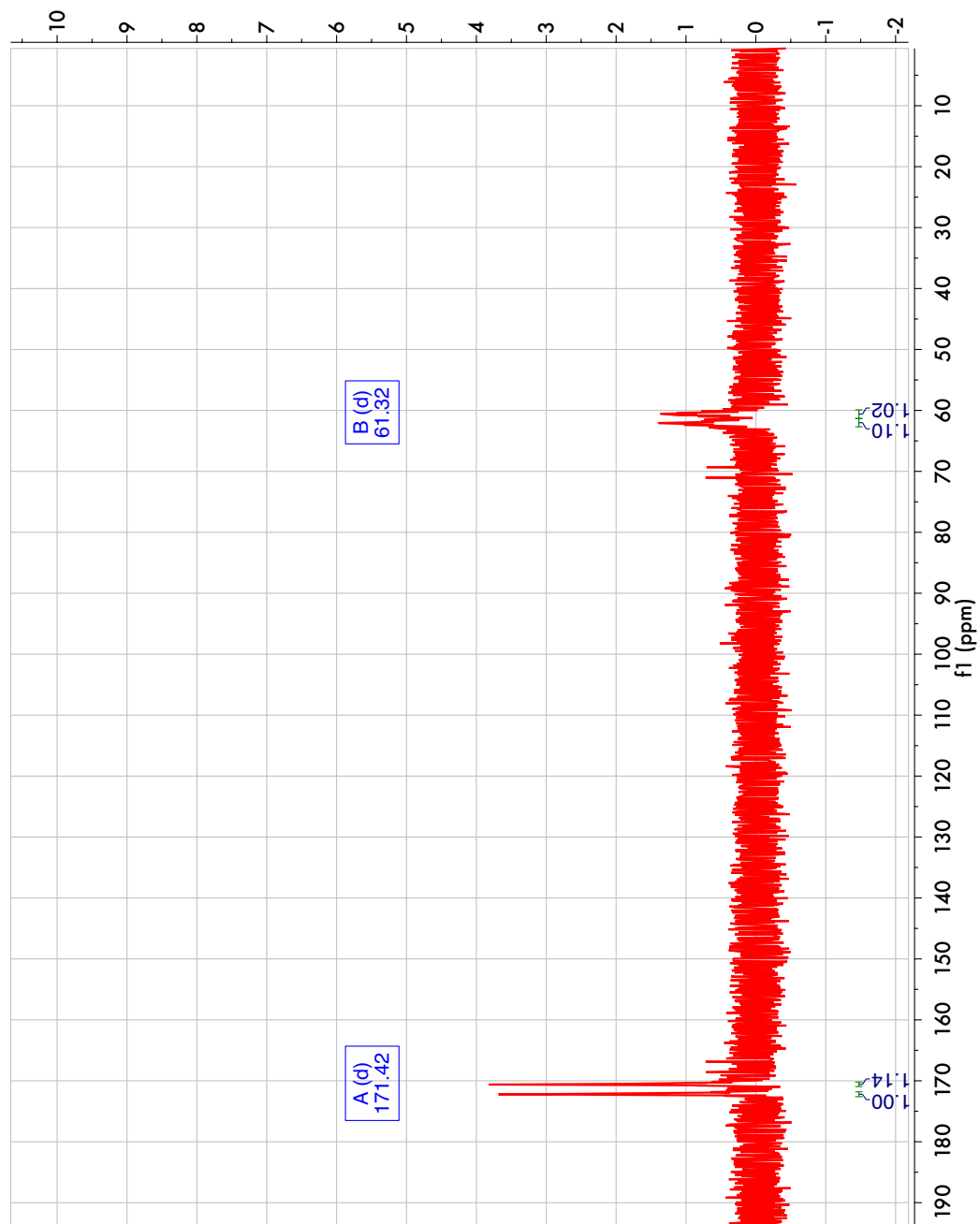
**Resting State of (<sup>t</sup>Bu<sup>4</sup>PCOP)Ir in Alkane Metathesis.** A solution of 10 mM <sup>t</sup>Bu<sup>4</sup>PCOPIr(H)<sub>2</sub> (**3-3**, 0.005 mmol), 16 mM **MoF12** catalyst (0.008 mmol), 40 mM TBE (0.020 mmol), and roughly 7.6 M *n*-hexane (total volume of solution: 0.5 ml) was added to an NMR tube along with an external PMe<sub>3</sub> in *p*-xylene-*d*<sub>10</sub> capillary insert, and the NMR tube was subsequently flame-sealed. This mixture was heated to 90 °C in the NMR spectrometer for *ca.* 60 minutes. After 60 minutes, <sup>31</sup>P NMR exhibited two main sets of peaks of differing intensity: a smaller set of peaks indicative of the dihydride species (**3-3**) (24 %) and larger set of peaks consisting of a doublet at 171.2 ppm and doublet at 61.6 ppm (76 %) indicative of an olefin-bound complex. To confirm the identity of this putative olefin-bound species, in a separate NMR tube 10 mM <sup>t</sup>Bu<sup>4</sup>PCOPIrH<sub>2</sub> and 40 mM 1-hexene (in *p*-xylene-*d*<sub>10</sub> solution, 0.5 ml total sample volume) were mixed, reproducing the sets of doublets at 171.2 and 61.6 ppm in the <sup>31</sup>P NMR and confirming that the larger set of peaks is attributable to an olefin-bound species.

### 3.6 Chapter 3 Appendix

3.6.1 Sample GC trace showing separation and identification of various *n*-alkanes produced from *n*-hexane metathesis.



3.6.2 **Figure 3.A1.**  $^{31}\text{P}$  NMR spectrum of ( $^t\text{Bu}^4\text{PCOP}$ )Ir(1-hexene) (used to confirm identity of resting state species)





### 3.6. References

- (1) This chapter is largely adapted from the following paper: Nawara-Hultzs, A. J.; Hackenberg, J. D.; Punji, B.; Supplee, C.; Emge, T. J.; Bailey, B. C.; Schrock, R. R.; Brookhart, M.; Goldman, A. S. *ACS Catalysis* **2013**, 3, 2505.
- (2) Brandt, A. R.; Millard-Ball, A.; Ganser, M.; Gorelick, S. M. *Environmental Science & Technology* **2013**.
- (3) Kerr, R. A. *Science* **2011**, 331, 1510–1511.
- (4) Murray, J.; King, D. *Nature* **2012**, 481, 433–435.
- (5) International Energy Agency (IAE) World Energy Outlook 2010; [http://www.worldenergyoutlook.org/docs/weo2010/WEO2010\\_es\\_english.pdf](http://www.worldenergyoutlook.org/docs/weo2010/WEO2010_es_english.pdf)
- (6) (a) Dry, M. E. *J. Chem. Tech. Biotech.* **2001**, 77, 43-50. (b) Dry, M. E. *Catalysis Today* **2002**, 71, 227-241. (c) Dry, M. E. *Applied Catalysis, A: General* **2004**, 276, 1-3.
- (7) Leckel, D. *Energy Fuels* **2009**, 23, 2342-2358.
- (8) Holdebrandt, D.; Glasser, D.; Hausberger, B.; Patel, B.; Glasser, B. J. *Science (Washington, DC, U. S.)* **2009**, 323, 1680-1681.
- (9) Zwart, R.; van Ree, R. *Biofuels* **2009**, 95-116.
- (10) Digman, B.; Joo, H. S.; Kim, D.-S. *Environ. Prog. Sustainable Energy* **2009**, 28, 47-51.
- (11) Demirbas, A. *Progress in Energy and Combustion Science* **2007**, 33, 1-18.
- (12) Huber, G. W.; Iborra, S.; Corma, A. *Chem. Rev.* **2006**, 106, 4044-4098.
- (13) Demirbas, A.; Dincer, K. *Energy Sources, Part A: Recovery, Utilization, and Environmental Effects* **2008**, 30, 1233-1241.
- (14) Centi, G.; Perathoner, S. *Catalysis Today* **2009**, 148, 191-205.
- (15) Wang, W.; Wang, S. P.; Ma, X. B.; Gong, J. L. *Chem. Soc. Rev.* **2011**, 40, 3703-3727.
- (16) Borodko, Y.; Somorjai, G. A. *Appl. Catal. A-Gen.* **1999**, 186, 355-362.
- (17) Graves, C.; Ebbesen, S. D.; Mogensen, M.; Lackner, K. S. *Renew. Sust. Energy Rev.* **2011**, 15, 1-23.
- (18) "The Outlook for Energy: A View to 2040", ExxonMobil report, 2012, p 19. [http://www.exxonmobil.com/Corporate/files/news\\_pub\\_eo.pdf](http://www.exxonmobil.com/Corporate/files/news_pub_eo.pdf)
- (19) Burnett, R. L.; Hughes, T. R. *J. Catalysis* **1973**, 31, 55-64.
- (20) (a) Basset, J. M.; Coperet, C.; Lefort, L.; Maunders, B. M.; Maury, O.; Le Roux, E.; Saggio, G.; Soignier, S.; Soulivong, D.; Sunley, G. J.; Taoufik, M.; Thivolle-Cazat, J. *J. Am. Chem. Soc.* **2005**, 127, 8604-8605. (b) Soulivong, D.; Coperet, C.; Thivolle-Cazat, J.; Basset, J.-M.; Maunders, B. M.; Pardy, R. B. A.; Sunley, G. J. *Angew. Chem., Int. Ed.* **2004**, 43, 5366-5369. (c) Vidal, V.; Theolier, A.; Thivolle-Cazat, J.; Basset, J.-M. *Science* **1997**, 276, 99-102.
- (21) Goldman, A. S.; Roy, A. H.; Huang, Z.; Ahuja, R.; Schinski, W.; Brookhart, M. *Science* **2006**, 312, 257-261.
- (22) Haibach, M. C.; Kundu, S.; Brookhart, M.; Goldman, A. S. *Acc. Chem. Res.* **2012**, 45, 947-958.
- (23) Bailey, B. C.; Schrock, R. R.; Kundu, S.; Goldman, A. S.; Huang, Z.; Brookhart, M. *Organometallics* **2009**, 28, 355-360.

- (24) (a) Huang, Z.; Brookhart, M.; Goldman, A. S.; Kundu, S.; Ray, A.; Scott, S. L.; Vicente, B. C. *Adv. Synth. Catal.* **2009**, 351, 188-206. (b) Huang, Z.; Rolfe, E.; Carson, E. C.; Brookhart, M.; Goldman, A. S.; El-Khalafy, S. H.; MacArthur, A. H. R. *Adv. Synth. Catal.* **2010**, 352, 125-135.
- (25) Kundu, S.; Choliy, Y.; Zhuo, G.; Ahuja, R.; Emge, T. J.; Warmuth, R.; Brookhart, M.; Krogh-Jespersen, K.; Goldman, A. S. *Organometallics* **2009**, 28, 5432-5444.
- (26) Eberhard, M. R.; Matsukawa, S.; Yamamoto, Y.; Jensen, C. M. *J. Organomet. Chem.* **2003**, 687, 185-189.
- (27) Moulton, C. J.; Shaw, B. L. *J. Chem. Soc., Dalton Trans.* **1976**, 1020-1024.
- (28) Zhu, K.; Achord, P. D.; Zhang, X.; Krogh-Jespersen, K.; Goldman, A. S. *J. Am. Chem. Soc.* **2004**, 126, 13044-13053.
- (29) Schrock, R. R.; Murdzek, J. S.; Bazan, G. C.; Robbins, J.; DiMare, M.; O'Regan, M. *J. Am. Chem. Soc.* **1990**, 112, 3875-3886.
- (30) Biswas, S.; Zhou, T.; Wang, D. Y.; Hackenberg, J.; Nawara- Hultzs, A.; Schrock, R. R.; Brookhart, M.; Krogh-Jespersen, K.; Goldman, A. S. Abstracts of Papers, 245th ACS National Meeting & Exposition, New Orleans, LA, April 7-11, 2013, INOR-681.
- (31) Gupta, M.; Hagen, C.; Kaska, W. C.; Cramer, R. E.; Jensen, C. M. *J. Am. Chem. Soc.* 1997, 119, 840-841.
- (32) Göttker-Schnetmann, I.; Brookhart, M. *J. Am. Chem. Soc.* 2004, 126, 9330-9338.
- (33) Schrock, R. R.; Murdzek, J. S.; Bazan, G. C.; Robbins, J.; DiMare, M.; O'Regan, M. *J. Am. Chem. Soc.* 1990, 112, 3875-3886.

## Chapter 4

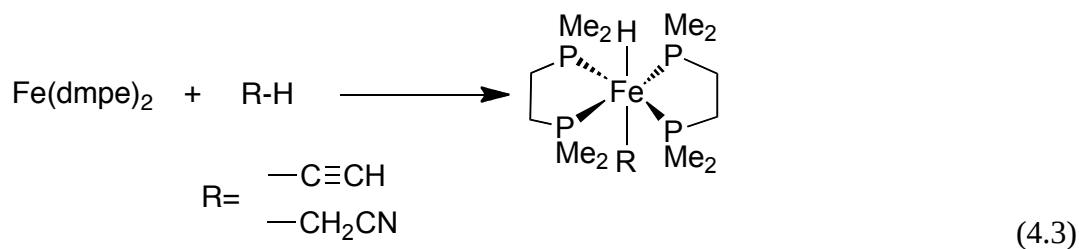
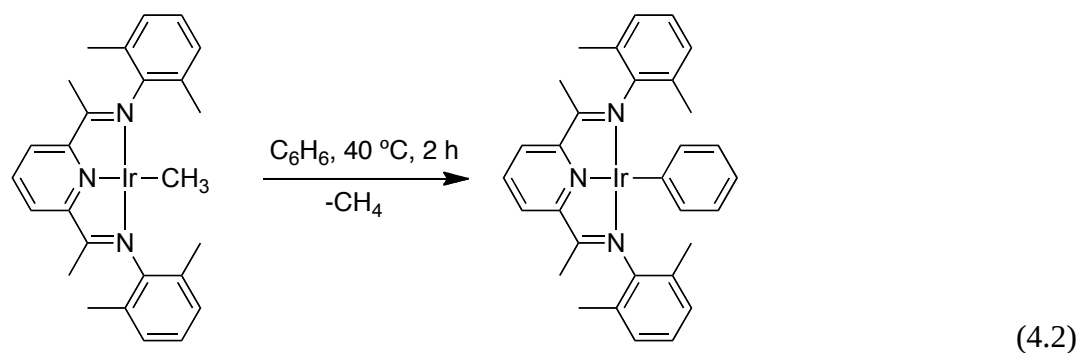
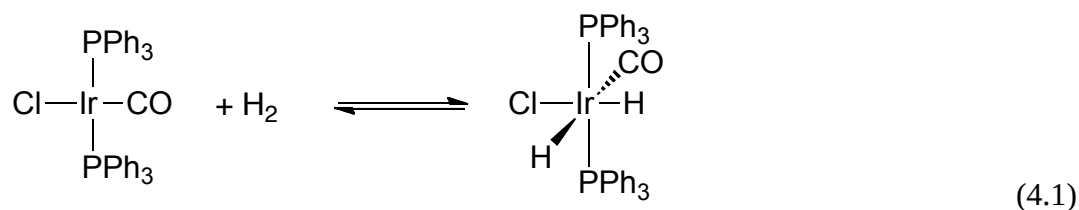
### Acid-catalyzed Oxidative Addition of PhCCH to (<sup>t</sup>Bu<sup>4</sup>PCP)Ir(CO)

#### Abstract

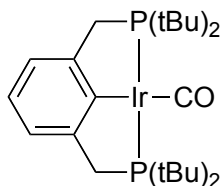
The oxidative addition of C-H bonds to square planar complexes is largely unprecedented. Herein, we describe the net oxidative addition of the alkynyl C-H bond of phenylacetylene to the square planar complex (<sup>t</sup>Bu<sup>4</sup>PCP)Ir(CO) (**4-1**) as catalyzed by simple Brønsted acids such as triethylammonium or phenol. This rare transformation relies on generation of a five-coordinate cationic intermediate, which subsequently undergoes electrophilic addition of phenylacetylene, losing the alkynyl proton to conjugate base in the rate-determining step. The mechanism is elucidated in detail based upon kinetics, isotope effect studies, and DFT calculations.

## 4.1 Introduction

Oxidative addition of covalent bonds to transition metal centers is a fundamental reaction in organometallic chemistry<sup>1,2</sup>. In the early 1960s, Vaska reported the square-planar d<sup>8</sup> iridium complex that now bears his name, (PPh<sub>3</sub>)<sub>2</sub>Ir(CO)Cl, along with its facile ability to oxidatively add H<sub>2</sub> (**eq. 4.1**), prompting a series of discoveries over the next several decades involving the oxidative addition of covalent bonds to square planar complexes<sup>1,3-5</sup>. Curiously, despite the glut of resulting examples, the oxidative addition of C-H bonds to square planar complexes has relatively little precedent. Several examples have been reported in which a ligand already attached to a metal center undergoes metathesis with a free ligand to yield a new four-coordinate square planar species, frequently presumed to occur via an unobserved oxidative addition/reductive elimination pathway (**eq. 4.2**)<sup>6</sup>. Likewise, Sola *et al.* have described how the addition of a fifth ligand to a four-coordinate complex has been observed to promote the apparent oxidative addition of a C-H bond of one of the previously-coordinated ligands to yield a new six-coordinate complex; this process, however, requires incorporation of the “fifth ligand” into the metal complex and subsequent generation of distorted (non-square planar) four-coordinate species to undergo C-H oxidative addition<sup>7</sup>. The most prominent example of direct C-H oxidative addition to a four-coordinate complex (*i.e.* simple addition of a substrate C-H bond to a four-coordinate complex without additional ligands) was reported in the late 1970s by Ittel and Tolman, who reported the oxidative addition of acetonitrile and acetylene to an *in situ* generated Fe(dmpe)<sub>2</sub> complex (**eq. 4.3**); however, Eisenstein and Perutz have proposed (on the basis of DFT calculations and *in situ* spectroscopy) that the structure of the putative four-coordinate Fe(dmpe)<sub>2</sub> species is not



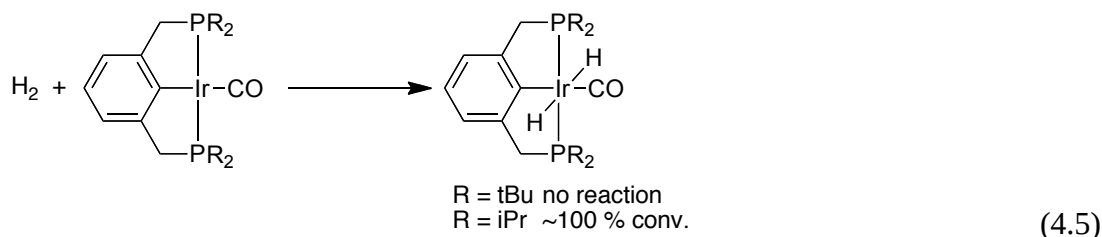
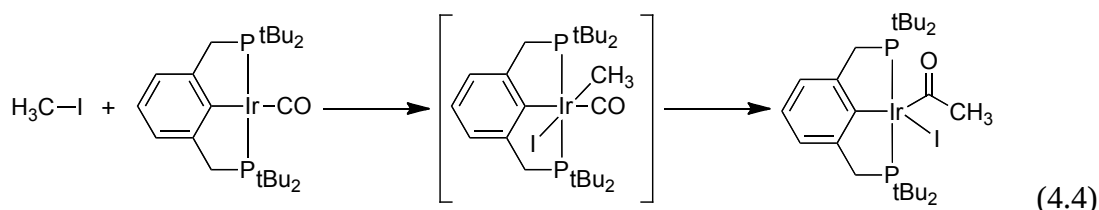
Of course, four-coordinate  $d^8$  complexes are encountered frequently as stable precursors to more active three-coordinate complexes that are capable of readily adding C-H bonds (e.g.  $(^t\text{Bu}^4\text{PCP})\text{Ir}(\text{ethylene})$ ). Many four-coordinate complexes are exploited thus, but others contain ligands that are not particularly labile, such as carbonyls or isocyanides, and are consequently precluded from adding C-H bonds via a ligand-dissociation route, perhaps unless photolysis of the ligand is possible. Even classes of complexes that are superb at C-H oxidative addition as three-coordinate species experience loss of activity toward oxidative addition as four-coordinate complexes. An archetypal example of this dichotomy is  $(^t\text{Bu}^4\text{PCP})\text{Ir}(\text{CO})$  (**4-1**), which is unreactive to the wide variety of C-H bonds that its three-coordinate 14-electron analogue ( $(^t\text{Bu}^4\text{PCP})\text{Ir}$ ) so readily activates.



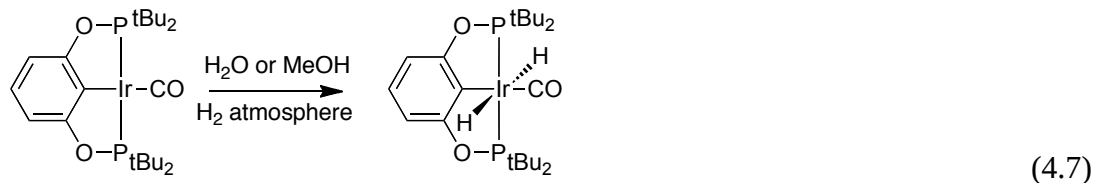
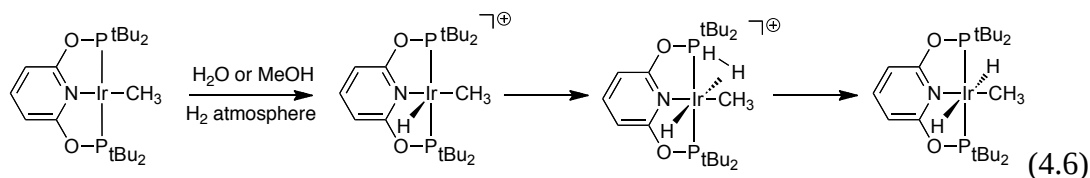
**4-1**

Four-coordinate square planar iridium-pincer complexes are not entirely chemically inert, having the ability to undergo similar reactions to Vaska's complex.  $(^t\text{Bu}^4\text{PCP})\text{Ir}(\text{CO})$ , for instance, adds methyl iodide, but the resulting putative six-coordinate species rapidly undergoes migratory insertion of the CO ligand into the Ir-methyl bond to generate the five-coordinate acyl iodide complex,  $(^t\text{Bu}^4\text{PCP})\text{Ir}(\text{I})(\text{COCH}_3)$  (**eq. 4.4**)<sup>12</sup>. Interestingly,  $(^t\text{Bu}^4\text{PCP})\text{Ir}(\text{CO})$  does not readily undergo  $\text{H}_2$  oxidative addition (the archetypal example of oxidative addition to Vaska's complex), while the less sterically-hindered *iso*-propyl analogue,  $(^i\text{Pr}^4\text{PCP})\text{Ir}(\text{CO})$ , readily forms the six-coordinate

dihydride product in quantitative yield at room temperature under a hydrogen atmosphere (**eq. 4.5**), so it is further possible that  $(^t\text{Bu}^4\text{PCP})\text{Ir}(\text{CO})$  represents a truly unreactive intermediate, particularly with respect to nonpolar covalent bonds (e.g. H-H or C-H)<sup>13,14</sup>.



A relatively recent discovery is the Brønsted acid-catalyzed net oxidative addition of bonds to square-planar complexes. Brookhart was the first to report this type of process, when he found that  $\text{H}_2$  could add to a  $(\text{PONOP})\text{Ir}(\text{CH}_3)$  complex in the presence of a weak Brønsted acid (water or methanol) to generate the exclusively *trans*-dihydride complex,  $(\text{PONOP})\text{Ir}(\text{CH}_3)(\text{H})_2$  (**eq. 4.6**)<sup>15</sup>. Instead of occurring in a concerted fashion via a three-center two-electron intermediate like a traditional oxidative addition event, Brookhart proposed a mechanism in which the four-coordinate complex is first protonated to generate a five-coordinate cationic intermediate, followed by coordination of dihydrogen and subsequent deprotonation by conjugate base to yield the six-coordinate oxidative addition product with the observed *trans* stereochemistry. More recently, Goldberg and Heinekey have described a related acid-catalyzed addition of  $\text{H}_2$  to  $(^t\text{Bu}^4\text{POCOP})\text{Ir}(\text{CO})$ , proceeding by an analogous mechanism (**eq. 4.7**).<sup>16</sup>



These acid-catalyzed processes represent a novel means of promoting the net oxidative addition of bonds to otherwise unreactive four-coordinate complexes, particularly square planar carbonyl species. Although the only known examples involve H<sub>2</sub> addition, this route holds promise for a variety of X-H bonds (e.g. O-H, N-H), but would prove most valuable for C-H bonds, which as described earlier, are particularly unreactive toward oxidative addition involving four-coordinate complexes and have similar properties to H-H bonds in terms of both polarity and bond strengths<sup>17</sup>. In this chapter, we describe the acid-catalyzed oxidative addition of the alkynyl C-H bond of phenylacetylene to (<sup>t</sup>Bu<sup>4</sup>PCP)Ir(CO), which represents not only the first example of C-H addition to a square planar carbonyl complex, but also the first example of an acid-catalyzed C-H oxidative addition event.

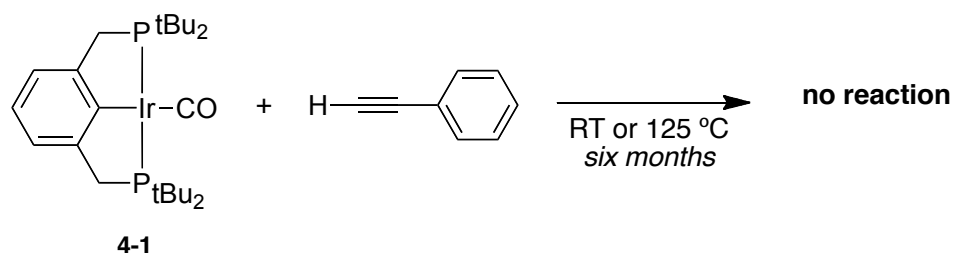
## 4.2 Results and Discussion

### 4.2.1 Attempts to add C-H bonds to (<sup>t</sup>Bu<sup>4</sup>PCP)Ir(CO)



It has long been established that numerous 16-electron square planar complexes fail to undergo C-H oxidative addition; in no respect is this more unfortunate than for square planar carbonyl complexes, given that C-H activation under a CO atmosphere and subsequent insertion of a carbonyl ligand into the C-H bond would be an attractive, straightforward route to oxygenated species from unfunctionalized hydrocarbon substrates. The inactivity toward C-H oxidative addition is no different for (pincer)Ir(CO) complexes, despite the unparalleled ability of the 14-electron (pincer)Ir species to activate C-H bonds. Consequently, (<sup>t</sup>Bu<sup>4</sup>PCP)Ir(CO) (**4-1**) is stable to a wide variety of C-H bonds, including those of simple alkanes like *n*-pentane, aromatics like benzene, and even relatively “activated” C-H bonds, like those in acetonitrile or trifluoromethane. Indeed, not even H<sub>2</sub> has been observed to oxidatively add to (<sup>t</sup>Bu<sup>4</sup>PCP)Ir(CO) (**4-1**) at relatively low pressures (1-2 atm), despite the relative ease with which H<sub>2</sub> adds to Vaska’s complex.<sup>18</sup> Phenylacetylene (PhCCH) therefore predictably also fails to undergo any reaction with (<sup>t</sup>Bu<sup>4</sup>PCP)Ir(CO) (**4-1**), even after allowing the reaction to proceed for *six months* at room temperature or 125 °C (**scheme 4.1**).

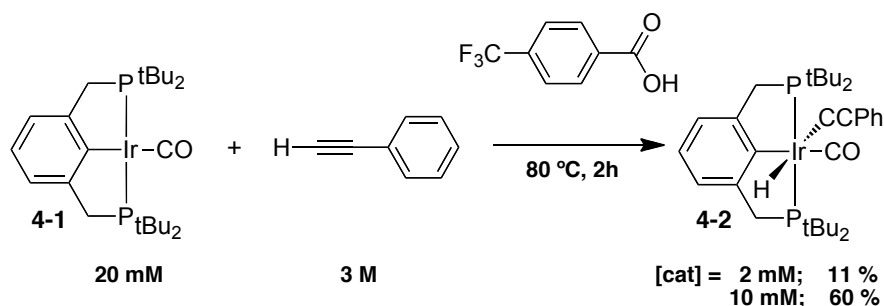
**Scheme 4.1.** No reaction takes place between (<sup>t</sup>Bu<sup>4</sup>PCP)Ir(CO) and PhCCH at room temperature or 125 °C over the course of six months in the absence of a catalyst.

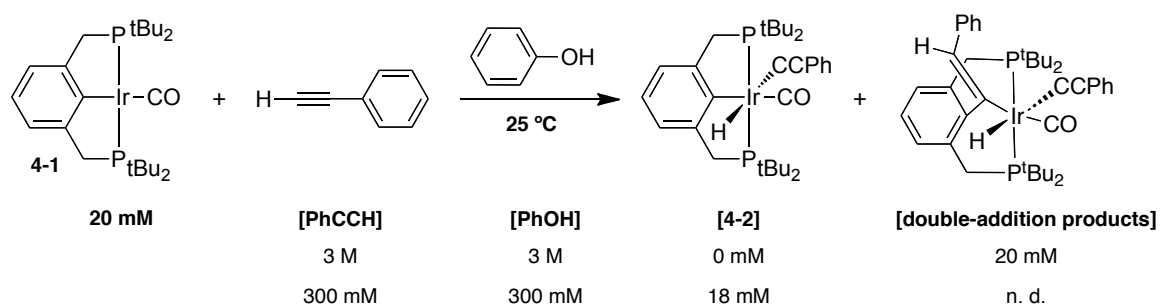


#### 4.2.2 Early studies involving acid-catalyzed addition of PhCCH to (<sup>t</sup>Bu<sup>4</sup>PCP)Ir(CO)<sup>19</sup>

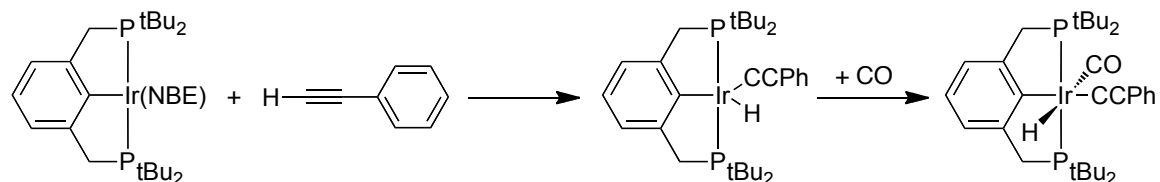
Given that (<sup>t</sup>Bu<sup>4</sup>PCP)Ir(CO) was essentially considered a dead-end in terms of C-H activation catalysis, it was truly surprising when it was serendipitously discovered that 2 mM of 4-(trifluoromethyl)benzoic acid could catalyze the addition of PhCCH (3M) to (<sup>t</sup>Bu<sup>4</sup>PCP)Ir(CO) at 80 °C to give the *trans* oxidative addition product (**4-2**) in 11 % yield after heating for two hours; increasing the acid concentration to 10 mM improved the yield of **4-2** after two hours at 80 °C to 60 % (**scheme 4.2**).<sup>20</sup> Subsequent reaction optimization found that phenol (PhOH), in relatively high concentrations (3 M), could catalyze the room-temperature addition of PhCCH to **4-1** (**scheme 4.3**). This reaction, however, did not yield the *trans*-addition product (**4-2**), but instead a mixture of products determined by nmr spectroscopy and x-ray crystallography to have resulted from addition of two equivalents of PhCCH to a single metal complex, likely as a result of C-H oxidative addition, acetylide migratory insertion into the (PCP)C<sub>ispo</sub>-Ir bond, and subsequent second addition of another molecule of PhCCH.<sup>20</sup> These “double-addition” products could be mitigated by reducing the concentrations of phenol and PhCCH (both 300 mM), forming the *trans* “single-addition” product **4-2** in 90 % yield.

**Scheme 4.2.** 4-(trifluoromethyl)benzoic acid-catalyzed oxidative addition of PhCCH to (<sup>t</sup>Bu<sup>4</sup>PCP)Ir(CO).



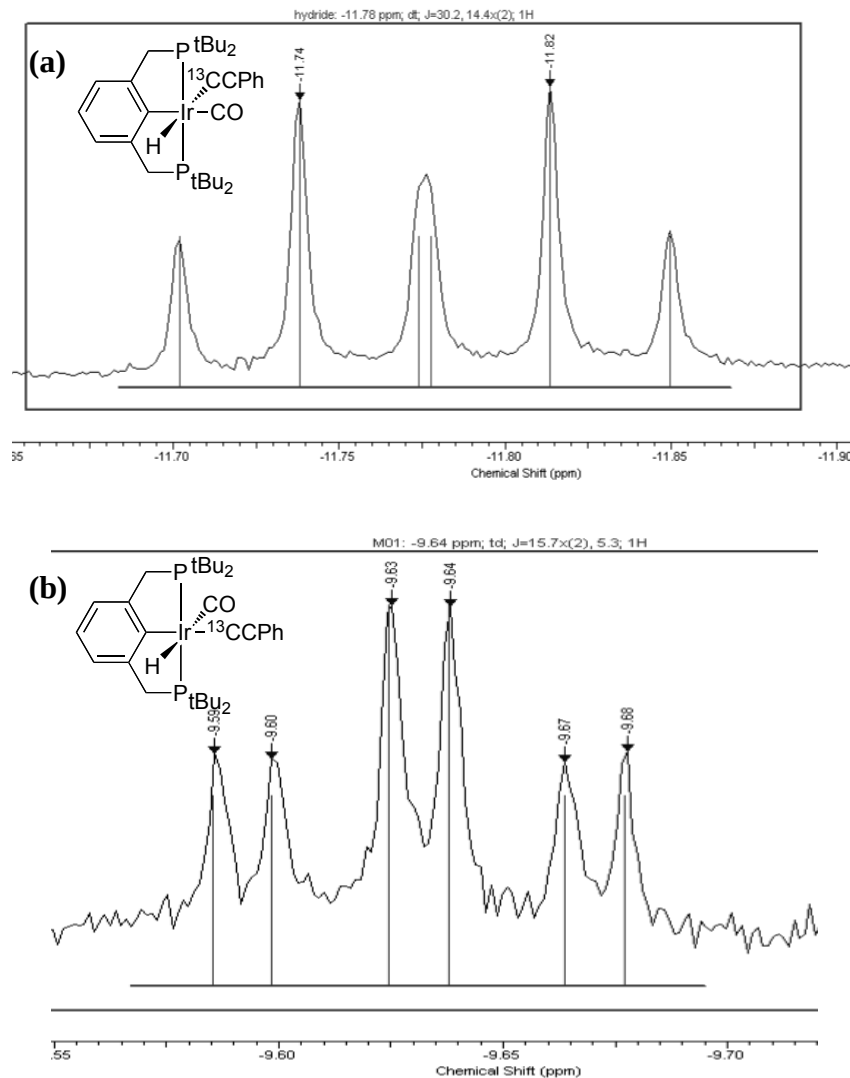
**Scheme 4.3.** Phenol-catalyzed oxidative addition of PhCCH to (<sup>t</sup>Bu<sub>4</sub>PCP)Ir(CO).

Isolating the single-addition product **4-2** proved difficult in several respects. Attempts to remove the solvent effectively increase the concentration of acid and PhCCH, which results in conversion of **4-2** to the double-addition product via rapid addition of a second equivalent of PhCCH. Likewise, careful low temperature sublimation of the frozen solvent avoids the double-addition formation, but subsequent dissolution of the residue (which is a mixture of single-addition product and acid catalyst) prompts the apparent acid-catalyzed elimination of the PhCCH (the reverse of the oxidative addition reaction under study) to yield (<sup>t</sup>Bu<sub>4</sub>PCP)Ir(CO) (**4-1**). To help establish the identity of the single-addition product, one could imagine independent synthesis of the product via addition of CO to (<sup>t</sup>Bu<sub>4</sub>PCP)Ir(H)(CCPh) (**scheme 4.4**). This route, how-

**Scheme 4.4.** Synthesis of *cis*-(<sup>t</sup>Bu<sub>4</sub>PCP)Ir(CO)(H)(CCPh) via CO addition to (<sup>t</sup>Bu<sub>4</sub>PCP)Ir(H)(CCPh).

ever, does not yield the product we observed, but instead presents as a singlet in the  $^{31}\text{P}\{^1\text{H}\}$  nmr at 58.1 ppm and a triplet in  $^1\text{H}$  nmr at -9.5 ppm ( $J_{\text{PH}}=15.6$  Hz); x-ray crystallography showed this product to have a *cis* relationship between the hydride and acetylide ligands, thus implying that the acid-catalyzed product was the *trans* addition product.<sup>20</sup> Using isotopically-labeled  $\text{PhC}\equiv^{13}\text{CH}$ , we could determine the  $J_{\text{CH}}$  coupling

**Figure 4.1.** Hydride signals exhibiting  $^{13}\text{C}$ -splitting in  $^1\text{H}$  nmr for (a) *trans*-( $^{\text{tBu}}_4\text{PCP}$ )Ir(CO)(H)( $^{13}\text{CCPh}$ ) (top) and (b) *cis*-( $^{\text{tBu}}_4\text{PCP}$ )Ir(CO)(H)( $^{13}\text{CCPh}$ ) (bottom).



constants associated with the hydride produced by both routes to firmly establish the stereochemistry of the products. The acid-catalyzed product displayed a doublet of triplets at -11.78 with  $J_{CH}$  equal to 30.2 Hz (**figure 4.1a**), while the previously crystallographically-confirmed *cis*-product displayed a triplet of doublets at -9.54 ppm, with  $J_{CH}$  equal to 5.3 Hz (**figure 4.1b**); the larger  $J_{CH}$  coupling value is fully consistent with a *trans* stereochemical relationship, suggesting that the acid-catalyzed route affords the *trans* isomer exclusively.

At this point, it seemed quite likely that the mechanism of addition relied upon proton transfer from the acid to the carbonyl species. To support this idea, we first attempted to use a Lewis acid,  $(\text{Ph}_3\text{C})^+ \text{B}(\text{C}_6\text{H}_5\text{F}_6)_4^-$  (“trityl BAr<sup>F</sup>”), to rule out an alternative mechanism relying on activation of the carbonyl ligand. However, to our surprise, the addition of PhCCH to  $(^{\text{tBu}}\text{PCP})\text{Ir}(\text{CO})$  proceeded very rapidly in the presence of 1 mM trityl BAr<sup>F</sup>, forming double-addition products exclusively in less than a minute (**scheme 4.5**). Careful monitoring of this reaction at low temperature (-30 °C) showed formation of both the single-addition and the double-addition products, with rapid conversion of **4-2** to the double addition product upon warming to room temperature (**figure 4.2**). One possible suggestion for this unexpected reactivity could be an alternate mechanism operates for Lewis acid catalysts (for example, the Lewis acid could activate the CO ligand, weakening the Ir-CO interaction and favoring oxidative addition). However, such a mechanism would likely favor formation of the *cis* product or at least not favor *exclusive trans* product formation. A more consistent explanation involves coordination of adventitious water to the trityl cation, generating an acidic oxonium species that carries out Bronsted acid catalysis. As such, addition of a strong

non-nucleophilic base (sodium *tert*-butoxide) was found to completely shut down the catalytic oxidative addition pathway.

**Scheme 4.5.** Lewis-acid (trityl  $\text{BAr}^{\text{F}}$ )-catalyzed addition of  $\text{PhCCH}$  to  $(^{\text{tBu}}\text{PCP})\text{Ir}(\text{CO})$ .

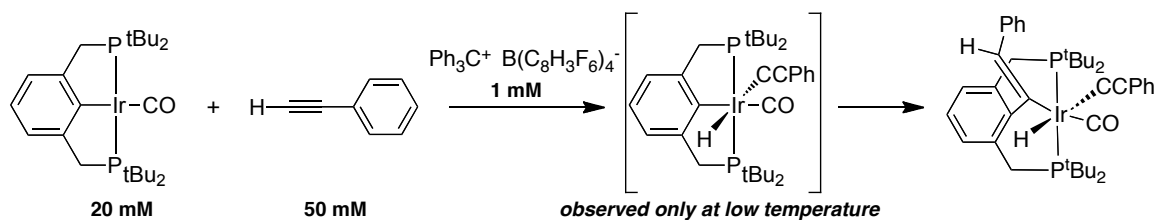
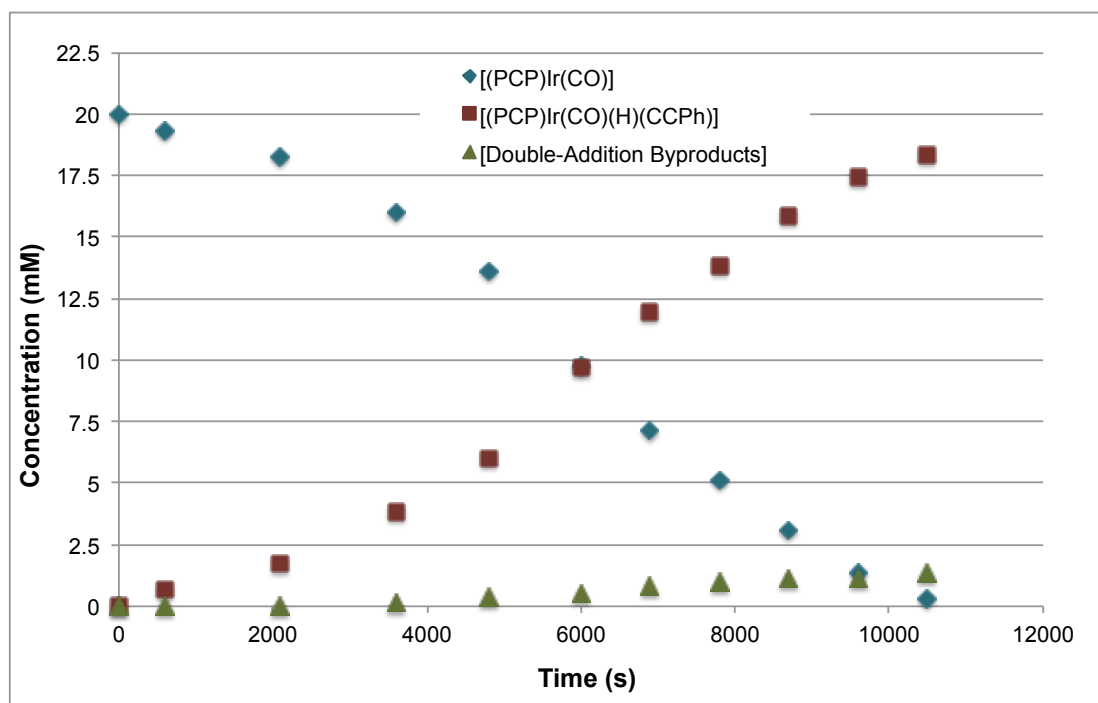


**Figure 4.2.** Conversion of  $(^{\text{tBu}}\text{PCP})\text{Ir}(\text{CO})$  to  $(^{\text{tBu}}\text{PCP})\text{Ir}(\text{CO})(\text{H})(\text{CCPh})$  and double-addition byproducts as catalyzed by 1 mM trityl  $\text{BAr}^{\text{F}}$  at  $-30^\circ\text{C}$ .



### 4.2.3 Synthesis and characterization of the putative cationic intermediate, $(^t\text{Bu}^4\text{PCP})\text{Ir}(\text{CO})(\text{H})^+$

Given the apparent pKa dependence on the rate of reaction, we sought to independently generate the proposed five-coordinate cationic intermediate,  $(^t\text{Bu}^4\text{PCP})\text{Ir}(\text{CO})(\text{H})^+$ , which should react rapidly with PhCCH. A prior attempt to synthesize this species involved adding CO to the previously-reported cationic species  $(^t\text{Bu}^4\text{PCP})\text{Ir}(\text{H})^+ \text{BAr}^{\text{F}-}$ ; this, however, did not generate the five-coordinate species, but rather more likely the six-coordinate bis-carbonyl complex,  $(^t\text{Bu}^4\text{PCP})\text{Ir}(\text{H})(\text{CO})_2^+$ .<sup>20</sup> Nevertheless, this bis-carbonyl complex was found to catalyze C-H addition, likely by acting as proton donor rather than as an intermediate in the catalytic cycle. The true five-coordinate cationic intermediate (proposed to be formed during the catalytic cycle) could be generated by direct protonation of the  $(^t\text{Bu}^4\text{PCP})\text{Ir}(\text{CO})$  with a strong acid (**scheme 4.6**). As such, addition of Brookhart's oxonium acid ( $[\text{H}(\text{OEt}_2)_2^+ \text{B}(\text{C}_8\text{H}_3\text{F}_6)_4^-]$ ) or "H-BAr<sup>F</sup>") to  $(^t\text{Bu}^4\text{PCP})\text{Ir}(\text{CO})$  in *n*-pentane immediately precipitates out the cationic intermediate as yellow crystals.<sup>21</sup> The nmr spectra of  $(^t\text{Bu}^4\text{PCP})\text{Ir}(\text{CO})(\text{H})^+ \text{BAr}^{\text{F}-}$  (**4-3**) are nearly identical to that of the four-coordinate complex, with a subtle shift in the <sup>31</sup>P nmr spectrum ( $\delta$  81.8 ppm—a 0.6 ppm downfield shift) and a broad hydride signal at -36 ppm. The crystals that precipitated after addition of acid were of suitable quality to obtain an x-ray crystal structure (**figure 4.3**); the crystal structure was highly ordered, with the hydride unambiguously located in the residual electron density map as a 0.61(10) e/Å<sup>3</sup> peak on the side of the cation where the *tert*-butyl groups are further apart, having an Ir-H distance of 1.62 Å.

**Scheme 4.6.** Independent synthesis of the putative cationic intermediate **4-3** via direct protonation of **4-1**.

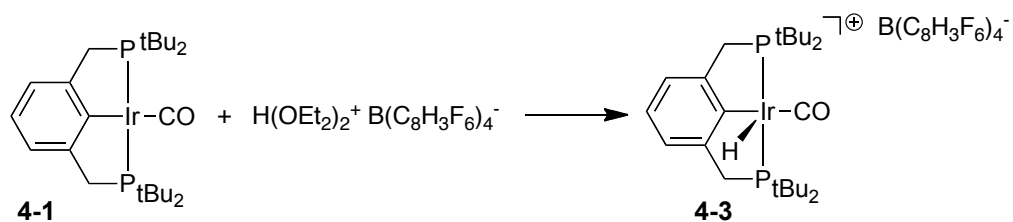
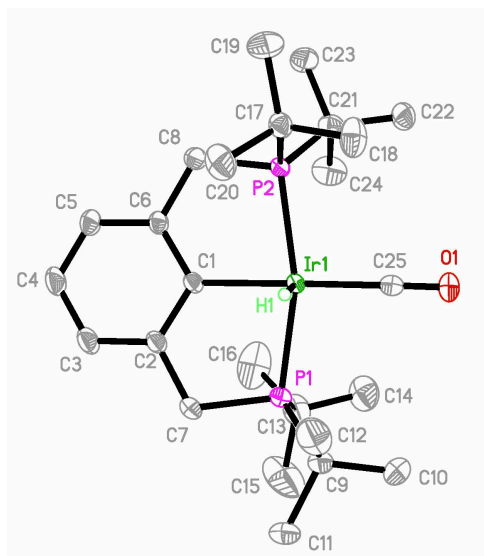


**Figure 4.3.** Thermal ellipsoid plot of  $(^{t\text{Bu}}_4\text{PCP})\text{Ir}(\text{CO})(\text{H})^+$  (**4-3**) ( $\text{BAR}^{\text{F}}$  counteranion not shown).



#### 4.2.4 Establishing the intermediacy of $(^{t\text{Bu}}_4\text{PCP})\text{Ir}(\text{CO})(\text{H})^+$ (**4-3**)

With  $(^{t\text{Bu}}_4\text{PCP})\text{Ir}(\text{CO})\text{H}^+$  in hand, we examined its ability to add PhCCH. At room temperature, 10 mM of  $(^{t\text{Bu}}_4\text{PCP})\text{Ir}(\text{CO})(\text{H})^+ \text{BAR}^{\text{F}}$  (**4-3**) reacts rapidly with 50 mM PhCCH to generate exclusively the double addition product. Using a catalytic amount of  $(^{t\text{Bu}}_4\text{PCP})\text{Ir}(\text{CO})(\text{H})^+$  (1 mM), a 20 mM solution of  $(^{t\text{Bu}}_4\text{PCP})\text{Ir}(\text{CO})$  and 50 mM PhCCH is also rapidly converted to double-addition product (**scheme 4.7**). Interestingly, monitoring of this reaction at low temperature ( $-25\text{ }^\circ\text{C}$ ) shows nearly simultaneously



formation of both the single and double addition products, with rapid conversion to the double-addition product upon warming to higher temperatures (**figure 4.4**). These results are consistent with a mechanism in which an acid protonates the four-coordinate carbonyl species to generate a more reactive five-coordinate cationic intermediate that is capable of adding PhCCH.

**Scheme 4.7.** Addition of PhCCH (50 mM) to (<sup>t</sup>Bu<sup>4</sup>PCP)Ir(CO) (20 mM) catalyzed by **4-3** (1 mM).

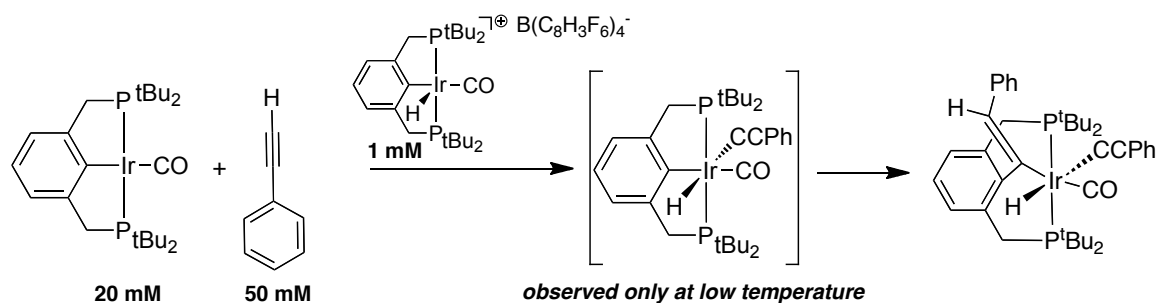
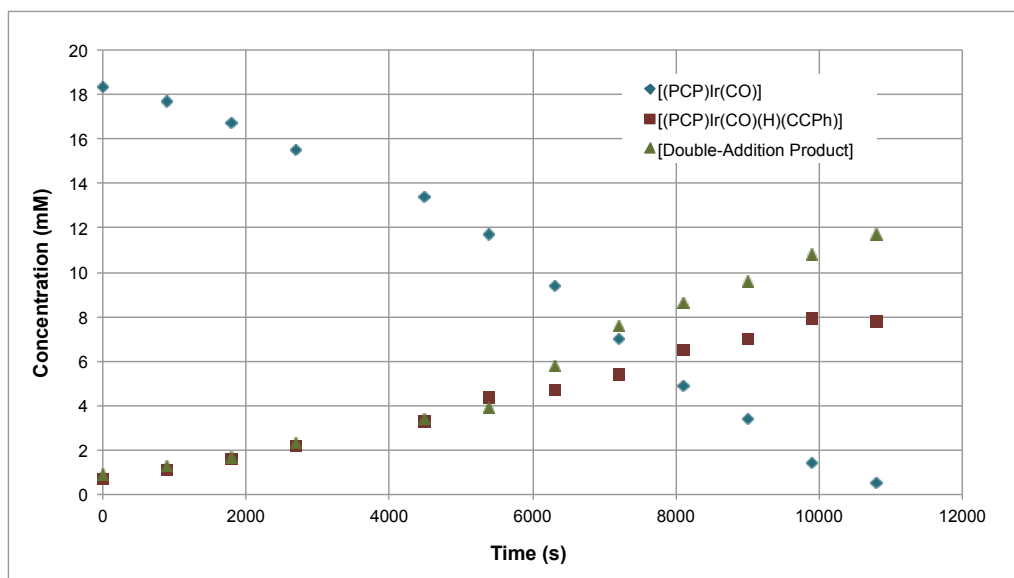


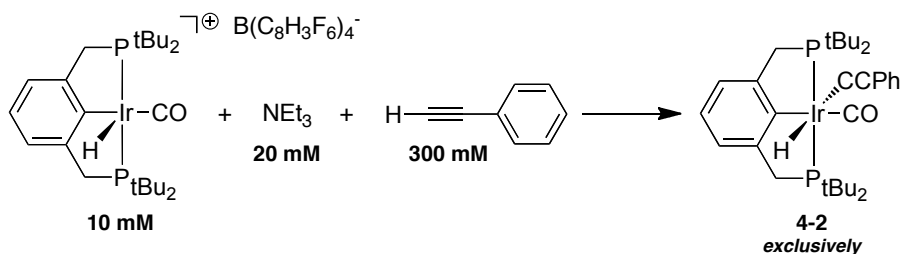
**Figure 4.4.** Conversion of (<sup>t</sup>Bu<sup>4</sup>PCP)Ir(CO) to (<sup>t</sup>Bu<sup>4</sup>PCP)Ir(CO)(H)(CCPh) and double-addition byproduct as catalyzed by (<sup>t</sup>Bu<sup>4</sup>PCP)Ir(CO)(H)<sup>+</sup> BAr<sup>F-</sup> at -25 °C.



#### 4.2.5 Strategies to minimize the production of double-addition product

To facilitate studying the mechanism of this unprecedented transformation, we sought to minimize the production of the unwanted double-addition byproduct. It appeared that double-addition product predominated when highly acidic catalysts (such as  $\text{H}(\text{OEt}_2)_2^+ \text{B}(\text{C}_8\text{H}_3\text{F}_6)_4^-$  or  $(\text{PCP})\text{Ir}(\text{CO})(\text{H})^+ \text{B}(\text{C}_8\text{H}_3\text{F}_6)_4^-$ , neither of which have strong conjugate bases) were employed, suggesting that the addition of a second equivalent of PhCCH was also acid-catalyzed; as such, we proposed that adding a base to the reaction system might disfavor double-addition product formation by readily deprotonating any highly acidic intermediate that would lead to acetylene insertion/second addition. To a 10 mM solution of  $(^{\text{tBu}}_4\text{PCP})\text{Ir}(\text{CO})\text{H}^+ \text{B}(\text{C}_8\text{H}_3\text{F}_6)_4^-$  was added 20 mM of triethylamine, which resulted in apparently complete deprotonation of the cationic intermediate to yield 10 mM  $(^{\text{tBu}}_4\text{PCP})\text{Ir}(\text{CO})$ , 10 mM  $\text{HNEt}_3^+ \text{B}(\text{C}_8\text{H}_3\text{F}_6)_4^-$ , and 10 mM of free triethylamine. 300 mM PhCCH was then added to this mixture. After reacting for 30 minutes at room temperature, the solution had turned a light, pale yellow, and  $^{31}\text{P}$  and  $^1\text{H}$  nmr indicated *exclusive formation of the single-addition product* in quantitative yield (**scheme 4.8**), which upon standing for several hours only slowly began to form double-addition product; in the *absence* of base, the same reaction conditions lead exclusively to the double-addition product in less than a minute.

**Scheme 4.8.** Acid-catalyzed addition of PhCCH to  $(^{\text{tBu}}_4\text{PCP})\text{Ir}(\text{CO})$  in presence of base.



As a prelude to studying the kinetics of addition, we optimized the reaction conditions and developed a “buffered” reaction system by utilizing an acid/conjugate base pair,  $\text{HNEt}_3^+ \text{B}(\text{C}_6\text{F}_5)_4^-$  and triethylamine, in a 1:4 ratio of acid:base. Utilizing a higher ratio of base to acid was observed to significantly disfavor the production of double-addition product, particularly when the reaction mixture was left to react over longer periods of time.

#### 4.2.6 Kinetics of PhCCH Addition

We began examining the kinetics of C-H addition to  $(^t\text{Bu}^4\text{PCP})\text{Ir}(\text{CO})$  by determining the order of reaction with respect to each reagent (PhCCH,  $\text{HNEt}_3^+ \text{B}(\text{C}_6\text{F}_5)_4^-$ ,  $\text{NEt}_3$ , and  $(^t\text{Bu}^4\text{PCP})\text{Ir}(\text{CO})$ ). To do so, we systematically varied the concentration of each reagent by 1-, 2-, 4-, and 8-fold increments and determined the effect on the rate of disappearance of  $(^t\text{Bu}^4\text{PCP})\text{Ir}(\text{CO})$  (**4-1**) and the appearance of *trans*-addition product (**4-2**) based on monitoring concentrations of each species by  $^1\text{H}$  nmr. **Table 4.1** summarizes the initial rates of reactions under each set of conditions; the acid-catalyzed route was found to be first order in acid ( $\text{HNEt}_3^+$ ), PhCCH, and  $(^t\text{Bu}^4\text{PCP})\text{Ir}(\text{CO})$ , and zero-order in base ( $\text{NEt}_3$ ) (presumably, the addition of a second equivalent of PhCCH to form double addition product is inverse order in base, such that the presence of base disfavors subsequent addition).

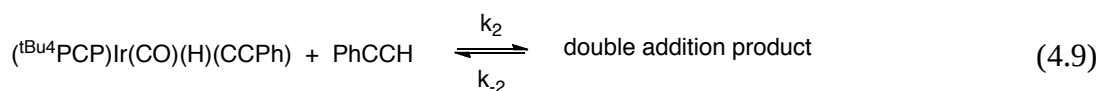
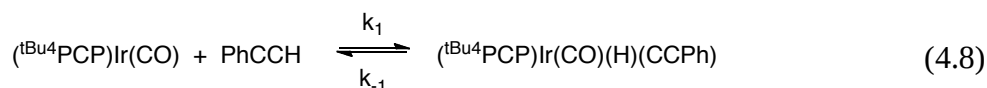
**Table 4.1.** Initial rates of reaction for buffer-catalyzed addition of PhCCH to **4-1** under various concentration conditions.

Initial rate of			Initial rate of		
[HNEt <sub>3</sub> + BArF-] mM	4-2 formation mM s <sup>-1</sup>	4-1 loss mM s <sup>-1</sup>	[NEt <sub>3</sub> ] mM	4-2 formation mM s <sup>-1</sup>	4-1 loss mM s <sup>-1</sup>
1	4.95E-04	4.15E-04	4	4.95E-04	4.15E-04
2	8.13E-04	7.15E-04	8	3.72E-04	4.01E-04
4	1.54E-03	1.38E-03	16	3.12E-04	3.15E-04
8	2.59E-03	2.44E-03	32	3.13E-04	3.23E-04

Initial rate of			Initial rate of		
[PhCCH] mM	4-2 formation mM s <sup>-1</sup>	4-1 loss mM s <sup>-1</sup>	[(PCP)Ir(CO)] mM	4-2 formation mM s <sup>-1</sup>	4-1 loss mM s <sup>-1</sup>
50	4.34E-04	4.72E-04	10	4.52E-04	4.59E-04
100	7.73E-04	8.42E-04	20	7.05E-04	7.87E-04
200	1.26E-03	1.40E-03	40	1.48E-03	1.62E-03
400	1.31E-03	1.57E-03	80	2.25E-03	2.29E-03

The results of our kinetics experiments were analyzed with COPASI to determine actual third-order rate constants by simulating and fitting the experimental data<sup>22</sup>. We modeled the mechanism as shown in **equations 4.8** and **4.9**, including the experimentally-determined concentrations of (<sup>t</sup>Bu<sup>4</sup>PCP)Ir(CO) (**4-1**) and product **4-2** measured at each point in time.



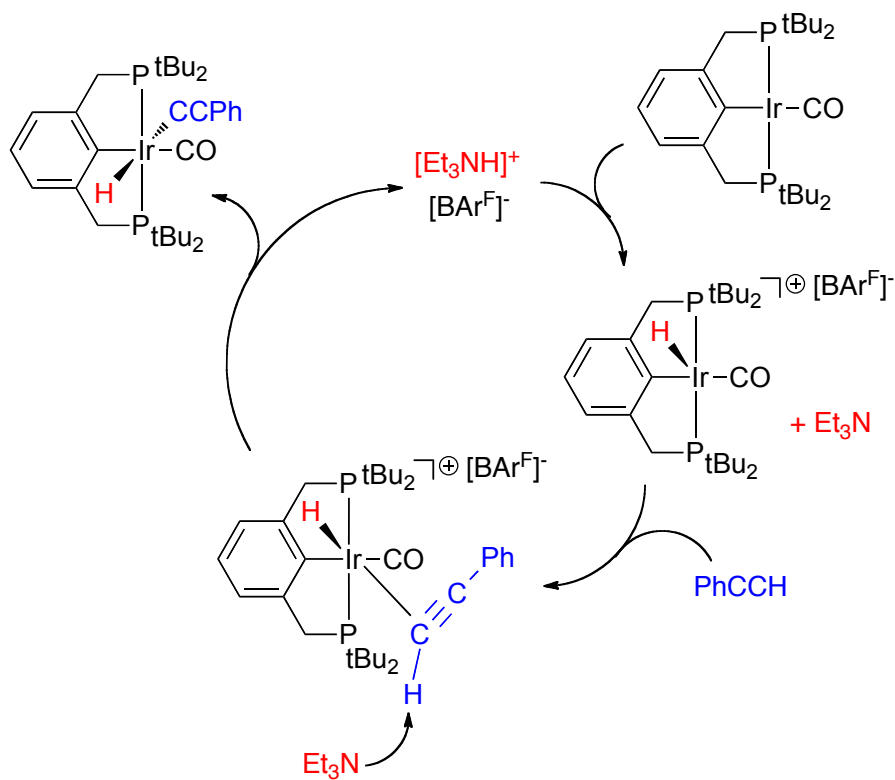
As the reaction to form single-addition product (**4-2**) was found to be zero-order in base, triethylamine was omitted from the model, as was the triethylammonium since it is a catalyst and its concentration does not change during the course of the reaction. Simulation and fitting of the data from each experiment (13 unique experiments) afforded an average rate constant ( $k_1$ ) of  $9.0(\pm 0.9) \times 10^{-1} \text{ M}^{-2} \text{ s}^{-1}$  for acid-catalyzed addition of phenylacetylene to (<sup>t</sup>Bu<sup>4</sup>PCP)Ir(CO), while the rate constant for the reverse reaction

(reductive elimination,  $k_{-1}$ ) was found to be more than an order of magnitude slower,  $1.2(\pm 0.3) \times 10^{-2} \text{ M}^{-2} \text{ s}^{-1}$ .

#### 4.2.7 Proposed Mechanism

Based upon these kinetics studies and the observed reactivity of the independently-generated cationic complex, the mechanism in **scheme 4.9** is proposed. Upon protonation of ( $^t\text{Bu}^4\text{PCP}$ )Ir(CO) by the Brønsted acid, a five-coordinate cationic intermediate is formed, which is capable of undergoing electrophilic attack of phenylacetylene to yield a presumably highly-acidic coordinated phenylacetylene adduct. In the absence of base, this intermediate can undergo fast insertion of the acetylene ligand into the Ir-C bond and react with a second PhCCH equivalent to yield double-addition product. However, in the presence of a sufficiently strong conjugate base, the coordinated acetylene can be readily deprotonated to generate the exclusively-*trans* single-addition product and regenerate the acid catalyst. This mechanism is highly consistent with Brookhart's analogous mechanism for proton-catalyzed *trans*-addition of  $\text{H}_2$  to the four-coordinate (PONOP)Ir( $\text{CH}_3$ ) species<sup>15</sup>. Further, as shown in **scheme 4.10**, a cross-labeling experiment using a mixture of *para*-methylphenylacetylene and phenylacetylene-*d1* showed significant scrambling of the H/D signal, as expected based on the proposed mechanism. Deconvolution of the overlapping hydride signals (**figure 4.5**) indicated a mixture of *protio*-products (58 %: 39 % *p*-methylphenylacetylene and 19 % phenylacetylene), and as the reaction proceeded to completion, presumably 42 % deuterated products.

**Scheme 4.9.** Proposed mechanism for the acid-catalyzed oxidative addition of PhCCH to  $(^t\text{Bu}_4\text{PCP})\text{Ir}(\text{CO})$ .



**Scheme 4.10.** Cross-labeling experiment involving *p*-methylphenylacetylene (150 mM) and phenylacetylene-*d*1 (150 mM).

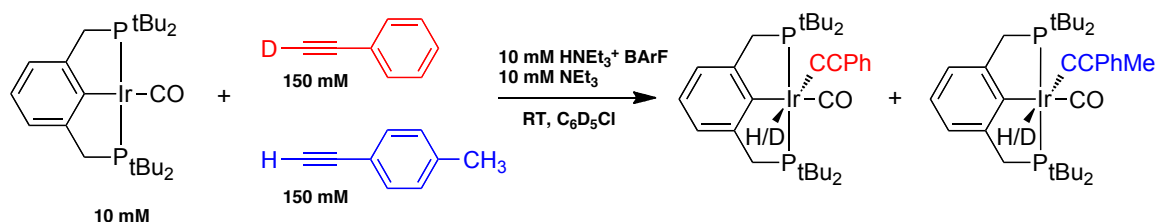
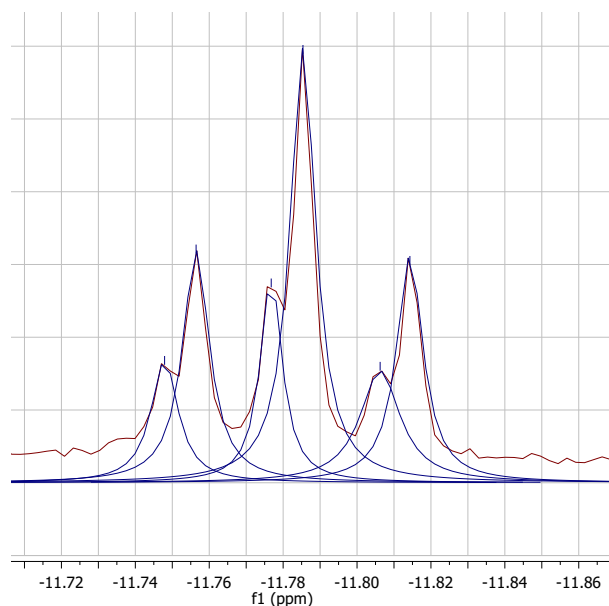


**Figure 4.5.** Deconvoluted hydride signals in the  $^1\text{H}$  nmr spectrum of the products obtained in the cross-labeling experiment shown in scheme 4.10. The larger set of peaks corresponds to the *para*-methylphenylacetylene product, while the smaller set corresponds to the phenylacetylene product.



#### 4.2.8 DFT Calculations

To further support our mechanism, DFT calculations were performed in the presence of a polarizable continuum modeling chlorobenzene (**figure 4.6**). Interestingly, DFT calculations show that addition of the alkyne to the five-coordinate protonated carbonyl complex yields a six-coordinate phenylacetylene adduct (likely resulting from electrophilic addition of  $\text{PhCCH}$ ) in which distortion of the alkyne C-H bond has resulted in a  $\text{C}\equiv\text{C-H}$  angle of  $157^\circ$  (significantly distorted from the expected *ca.*  $180^\circ$  bond angle present in free  $\text{PhCCH}$ ). This orientation apparently prepares the adduct for subsequent deprotonation by the base. The transition state for the transfer of the proton from the alkyne to the base is calculated to have an activation energy of 15.9 kcal/mol, and is the

likely rate-determining step (**figure 4.7**). Note, however, that DFT calculations predict that the overall reaction is endothermic by roughly 8 kcal/mol, and that the acid-base equilibrium between  $(^{\text{tBu}}_4\text{PCP})\text{Ir}(\text{CO})$  and  $\text{HNEt}_3^+$  slightly favors formation of the cationic intermediate via protonation, neither of which agrees with experimental observation. These deviations from experimental observation persist with other functionals (PBE or B3LYP) as well; regardless of the apparently poor modeling of the thermodynamics, the kinetics describing the barriers to addition are consistent with experimental observations of a facile room-temperature reaction.

**Figure 4.6.** DFT-calculated pathway for acid-catalyzed addition of  $\text{PhCCH}$  to **4-1** ( $\Delta G$  values in kcal/mol).

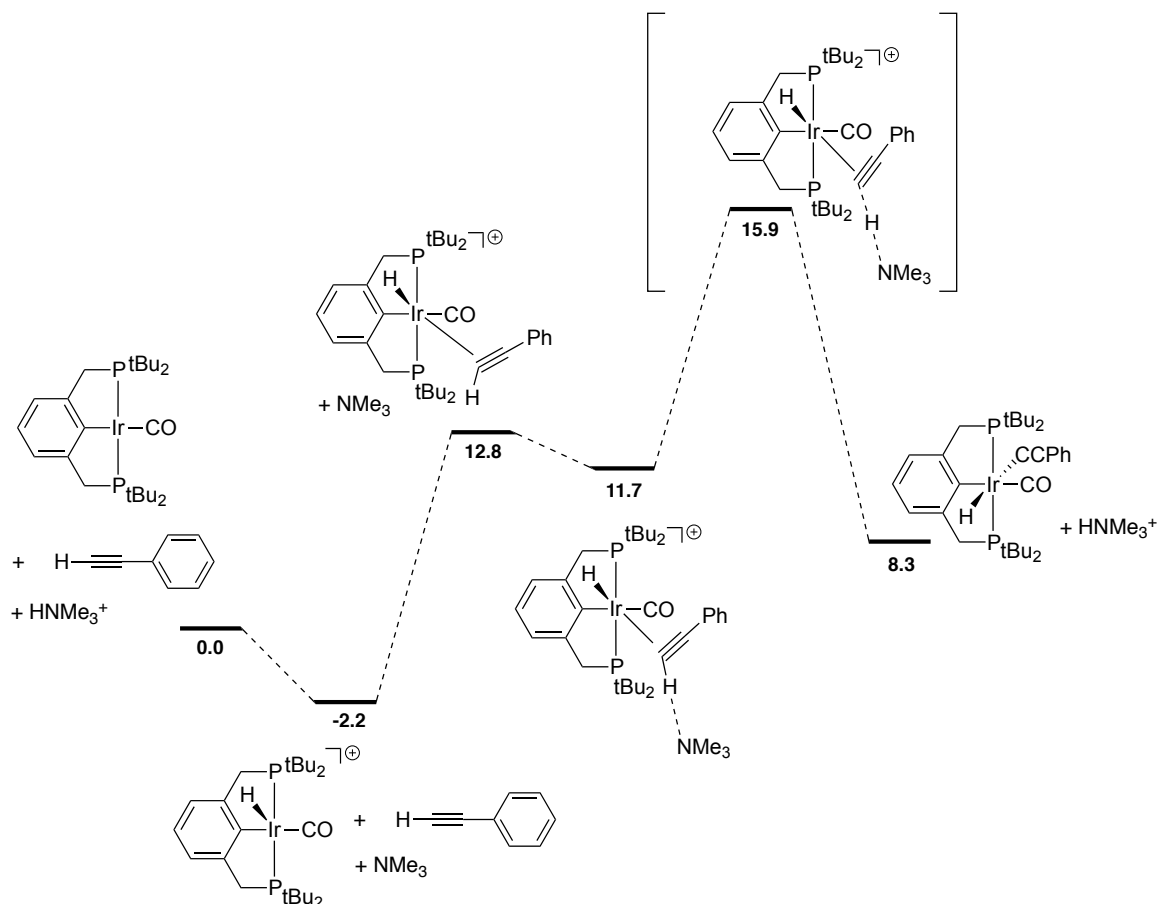
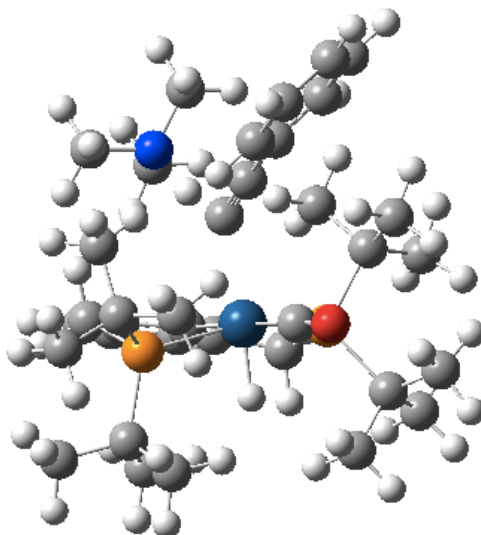


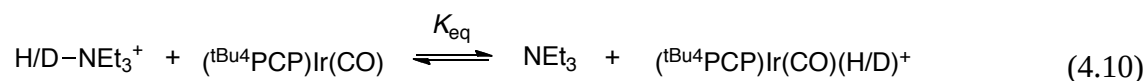


**Figure 4.7.** DFT-calculated transition state for deprotonation of the phenylacetylene adduct ( $\Delta G^\ddagger = 15.9$  kcal/mol).



#### 4.2.9 Isotope Effects

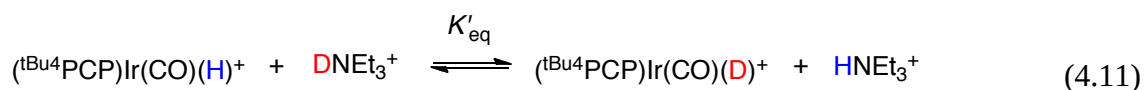
Further insight into the mechanism, and particularly the rate-determining step, can be gained by examining the kinetic isotope effect arising from isotopic substitution of the alkyne C-H bond. To determine the overall kinetic isotope effect, we need to account for both an isotope effect for the equilibrium described by **eq. 4.10** (an *equilibrium isotope effect*, EIE)



as well as the isotope effect arising from isotopic substitution of PhCCH. Individual experiments employing either PhCCH or PhCCD would be subject to *both* effects, while competition experiments (where both PhCCH and PhCCD are present in the same sample and have access to the same small equilibrium amount of protonated carbonyl complex)

would be dominated by just the KIE associated with phenylacetylene isotopic substitution. Accordingly, comparison of the observed rate constants for PhCCH and PhCCD (*i.e.* the individual experiments) indicated a large normal, primary isotope effect of 7.8 (in actuality, a product of both an EIE and a KIE) (**figure 4.8**), while the competition experiment utilizing 5 eq. PhCCD : 1 eq. PhCCH yielded a normal, primary KIE of 2.0 (**figure 4.9**) (KIE obtained as  $([4-2]_{\text{H}}/[4-2]_{\text{D}}) \times 5 = (2/5) \times 5 = 2$ )<sup>23</sup>.

Based on these values, the EIE would be expected to be *ca.* 3.9 (7.8/2.0, the quotient of the total KIE and PhCCH/D KIE). Unfortunately, the equilibrium between (PCP)Ir(CO) and (PCP)Ir(CO)H/D<sup>+</sup> described by **eq. 4.10** lies too far to the left to measure directly at room temperature. DFT calculations predict an EIE of 3.76, which is in excellent agreement with the expected value. However, a measurable surrogate equilibrium ( $K'_{\text{eq}}$ ) described by **equation 4.11** leads to an indirect means of calculating the EIE.



$K'_{\text{eq}}$  was measured and found to be 0.267 (DFT calculation value: 0.266) which corresponds to an EIE of 3.75. Based upon these isotope effect studies and DFT calculations, it is highly likely that breakage of the C-H bond of PhCCH occurs in the rate-determining step.

**Figure 4.8.** Kinetic isotope effect observed for the addition of (a) PhCCH (200 mM) or (b) PhCCH-*d*1 (200 mM) to ( $^{t}\text{Bu}^4\text{PCP}$ )Ir(CO) catalyzed by 1 mM HNEt<sub>3</sub><sup>+</sup> BAr<sup>F</sup> and 4 mM NEt<sub>3</sub> (individual experiments). Pink curve describes [4-1]; orange curve describes [4-2].

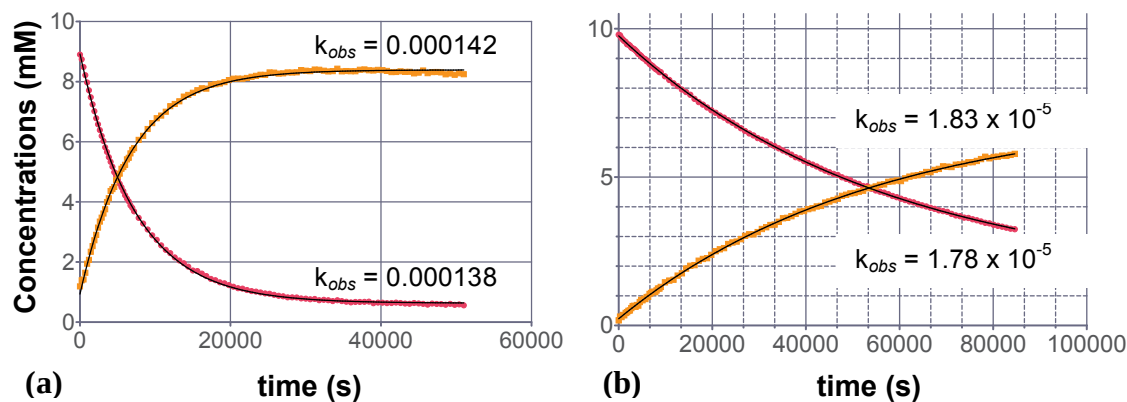
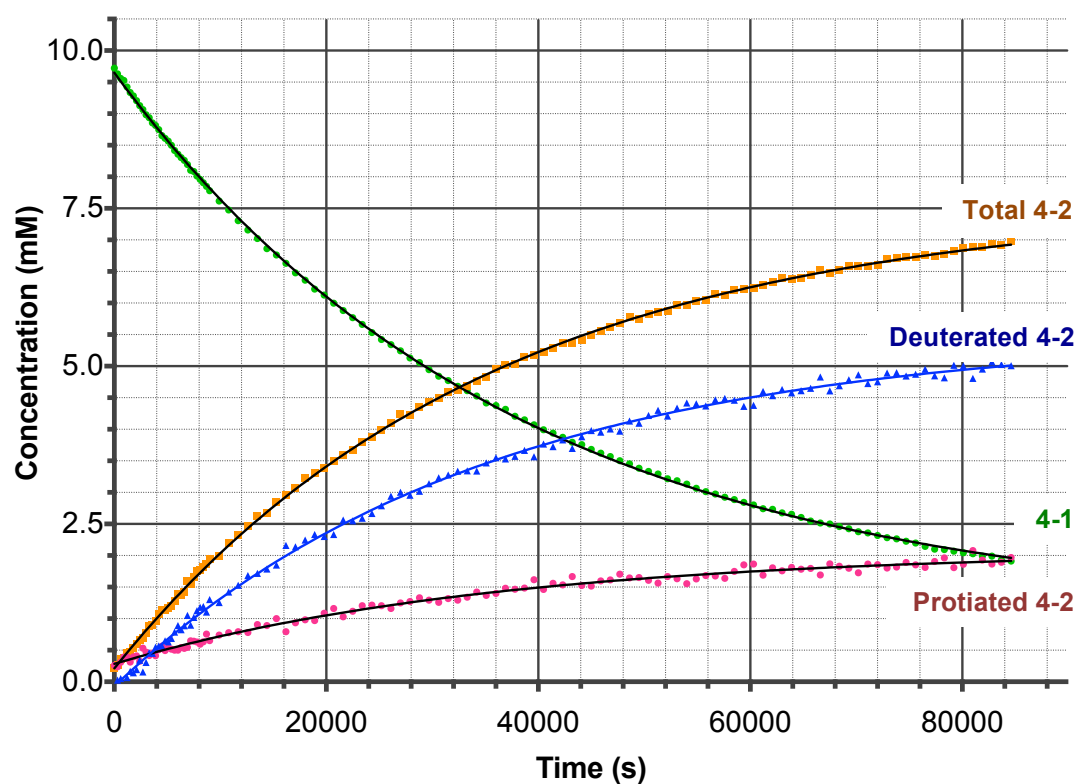


**Figure 4.9.** Competition kinetic isotope effect experiments for the buffer-catalyzed (1 mM HNEt<sub>3</sub><sup>+</sup> BAr<sup>F</sup> and 4 mM NEt<sub>3</sub>) reaction between 167 mM PhCCH-*d*1, 33 mM PhCCH, and 10 mM ( $^{t}\text{Bu}^4\text{PCP}$ )Ir(CO) (4-1).



### 4.3 Summary

In summary, we have reported a very rare, if not unprecedented, acid-catalyzed *trans* C-H addition to a square-planar d<sup>8</sup> iridium carbonyl complex, a reaction that surprisingly proceeds whereas subsequent addition of a CO ligand to the same square planar complex does not. This opens up the possibility of carrying out C-H activation catalysis under a CO atmosphere, allowing for potential carbonylation of *n*-alkanes. The proposed mechanism involves generation of a five-coordinate Ir(III) cationic intermediate, which is capable of adding phenylacetylene to form an alkynyl adduct that is then deprotonated in the rate-determining step to regenerate the acid catalyst and yield the exclusively *trans* C-H addition product. Kinetics studies to determine the order of the reaction and probe the rate-determining step are consistent with our proposed mechanism, which is further supported by DFT calculations. In future work, we hope to extend this novel reactivity of four-coordinate square-planar complexes to other transformations, with an ultimate goal of designing four-coordinate pincer complexes that are capable of adding and catalytically transforming less reactive C-H bonds.

**4.4. Acknowledgments.** We thank Dr. Tom Emge for performing x-ray diffraction studies of complex **4-3**.

### 4.5. Experimental

**General Considerations.** All reactions were conducted under an argon atmosphere in a drybox or using standard Schlenk techniques. Triethylamine, phenylacetylene and phenylacetylene-*d*1 were purchased from Sigma-Aldrich, dried over CaH<sub>2</sub> and vacuum-

transferred to yield colorless liquids, which were stored in a dark, -40 °C glovebox freezer. C<sub>6</sub>D<sub>5</sub>Cl and CD<sub>2</sub>Cl<sub>2</sub> were purchased from Cambridge Isotope Labs, dried over P<sub>2</sub>O<sub>5</sub> and vacuum-transferred. Triethylammonium B(C<sub>6</sub>F<sub>5</sub>)<sub>4</sub><sup>-</sup> was prepared by metathesis of triethylammonium chloride with LiB(C<sub>6</sub>F<sub>5</sub>)<sub>4</sub><sup>-</sup>·2.5Et<sub>2</sub>O.<sup>24</sup> (<sup>t</sup>Bu<sup>4</sup>PCP)Ir(CO) was prepared by exposing (<sup>t</sup>Bu<sup>4</sup>PCP)IrH<sub>4</sub> to a carbon monoxide atmosphere. All other reagents were purchased from commercial suppliers and used without further purification, other than freeze-pump-thaw degassing. NMR spectra were acquired on 400 or 500 MHz Varian VNMRS nmr spectrometers. <sup>1</sup>H and <sup>13</sup>C spectra are referenced to residual solvent peaks, while <sup>31</sup>P spectra are referenced to an external PMe<sub>3</sub> standard. NMR characterization of the double-addition products has been previously reported<sup>20</sup>. For kinetics experiments, the actual temperature of the probe was calibrated using a neat methanol standard before and after acquiring data. Kinetic simulation and fitting to afford rate constants was performed using COPASI.<sup>22</sup>

**Synthesis of *trans*-(PCP)Ir(CO)(H)(CCPh)** 10 mM (PCP)Ir(CO), 1 mM HNEt<sub>3</sub><sup>+</sup> B(C<sub>6</sub>F<sub>5</sub>)<sub>4</sub><sup>-</sup>, 4 mM NEt<sub>3</sub>, and 50 mM of PhCCH were mixed in a J. Young nmr tube to yield a bright yellow solution. After reacting for 24 hours at room temperature, the solution had turned very faint yellow (nearly colorless), and analysis of the resulting <sup>31</sup>P and <sup>1</sup>H nmr showed conversion to the single addition product (**1**) in 90% yield. <sup>31</sup>P{<sup>1</sup>H} NMR (C<sub>6</sub>D<sub>6</sub>, 202 MHz): δ 64.3 (s), <sup>1</sup>H NMR (C<sub>6</sub>D<sub>6</sub>, 500 MHz): δ 7.37 (d, J<sub>HH</sub> = 8.41, 2 H), 7.08 (t, J<sub>HH</sub> = 7.6, 2H), 7.05-7.0 (m, 2H) 6.96 – 6.90 (m, 2 H), 3.75 (d of vt, J<sub>PH</sub> = 3.5Hz, J<sub>HH</sub> = 16.0Hz, 2H, CH<sub>2</sub>PCP), 3.12 (d of vt, J<sub>PH</sub> = 3.6Hz, J<sub>HH</sub> = 15.6Hz, 2H, CH<sub>2</sub>PCP), 1.44 (t, J<sub>PH</sub> = 6.8 Hz, 18H, PC(CH<sub>3</sub>)<sub>3</sub>), 1.08 (t, J<sub>PH</sub> = 6.8 Hz, 18H, PC(CH<sub>3</sub>)<sub>3</sub>), -11.78 (t, J<sub>PH</sub> =

14.4 Hz, 1H, Ir-H).  $^{13}\text{C}\{^1\text{H}\}$  NMR ( $\text{C}_6\text{D}_6$ , 125 MHz): 177.38 (t,  $J_{\text{PC}}=6.2$  Hz, Ir-CO), 147.42 (t,  $J_{\text{PC}}=7.4$  Hz PCP *ortho* C), 135.5 (t,  $J_{\text{PC}}=12.7$  Ir-C=C), 131.2 (d  $J_{\text{PC}}=2.9$  PCP *ipso* C), 129.92 (s), 128.84 (s), 126.51 (s), 124.4 (s), 124.3 (s), 121.02 (t,  $J_{\text{PC}}=7.5$ , PCP *meta* C), 95.99 (t,  $J_{\text{PC}}=10.4$  Hz, Ir C=C), 39.6 (t,  $-\text{CH}_2\text{PCP}$ ,  $J_{\text{PC}}=14.9$  Hz), 36.9 (t,  $J_{\text{PC}} = 10.2$  Hz,  $\text{PC}(\text{CH}_3)_3$ ), 35.46 (t,  $J_{\text{PC}}=13.1$  Hz,  $(\text{PC}(\text{CH}_3)_3)$ , 30.2 (s,  $\text{PC}(\text{CH}_3)_3$ ), 29.9 (s,  $\text{PC}(\text{CH}_3)_3$ ).

**Synthesis of *cis*-(PCP)Ir(CO)(H)(CCPh)** To a 0.5 mL  $\text{C}_6\text{D}_6$  solution, 5 mg (PCP)IrH<sub>4</sub> (0.0083 mmol), 2.7  $\mu\text{L}$  3,3-dimethyl-1-butene (0.0207 mmol) and 0.92  $\mu\text{L}$  PhCCH (0.0083 mmol) were added. After 5 minutes at room temperature, NMR spectra indicated formation of (PCP)Ir(H)(CCPh). 1 atm CO was then added to the solution, and the *cis* product was formed immediately upon warming to room temperature. Solvent was removed under vacuum and NMR spectrum showed the formation of compound **3** in 95% yield.  $^{31}\text{P}\{^1\text{H}\}$  NMR ( $\text{C}_6\text{D}_6$ , 202 MHz):  $\delta$  58.05 (s).  $^1\text{H}$  NMR ( $\text{C}_6\text{D}_6$ , 400 MHz):  $\delta$  7.59 (d,  $J_{\text{HH}} = 6.8$  Hz, 2H, PCP), 7.25 (m, 1H, Ar), 7.02 (m, 5H, Ar), 3.18 (d of vt,  $J_{\text{PH}} = 4.0$  Hz,  $J_{\text{HH}} = 16.0$  Hz, 2H,  $\text{CH}_2\text{PCP}$ ), 3.14 (d of vt,  $J_{\text{PH}} = 3.5$  Hz,  $J_{\text{HH}} = 16.5$  Hz, 2H,  $\text{CH}_2\text{PCP}$ ), 1.34 (t,  $J_{\text{PH}} = 6.8$  Hz, 18H,  $\text{PC}(\text{CH}_3)_3$ ), 1.23 (t,  $J_{\text{PH}} = 6.8$  Hz, 18H,  $\text{PC}(\text{CH}_3)_3$ ), -9.64 (t,  $J_{\text{PH}} = 15.6$  Hz, 1H, Ir-H).

**Synthesis of (PCP)Ir(CO)H<sup>+</sup> BAr<sup>F</sup>** To a solution of 20 mg (0.032 mmol) of (PCP)Ir(CO) in 3 mL *n*-pentane was added 32.5 mg (0.032 mmol) of Brookhart's oxonium acid ( $\text{H}(\text{OEt}_2)_2^+ \text{B}(\text{C}_8\text{H}_3\text{F}_6)_4^-$ ). This resulted in rapid precipitation of the product as a bright yellow microcrystalline solid, which was collected by decanting the mother

liquor and washing several times with cold *n*-pentane until the mother liquor remained colorless. The product was recovered in 75 % yield. X-ray quality crystals were grown from slow evaporation of 1:1 mixture of benzene/pentane stored in the glovebox freezer for 48 hours. Alternatively, the  $\text{B}(\text{C}_6\text{F}_5)_4^-$  analogue can be prepared by mixing  $(\text{PCP})\text{Ir}(\text{CO})$  and dimethylanilinium  $\text{B}(\text{C}_6\text{F}_5)_4^-$  in  $\text{CH}_2\text{Cl}_2$ , and then adding cold *n*-pentane to precipitate out the product.  $^{31}\text{P}\{^1\text{H}\}$  nmr ( $\text{CD}_2\text{Cl}_2$ ): 82.99 (s)  $^1\text{H}$  nmr ( $\text{CD}_2\text{Cl}_2$ ): 7.72 (s, 8 H,  $\text{BAr}^{\text{F}}$ ), 7.56 (s, 4 H,  $\text{BAr}^{\text{F}}$ ), 7.38 (d,  $J_{\text{HH}}=7.38$  Hz, 2H, Ar-H), 7.28 (m, 1 H, Ar-H), 3.73 (qt,  $J_{\text{HH}}=18.0$  Hz,  $J_{\text{PH}}=4.11$  Hz, 4H,  $\text{CH}_2\text{PCP}$ ), 1.36 (t,  $J_{\text{PH}}=7.4$  Hz, 18 H,  $\text{PC}(\text{CH}_3)_3$ ), 1.32 (t,  $J_{\text{PH}}=7.4$  Hz, 18H,  $\text{PC}(\text{CH}_3)_3$ ), -36.8 (br s, 1H, Ir-H)  $^{19}\text{F}$  nmr: -63.3 (s).

**Typical procedure for kinetics experiments.** Stock solutions of each reagent were prepared and the appropriate amounts added via syringe to a J. Young nmr tube. Solvent, ( $^{\text{tBu}}_4\text{PCP}$ ) $\text{Ir}(\text{CO})$ , acid, base, and internal standard (1,2,4,5-tetramethylbenzene) were always added prior to  $\text{PhCCH}$ . Upon addition of  $\text{PhCCH}$ , the nmr tube was sealed and quickly frozen in liquid nitrogen until nmr acquisition could begin. All data was collected in a temperature regulated nmr probe with an actual temperature of 26.2 °C as determined by calibration with a methanol standard before and after data acquisition. The sample was quickly thawed and allowed to equilibrate at the probe temperature for *circa* 5 minutes before starting data acquisition. To ensure quantitative integration, the acquisition (*at*) and delay (*d1*) time nmr parameters were set to 5 and 15 seconds, respectively. The concentrations of ( $^{\text{tBu}}_4\text{PCP}$ ) $\text{Ir}(\text{CO})$  and ( $^{\text{tBu}}_4\text{PCP}$ ) $\text{Ir}(\text{CO})(\text{H})(\text{CCPh})$  were determined by integrating the signal due to the methylene protons and comparing those integrals to the 1,2,4,5-tetramethylbenzene internal standard integrals ( $-\text{CH}_3$  protons).

### Kinetic Isotope Effect Experiment Details.

(a) *individual experiment*: In two separate J. Young nmr tubes, 10 mM (PCP)Ir(CO), 1 mM  $\text{HNEt}_3^+ \text{B}(\text{C}_6\text{F}_5)_4^-$ , 4 mM  $\text{NEt}_3$ , and 200 mM of either PhCCH or PhCCH-*d1* were added (total reaction mixture volume of 0.5 mL). The reaction was monitored by  $^1\text{H}$  nmr over several hours, and product concentrations were determined as described above using a durene internal standard. The concentrations were fit to an exponential plot to yield a first-order rate constant. The ratio of  $k_{\text{H}}/k_{\text{D}}$  was found to be 7.8.

(b) *competition experiment*: In a J. Young nmr tube, 10 mM (PCP)Ir(CO), 1 mM  $\text{HNEt}_3^+ \text{B}(\text{C}_6\text{F}_5)_4^-$ , 4 mM  $\text{NEt}_3$ , 133.3 mM PhCCH-*d1*, and 66.7 mM PhCCH were added (total reaction mixture volume of 0.5 mL). The reaction was monitored by  $^1\text{H}$  nmr over several hours, and product concentrations were determined as described above using a durene internal standard. Once the reaction had reached completion, the ratio of the concentrations of (PCP)Ir(CO)(H)(CCPh) to (PCP)Ir(CO)(D)(CCPh) was determined and found to be 1:1, consistent with an isotope effect of 2 ( $\text{KIE} = ([\text{IrH}]/[\text{IrD}]) \times 2 = 2$ ).

(c) *EIE experiment*: In a vial was weighed 1.9 mg (PCP)Ir(CO)H $^+ \text{B}(\text{C}_6\text{F}_5)_4^-$  and 2.3 mg  $\text{DNEt}_3^+ \text{B}(\text{C}_6\text{F}_5)_4^-$ , which were subsequently dissolved in 490 microliters of  $\text{C}_6\text{D}_5\text{Cl}$  and 10 microliters of a 100 mM durene stock solution. The mixture was left to stand for 24 hours and then analyzed by  $^1\text{H}$  nmr. Total concentration of (PCP)Ir(CO)X $^+ \text{B}(\text{C}_6\text{F}_5)_4^-$  was determined by integration of the methylene signals, while [(PCP)Ir(CO)H $^+ \text{B}(\text{C}_6\text{F}_5)_4^-$ ] was found by integrating the hydride signal. The difference between these



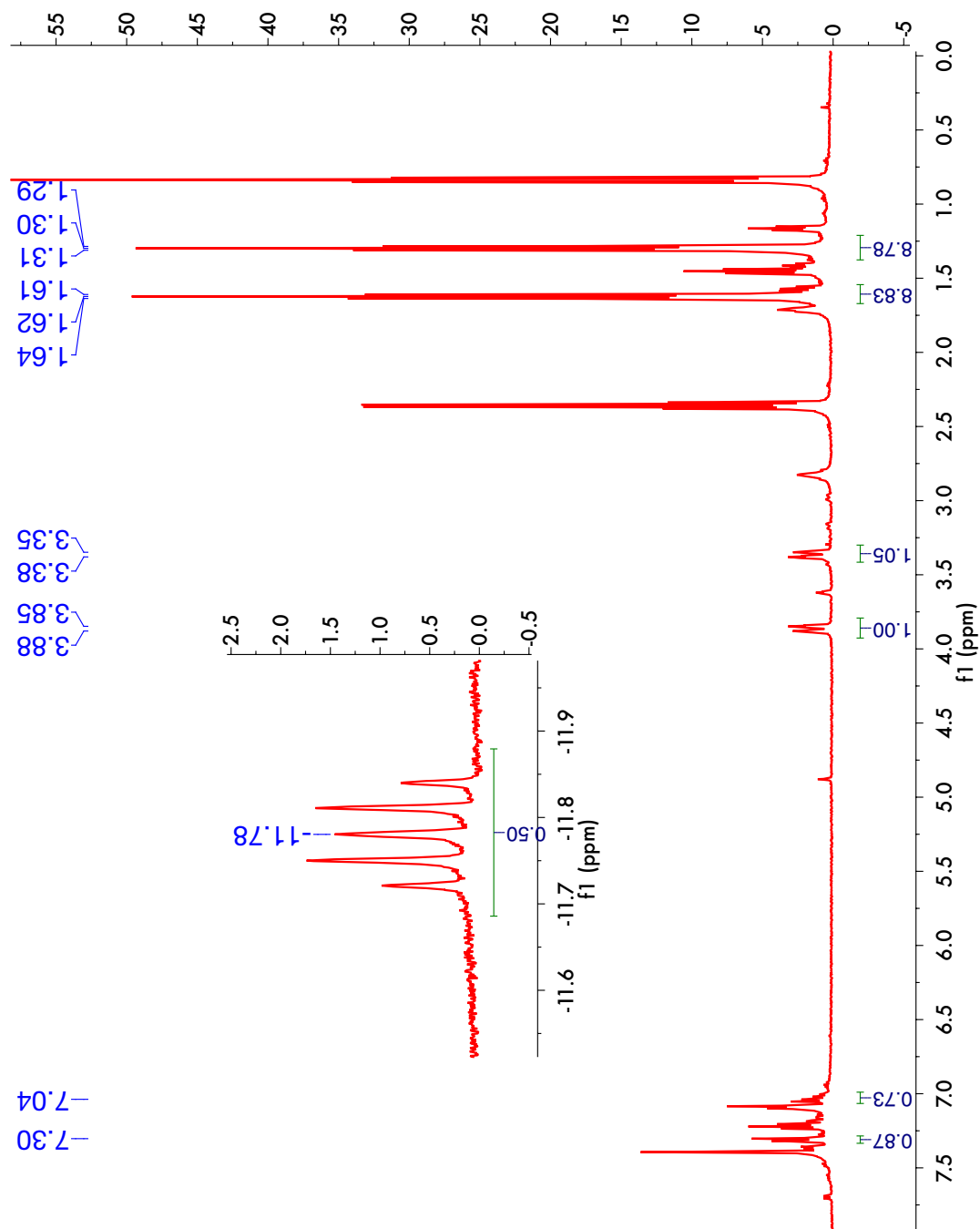
concentrations is the concentration of  $(\text{PCP})\text{Ir}(\text{CO})\text{D}^+ \text{B}(\text{C}_6\text{F}_5)_4^-$ . Likewise, total concentration of  $\text{XNEt}_3^+ \text{B}(\text{C}_6\text{F}_5)_4^-$  was determined by integration of the methyl signals,  $[\text{HNEt}_3^+ \text{B}(\text{C}_6\text{F}_5)_4^-]$  was determined by integration of the proton signal, and  $[\text{DNEt}_3^+ \text{B}(\text{C}_6\text{F}_5)_4^-]$  was found as the difference. Using the equation  $K'_{\text{eq}} = ([\text{IrD}^+][\text{HNEt}_3^+]/[\text{IrH}^+][\text{DNEt}_3^+])$ , the  $K'_{\text{eq}}$  was found to be 0.266. In this case, the EIE is equal to the reciprocal of  $K'_{\text{eq}}$ , so  $\text{EIE} = 1/0.266 = 3.76$ .

**Computational Methods.** All calculations were performed by the *Gaussian09* suite of molecular modeling software.<sup>25</sup> DFT calculations employing the M06L functional were used<sup>26</sup>. Ir atoms were described by a LANL2TZ basis set augmented by a diffuse d-type function (exponent = 0.07645) (value obtained as one-half times the exponent of the outermost d-type function in the LANL2TZ basis set for Ir).<sup>27</sup> All other atoms were described by a 6-311G(d,p) basis set<sup>28</sup>. All calculations made use of a conductor-like polarizable continuum model (c-PCM) representing chlorobenzene and were conducted at standard temperature and pressure.<sup>29</sup>

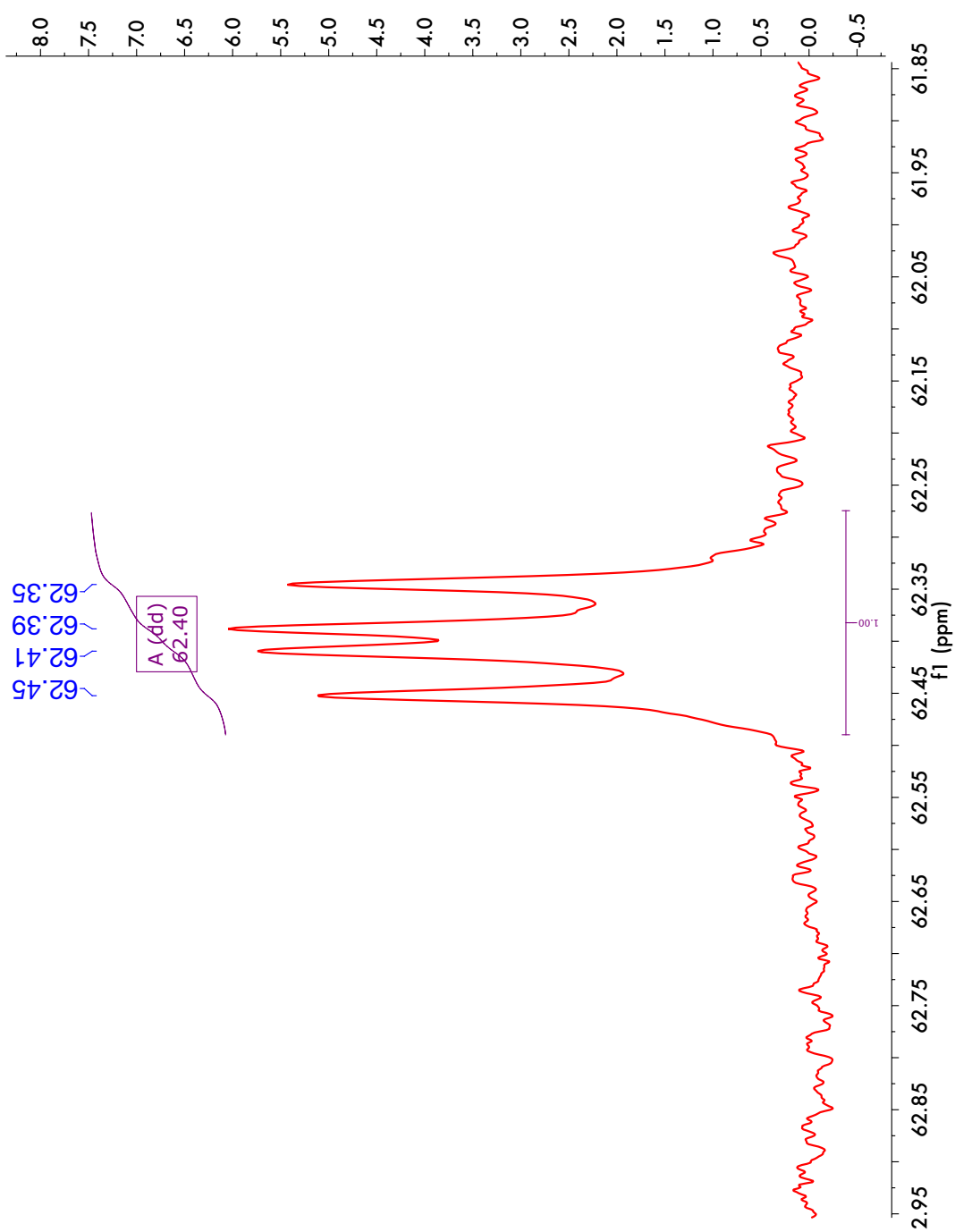
## 4.6 Chapter 4 Appendix

### 4.6.1 NMR spectra

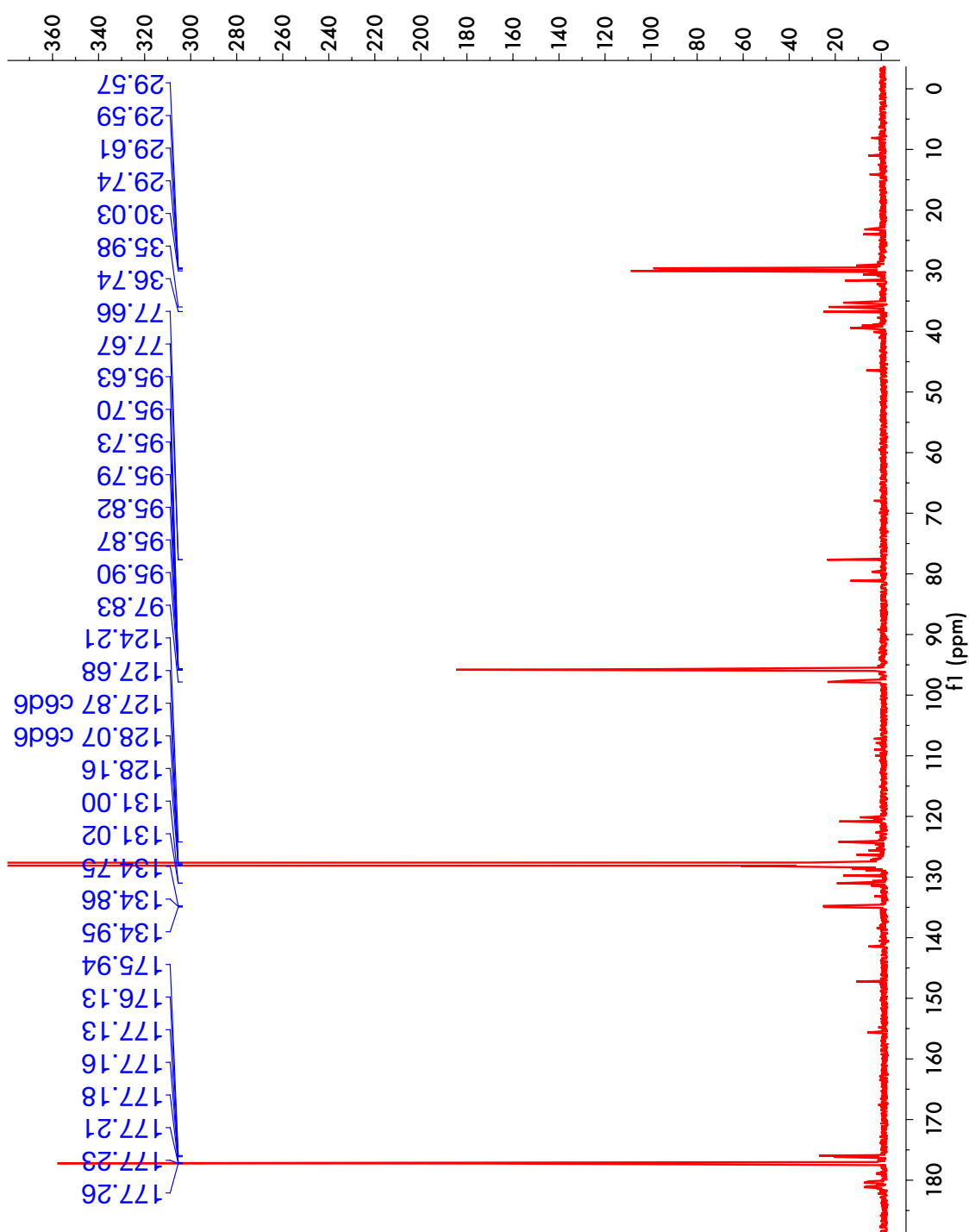
**Figure 4A.1.**  $^1\text{H}$  nmr spectrum of **4-2** ( $^{13}\text{C}$ -labelled  $\text{PhC}^{13}\text{CH}$  product)

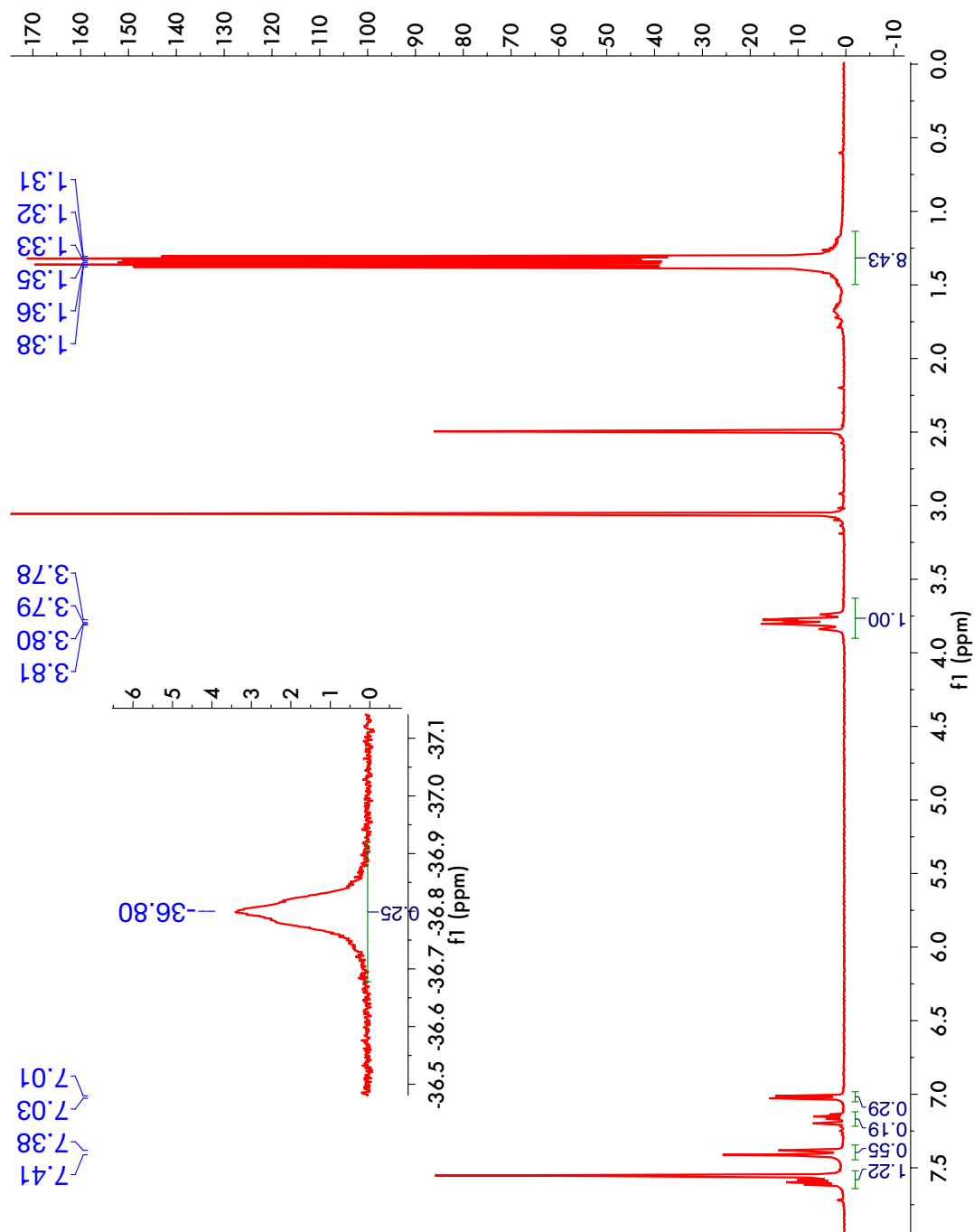


**Figure 4A.2.**  $^{31}\text{P}$  nmr spectrum of **4-2** ( $^{13}\text{C}$ -labelled  $\text{PhC}^{13}\text{CH}$  product)

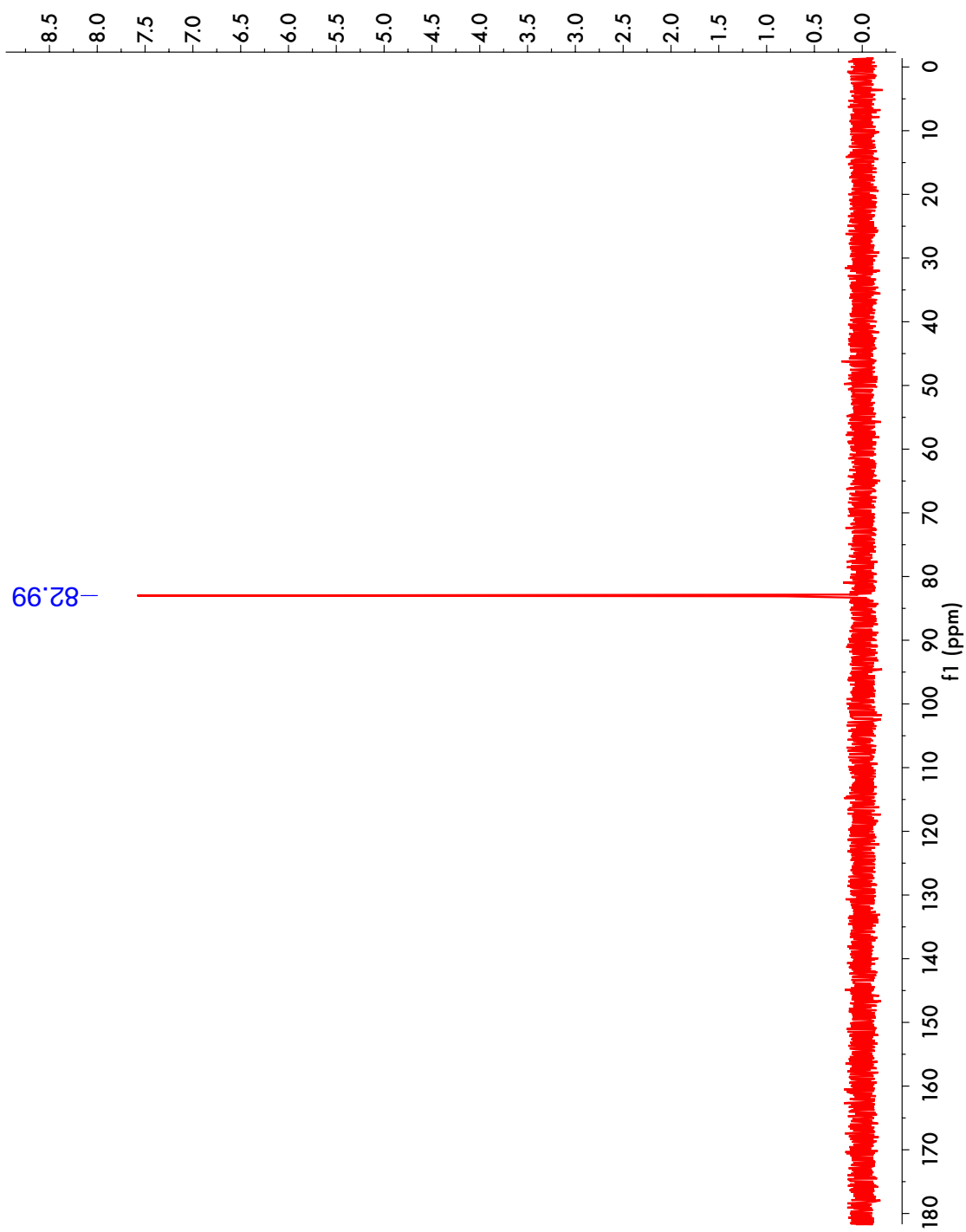


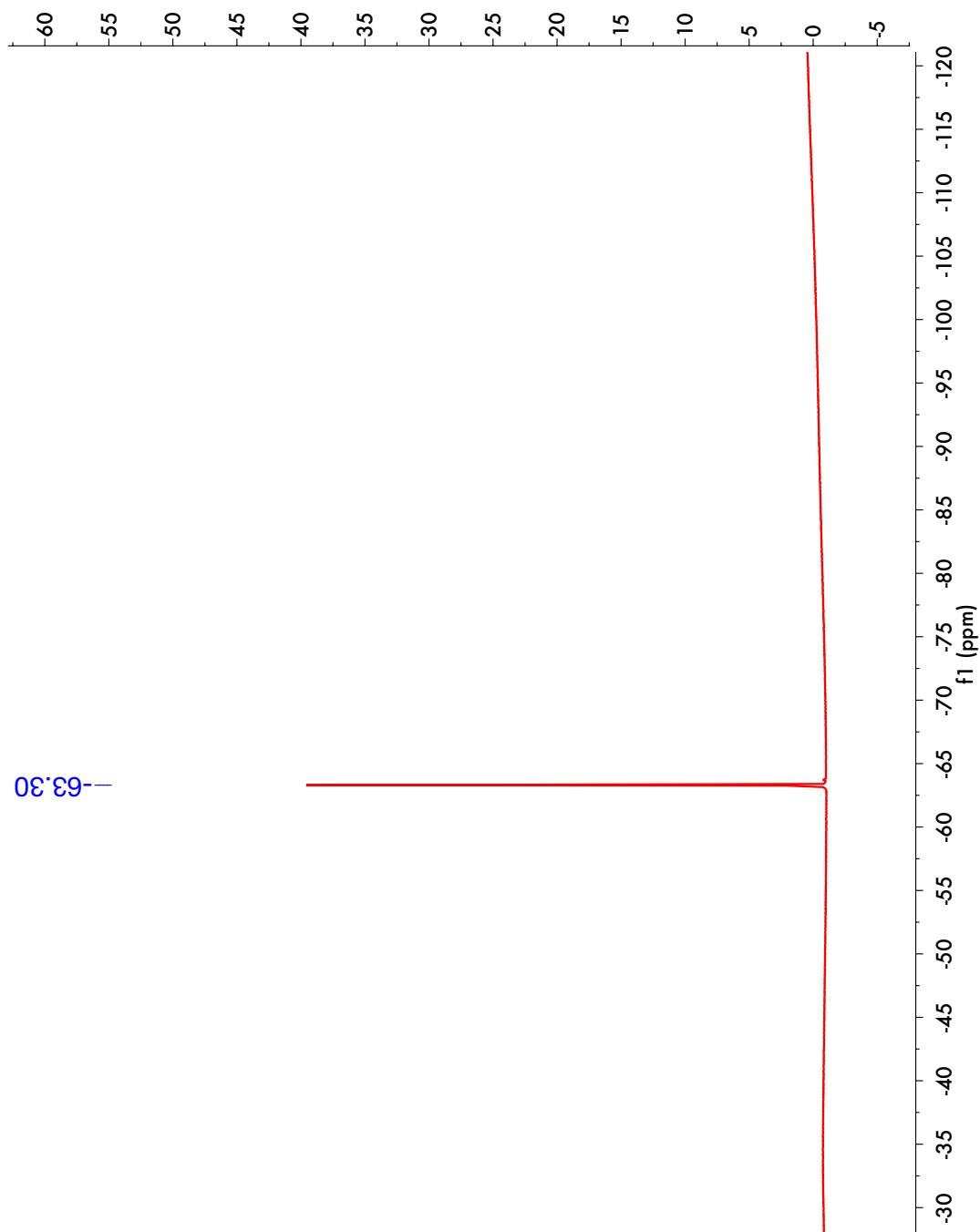
**Figure 4A.3.**  $^{13}\text{C}$  nmr spectrum of **4-2** ( $^{13}\text{C}$ -labelled  $\text{PhC}^{13}\text{CH}$  product)



**Figure 4A.4.**  $^1\text{H}$  nmr spectrum of 4-3

**Figure 4A.5.**  $^{31}\text{P}$  nmr spectrum of 4-3



**Figure 4A.6.**  $^{19}\text{F}$  nmr spectrum of 4-3

#### 4.6.2 Full crystal data of (<sup>t</sup>Bu<sup>4</sup>PCP)Ir(CO)(H)<sup>+</sup> BAr<sup>F</sup><sup>-</sup> (4-3)

**X-ray Structure Determination.** X-ray diffraction data were collected on a Bruker Smart APEX CCD diffractometer with graphite monochromatized Mo K $\alpha$  radiation ( $\lambda$  = 0.71073 Å) at 100 K. Crystals were immersed in Paratone oil, placed on a glass needle, and examined at 100 K. The data were corrected for Lorentz effects, polarization, and absorption, the latter by a multi-scan (SADABS) method.<sup>30</sup> The structures were solved by direct methods (SHELXS86).<sup>31</sup> All non-hydrogen atoms were refined (SHELXL97)<sup>32</sup> based upon  $F_{\text{obs}}^2$ . All hydrogen atom coordinates were calculated with idealized geometries (SHELXL97). Scattering factors ( $f_0$ ,  $f'$ ,  $f''$ ) are as described in SHELXL97.<sup>32</sup>

**Figure 4A.7.** Full crystal Structure of 4-3 (including BAr<sup>F</sup> counteranion).

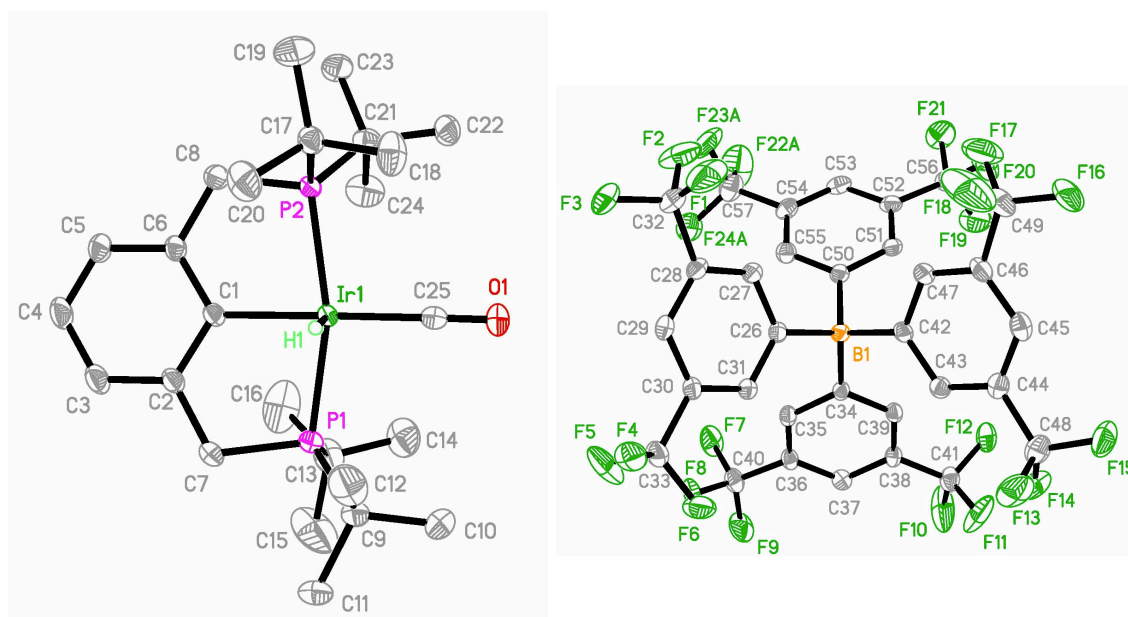




**Table 4A.1.** Crystal data and structure refinement for **4-3**.

Identification code	jh-xr1a	
Empirical formula	C <sub>57</sub> H <sub>56</sub> B F <sub>24</sub> Ir O P <sub>2</sub>	
Formula weight	1477.97	
Temperature	100(2) K	
Wavelength	0.71073 Å	
Crystal system	Monoclinic	
Space group	P2(1)/c	
Unit cell dimensions	a = 12.5713(6) Å	a = 90°.
	b = 12.3816(6) Å	b = 96.220(1)°.
	c = 38.9538(18) Å	g = 90°.
Volume	6027.6(5) Å <sup>3</sup>	
Z	4	
Density (calculated)	1.629 Mg/m <sup>3</sup>	
Absorption coefficient	2.381 mm <sup>-1</sup>	
F(000)	2936	
Crystal size	0.21 x 0.12 x 0.05 mm <sup>3</sup>	
Theta range for data collection	1.73 to 31.62°.	
Index ranges	-18 ≤ h ≤ 18, -18 ≤ k ≤ 18, -57 ≤ l ≤ 55	
Reflections collected	75452	
Independent reflections	20196 [R(int) = 0.0263]	
Completeness to theta = 31.62°	99.6 %	
Absorption correction	Semi-empirical from equivalents	
Max. and min. transmission	0.8902 and 0.6347	
Refinement method	Full-matrix least-squares on F <sup>2</sup>	
Data / restraints / parameters	20196 / 173 / 819	
Goodness-of-fit on F <sup>2</sup>	1.004	
Final R indices [I > 2σ(I)]	R1 = 0.0336, wR2 = 0.0754	
R indices (all data)	R1 = 0.0395, wR2 = 0.0781	
Largest diff. peak and hole	2.344 and -1.267 e.Å <sup>-3</sup>	

**Table 4A.2.** Atomic coordinates ( $\times 10^4$ ) and equivalent isotropic displacement parameters ( $\text{\AA}^2 \times 10^3$ ) for **4-3**.  $U(\text{eq})$  is defined as one third of the trace of the orthogonalized  $U^{ij}$  tensor.

	x	y	z	$U(\text{eq})$
Ir(1)	7079(1)	7219(1)	3800(1)	17(1)
P(1)	7722(1)	6687(1)	3286(1)	23(1)
P(2)	6797(1)	8113(1)	4310(1)	18(1)
C(1)	8026(2)	8561(2)	3736(1)	18(1)
C(2)	8468(2)	8743(2)	3422(1)	21(1)
C(3)	9065(2)	9671(2)	3376(1)	29(1)
C(4)	9218(2)	10438(2)	3634(1)	31(1)
C(5)	8806(2)	10276(2)	3946(1)	26(1)
C(6)	8223(2)	9344(2)	3999(1)	20(1)
C(7)	8259(2)	7947(2)	3130(1)	26(1)
C(8)	7832(2)	9164(2)	4346(1)	26(1)
C(9)	6748(3)	6209(3)	2921(1)	37(1)
C(10)	6413(3)	5026(3)	2973(1)	50(1)
C(11)	7204(4)	6303(3)	2570(1)	56(1)
C(12)	5768(3)	6928(3)	2918(1)	49(1)
C(13)	8898(3)	5770(3)	3396(1)	40(1)
C(14)	8565(3)	4747(3)	3578(1)	48(1)
C(15)	9452(5)	5439(4)	3080(1)	86(2)
C(16)	9697(3)	6389(3)	3651(1)	64(1)
C(17)	5494(2)	8842(2)	4284(1)	23(1)
C(18)	4566(2)	8052(2)	4209(1)	36(1)
C(19)	5345(3)	9477(3)	4613(1)	39(1)
C(20)	5485(3)	9632(3)	3982(1)	38(1)
C(21)	7108(2)	7266(2)	4705(1)	24(1)
C(22)	6207(2)	6458(2)	4752(1)	31(1)
C(23)	7339(3)	7934(2)	5035(1)	34(1)
C(24)	8119(3)	6620(3)	4642(1)	42(1)
C(25)	6143(2)	6009(2)	3844(1)	27(1)
O(1)	5564(2)	5314(2)	3862(1)	44(1)
B(1)	2669(2)	2397(2)	3757(1)	18(1)

C(26)	3980(2)	2436(2)	3808(1)	18(1)
C(27)	4572(2)	2228(2)	3529(1)	19(1)
C(28)	5687(2)	2184(2)	3568(1)	20(1)
C(29)	6263(2)	2353(2)	3888(1)	20(1)
C(30)	5691(2)	2540(2)	4168(1)	20(1)
C(31)	4578(2)	2574(2)	4129(1)	19(1)
C(32)	6263(2)	1898(2)	3264(1)	28(1)
C(33)	6299(2)	2733(2)	4516(1)	27(1)
C(34)	2112(2)	3187(2)	4024(1)	17(1)
C(35)	2588(2)	4160(2)	4147(1)	19(1)
C(36)	2087(2)	4862(2)	4359(1)	20(1)
C(37)	1089(2)	4627(2)	4460(1)	21(1)
C(38)	597(2)	3676(2)	4338(1)	19(1)
C(39)	1084(2)	2990(2)	4122(1)	18(1)
C(40)	2631(2)	5897(2)	4470(1)	26(1)
C(41)	-458(2)	3354(2)	4454(1)	28(1)
C(42)	2352(2)	1124(2)	3801(1)	18(1)
C(43)	2026(2)	683(2)	4105(1)	20(1)
C(44)	1751(2)	-399(2)	4131(1)	22(1)
C(45)	1824(2)	-1110(2)	3860(1)	25(1)
C(46)	2197(2)	-705(2)	3563(1)	25(1)
C(47)	2443(2)	380(2)	3534(1)	22(1)
C(48)	1389(2)	-801(2)	4463(1)	30(1)
C(49)	2380(3)	-1463(3)	3274(1)	39(1)
C(50)	2204(2)	2863(2)	3375(1)	20(1)
C(51)	1261(2)	2468(2)	3196(1)	22(1)
C(52)	814(2)	2924(2)	2887(1)	24(1)
C(53)	1298(2)	3792(2)	2741(1)	25(1)
C(54)	2242(2)	4194(2)	2913(1)	24(1)
C(55)	2679(2)	3744(2)	3225(1)	22(1)
C(56)	-206(2)	2452(3)	2717(1)	33(1)
C(57)	2819(2)	5097(2)	2756(1)	35(1)
F(1)	6320(2)	836(2)	3221(1)	59(1)
F(2)	5792(2)	2304(2)	2969(1)	55(1)
F(3)	7266(1)	2255(2)	3292(1)	47(1)
F(4)	7170(1)	2112(2)	4571(1)	37(1)

F(5)	6650(2)	3744(2)	4552(1)	56(1)
F(6)	5719(1)	2517(2)	4776(1)	51(1)
F(7)	2593(2)	6607(1)	4209(1)	41(1)
F(8)	3674(1)	5751(1)	4578(1)	34(1)
F(9)	2200(2)	6384(2)	4727(1)	43(1)
F(10)	-942(2)	4149(2)	4599(1)	76(1)
F(11)	-355(2)	2543(2)	4679(1)	62(1)
F(12)	-1138(1)	2983(2)	4195(1)	43(1)
F(13)	2213(2)	-1037(2)	4698(1)	49(1)
F(14)	791(2)	-70(2)	4611(1)	41(1)
F(15)	791(2)	-1699(2)	4421(1)	44(1)
F(16)	1765(2)	-2331(2)	3262(1)	56(1)
F(17)	2221(3)	-1005(2)	2967(1)	72(1)
F(18)	3394(2)	-1820(3)	3301(1)	90(1)
F(19)	-1026(2)	2646(3)	2891(1)	67(1)
F(20)	-142(2)	1361(2)	2695(1)	58(1)
F(21)	-447(2)	2779(2)	2395(1)	52(1)
F(22A)	2221(3)	5723(3)	2551(1)	79(1)
F(23A)	3565(3)	4712(2)	2564(1)	60(1)
F(24A)	3397(3)	5709(2)	2989(1)	58(1)
F(22B)	3747(9)	5140(12)	2833(4)	66(3)
F(23B)	2223(10)	6028(7)	2787(3)	53(2)
F(24B)	2523(11)	5149(10)	2404(2)	58(2)

---

**Table 4A.3.** Bond lengths [Å] and angles [°] for **4-3**.

Ir(1)-C(25)	1.924(3)	C(11)-H(11C)	0.9800
Ir(1)-C(1)	2.074(2)	C(12)-H(12A)	0.9800
Ir(1)-P(1)	2.3321(6)	C(12)-H(12B)	0.9800
Ir(1)-P(2)	2.3360(6)	C(12)-H(12C)	0.9800
Ir(1)-H(1)	1.59(6)	C(13)-C(14)	1.532(5)
P(1)-C(7)	1.829(3)	C(13)-C(15)	1.535(5)
P(1)-C(9)	1.869(3)	C(13)-C(16)	1.538(6)
P(1)-C(13)	1.876(3)	C(14)-H(14A)	0.9800
P(2)-C(8)	1.835(2)	C(14)-H(14B)	0.9800
P(2)-C(17)	1.863(2)	C(14)-H(14C)	0.9800
P(2)-C(21)	1.866(2)	C(15)-H(15A)	0.9800
C(1)-C(2)	1.412(3)	C(15)-H(15B)	0.9800
C(1)-C(6)	1.413(3)	C(15)-H(15C)	0.9800
C(2)-C(3)	1.396(3)	C(16)-H(16A)	0.9800
C(2)-C(7)	1.506(3)	C(16)-H(16B)	0.9800
C(3)-C(4)	1.383(4)	C(16)-H(16C)	0.9800
C(3)-H(3)	0.9500	C(17)-C(18)	1.526(4)
C(4)-C(5)	1.385(4)	C(17)-C(19)	1.530(4)
C(4)-H(4)	0.9500	C(17)-C(20)	1.532(4)
C(5)-C(6)	1.395(3)	C(18)-H(18A)	0.9800
C(5)-H(5)	0.9500	C(18)-H(18B)	0.9800
C(6)-C(8)	1.507(3)	C(18)-H(18C)	0.9800
C(7)-H(7A)	0.9900	C(19)-H(19A)	0.9800
C(7)-H(7B)	0.9900	C(19)-H(19B)	0.9800
C(8)-H(8A)	0.9900	C(19)-H(19C)	0.9800
C(8)-H(8B)	0.9900	C(20)-H(20A)	0.9800
C(9)-C(12)	1.519(5)	C(20)-H(20B)	0.9800
C(9)-C(10)	1.543(4)	C(20)-H(20C)	0.9800
C(9)-C(11)	1.547(4)	C(21)-C(23)	1.531(4)
C(10)-H(10A)	0.9800	C(21)-C(22)	1.537(4)
C(10)-H(10B)	0.9800	C(21)-C(24)	1.543(4)
C(10)-H(10C)	0.9800	C(22)-H(22A)	0.9800
C(11)-H(11A)	0.9800	C(22)-H(22B)	0.9800
C(11)-H(11B)	0.9800	C(22)-H(22C)	0.9800

C(23)-H(23A)	0.9800	C(38)-C(39)	1.385(3)
C(23)-H(23B)	0.9800	C(38)-C(41)	1.500(3)
C(23)-H(23C)	0.9800	C(39)-H(39)	0.9500
C(24)-H(24A)	0.9800	C(40)-F(9)	1.333(3)
C(24)-H(24B)	0.9800	C(40)-F(7)	1.341(3)
C(24)-H(24C)	0.9800	C(40)-F(8)	1.345(3)
C(25)-O(1)	1.134(3)	C(41)-F(10)	1.316(3)
B(1)-C(42)	1.639(3)	C(41)-F(11)	1.331(3)
B(1)-C(26)	1.640(3)	C(41)-F(12)	1.331(3)
B(1)-C(34)	1.641(3)	C(42)-C(43)	1.402(3)
B(1)-C(50)	1.643(3)	C(42)-C(47)	1.405(3)
C(26)-C(31)	1.397(3)	C(43)-C(44)	1.391(3)
C(26)-C(27)	1.405(3)	C(43)-H(43)	0.9500
C(27)-C(28)	1.395(3)	C(44)-C(45)	1.385(4)
C(27)-H(27)	0.9500	C(44)-C(48)	1.501(4)
C(28)-C(29)	1.390(3)	C(45)-C(46)	1.390(4)
C(28)-C(32)	1.495(3)	C(45)-H(45)	0.9500
C(29)-C(30)	1.389(3)	C(46)-C(47)	1.386(3)
C(29)-H(29)	0.9500	C(46)-C(49)	1.501(4)
C(30)-C(31)	1.392(3)	C(47)-H(47)	0.9500
C(30)-C(33)	1.501(3)	C(48)-F(13)	1.339(3)
C(31)-H(31)	0.9500	C(48)-F(15)	1.343(3)
C(32)-F(1)	1.329(3)	C(48)-F(14)	1.344(3)
C(32)-F(3)	1.330(3)	C(49)-F(17)	1.320(4)
C(32)-F(2)	1.333(3)	C(49)-F(16)	1.321(4)
C(33)-F(5)	1.330(3)	C(49)-F(18)	1.342(4)
C(33)-F(4)	1.336(3)	C(50)-C(51)	1.397(3)
C(33)-F(6)	1.338(3)	C(50)-C(55)	1.402(3)
C(34)-C(35)	1.406(3)	C(51)-C(52)	1.391(3)
C(34)-C(39)	1.407(3)	C(51)-H(51)	0.9500
C(35)-C(36)	1.394(3)	C(52)-C(53)	1.385(4)
C(35)-H(35)	0.9500	C(52)-C(56)	1.497(4)
C(36)-C(37)	1.387(3)	C(53)-C(54)	1.390(4)
C(36)-C(40)	1.494(3)	C(53)-H(53)	0.9500
C(37)-C(38)	1.390(3)	C(54)-C(55)	1.394(3)
C(37)-H(37)	0.9500	C(54)-C(57)	1.498(4)

C(55)-H(55)	0.9500	C(57)-F(24B)	1.382(10)
C(56)-F(19)	1.316(3)	C(57)-F(23B)	1.388(10)
C(56)-F(21)	1.323(3)	F(22A)-F(23B)	0.994(12)
C(56)-F(20)	1.356(4)	F(22A)-F(24B)	1.011(13)
C(57)-F(22B)	1.174(12)	F(23A)-F(22B)	1.172(17)
C(57)-F(22A)	1.294(4)	F(23A)-F(24B)	1.490(15)
C(57)-F(24A)	1.335(4)	F(24A)-F(22B)	1.057(17)
C(57)-F(23A)	1.348(4)	F(24A)-F(23B)	1.643(13)
C(25)-Ir(1)-C(1)	177.04(10)	C(1)-C(2)-C(7)	119.7(2)
C(25)-Ir(1)-P(1)	97.39(7)	C(4)-C(3)-C(2)	120.3(2)
C(1)-Ir(1)-P(1)	82.31(6)	C(4)-C(3)-H(3)	119.9
C(25)-Ir(1)-P(2)	98.17(7)	C(2)-C(3)-H(3)	119.9
C(1)-Ir(1)-P(2)	82.26(6)	C(3)-C(4)-C(5)	120.2(2)
P(1)-Ir(1)-P(2)	164.28(2)	C(3)-C(4)-H(4)	119.9
C(25)-Ir(1)-H(1)	88(3)	C(5)-C(4)-H(4)	119.9
C(1)-Ir(1)-H(1)	89(3)	C(4)-C(5)-C(6)	120.1(2)
P(1)-Ir(1)-H(1)	89(3)	C(4)-C(5)-H(5)	119.9
P(2)-Ir(1)-H(1)	94(3)	C(6)-C(5)-H(5)	119.9
C(7)-P(1)-C(9)	104.61(13)	C(5)-C(6)-C(1)	121.0(2)
C(7)-P(1)-C(13)	106.38(14)	C(5)-C(6)-C(8)	118.9(2)
C(9)-P(1)-C(13)	114.67(16)	C(1)-C(6)-C(8)	120.1(2)
C(7)-P(1)-Ir(1)	102.61(8)	C(2)-C(7)-P(1)	110.34(16)
C(9)-P(1)-Ir(1)	118.84(10)	C(2)-C(7)-H(7A)	109.6
C(13)-P(1)-Ir(1)	108.23(11)	P(1)-C(7)-H(7A)	109.6
C(8)-P(2)-C(17)	105.82(12)	C(2)-C(7)-H(7B)	109.6
C(8)-P(2)-C(21)	104.58(12)	P(1)-C(7)-H(7B)	109.6
C(17)-P(2)-C(21)	114.94(11)	H(7A)-C(7)-H(7B)	108.1
C(8)-P(2)-Ir(1)	103.26(8)	C(6)-C(8)-P(2)	109.49(16)
C(17)-P(2)-Ir(1)	113.38(8)	C(6)-C(8)-H(8A)	109.8
C(21)-P(2)-Ir(1)	113.38(8)	P(2)-C(8)-H(8A)	109.8
C(2)-C(1)-C(6)	117.5(2)	C(6)-C(8)-H(8B)	109.8
C(2)-C(1)-Ir(1)	121.10(16)	P(2)-C(8)-H(8B)	109.8
C(6)-C(1)-Ir(1)	121.32(15)	H(8A)-C(8)-H(8B)	108.2
C(3)-C(2)-C(1)	120.8(2)	C(12)-C(9)-C(10)	109.0(3)
C(3)-C(2)-C(7)	119.5(2)	C(12)-C(9)-C(11)	109.0(3)

C(10)-C(9)-C(11)	108.7(3)	H(15A)-C(15)-H(15B)	109.5
C(12)-C(9)-P(1)	106.6(2)	C(13)-C(15)-H(15C)	109.5
C(10)-C(9)-P(1)	111.5(2)	H(15A)-C(15)-H(15C)	109.5
C(11)-C(9)-P(1)	112.0(2)	H(15B)-C(15)-H(15C)	109.5
C(9)-C(10)-H(10A)	109.5	C(13)-C(16)-H(16A)	109.5
C(9)-C(10)-H(10B)	109.5	C(13)-C(16)-H(16B)	109.5
H(10A)-C(10)-H(10B)	109.5	H(16A)-C(16)-H(16B)	109.5
C(9)-C(10)-H(10C)	109.5	C(13)-C(16)-H(16C)	109.5
H(10A)-C(10)-H(10C)	109.5	H(16A)-C(16)-H(16C)	109.5
H(10B)-C(10)-H(10C)	109.5	H(16B)-C(16)-H(16C)	109.5
C(9)-C(11)-H(11A)	109.5	C(18)-C(17)-C(19)	109.2(2)
C(9)-C(11)-H(11B)	109.5	C(18)-C(17)-C(20)	108.7(2)
H(11A)-C(11)-H(11B)	109.5	C(19)-C(17)-C(20)	108.9(2)
C(9)-C(11)-H(11C)	109.5	C(18)-C(17)-P(2)	110.46(17)
H(11A)-C(11)-H(11C)	109.5	C(19)-C(17)-P(2)	112.96(19)
H(11B)-C(11)-H(11C)	109.5	C(20)-C(17)-P(2)	106.51(18)
C(9)-C(12)-H(12A)	109.5	C(17)-C(18)-H(18A)	109.5
C(9)-C(12)-H(12B)	109.5	C(17)-C(18)-H(18B)	109.5
H(12A)-C(12)-H(12B)	109.5	H(18A)-C(18)-H(18B)	109.5
C(9)-C(12)-H(12C)	109.5	C(17)-C(18)-H(18C)	109.5
H(12A)-C(12)-H(12C)	109.5	H(18A)-C(18)-H(18C)	109.5
H(12B)-C(12)-H(12C)	109.5	H(18B)-C(18)-H(18C)	109.5
C(14)-C(13)-C(15)	108.7(3)	C(17)-C(19)-H(19A)	109.5
C(14)-C(13)-C(16)	107.8(3)	C(17)-C(19)-H(19B)	109.5
C(15)-C(13)-C(16)	109.2(4)	H(19A)-C(19)-H(19B)	109.5
C(14)-C(13)-P(1)	111.0(2)	C(17)-C(19)-H(19C)	109.5
C(15)-C(13)-P(1)	113.1(3)	H(19A)-C(19)-H(19C)	109.5
C(16)-C(13)-P(1)	106.8(2)	H(19B)-C(19)-H(19C)	109.5
C(13)-C(14)-H(14A)	109.5	C(17)-C(20)-H(20A)	109.5
C(13)-C(14)-H(14B)	109.5	C(17)-C(20)-H(20B)	109.5
H(14A)-C(14)-H(14B)	109.5	H(20A)-C(20)-H(20B)	109.5
C(13)-C(14)-H(14C)	109.5	C(17)-C(20)-H(20C)	109.5
H(14A)-C(14)-H(14C)	109.5	H(20A)-C(20)-H(20C)	109.5
H(14B)-C(14)-H(14C)	109.5	H(20B)-C(20)-H(20C)	109.5
C(13)-C(15)-H(15A)	109.5	C(23)-C(21)-C(22)	109.0(2)
C(13)-C(15)-H(15B)	109.5	C(23)-C(21)-C(24)	109.2(2)



C(22)-C(21)-C(24)	108.2(2)	C(29)-C(28)-C(32)	119.8(2)
C(23)-C(21)-P(2)	113.07(18)	C(27)-C(28)-C(32)	119.5(2)
C(22)-C(21)-P(2)	111.88(17)	C(30)-C(29)-C(28)	117.8(2)
C(24)-C(21)-P(2)	105.28(18)	C(30)-C(29)-H(29)	121.1
C(21)-C(22)-H(22A)	109.5	C(28)-C(29)-H(29)	121.1
C(21)-C(22)-H(22B)	109.5	C(29)-C(30)-C(31)	121.3(2)
H(22A)-C(22)-H(22B)	109.5	C(29)-C(30)-C(33)	118.6(2)
C(21)-C(22)-H(22C)	109.5	C(31)-C(30)-C(33)	120.1(2)
H(22A)-C(22)-H(22C)	109.5	C(30)-C(31)-C(26)	122.1(2)
H(22B)-C(22)-H(22C)	109.5	C(30)-C(31)-H(31)	119.0
C(21)-C(23)-H(23A)	109.5	C(26)-C(31)-H(31)	119.0
C(21)-C(23)-H(23B)	109.5	F(1)-C(32)-F(3)	106.0(2)
H(23A)-C(23)-H(23B)	109.5	F(1)-C(32)-F(2)	106.9(3)
C(21)-C(23)-H(23C)	109.5	F(3)-C(32)-F(2)	106.0(2)
H(23A)-C(23)-H(23C)	109.5	F(1)-C(32)-C(28)	111.8(2)
H(23B)-C(23)-H(23C)	109.5	F(3)-C(32)-C(28)	113.1(2)
C(21)-C(24)-H(24A)	109.5	F(2)-C(32)-C(28)	112.6(2)
C(21)-C(24)-H(24B)	109.5	F(5)-C(33)-F(4)	105.6(2)
H(24A)-C(24)-H(24B)	109.5	F(5)-C(33)-F(6)	108.1(2)
C(21)-C(24)-H(24C)	109.5	F(4)-C(33)-F(6)	105.4(2)
H(24A)-C(24)-H(24C)	109.5	F(5)-C(33)-C(30)	112.1(2)
H(24B)-C(24)-H(24C)	109.5	F(4)-C(33)-C(30)	112.5(2)
O(1)-C(25)-Ir(1)	177.5(3)	F(6)-C(33)-C(30)	112.6(2)
C(42)-B(1)-C(26)	105.56(18)	C(35)-C(34)-C(39)	115.2(2)
C(42)-B(1)-C(34)	112.41(18)	C(35)-C(34)-B(1)	122.19(19)
C(26)-B(1)-C(34)	113.42(18)	C(39)-C(34)-B(1)	122.33(19)
C(42)-B(1)-C(50)	111.52(18)	C(36)-C(35)-C(34)	122.2(2)
C(26)-B(1)-C(50)	110.72(18)	C(36)-C(35)-H(35)	118.9
C(34)-B(1)-C(50)	103.36(18)	C(34)-C(35)-H(35)	118.9
C(31)-C(26)-C(27)	115.8(2)	C(37)-C(36)-C(35)	121.2(2)
C(31)-C(26)-B(1)	123.3(2)	C(37)-C(36)-C(40)	119.8(2)
C(27)-C(26)-B(1)	120.69(19)	C(35)-C(36)-C(40)	119.0(2)
C(28)-C(27)-C(26)	122.4(2)	C(36)-C(37)-C(38)	117.6(2)
C(28)-C(27)-H(27)	118.8	C(36)-C(37)-H(37)	121.2
C(26)-C(27)-H(27)	118.8	C(38)-C(37)-H(37)	121.2
C(29)-C(28)-C(27)	120.6(2)	C(39)-C(38)-C(37)	121.2(2)

C(39)-C(38)-C(41)	118.9(2)	F(13)-C(48)-F(14)	106.3(2)
C(37)-C(38)-C(41)	119.8(2)	F(15)-C(48)-F(14)	106.2(2)
C(38)-C(39)-C(34)	122.5(2)	F(13)-C(48)-C(44)	112.2(2)
C(38)-C(39)-H(39)	118.8	F(15)-C(48)-C(44)	112.8(2)
C(34)-C(39)-H(39)	118.8	F(14)-C(48)-C(44)	112.4(2)
F(9)-C(40)-F(7)	106.8(2)	F(17)-C(49)-F(16)	106.7(3)
F(9)-C(40)-F(8)	106.7(2)	F(17)-C(49)-F(18)	105.2(3)
F(7)-C(40)-F(8)	106.2(2)	F(16)-C(49)-F(18)	106.4(3)
F(9)-C(40)-C(36)	113.3(2)	F(17)-C(49)-C(46)	113.0(3)
F(7)-C(40)-C(36)	111.4(2)	F(16)-C(49)-C(46)	113.4(3)
F(8)-C(40)-C(36)	112.0(2)	F(18)-C(49)-C(46)	111.6(2)
F(10)-C(41)-F(11)	107.3(3)	C(51)-C(50)-C(55)	116.1(2)
F(10)-C(41)-F(12)	107.1(2)	C(51)-C(50)-B(1)	122.0(2)
F(11)-C(41)-F(12)	104.4(2)	C(55)-C(50)-B(1)	121.7(2)
F(10)-C(41)-C(38)	113.3(2)	C(52)-C(51)-C(50)	122.2(2)
F(11)-C(41)-C(38)	111.9(2)	C(52)-C(51)-H(51)	118.9
F(12)-C(41)-C(38)	112.3(2)	C(50)-C(51)-H(51)	118.9
C(43)-C(42)-C(47)	115.2(2)	C(53)-C(52)-C(51)	120.9(2)
C(43)-C(42)-B(1)	124.0(2)	C(53)-C(52)-C(56)	121.1(2)
C(47)-C(42)-B(1)	120.8(2)	C(51)-C(52)-C(56)	118.0(2)
C(44)-C(43)-C(42)	122.3(2)	C(52)-C(53)-C(54)	118.1(2)
C(44)-C(43)-H(43)	118.8	C(52)-C(53)-H(53)	120.9
C(42)-C(43)-H(43)	118.8	C(54)-C(53)-H(53)	120.9
C(45)-C(44)-C(43)	121.2(2)	C(53)-C(54)-C(55)	120.7(2)
C(45)-C(44)-C(48)	119.8(2)	C(53)-C(54)-C(57)	119.8(2)
C(43)-C(44)-C(48)	119.0(2)	C(55)-C(54)-C(57)	119.4(2)
C(44)-C(45)-C(46)	117.6(2)	C(54)-C(55)-C(50)	121.9(2)
C(44)-C(45)-H(45)	121.2	C(54)-C(55)-H(55)	119.0
C(46)-C(45)-H(45)	121.2	C(50)-C(55)-H(55)	119.0
C(47)-C(46)-C(45)	121.0(2)	F(19)-C(56)-F(21)	108.7(3)
C(47)-C(46)-C(49)	119.4(2)	F(19)-C(56)-F(20)	105.6(3)
C(45)-C(46)-C(49)	119.5(2)	F(21)-C(56)-F(20)	104.7(2)
C(46)-C(47)-C(42)	122.6(2)	F(19)-C(56)-C(52)	112.5(2)
C(46)-C(47)-H(47)	118.7	F(21)-C(56)-C(52)	113.3(2)
C(42)-C(47)-H(47)	118.7	F(20)-C(56)-C(52)	111.3(2)
F(13)-C(48)-F(15)	106.5(2)	F(22A)-C(57)-F(24A)	108.4(4)

F(22A)-C(57)-F(23A)	105.2(3)
F(24A)-C(57)-F(23A)	102.5(3)
F(22B)-C(57)-F(24B)	113.8(9)
F(22B)-C(57)-F(23B)	118.1(10)
F(24B)-C(57)-F(23B)	87.6(8)
F(22B)-C(57)-C(54)	116.2(6)
F(22A)-C(57)-C(54)	115.1(3)
F(24A)-C(57)-C(54)	113.5(3)
F(23A)-C(57)-C(54)	111.0(3)
F(24B)-C(57)-C(54)	110.5(4)
F(23B)-C(57)-C(54)	107.2(5)

**Table 4A.4.** Anisotropic displacement parameters ( $\text{\AA}^2 \times 10^3$ ) for **4-3**. The anisotropic displacement factor exponent takes the form:  $-2p^2[ h^2 a^{*2} U^{11} + \dots + 2 h k a^* b^* U^{12} ]$

	U <sup>11</sup>	U <sup>22</sup>	U <sup>33</sup>	U <sup>23</sup>	U <sup>13</sup>	U <sup>12</sup>
Ir(1)	20(1)	16(1)	16(1)	0(1)	5(1)	-4(1)
P(1)	29(1)	21(1)	20(1)	-3(1)	10(1)	-3(1)
P(2)	19(1)	19(1)	15(1)	-1(1)	4(1)	-3(1)
C(1)	17(1)	20(1)	18(1)	1(1)	4(1)	-2(1)
C(2)	20(1)	23(1)	19(1)	2(1)	5(1)	-4(1)
C(3)	28(1)	33(1)	27(1)	4(1)	7(1)	-12(1)
C(4)	32(1)	31(1)	31(1)	3(1)	5(1)	-16(1)
C(5)	25(1)	25(1)	28(1)	-2(1)	2(1)	-11(1)
C(6)	16(1)	21(1)	22(1)	0(1)	3(1)	-5(1)
C(7)	32(1)	28(1)	21(1)	0(1)	11(1)	-7(1)
C(8)	27(1)	31(1)	22(1)	-6(1)	6(1)	-12(1)
C(9)	52(2)	40(2)	20(1)	-6(1)	7(1)	-21(1)
C(10)	74(2)	45(2)	32(2)	-11(1)	10(2)	-30(2)
C(11)	88(3)	62(2)	22(1)	-13(1)	16(2)	-35(2)
C(12)	43(2)	66(2)	35(2)	11(2)	-9(1)	-14(2)
C(13)	39(2)	30(1)	56(2)	5(1)	22(1)	10(1)
C(14)	52(2)	31(2)	61(2)	9(2)	11(2)	10(1)
C(15)	109(4)	62(3)	103(4)	16(3)	79(3)	39(3)
C(16)	30(2)	49(2)	110(4)	8(2)	-10(2)	9(2)
C(17)	24(1)	20(1)	26(1)	3(1)	6(1)	2(1)
C(18)	19(1)	30(1)	59(2)	6(1)	2(1)	-1(1)
C(19)	38(2)	40(2)	42(2)	-9(1)	11(1)	11(1)
C(20)	43(2)	33(1)	38(2)	14(1)	3(1)	6(1)
C(21)	27(1)	27(1)	19(1)	2(1)	2(1)	4(1)
C(22)	44(2)	26(1)	24(1)	6(1)	3(1)	-5(1)
C(23)	48(2)	35(1)	18(1)	0(1)	-1(1)	-4(1)
C(24)	34(2)	49(2)	40(2)	3(1)	1(1)	16(1)
C(25)	36(1)	27(1)	18(1)	-4(1)	8(1)	-7(1)
O(1)	62(2)	36(1)	39(1)	-7(1)	19(1)	-29(1)
B(1)	16(1)	22(1)	16(1)	0(1)	2(1)	-2(1)
C(26)	17(1)	19(1)	18(1)	1(1)	2(1)	-2(1)

C(27)	18(1)	22(1)	18(1)	0(1)	2(1)	-1(1)
C(28)	20(1)	22(1)	20(1)	0(1)	7(1)	-1(1)
C(29)	14(1)	22(1)	25(1)	1(1)	4(1)	-2(1)
C(30)	16(1)	22(1)	20(1)	0(1)	0(1)	-4(1)
C(31)	16(1)	22(1)	18(1)	0(1)	2(1)	-2(1)
C(32)	26(1)	34(1)	27(1)	1(1)	11(1)	0(1)
C(33)	17(1)	36(1)	27(1)	-3(1)	-1(1)	-2(1)
C(34)	14(1)	20(1)	16(1)	3(1)	0(1)	-2(1)
C(35)	16(1)	20(1)	22(1)	3(1)	0(1)	-3(1)
C(36)	19(1)	16(1)	23(1)	3(1)	-2(1)	-2(1)
C(37)	20(1)	19(1)	23(1)	-1(1)	1(1)	2(1)
C(38)	15(1)	20(1)	24(1)	1(1)	2(1)	-1(1)
C(39)	15(1)	19(1)	20(1)	1(1)	0(1)	-3(1)
C(40)	26(1)	18(1)	33(1)	0(1)	-2(1)	-4(1)
C(41)	19(1)	29(1)	36(1)	-4(1)	9(1)	-2(1)
C(42)	14(1)	23(1)	18(1)	-2(1)	-1(1)	-1(1)
C(43)	18(1)	22(1)	20(1)	0(1)	0(1)	0(1)
C(44)	17(1)	23(1)	26(1)	4(1)	0(1)	1(1)
C(45)	21(1)	21(1)	32(1)	2(1)	-4(1)	-2(1)
C(46)	22(1)	26(1)	25(1)	-6(1)	-2(1)	-4(1)
C(47)	20(1)	27(1)	19(1)	-2(1)	1(1)	-4(1)
C(48)	32(1)	26(1)	34(1)	8(1)	5(1)	0(1)
C(49)	47(2)	33(1)	36(2)	-13(1)	1(1)	-7(1)
C(50)	17(1)	25(1)	18(1)	-1(1)	2(1)	-1(1)
C(51)	17(1)	32(1)	16(1)	-1(1)	2(1)	-4(1)
C(52)	17(1)	39(1)	15(1)	-2(1)	1(1)	2(1)
C(53)	22(1)	35(1)	18(1)	3(1)	5(1)	8(1)
C(54)	22(1)	26(1)	24(1)	4(1)	7(1)	5(1)
C(55)	20(1)	22(1)	23(1)	0(1)	1(1)	0(1)
C(56)	22(1)	55(2)	21(1)	-1(1)	-2(1)	-4(1)
C(57)	34(1)	32(1)	38(2)	13(1)	5(1)	0(1)
F(1)	87(2)	36(1)	64(1)	-15(1)	49(1)	-4(1)
F(2)	45(1)	98(2)	24(1)	12(1)	12(1)	20(1)
F(3)	26(1)	74(2)	44(1)	-6(1)	19(1)	-8(1)
F(4)	24(1)	56(1)	29(1)	4(1)	-4(1)	8(1)
F(5)	69(1)	36(1)	55(1)	-9(1)	-30(1)	-10(1)

F(6)	23(1)	108(2)	21(1)	-8(1)	2(1)	-6(1)
F(7)	48(1)	22(1)	49(1)	13(1)	-10(1)	-11(1)
F(8)	25(1)	25(1)	49(1)	0(1)	-10(1)	-8(1)
F(9)	46(1)	31(1)	53(1)	-20(1)	8(1)	-8(1)
F(10)	41(1)	55(1)	143(2)	-52(2)	55(1)	-17(1)
F(11)	32(1)	89(2)	66(1)	46(1)	15(1)	-4(1)
F(12)	22(1)	59(1)	48(1)	-1(1)	2(1)	-18(1)
F(13)	45(1)	64(1)	36(1)	25(1)	-2(1)	4(1)
F(14)	54(1)	35(1)	37(1)	9(1)	22(1)	5(1)
F(15)	50(1)	31(1)	53(1)	9(1)	17(1)	-10(1)
F(16)	90(2)	33(1)	45(1)	-16(1)	8(1)	-24(1)
F(17)	145(3)	44(1)	31(1)	-14(1)	18(1)	-26(1)
F(18)	58(2)	112(2)	100(2)	-75(2)	4(1)	19(2)
F(19)	21(1)	134(2)	48(1)	-32(1)	13(1)	-18(1)
F(20)	53(1)	59(1)	57(1)	-3(1)	-23(1)	-19(1)
F(21)	34(1)	92(2)	28(1)	13(1)	-11(1)	-11(1)
F(22A)	64(2)	73(2)	97(2)	54(2)	-8(2)	3(2)
F(23A)	76(2)	52(2)	63(2)	2(1)	50(2)	-15(1)
F(24A)	85(2)	45(2)	46(2)	-1(1)	19(1)	-37(2)
F(22B)	47(4)	69(6)	82(5)	34(4)	2(4)	-15(4)
F(23B)	74(5)	17(3)	74(5)	11(4)	35(4)	2(3)
F(24B)	90(5)	56(5)	30(4)	11(3)	16(3)	-44(4)

---

**Table 4A.5.** Hydrogen coordinates ( $\times 10^4$ ) and isotropic displacement parameters ( $\text{\AA}^2 \times 10^3$ ) for **4-3**.

	x	y	z	U(eq)
H(1)	6110(40)	7810(50)	3580(17)	150(30)
H(3)	9368	9776	3165	35
H(4)	9607	11078	3598	37
H(5)	8921	10801	4124	31
H(7A)	8934	7797	3030	32
H(7B)	7742	8259	2947	32
H(8A)	7534	9844	4429	32
H(8B)	8436	8939	4515	32
H(10A)	6239	4928	3210	75
H(10B)	7004	4544	2931	75
H(10C)	5784	4855	2811	75
H(11A)	6661	6072	2385	85
H(11B)	7838	5842	2570	85
H(11C)	7403	7055	2531	85
H(12A)	5270	6765	2713	73
H(12B)	5986	7687	2911	73
H(12C)	5416	6797	3126	73
H(14A)	8050	4339	3422	72
H(14B)	8234	4947	3786	72
H(14C)	9198	4299	3644	72
H(15A)	10078	4993	3154	129
H(15B)	9680	6088	2964	129
H(15C)	8951	5026	2920	129
H(16A)	10318	5929	3720	96
H(16B)	9351	6590	3855	96
H(16C)	9932	7043	3539	96
H(18A)	3890	8453	4179	54
H(18B)	4556	7548	4403	54
H(18C)	4655	7648	3998	54
H(19A)	5976	9928	4676	59

H(19B)	5253	8972	4801	59
H(19C)	4709	9937	4571	59
H(20A)	5540	9229	3768	57
H(20B)	6094	10128	4023	57
H(20C)	4817	10046	3960	57
H(22A)	6428	5982	4948	47
H(22B)	6058	6024	4542	47
H(22C)	5560	6853	4796	47
H(23A)	6695	8335	5078	51
H(23B)	7922	8442	5008	51
H(23C)	7549	7452	5230	51
H(24A)	8335	6163	4843	62
H(24B)	8700	7121	4606	62
H(24C)	7965	6165	4437	62
H(27)	4199	2112	3307	23
H(29)	7023	2341	3915	25
H(31)	4213	2695	4327	22
H(35)	3274	4345	4084	23
H(37)	754	5098	4608	25
H(39)	711	2362	4036	22
H(43)	1992	1140	4299	24
H(45)	1627	-1847	3877	30
H(47)	2682	630	3325	27
H(51)	914	1869	3287	26
H(53)	994	4103	2530	30
H(55)	3318	4044	3339	26

---



**Table 4A.6.** Torsion angles [°] for **4-3**.

C(25)-Ir(1)-P(1)-C(7)	161.28(13)	C(2)-C(1)-C(6)-C(8)	-176.2(2)
C(1)-Ir(1)-P(1)-C(7)	-15.75(11)	Ir(1)-C(1)-C(6)-C(8)	5.9(3)
P(2)-Ir(1)-P(1)-C(7)	-26.76(14)	C(3)-C(2)-C(7)-P(1)	167.7(2)
C(25)-Ir(1)-P(1)-C(9)	46.56(15)	C(1)-C(2)-C(7)-P(1)	-14.5(3)
C(1)-Ir(1)-P(1)-C(9)	-130.47(13)	C(9)-P(1)-C(7)-C(2)	144.6(2)
P(2)-Ir(1)-P(1)-C(9)	-141.48(13)	C(13)-P(1)-C(7)-C(2)	-93.6(2)
C(25)-Ir(1)-P(1)-C(13)	-86.52(14)	Ir(1)-P(1)-C(7)-C(2)	19.9(2)
C(1)-Ir(1)-P(1)-C(13)	96.45(13)	C(5)-C(6)-C(8)-P(2)	164.2(2)
P(2)-Ir(1)-P(1)-C(13)	85.44(14)	C(1)-C(6)-C(8)-P(2)	-17.7(3)
C(25)-Ir(1)-P(2)-C(8)	169.80(13)	C(17)-P(2)-C(8)-C(6)	-100.08(19)
C(1)-Ir(1)-P(2)-C(8)	-13.15(11)	C(21)-P(2)-C(8)-C(6)	138.15(18)
P(1)-Ir(1)-P(2)-C(8)	-2.14(14)	Ir(1)-P(2)-C(8)-C(6)	19.3(2)
C(25)-Ir(1)-P(2)-C(17)	-76.18(12)	C(7)-P(1)-C(9)-C(12)	-74.5(2)
C(1)-Ir(1)-P(2)-C(17)	100.87(10)	C(13)-P(1)-C(9)-C(12)	169.3(2)
P(1)-Ir(1)-P(2)-C(17)	111.88(11)	Ir(1)-P(1)-C(9)-C(12)	39.1(2)
C(25)-Ir(1)-P(2)-C(21)	57.24(13)	C(7)-P(1)-C(9)-C(10)	166.7(2)
C(1)-Ir(1)-P(2)-C(21)	-125.71(11)	C(13)-P(1)-C(9)-C(10)	50.5(3)
P(1)-Ir(1)-P(2)-C(21)	-114.70(12)	Ir(1)-P(1)-C(9)-C(10)	-79.7(3)
P(1)-Ir(1)-C(1)-C(2)	11.37(18)	C(7)-P(1)-C(9)-C(11)	44.6(3)
P(2)-Ir(1)-C(1)-C(2)	-171.62(19)	C(13)-P(1)-C(9)-C(11)	-71.5(3)
P(1)-Ir(1)-C(1)-C(6)	-170.80(19)	Ir(1)-P(1)-C(9)-C(11)	158.3(2)
P(2)-Ir(1)-C(1)-C(6)	6.21(17)	C(7)-P(1)-C(13)-C(14)	172.0(2)
C(6)-C(1)-C(2)-C(3)	-0.7(3)	C(9)-P(1)-C(13)-C(14)	-72.9(3)
Ir(1)-C(1)-C(2)-C(3)	177.19(19)	Ir(1)-P(1)-C(13)-C(14)	62.3(3)
C(6)-C(1)-C(2)-C(7)	-178.5(2)	C(7)-P(1)-C(13)-C(15)	-65.5(3)
Ir(1)-C(1)-C(2)-C(7)	-0.6(3)	C(9)-P(1)-C(13)-C(15)	49.6(3)
C(1)-C(2)-C(3)-C(4)	-1.1(4)	Ir(1)-P(1)-C(13)-C(15)	-175.2(3)
C(7)-C(2)-C(3)-C(4)	176.7(3)	C(7)-P(1)-C(13)-C(16)	54.6(3)
C(2)-C(3)-C(4)-C(5)	1.9(4)	C(9)-P(1)-C(13)-C(16)	169.7(3)
C(3)-C(4)-C(5)-C(6)	-0.8(4)	Ir(1)-P(1)-C(13)-C(16)	-55.0(3)
C(4)-C(5)-C(6)-C(1)	-1.1(4)	C(8)-P(2)-C(17)-C(18)	173.08(19)
C(4)-C(5)-C(6)-C(8)	177.0(3)	C(21)-P(2)-C(17)-C(18)	-72.1(2)
C(2)-C(1)-C(6)-C(5)	1.8(3)	Ir(1)-P(2)-C(17)-C(18)	60.6(2)
Ir(1)-C(1)-C(6)-C(5)	-176.09(18)	C(8)-P(2)-C(17)-C(19)	-64.3(2)

C(21)-P(2)-C(17)-C(19)	50.6(2)	C(29)-C(28)-C(32)-F(2)	-146.3(3)
Ir(1)-P(2)-C(17)-C(19)	-176.74(18)	C(27)-C(28)-C(32)-F(2)	36.8(3)
C(8)-P(2)-C(17)-C(20)	55.2(2)	C(29)-C(30)-C(33)-F(5)	80.5(3)
C(21)-P(2)-C(17)-C(20)	170.10(19)	C(31)-C(30)-C(33)-F(5)	-98.0(3)
Ir(1)-P(2)-C(17)-C(20)	-57.2(2)	C(29)-C(30)-C(33)-F(4)	-38.3(3)
C(8)-P(2)-C(21)-C(23)	46.3(2)	C(31)-C(30)-C(33)-F(4)	143.1(2)
C(17)-P(2)-C(21)-C(23)	-69.2(2)	C(29)-C(30)-C(33)-F(6)	-157.3(2)
Ir(1)-P(2)-C(21)-C(23)	158.09(17)	C(31)-C(30)-C(33)-F(6)	24.1(3)
C(8)-P(2)-C(21)-C(22)	169.91(18)	C(42)-B(1)-C(34)-C(35)	150.9(2)
C(17)-P(2)-C(21)-C(22)	54.3(2)	C(26)-B(1)-C(34)-C(35)	31.3(3)
Ir(1)-P(2)-C(21)-C(22)	-78.34(19)	C(50)-B(1)-C(34)-C(35)	-88.7(2)
C(8)-P(2)-C(21)-C(24)	-72.8(2)	C(42)-B(1)-C(34)-C(39)	-34.9(3)
C(17)-P(2)-C(21)-C(24)	171.63(19)	C(26)-B(1)-C(34)-C(39)	-154.6(2)
Ir(1)-P(2)-C(21)-C(24)	39.0(2)	C(50)-B(1)-C(34)-C(39)	85.5(2)
C(42)-B(1)-C(26)-C(31)	-89.3(2)	C(39)-C(34)-C(35)-C(36)	1.7(3)
C(34)-B(1)-C(26)-C(31)	34.2(3)	B(1)-C(34)-C(35)-C(36)	176.3(2)
C(50)-B(1)-C(26)-C(31)	149.9(2)	C(34)-C(35)-C(36)-C(37)	0.4(3)
C(42)-B(1)-C(26)-C(27)	84.7(2)	C(34)-C(35)-C(36)-C(40)	-178.1(2)
C(34)-B(1)-C(26)-C(27)	-151.8(2)	C(35)-C(36)-C(37)-C(38)	-1.2(3)
C(50)-B(1)-C(26)-C(27)	-36.1(3)	C(40)-C(36)-C(37)-C(38)	177.3(2)
C(31)-C(26)-C(27)-C(28)	-1.3(3)	C(36)-C(37)-C(38)-C(39)	-0.1(3)
B(1)-C(26)-C(27)-C(28)	-175.7(2)	C(36)-C(37)-C(38)-C(41)	176.9(2)
C(26)-C(27)-C(28)-C(29)	-0.3(4)	C(37)-C(38)-C(39)-C(34)	2.4(3)
C(26)-C(27)-C(28)-C(32)	176.6(2)	C(41)-C(38)-C(39)-C(34)	-174.6(2)
C(27)-C(28)-C(29)-C(30)	1.5(3)	C(35)-C(34)-C(39)-C(38)	-3.1(3)
C(32)-C(28)-C(29)-C(30)	-175.4(2)	B(1)-C(34)-C(39)-C(38)	-177.7(2)
C(28)-C(29)-C(30)-C(31)	-1.0(3)	C(37)-C(36)-C(40)-F(9)	15.1(3)
C(28)-C(29)-C(30)-C(33)	-179.5(2)	C(35)-C(36)-C(40)-F(9)	-166.4(2)
C(29)-C(30)-C(31)-C(26)	-0.7(4)	C(37)-C(36)-C(40)-F(7)	-105.3(3)
C(33)-C(30)-C(31)-C(26)	177.8(2)	C(35)-C(36)-C(40)-F(7)	73.2(3)
C(27)-C(26)-C(31)-C(30)	1.8(3)	C(37)-C(36)-C(40)-F(8)	135.9(2)
B(1)-C(26)-C(31)-C(30)	176.1(2)	C(35)-C(36)-C(40)-F(8)	-45.6(3)
C(29)-C(28)-C(32)-F(1)	93.4(3)	C(39)-C(38)-C(41)-F(10)	-167.2(3)
C(27)-C(28)-C(32)-F(1)	-83.6(3)	C(37)-C(38)-C(41)-F(10)	15.7(4)
C(29)-C(28)-C(32)-F(3)	-26.2(3)	C(39)-C(38)-C(41)-F(11)	71.3(3)
C(27)-C(28)-C(32)-F(3)	156.9(2)	C(37)-C(38)-C(41)-F(11)	-105.8(3)

C(39)-C(38)-C(41)-F(12)	-45.7(3)	C(26)-B(1)-C(50)-C(55)	-38.1(3)
C(37)-C(38)-C(41)-F(12)	137.2(2)	C(34)-B(1)-C(50)-C(55)	83.7(2)
C(26)-B(1)-C(42)-C(43)	100.1(2)	C(55)-C(50)-C(51)-C(52)	-0.3(3)
C(34)-B(1)-C(42)-C(43)	-24.0(3)	B(1)-C(50)-C(51)-C(52)	174.2(2)
C(50)-B(1)-C(42)-C(43)	-139.6(2)	C(50)-C(51)-C(52)-C(53)	0.7(4)
C(26)-B(1)-C(42)-C(47)	-76.8(2)	C(50)-C(51)-C(52)-C(56)	-179.1(2)
C(34)-B(1)-C(42)-C(47)	159.1(2)	C(51)-C(52)-C(53)-C(54)	0.0(4)
C(50)-B(1)-C(42)-C(47)	43.5(3)	C(56)-C(52)-C(53)-C(54)	179.7(2)
C(47)-C(42)-C(43)-C(44)	-3.7(3)	C(52)-C(53)-C(54)-C(55)	-0.9(4)
B(1)-C(42)-C(43)-C(44)	179.2(2)	C(52)-C(53)-C(54)-C(57)	177.1(2)
C(42)-C(43)-C(44)-C(45)	2.4(4)	C(53)-C(54)-C(55)-C(50)	1.2(4)
C(42)-C(43)-C(44)-C(48)	-178.7(2)	C(57)-C(54)-C(55)-C(50)	-176.7(2)
C(43)-C(44)-C(45)-C(46)	0.9(3)	C(51)-C(50)-C(55)-C(54)	-0.6(3)
C(48)-C(44)-C(45)-C(46)	-177.9(2)	B(1)-C(50)-C(55)-C(54)	-175.1(2)
C(44)-C(45)-C(46)-C(47)	-2.7(4)	C(53)-C(52)-C(56)-F(19)	-110.3(3)
C(44)-C(45)-C(46)-C(49)	174.8(2)	C(51)-C(52)-C(56)-F(19)	69.5(4)
C(45)-C(46)-C(47)-C(42)	1.2(4)	C(53)-C(52)-C(56)-F(21)	13.6(4)
C(49)-C(46)-C(47)-C(42)	-176.2(2)	C(51)-C(52)-C(56)-F(21)	-166.6(3)
C(43)-C(42)-C(47)-C(46)	1.9(3)	C(53)-C(52)-C(56)-F(20)	131.3(3)
B(1)-C(42)-C(47)-C(46)	179.1(2)	C(51)-C(52)-C(56)-F(20)	-48.9(3)
C(45)-C(44)-C(48)-F(13)	96.1(3)	C(53)-C(54)-C(57)-F(22B)	-152.8(10)
C(43)-C(44)-C(48)-F(13)	-82.8(3)	C(55)-C(54)-C(57)-F(22B)	25.2(11)
C(45)-C(44)-C(48)-F(15)	-24.2(3)	C(53)-C(54)-C(57)-F(22A)	26.7(5)
C(43)-C(44)-C(48)-F(15)	156.9(2)	C(55)-C(54)-C(57)-F(22A)	-155.3(4)
C(45)-C(44)-C(48)-F(14)	-144.2(2)	C(53)-C(54)-C(57)-F(24A)	152.5(3)
C(43)-C(44)-C(48)-F(14)	36.9(3)	C(55)-C(54)-C(57)-F(24A)	-29.5(4)
C(47)-C(46)-C(49)-F(17)	-33.5(4)	C(53)-C(54)-C(57)-F(23A)	-92.7(3)
C(45)-C(46)-C(49)-F(17)	149.0(3)	C(55)-C(54)-C(57)-F(23A)	85.3(3)
C(47)-C(46)-C(49)-F(16)	-155.1(3)	C(53)-C(54)-C(57)-F(24B)	-21.3(8)
C(45)-C(46)-C(49)-F(16)	27.5(4)	C(55)-C(54)-C(57)-F(24B)	156.7(7)
C(47)-C(46)-C(49)-F(18)	84.8(4)	C(53)-C(54)-C(57)-F(23B)	72.6(7)
C(45)-C(46)-C(49)-F(18)	-92.7(4)	C(55)-C(54)-C(57)-F(23B)	-109.4(7)
C(42)-B(1)-C(50)-C(51)	30.5(3)		
C(26)-B(1)-C(50)-C(51)	147.7(2)		
C(34)-B(1)-C(50)-C(51)	-90.5(2)		
C(42)-B(1)-C(50)-C(55)	-155.3(2)		

#### 4.7 References

- (1) Hartwig, J. F. *Organotransition Metal Chemistry*; University Science Books: Sausalito, CA, 2010.
- (2) Crabtree, R. H. *The Organometallic Chemistry of the Transition Metals*; 4th ed.; John Wiley & Sons: New York, 2005.
- (3) Vaska, L.; DiLuzio, J. W. *J. Am. Chem. Soc.* **1962**, *84*, 679.
- (4) Choi, J.; Goldman, A. S. *Top. Organomet. Chem.* **2011**, *34*, 139.
- (5) Deutsch, P. P.; Eisenberg, R. *Chem. Rev.* **1988**, *88*, 1147.
- (6) Nüchel, S. a. B., P. *Angewandte Chemie International Edition*, **2003**, *42*, 1632.
- (7) Martín, M.; Torres, O.; Oñate, E.; Sola, E.; Oro, L. A. *J. Am. Chem. Soc.* **2005**, *127*, 18074.
- (8) Ittel, S. D.; Tolman, C. A.; English, A. D.; Jesson, J. P. *J. Am. Chem. Soc.* **1976**, *98*, 6073.
- (9) Whittlesey, M. K.; Mawby, R. J.; Osman, R.; Perutz, R. N.; Field, L. D.; Wilkinson, M. P.; George, M. W. *J. Am. Chem. Soc.* **1993**, *115*, 8627.
- (10) Macgregor, S. A.; Eisenstein, O.; Whittlesey, M. K.; Perutz, R. N. *J. Chem. Soc., Dalton Trans.* **1998**, 291.
- (11) Saillard, J.; Hoffmann, R. *J. Am. Chem. Soc.* **1984**, *106*, 2006.
- (12) Kanzelberger, M. Ph.D. Thesis, Rutgers University, 2004.
- (13) Wang, D. Ph. D. Thesis, Rutgers University, 2012.
- (14) Rybtchinski, B.; Ben-David, Y.; Milstein, D. *Organometallics* **1997**, *16*, 3786.
- (15) Findlater, M.; Bernskoetter, W. H.; Brookhart, M. *J. Am. Chem. Soc.* **2010**, *132*, 4534.
- (16) Ahmed Foskey, T. J.; Heinekey, D. M.; Goldberg, K. I. *ACS Catalysis* **2012**, *2*, 1285.
- (17) Goldman, A. S.; Goldberg, K. I. In *Activation and Functionalization of C-H Bonds*; Goldberg, K. I., Goldman, A. S., Eds. 2004; Vol. ACS Symposium Series 885, p 1.
- (18) Liu, F.; Goldman, A. S. *Chem. Commun.* **1999**, 655.
- (19) This work was carried out by Sabuj Kundu; refer to reference 20.
- (20) Kundu, S. Ph. D. Thesis, Rutgers University, 2010.
- (21) Brookhart, M.; Grant, B.; Volpe, A. F. *Organometallics* **1992**, *11*, 3920.
- (22) Hoops, S.; Sahle, S.; Gauges, R.; Lee, C.; Pahle, J.; Simus, N.; Singhal, M.; Xu, L.; Mendes, P.; Kummer, U. *Bioinformatics* **2006**, *22*, 3067.
- (23) Simmons, E. M.; Hartwig, J. F. *Angew. Chem., Intl. Ed.* **2012**, *51*, 3066.
- (24) Wang, Q.; Quyoum, R.; Gillis, D. J.; Tudoret, M.-J.; Jeremic, D.; Hunter, B. K.; Baird, M. C. *Organometallics* **1996**, *15*, 693.
- (25) Frisch, M. J. T., G. W.; Schlegel, H. B.; Scuseria, G. E.; Robb, M. A.; Cheeseman, J. R.; Scalmani, G.; Barone, V.; Mennucci, B.; Petersson, G. A.; Nakatsuji, H.; Caricato, M.; Li, X.; Hratchian, H. P.; Izmaylov, A. F.; Bloino, J.; Zheng, G.; Sonnenberg, J. L.; Hada, M.; Ehara, M.; Toyota, K.; Fukuda, R.; Hasegawa, J.; Ishida, M.; Nakajima, T.; Honda, Y.; Kitao, O.; Nakai, H.; Vreven, T.; Montgomery, Jr., J. A.; Peralta, J. E.; Ogliaro, F.; Bearpark, M.; Heyd, J. J.; Brothers, E.; Kudin, K. N.; Staroverov, V. N.; Kobayashi, R.; Normand, J.; Raghavachari, K.; Rendell, A.; Burant, J. C.; Iyengar, S. S.; Tomasi, J.; Cossi, M.;

- Rega, N.; Millam, N. J.; Klene, M.; Knox, J. E.; Cross, J. B.; Bakken, V.; Adamo, C.; Jaramillo, J.; Gomperts, R.; Stratmann, R. E.; Yazyev, O.; Austin, A. J.; Cammi, R.; Pomelli, C.; Ochterski, J. W.; Martin, R. L.; Morokuma, K.; Zakrzewski, V. G.; Voth, G. A.; Salvador, P.; Dannenberg, J. J.; Dapprich, S.; Daniels, A. D.; Farkas, Ö.; Foresman, J. B.; Ortiz, J. V.; Cioslowski, J.; Fox, D. J.; Gaussian 09, Revision A.02 ed.; Gaussian, Inc.: Wallingford, CT, 2009.
- (26) Zhao, C. Y.; Truhlar, D. G. *Theo. Chem. Acc.* **2008**, *120*, 215.
- (27) Roy, L. E.; Hay, P. J.; Martin, R. L. *J. Chem. Theory Comput.* **2008**, *4*, 1029.
- (28) Krishnan, R.; Binkley, J. S.; Seeger, R.; Pople, J. A. *J. Chem. Phys.* **1980**, *72*, 650.
- (29) Barone, V.; Cossi, M. *J. Phys. Chem. A* **1998**, *102*, 1995.
- (30) Bruker-AXS. SADABS, Bruker area detector scaling and absorption correction, v2.05, Bruker-AXS Inc., Madison, Wisconsin, 2003; SAINTplus, Bruker area detector data reduction program, v6.45, Bruker-AXS Inc., Madison, Wisconsin, 2003.
- (31) Sheldrick, G. M. SHELX86, Program for the Solution of Crystal Structures, University of Göttingen, Germany, 1986.
- (32) Sheldrick, G. M. SHELXL97, Program for Crystal Structure Refinement, University of Göttingen, Germany, 1997.

## Chapter 5

### Acid-catalyzed reductive elimination of C-H bonds from six-coordinate (<sup>t</sup>Bu<sup>4</sup>PCP)Ir(CO)(H)(R) complexes

#### Abstract

In the presence of acid, six-coordinate (<sup>t</sup>Bu<sup>4</sup>PCP)Ir(CO)(H)(R) complexes can undergo net reductive elimination of C-H bonds to yield the four-coordinate carbonyl complex, (<sup>t</sup>Bu<sup>4</sup>PCP)Ir(CO), and free alkanes or arenes; this is the microscopic reverse of the reaction discussed in Chapter 4 as applied to aryl and alkyl C-H bonds. Interestingly, *cis* and *trans* diastereomers of the (<sup>t</sup>Bu<sup>4</sup>PCP)Ir(CO)(H)(R) undergo elimination at different rates, with the *trans* isomer eliminating more rapidly than the *cis*, likely via different mechanisms. Further, we have found that acid-catalyzed elimination of alkanes is more favorable (both kinetically and thermodynamically) than the elimination of arenes, which require higher reaction temperatures and longer reaction times.

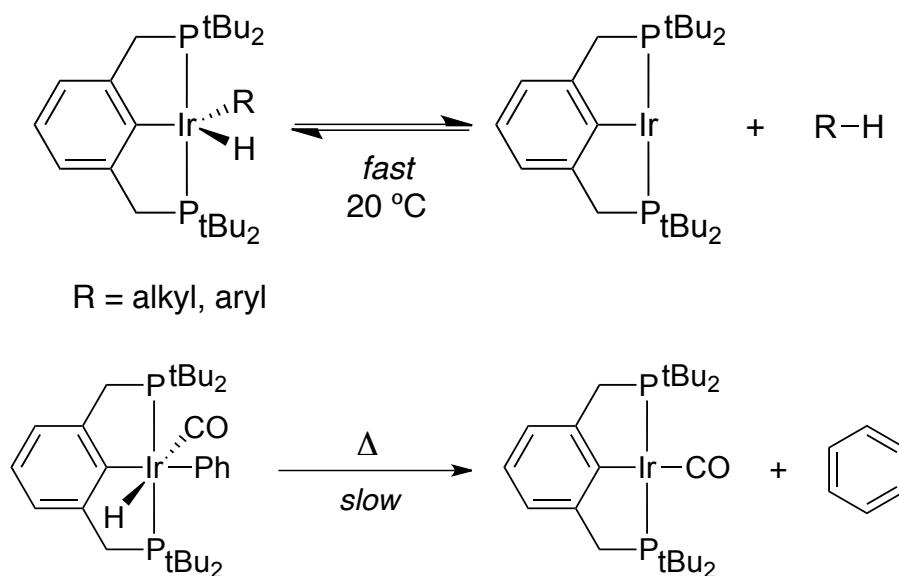
## 5.1 Introduction

The acid-catalyzed oxidative addition of the C-H bond of PhCCH to (<sup>t</sup>Bu<sup>4</sup>PCP)Ir(CO) was certainly unexpected and unprecedented, especially considering that oxidative addition is typically less thermodynamically favorable than its microscopic reverse, reductive elimination. While sp-hybridized C-H bonds appear to be particularly well-suited toward oxidative addition to (<sup>t</sup>Bu<sup>4</sup>PCP)Ir(CO), no reactivity was observed for either sp<sup>2</sup>- or sp<sup>3</sup>-hybridized C-H bonds, such as those in benzene or *n*-hexane, even at high temperatures (125 °C). It is quite possible that such reactions are kinetically feasible, but thermodynamically unfavorable, preventing formation of a stable six-coordinate product. This led us to consider the possibility that the reverse reaction, reductive elimination of C-H bonds from six-coordinate (PCP)Ir(CO)(H)(R) complexes, might be acid catalyzed as well.

The reductive elimination of C-H bonds from six-coordinate transition-metal complexes is well-precedented, though such eliminations tend to be slower compared to C-H reductive elimination from five-coordinate complexes, as formation of a product that has an occupied metal-ligand antibonding orbital occurs upon elimination from the six-coordinate species.<sup>1-3</sup> Likewise, reductive elimination of mutually *cis* ligands typically occurs faster than ligands with a *trans* disposition, as *trans*-positioned ligands are incapable of undergoing reductive elimination via a three-center concerted mechanism, and must instead occur via a stepwise (non-concerted) loss of ligands or isomerization to the *cis* isomer.<sup>1</sup> With higher coordination complexes, the requisite isomerization from *trans* to *cis* stereochemistry is likely difficult, further hindering reductive elimination of *trans* ligands from six-coordinate species. These general trends in reductive elimination

behavior are observed in iridium-pincer complexes as well: the reductive elimination of R-H bonds (R = alkyl or aryl, for instance) occurs rapidly at room-temperature for five-coordinate  $(^t\text{Bu}_4\text{PCP})\text{Ir}(\text{R})(\text{H})$  complexes (in equilibrium with equally facile oxidative addition), while loss of benzene from six-coordinate *cis*- $(^t\text{Bu}_4\text{PCP})\text{Ir}(\text{CO})(\text{Ph})(\text{H})$  requires elevated temperatures to occur (no arene exchange is observed).<sup>4,5</sup> (**scheme 5.1**).

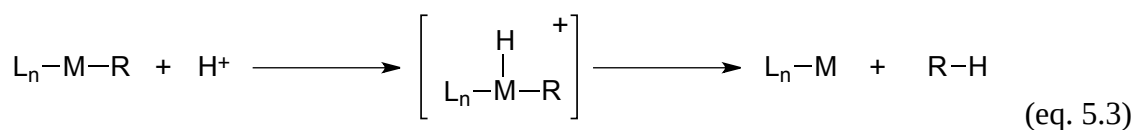
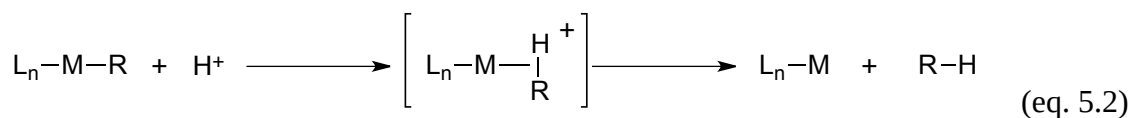
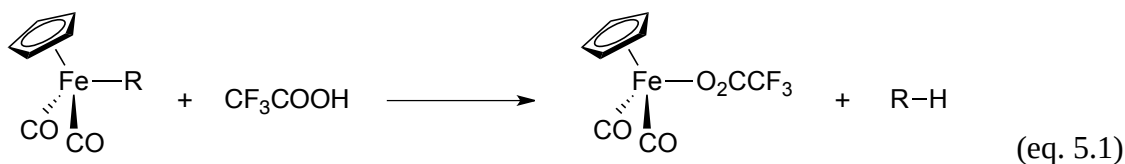
**Scheme 5.1.** Elimination of R-H bonds from five- and six-coordinate (pincer)Ir complexes.



Beyond thermally or photochemically-induced elimination, protonolysis of M-R bonds is another means of promoting R-H elimination, though it is generally non-catalytic, requiring a stoichiometric equivalent of a proton source and forming a new product with the same metal oxidation state (that is, formation of R-H bonds occurring by such protonolysis pathways is not necessarily a reductive elimination event) (for example, see **eq. 5.1**).<sup>6</sup> M-R bond protonolysis usually occurs in one of two ways, either



via direct protonation of the M-R bond to yield a M-(R-H)  $\sigma$ -complex (frequently observed for R=H) (**eq. 5.2**) or, more commonly for M-C bonds, by protonation of the metal (forming a M-H bond) followed by R-H reductive elimination (**eq. 5.3**).<sup>1</sup>



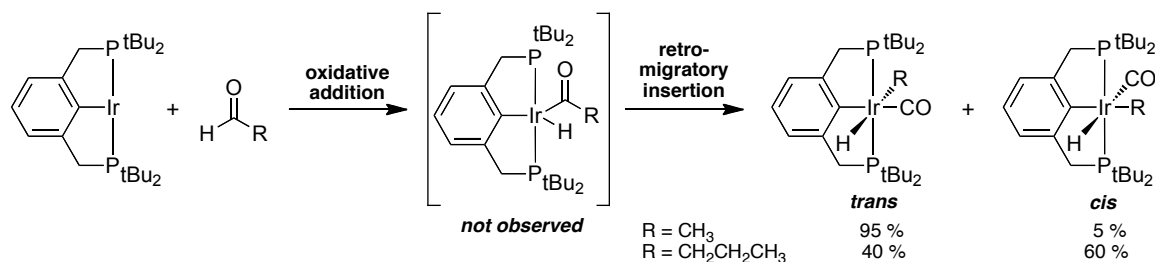
Assuming the reductive elimination of C-H bonds from (<sup>t</sup>Bu<sup>4</sup>PCP)Ir(CO)(R)(H) complexes is downhill (as expected based upon both precedent and the lack of reactivity of alkyl and aryl C-H bonds toward oxidative addition to the four-coordinate complex), acid-catalyzed reductive elimination (*i.e.* catalytic protonolysis) of alkanes or arenes may be possible. In this chapter we examine the behaviors of independently-generated six-coordinate carbonyl complexes, (<sup>t</sup>Bu<sup>4</sup>PCP)Ir(CO)(R)(H) (R= Me, Et, Ph), existing as both *cis* and *trans* stereoisomers, toward catalytic protonolysis.

## 5.2 Results and Discussion

### 5.2.1. Syntheses of (<sup>t</sup>Bu<sup>4</sup>PCP)Ir(CO)(H)(R) complexes

The synthesis of (<sup>t</sup>Bu<sup>4</sup>PCP)Ir(CO)(H)(alkyl) complexes had been extensively studied by Mira Kanzelberger in her efforts to observe the far less stable catalytic intermediate, (<sup>t</sup>Bu<sup>4</sup>PCP)Ir(H)(alkyl).<sup>7</sup> The addition of CO to five-coordinate (pincer)Ir(R)(H) complexes most typically results in formation of the six-coordinate carbonyl complex where the R and H groups are mutually *cis*.<sup>4</sup> Kanzelberger, however, found that addition of an aldehyde to (<sup>t</sup>Bu<sup>4</sup>PCP)Ir(NBE) formed a mixture of *cis* and *trans* diastereomers of the six-coordinate carbonyl complex (with ratios of *cis* : *trans* diastereomers varying with the chain length of alkyl group), likely proceeding by initial aldehyde C-H oxidative addition followed by retro-migratory insertion of CO (**Scheme 5.2**).<sup>7</sup> In the case of acetaldehyde, the *trans* six-coordinate carbonyl is formed almost exclusively ( $\geq 95$  % *trans* : 5 % *cis*). Analogously, addition of butyraldehyde yields a mixture of *cis* and *trans* (<sup>t</sup>Bu<sup>4</sup>PCP)Ir(CO)(H)(propyl); however, in this case, the *cis* isomer is the major product, with a *cis* : *trans* ratio of *ca.* 3:2. In general, these six-coordinate complexes were found to be highly stable, capable of undergoing column chromatography and manipulation under air for prolonged periods of time without significant decomposition. A testament to its stability, analytically pure *trans*-(<sup>t</sup>Bu<sup>4</sup>PCP)Ir(CO)(H)(CH<sub>3</sub>) was found in the glovebox after a *ca.* ten year “hibernation.”

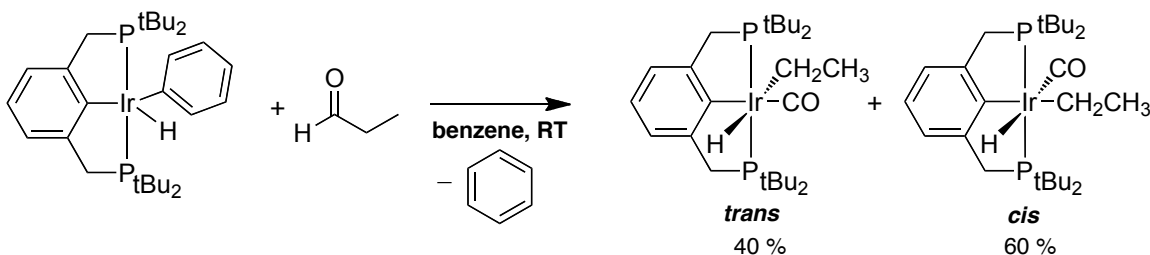
**Scheme 5.2.** Previously reported synthesis of *cis/trans*-(<sup>t</sup>Bu<sup>4</sup>PCP)Ir(CO)(R)(H) complexes.



To better understand acid-catalyzed processes (oxidative addition or reductive elimination), we further synthesized a series of six-coordinate carbonyl complexes exhibiting both *cis* and *trans* stereoisomers. In addition to the purely *trans*-(<sup>t</sup>Bu<sup>4</sup>PCP)Ir(CO)(H)(Me) that Kanzelberger reported, we synthesized the *cis/trans* mixture of (<sup>t</sup>Bu<sup>4</sup>PCP)Ir(CO)(H)(Et) (60 % *cis* : 40 % *trans* based on the ratio of hydride signal integrals) in quantitative yield (**scheme 5.3**) via propionaldehyde addition to a solution of (PCP)Ir(H)(Ph). Interestingly, it appears that homologation of the alkyl ligand (from methane to ethane) creates a large enough steric effect to discriminate between *cis* and *trans* six-coordinate carbonyl formation, slightly favoring the less sterically crowded *cis* isomer in spite of the apparent electronic preference for the *trans* stereochemistry. This result is essentially identical to the stereoisomer mixture that was found for the propyl hydride carbonyl complexes.<sup>7</sup> NMR spectra are consistent with previous results as well—the <sup>1</sup>H nmr exhibits a hydride triplet at -12.0 ppm (*J*<sub>PH</sub> = 16.4 Hz) consistent with a *trans* relationship between alkyl and hydride ligands, and another hydride triplet at -9.63 ppm (*J*<sub>PH</sub> = 17.3 Hz) consistent with a *cis* relationship between the ethyl and hydride

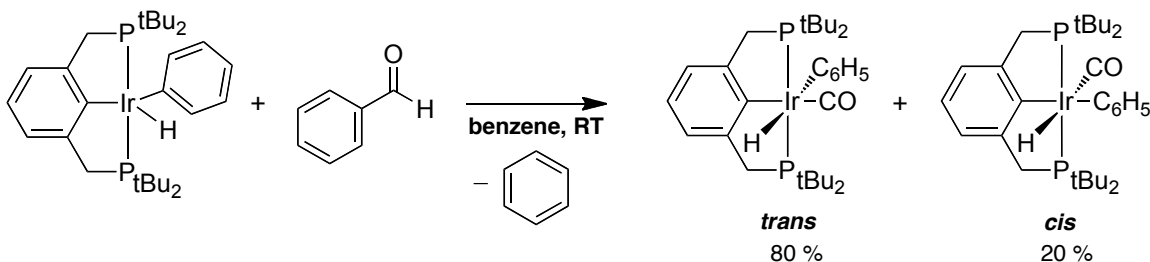
ligands. The *cis* stereoisomers presents as a doublet in the  $^{31}\text{P}$  nmr spectrum at 52.4 ppm, while the *trans* stereoisomer presents as a doublet at 56.8 ppm.

**Scheme 5.3.** Synthesis of *cis/trans*- $(^{\text{tBu}}\text{PCP})\text{Ir}(\text{CO})(\text{H})(\text{C}_2\text{H}_5)$  complexes.



Moving beyond alkyl groups, we further synthesized the *cis/trans* mixture of  $(^{\text{tBu}}\text{PCP})\text{Ir}(\text{CO})(\text{H})(\text{Ph})$  in quantitative yield (**scheme 5.4**). In this case, the ratio of *cis* : *trans* is much smaller (20 % *cis*: 80 % *trans* based on ratio of  $^{31}\text{P}$  signal integrals); the significant preference for the *trans* stereoisomer likely results from the relatively compact nature of the planar aryl ligand, allowing for positioning *trans* to the hydride ligand. The *trans* isomer presents as hydride triplet in the  $^1\text{H}$  nmr spectrum at -12.1 ppm ( $J_{\text{PH}} = 15.2$  Hz), while the *cis* presents as a triplet at -8.8 ppm ( $J_{\text{PH}} = 17.3$  Hz). The  $^{31}\text{P}$  nmr exhibits a singlet at 56.8 ppm for the *trans* stereoisomer and a singlet at 53.5 ppm for the *cis* stereoisomer.

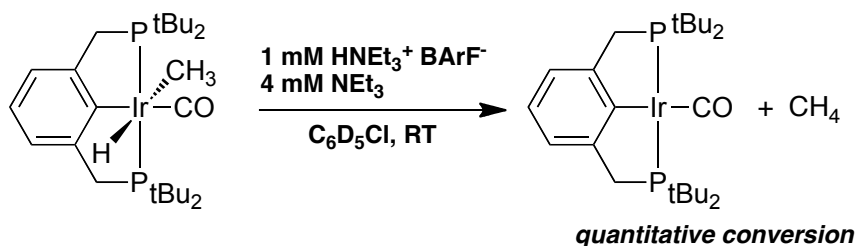
**Scheme 5.4.** Synthesis of *cis/trans*- $(^{\text{tBu}}\text{PCP})\text{Ir}(\text{CO})(\text{H})(\text{C}_6\text{H}_5)$  complexes.



### 5.2.2. Acid-catalyzed reductive elimination of methane from *trans*-(<sup>t</sup>Bu<sup>4</sup>PCP)Ir(CO)(Me)(H)

With a variety of alkyl and aryl hydride carbonyl complexes in hand, we set about examining potential acid-catalyzed reductive elimination of alkane and arene molecules. To our delight we found that treating 10 mM of *trans*-(<sup>t</sup>Bu<sup>4</sup>PCP)Ir(CO)(H)(CH<sub>3</sub>) with our standard “buffer” solution (1 mM HNEt<sub>3</sub><sup>+</sup> B(C<sub>6</sub>F<sub>5</sub>)<sub>4</sub><sup>-</sup> and 4 mM NEt<sub>3</sub>) in chlorobenzene-*d*<sub>5</sub> led to complete reductive elimination of methane in quantitative yield at room temperature (**scheme 5.5**). The reaction occurred very rapidly, with the initially nearly colorless solution turning the bright yellow color of the four-coordinate carbonyl complex within *ca.* 30 seconds of buffer addition. Of note, the appearance of a singlet at 0.17 ppm in <sup>1</sup>H nmr indicates the presence of free methane, and complete loss of the hydride signal indicates that no equilibrium between the six-coordinate species and the four-coordinate species/free methane exists (*i.e.* the loss of methane from the six-coordinate complex is highly thermodynamically favored and therefore *irreversible*).

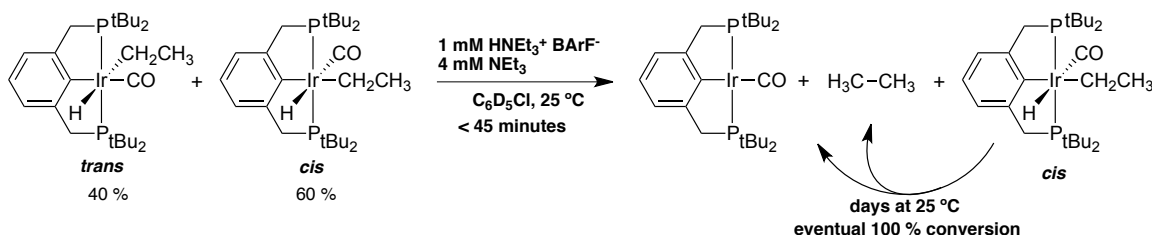
**Scheme 5.5.** Acid-catalyzed reductive elimination of methane from *trans*-(<sup>t</sup>Bu<sup>4</sup>PCP)Ir(CO)(H)(CH<sub>3</sub>).



### 5.2.3. Acid-catalyzed reductive elimination of ethane from a mixture of *cis/trans*- $(^t\text{Bu}^4\text{PCP})\text{Ir}(\text{CO})(\text{Et})(\text{H})$

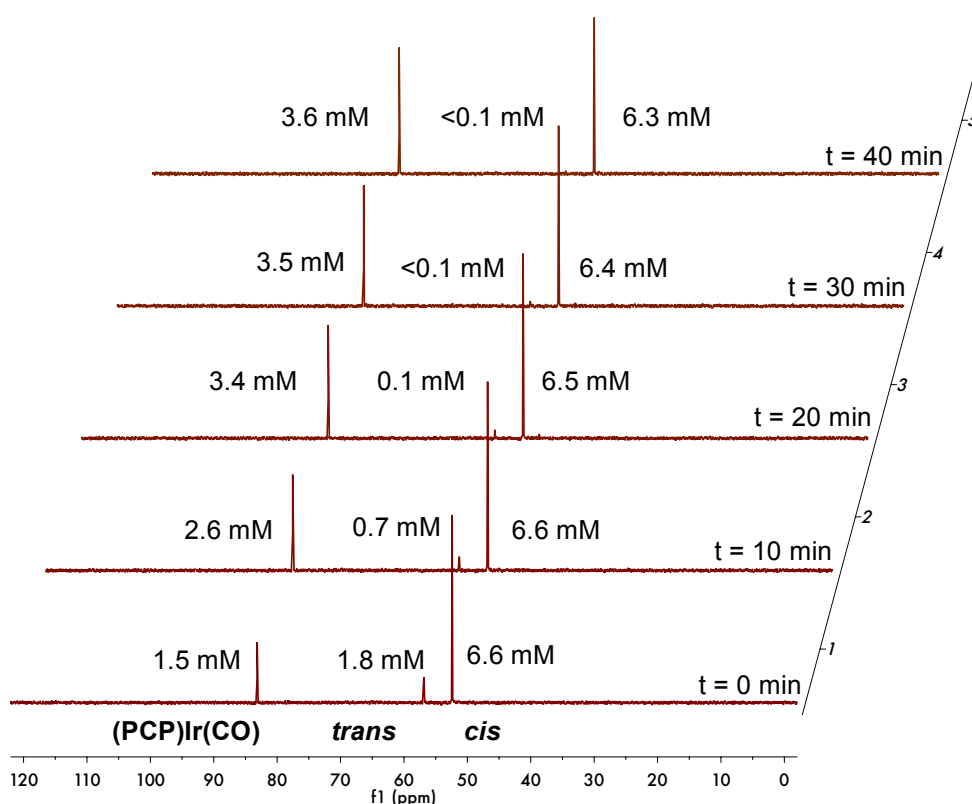
Whereas the  $(^t\text{Bu}^4\text{PCP})\text{Ir}(\text{CO})(\text{H})(\text{Me})$  complex used above was a single stereoisomer (*trans*),  $(^t\text{Bu}^4\text{PCP})\text{Ir}(\text{CO})(\text{H})(\text{Et})$  existed as a mixture of *cis* and *trans* stereoisomers. Interestingly, treating this mixture of stereoisomers with buffer resulted in different rates of reductive elimination for the *cis* and *trans* isomers (**scheme 5.6**). The *trans* isomer is fairly rapidly decomposed in the presence of acid, with no *trans* stereoisomer existing in solution after *ca.* 40 minutes of reaction (**figure 5.1**), while the *cis* isomer eliminates more slowly (**figure 5.2**), requiring *ca.* five days to reach completion at room temperature.

**Scheme 5.6.** Acid-catalyzed reductive elimination of ethane from *cis*- and *trans*- $(^t\text{Bu}^4\text{PCP})\text{Ir}(\text{CO})(\text{H})(\text{C}_2\text{H}_5)$ .



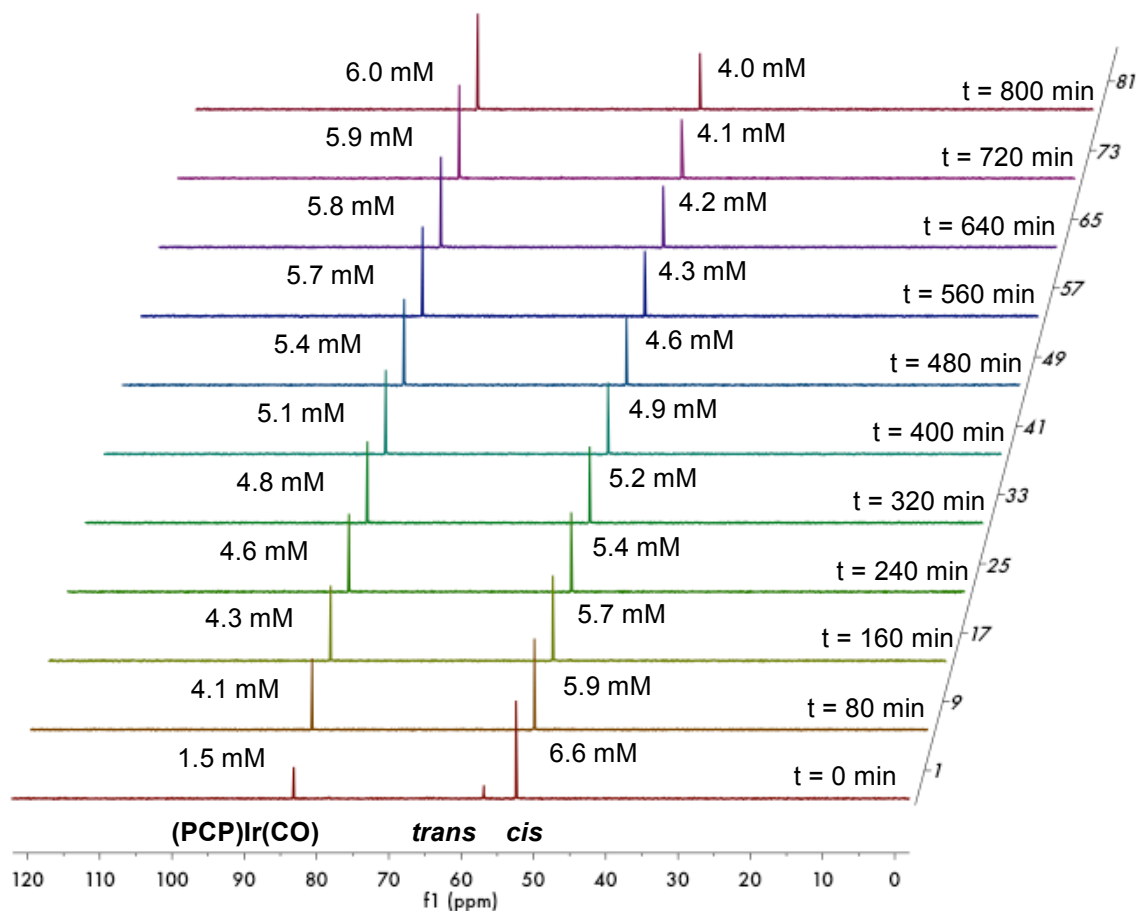
This result initially suggested that perhaps only the *trans* isomer was catalytically eliminated by acid, while the *cis* isomer underwent concerted (non-catalyzed) reductive elimination without the assistance of the acid; however, a control experiment utilizing the same mixture of stereoisomers but omitting buffer solution did not result in loss of either isomer over the same time period, indicating that both elimination processes are catalyzed by acid. Much like the *trans* isomer, it is possible that the *cis* isomer is protonated directly by acid, but, unlike the *trans* isomer, the resulting alkane adduct

**Figure 5.1.**  $^{31}\text{P}$  NMR spectra of acid-catalyzed elimination reaction involving *cis*- and *trans*-( $^{\text{tBu}}\text{PCP}$ )Ir(CO)(H)(C<sub>2</sub>H<sub>3</sub>) over the first 40 minutes of reaction. Values are approximate based upon initial 10 mM total concentration of isomer mixture.



dissociates more slowly owing to the weaker *trans* influence of the phenyl ligand *trans* to the alkyl group in the *cis* stereoisomer (in the *trans* stereoisomer, the ligand *trans* to the alkyl group is a comparably stronger  $\sigma$ -donating *trans* influence ligand (H<sup>-</sup>) which should weaken the bond M-C<sub>alkyl</sub> bond and favor protonation/dissociation of the alkane). It may also be possible that slow isomerization of the *cis* isomer to the putatively more thermodynamically favored *trans* isomer occurs via an acid-catalyzed route (with subsequent rapid acid-catalyzed elimination occurring from the *trans* stereoisomer).

**Figure 5.2.**  $^{31}\text{P}$  NMR spectra of acid-catalyzed elimination reaction involving *cis*- and *trans*-( $^t\text{Bu}^4\text{PCP}$ )Ir(CO)(H)(C<sub>2</sub>H<sub>3</sub>) over the first ca. 13 hours of reaction.



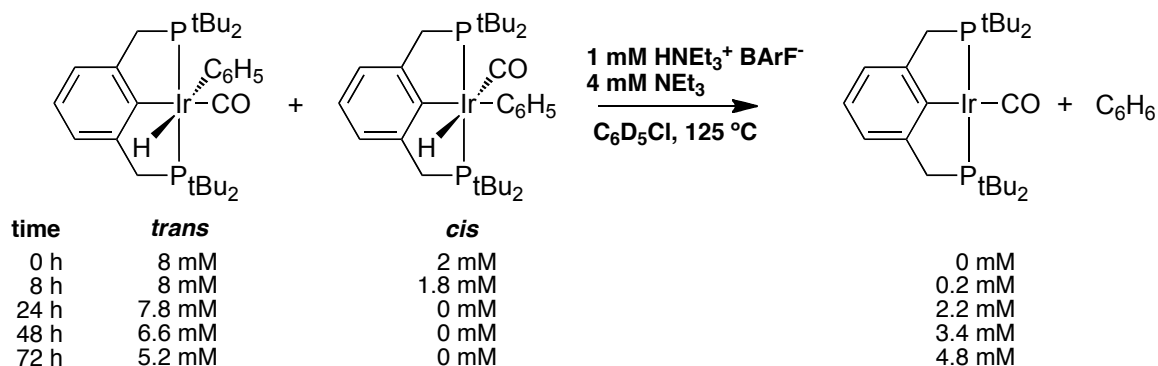
#### 5.2.4. Elimination of benzene from *cis/trans* ( $^t\text{Bu}^4\text{PCP}$ )Ir(CO)(H)(Ph) complexes

Unlike the reaction observed with the alkyl hydride carbonyl complexes, no reaction occurred with either the *cis* or *trans* six-coordinate phenyl carbonyl complexes when treated with buffer solution at room temperature; even following this reaction over the course of two weeks by  $^{31}\text{P}$  nmr showed no loss of starting materials. However, heating the reaction mixture to 125 °C for several days resulted in slow decomposition of the *cis* and *trans* diastereomers to free benzene and ( $^t\text{Bu}^4\text{PCP}$ )Ir(CO); curiously, in spite of our earlier observations regarding faster loss of *trans*-( $^t\text{Bu}^4\text{PCP}$ )Ir(CO)(H)(Et) relative to

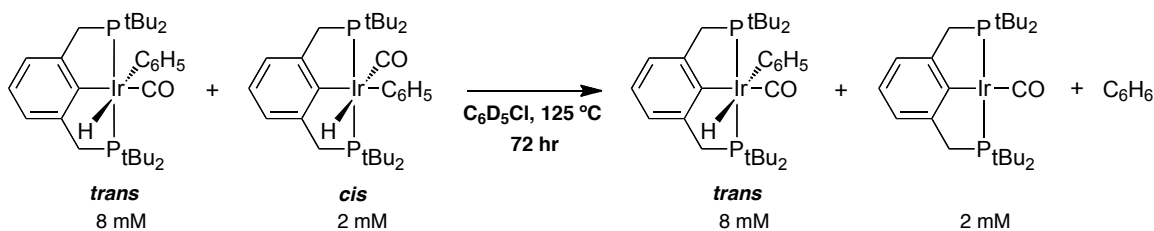


*cis*-(<sup>t</sup>Bu<sub>4</sub>PCP)Ir(CO)(H)(Et), it was observed that loss of the *cis* isomer occurred more readily than loss of the *trans* isomer (**scheme 5.7**). A control experiment was performed in which buffer solution was omitted (**scheme 5.8**): heating a solution of the *cis/trans* six-coordinate starting materials to 125 °C over the equivalent time period resulted only in loss of the *cis*-starting material with concomitant formation of the four-coordinate complex, indicating that direct thermolytic reductive elimination of *only* the *cis*-stereoisomer occurs at elevated temperature. The *trans* stereoisomer must therefore *exclusively* undergo acid-catalyzed elimination. Several reasons may exist for the slow and poor reactivity of the phenyl species compared to the alkyl-ligated species. It may be that the phenyl ligand is too crowded and therefore kinetically inaccessible to the Brønsted acid, perhaps requiring unfavorable canting of benzene ring (in an already sterically-hindered system) to accept the proton. It could also be simply that the phenyl ligand is several orders of magnitude a weaker base than the alkyl ligands (compare the pK<sub>a</sub> values of free benzene (43) to that of methane (50))<sup>8</sup>, and as result the kinetics of protonation are much less favorable.

**Scheme 5.7.** Buffer-catalyzed reductive elimination of benzene from *cis*- and *trans*-(<sup>t</sup>Bu<sub>4</sub>PCP)Ir(CO)(H)(Ph).



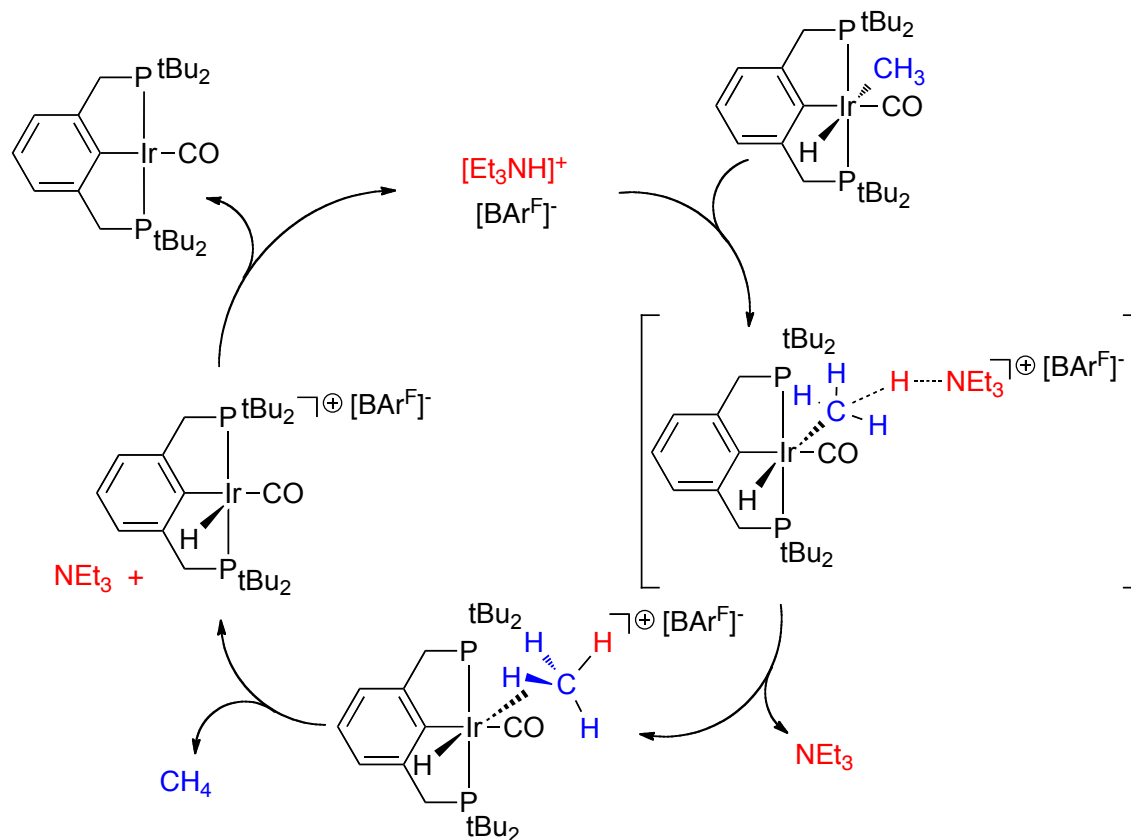
**Scheme 5.8.** Thermolytic loss of benzene exclusively from *cis*-(<sup>t</sup>Bu<sup>4</sup>PCP)Ir(CO)(H)(Ph)



### 5.2.5. Proposed mechanism for elimination of *trans*-(<sup>t</sup>Bu<sup>4</sup>PCP)Ir(CO)(H)(R) complexes.

Owing to the rapid rate of reductive elimination of the *trans* methyl hydride carbonyl species (and the presence of *cis* stereoisomers byproduct in higher alkyl species), kinetic studies are not easily accomplished. However, based upon the reactivity of the various six-coordinate substrates and the mechanism for the acid-catalyzed oxidative addition of  $\text{PhCCH}$ , the mechanism presented in **scheme 5.9** seems highly plausible. Protonation of the alkyl or aryl ligand results in a cationic  $\sigma$ -complex intermediate, which quickly decomposes into free R-H molecules (alkane or arene) and  $(^t\text{Bu}^4\text{PCP})\text{Ir}(\text{CO})(\text{H})^+ \text{BAR}^{\text{F}-}$ . As we observed in chapter 4,  $(^t\text{Bu}^4\text{PCP})\text{Ir}(\text{CO})(\text{H})^+ \text{BAR}^{\text{F}-}$  is readily deprotonated by free triethylamine, as equilibrium heavily favors the  $\text{HNEt}_3^+ \text{BAR}^{\text{F}-} / (^t\text{Bu}^4\text{PCP})\text{Ir}(\text{CO})$  side of the reaction, forming the four-coordinate carbonyl species and regenerating the triethylammonium acid catalyst.

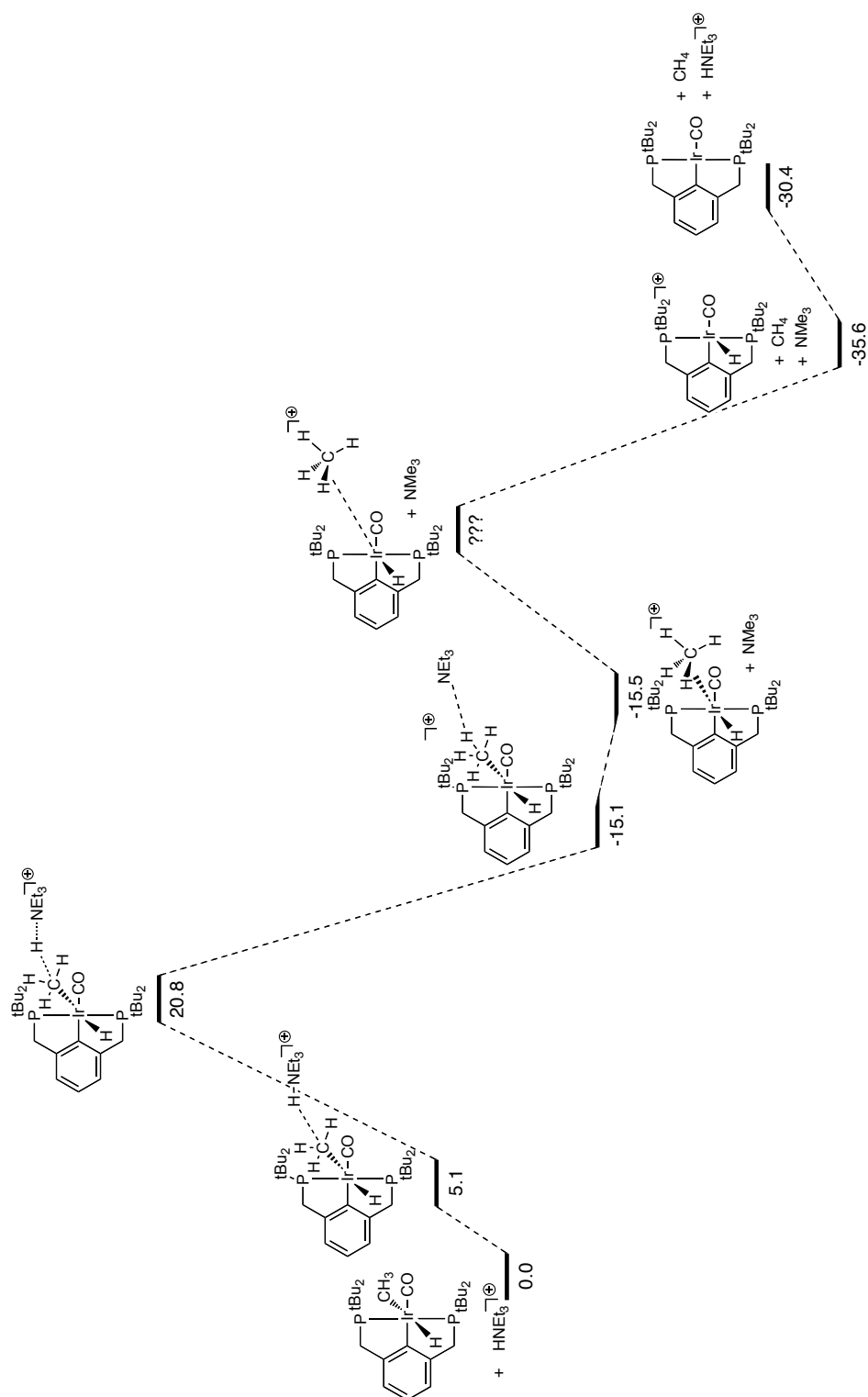
**Scheme 5.9.** Proposed mechanism for acid-catalyzed reductive elimination of methane from  $trans\text{-}(\text{tBu}^4\text{PCP})\text{Ir}(\text{CO})(\text{H})(\text{CH}_3)$ .



### 5.2.6. DFT Calculations

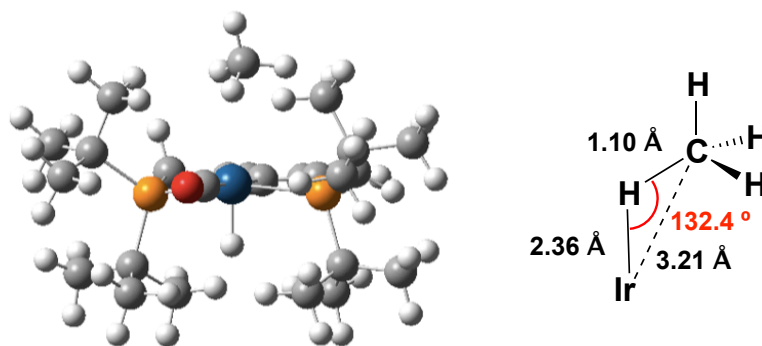
Further support for this mechanism is gained from DFT calculations regarding the acid-catalyzed elimination of methane from  $trans\text{-}(\text{tBu}^4\text{PCP})\text{Ir}(\text{CO})(\text{H})(\text{CH}_3)$ . As shown in the free energy diagram in **figure 5.3**, the acid-catalyzed reductive elimination of methane is highly kinetically and thermodynamically favorable. The transition state corresponding to proton-transfer from acid to the methyl ligand has an activation barrier of *ca.* 21 kcal/mol, about the upper limit of what we would expect for a reaction that

**Figure 5.3.** DFT-calculated pathway for acid-catalyzed elimination of methane from *trans*-(<sup>t</sup>Bu<sub>4</sub>PCP)Ir(CO)(CH<sub>3</sub>)(H) ( $\Delta G$  values in kcal/mol).



occurs readily at room-temperature. The formation of a cationic methane adduct  $(^t\text{Bu}_4\text{PCP})\text{Ir}(\text{CO})(\text{H})(\text{CH}_4)^+$  is significantly downhill; the DFT-optimized geometry indicates the formation of an agostic methane complex having an Ir-H bond length of 2.36 Å and Ir-C bond length of 3.16 Å (**figure 5.4**). The transition state for methane dissociation was not found, but is presumably relatively facile, as the methane adduct is not observed spectroscopically and is *trans* to strong  $\sigma$ -donating ligand. Loss of methane and deprotonation of the cationic intermediate to give  $(^t\text{Bu}_4\text{PCP})\text{Ir}(\text{CO})$  is further downhill by 15 kcal/mol; overall, the formation of  $(^t\text{Bu}_4\text{PCP})\text{Ir}(\text{CO})$  and methane from *trans*- $(^t\text{Bu}_4\text{PCP})\text{Ir}(\text{CO})(\text{H})(\text{CH}_3)$  is downhill by *ca.* 30 kcal/mol, indicating that reductive elimination is indeed highly thermodynamically favored. Conversely, looking at this scheme in reverse (*i.e.* oxidative addition of methane to  $(^t\text{Bu}_4\text{PCP})\text{Ir}(\text{CO})$ ), not only does the reaction suffer from very poor thermodynamics (uphill by 30 kcal/mol), but the transition state for proton transfer from  $(^t\text{Bu}_4\text{PCP})\text{Ir}(\text{CO})(\text{H})(\text{CH}_4)^+$  to base (analogous to the rate-determining step for PhCCH addition) has a prohibitively high barrier of *ca.* 51 kcal/mol relative to free  $(^t\text{Bu}_4\text{PCP})\text{Ir}(\text{CO})$ , methane, and acid catalyst.

**Figure 5.4.** DFT-calculated methane intermediate exhibiting an agostic interaction.



### 5.3 Summary

Six-coordinate (PCP)Ir(CO)(H)(R) (R=alkyl or aryl) complexes can undergo acid-catalyzed net reductive elimination of R-H bonds to form the four-coordinate carbonyl complex and free alkanes or arenes. In direct contrast to conventional reductive elimination behavior, elimination of *trans*-disposed alkyl and hydride ligands is observed to occur more rapidly than it does for the *cis*-disposed isomer, consistent with the microscopic reverse of the acid-catalyzed oxidative addition process elucidated in Chapter 4. Further, the rate of elimination is greater for alkyl substrates than for aryl substrates, which only undergo elimination at elevated temperatures. While elimination of *cis*-disposed C-H bonds in (<sup>t</sup>Bu<sup>4</sup>PCP)Ir(CO)(R)(H) may occur thermochemically in the absence of an acid catalyst, the *trans* isomers are only observed to eliminate in the presence of an acid. These results suggest that oxidative addition of alkyl and aryl C-H bonds may be kinetically possible, but would occur only if the thermodynamics of addition could be improved. Expanding the scope of these acid-catalyzed transformation (reductive elimination or, perhaps more importantly, oxidative addition) may yield more general means of C-H bond activation; exploring the factors that favor such transformations, particularly enhancing the thermodynamics of addition, is the focus of the next chapter.

### 5.4 Experimental

**General Considerations.** All reactions were conducted under an argon atmosphere in a drybox or using standard Schlenk techniques. Acetaldehyde, propionaldehyde, and benzaldehyde were all purchased from Sigma-Aldrich, dried over CaSO<sub>4</sub> and vacuum-

transferred to yield colorless liquids, which were stored in a -40 °C glovebox freezer. Norbornene was purchased from Sigma-Aldrich and purified by sublimation. C<sub>6</sub>D<sub>5</sub>Cl was purchased from Cambridge Isotope Labs, dried over P<sub>2</sub>O<sub>5</sub> and vacuum-transferred. Triethylammonium B(C<sub>6</sub>F<sub>5</sub>)<sub>4</sub><sup>-</sup> was prepared as described in chapter 4. All other reagents were purchased from commercial suppliers and used without further purification, other than freeze-pump-thaw degassing. NMR spectra were acquired on 400 or 500 MHz Varian VNMRs nmr spectrometers. <sup>1</sup>H spectra are referenced to residual solvent peaks, while <sup>31</sup>P spectra are referenced to an external PMe<sub>3</sub> standard.

***trans*-(<sup>t</sup>Bu<sup>4</sup>PCP)Ir(CO)(H)(Me).** In a 20 mL glass vial was weighed 50 mg (0.085 mmol) of (<sup>t</sup>Bu<sup>4</sup>PCP)IrH<sub>2</sub> and 8.5 mg (0.09 mmol) of norbornene. These solids were promptly dissolved in benzene (approximately 4 mL), and the solution was thoroughly stirred for 10 min. 5.6 µL (0.10 mmol) of acetaldehyde was then added via syringe, causing the deep red solution to rapidly turn colorless. After a further 10 minutes of mixing, the solvent was removed under vacuum to yield pale yellow microcrystals in 100 % yield (based on NMR spectroscopy). The ratio of stereoisomers was 95% *trans* and 5 % *cis*, but *cis*-product formation could be minimized by adding the aldehyde at low temperature. <sup>31</sup>P{<sup>1</sup>H} NMR (C<sub>6</sub>D<sub>6</sub>, 200 MHz): δ 56.9 ppm (s). <sup>1</sup>H NMR (C<sub>6</sub>D<sub>6</sub>, 400 MHz): δ 7.0 (d, J = 7.6 Hz, 2H), 6.80 (t, J = 7.5 Hz, 1H), 3.27 (t, J<sub>PH</sub> = 3.8 Hz, 4H), 1.24 (vt, J<sub>PH</sub> = 6.5 Hz, 18 H), 1.18 (vt, J<sub>PH</sub> = 6.5 Hz, 18H), -11.2 (t, J<sub>PH</sub> = 14.9 Hz, 1H).

**Synthesis of the mixture of *cis*- and *trans*-(<sup>t</sup>Bu<sup>4</sup>PCP)Ir(CO)(H)(Et).** In a 20 mL glass vial was weighed 50 mg (0.085 mmol) of (<sup>t</sup>Bu<sup>4</sup>PCP)IrH<sub>2</sub> and 8.5 mg (0.09 mmol) of

norbornene. These solids were promptly dissolved in benzene (approximately 4 mL), and the solution was thoroughly stirred for 10 min. 7.2  $\mu\text{L}$  (0.10 mmol) of propionaldehyde was then added via syringe, causing the deep red solution to rapidly turn pale yellow. After a further 10 minutes of mixing, the solvent was removed under vacuum to yield pale yellow microcrystals in 100 % yield (based on NMR spectroscopy). The ratio of stereoisomers was 40% *trans* and 60 % *cis*.  $^{31}\text{P}\{^1\text{H}\}$  NMR ( $\text{C}_6\text{D}_6$ , 200 MHz):  $\delta$  56.8 (d,  $J = 3.3$  Hz, *trans* isomer), 52.4 (d,  $J = 4.2$  Hz, *cis* isomer).  $^1\text{H}$  NMR ( $\text{C}_6\text{D}_6$ , 500 MHz):  $\delta$  7.08 (br s, 1H), 7.05 (m, 2H), 3.32 (dvt,  $J_{\text{PH}} = 16.4$  Hz,  $J_{\text{HH}} = 4.1$  Hz, 2H, *cis* isomer), 3.24 (t,  $J = 3.7$  Hz, 4H, *trans* isomer) 3.13 (dvt,  $J_{\text{PH}} = 16.4$  Hz,  $J_{\text{HH}} = 4.1$  Hz, 2H, *cis* isomer), 2.31 (t,  $J = 7.8$  Hz, overlapping  $\text{CH}_3$  signals), 1.92 (t,  $J = 7.6$  Hz, 2H,  $\text{CH}_2$  signal of *trans* isomer), 1.79 (sextet,  $J = 7.5$  Hz, 2H,  $\text{CH}_2$  signal of *cis* isomer), 1.24 (vt,  $J_{\text{PH}} = 6.4$  Hz, 18 H), 1.12 (vt,  $J_{\text{PH}} = 6.5$  Hz, 18H), -9.6 (t,  $J_{\text{PH}} = 17.3$  Hz, 1H, *cis* isomer), -11.8 (t,  $J_{\text{PH}} = 16.6$  Hz, 1H, *trans* isomer).

**Synthesis of the mixture of *cis*- and *trans*-( $^{\text{tBu}}\text{PCP}$ )Ir(CO)(H)(Ph).** In a 20 mL glass vial was weighed 50 mg (0.085 mmol) of ( $^{\text{tBu}}\text{PCP}$ )IrH<sub>2</sub> and 8.5 mg (0.09 mmol) of norbornene. These solids were promptly dissolved in benzene (approximately 4 mL), and the solution was thoroughly stirred for 10 min. 10.2  $\mu\text{L}$  (0.10 mmol) of benzaldehyde was then added via syringe, causing the deep red solution to rapidly turn a pale orange. After a further 10 minutes of mixing, the solvent was removed under vacuum to yield pale orange microcrystals in 100 % yield (based on NMR spectroscopy). The ratio of stereoisomers was 80 % *trans* and 20 % *cis*.  $^{31}\text{P}\{^1\text{H}\}$  NMR ( $\text{CD}_2\text{Cl}_2$ , 200 MHz):  $\delta$  56.8 (d,  $J = 4.7$  Hz, *trans* isomer), 52.9 (d,  $J = 2.4$  Hz, *cis* isomer).  $^1\text{H}$  NMR ( $\text{CD}_2\text{Cl}_2$ , 500



MHz):  $\delta$  7.02 (d,  $J = 7.4$  Hz, 2H, *trans* isomer), 6.98 (d,  $J = 7.4$  Hz, 2H, *cis* isomer), 6.91 (t,  $J = 7.4$  Hz, 1H, *trans* isomer), 6.82 (t,  $J = 7.4$  Hz, 1H, *cis* isomer), 6.73 (td,  $J = 16.5$  Hz,  $J = 4.3$  Hz, 1H, *trans* isomer), 6.69 (tt,  $J = 7.1$  Hz,  $J = 1.4$  Hz, 1H, *trans* isomer), 6.60 (td,  $J = 7.3$  Hz,  $J = 1.7$  Hz, 1H, *trans* isomer), 6.54 (d,  $J = 7.4$  Hz, 1H, *trans* isomer), 3.54 (dvt,  $J_{\text{PH}} = 16.4$  Hz,  $J_{\text{HH}} = 4.2$  Hz, 2H, *cis* isomer, note the upfield part of this AB pattern is buried under the larger signal for the *trans* isomer, reflected by both the appearance of the tail portion of the dvt and the integral of the larger signal), 3.43 (dvt,  $J_{\text{PH}} = 16.4$  Hz,  $J_{\text{HH}} = 3.9$  Hz, 2H, *trans* isomer), 3.3 (dvt,  $J_{\text{PH}} = 16.5$  Hz,  $J_{\text{HH}} = 4.3$  Hz, 2H, *trans* isomer), 1.28 (vt,  $J_{\text{PH}} = 6.6$  Hz, 18 H), 1.01 (vt,  $J_{\text{PH}} = 6.7$  Hz, 18H), -9.02 (t,  $J_{\text{PH}} = 17.5$  Hz, 1H, *cis* isomer), -12.2 (t,  $J_{\text{PH}} = 15.4$  Hz, 1H, *trans* isomer).

**General Procedure for acid-catalyzed reductive elimination reactions.** A 50 mM stock solution of ( $^{\text{tBu}}\text{PCP}$ )Ir(CO)(H)(R) in chlorobenzene- $d_5$  was prepared, along with a separate buffer solution containing a 1:4 mixture of  $\text{HNEt}_3^+ \text{BAr}^{\text{F}-}$  (10 mM) and  $\text{NEt}_3$  (40 mM) in chlorobenzene- $d_5$ . 100  $\mu\text{L}$  of the ( $^{\text{tBu}}\text{PCP}$ )Ir(CO)(H)(R) stock solution was then added to a J. Young NMR tube and further diluted with 350  $\mu\text{L}$  of  $\text{C}_6\text{D}_5\text{Cl}$ . Immediately prior to NMR data acquisition, 50  $\mu\text{L}$  of the buffer stock solution was added (total volume of reaction mixture: 0.5 mL) and, as quickly as possible, the sealed J. Young tube was removed from the glovebox and frozen in liquid nitrogen. The sample was kept frozen until ready for analysis.

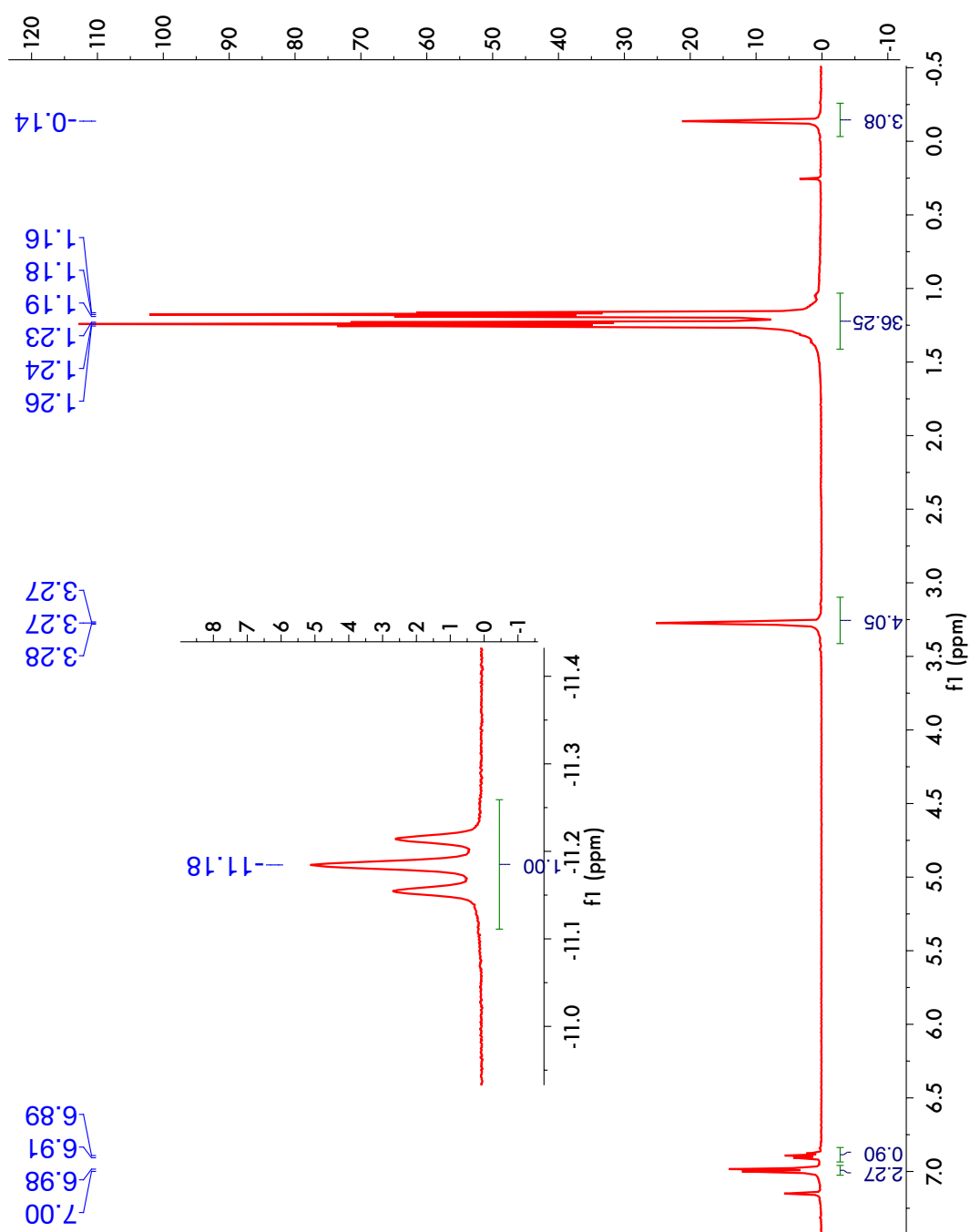
**Computational Methods.** All calculations were performed by the *Gaussian09* suite of molecular modeling software.<sup>9</sup> DFT<sup>10</sup> calculations employing the M06L functional were

used.<sup>11</sup> Ir atoms were described by a LANL2TZ basis set augmented by a diffuse d-type function (exponent = 0.07645) (value obtained as one-half times the exponent of the outermost d-type function in the LANL2TZ basis set for Ir).<sup>12</sup> All other atoms were described by a 6-311G(d,p) basis set.<sup>13</sup> All calculations made use of a conductor-like polarizable continuum model (c-PCM)<sup>14</sup> representing chlorobenzene and were conducted at standard temperature and pressure.

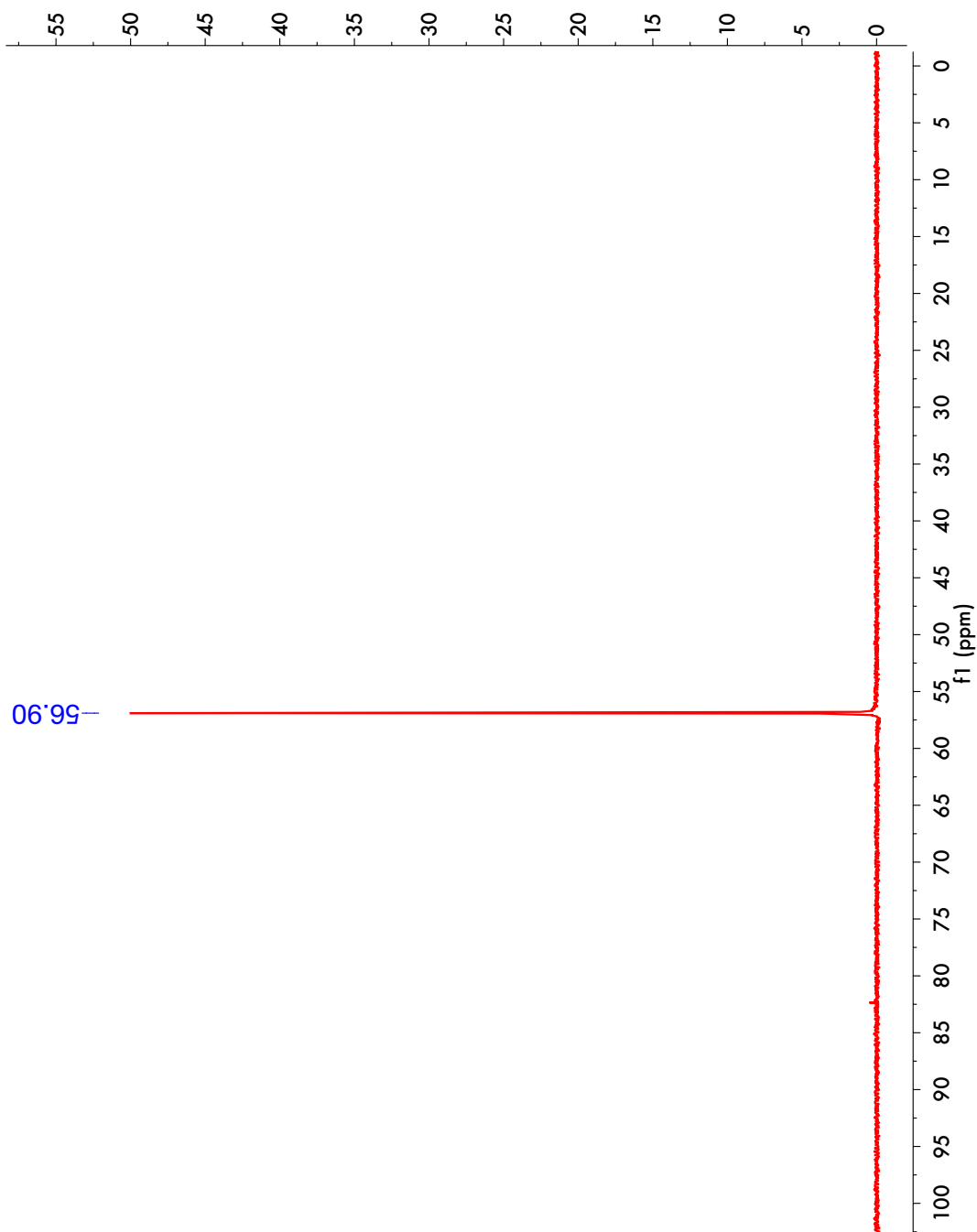
## 5.5 Chapter 5 Appendix

### 5.5.1 NMR Spectra

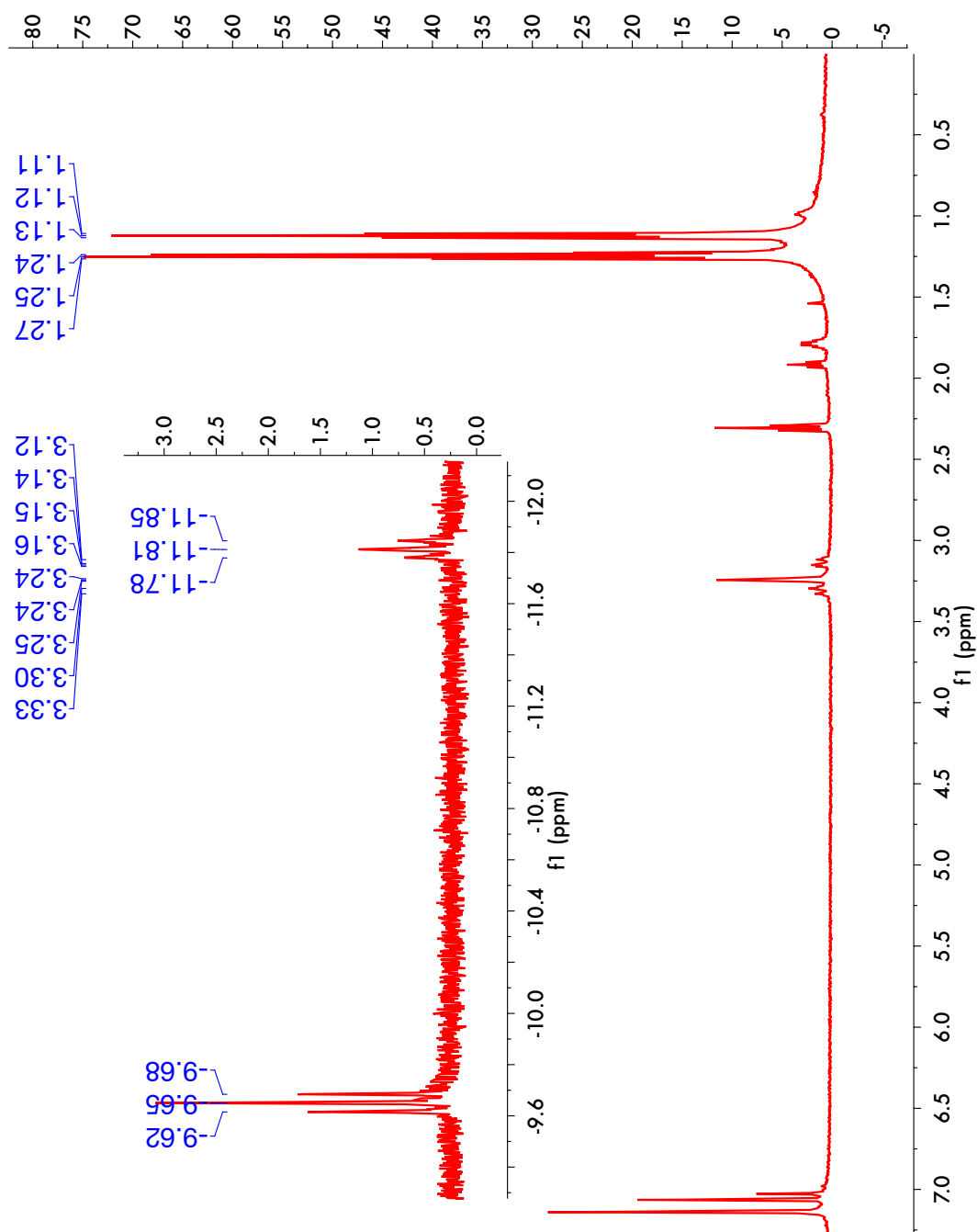
**Figure 5A.1.**  $^1\text{H}$  nmr spectrum of  $(^t\text{Bu}^4\text{PCP})\text{Ir}(\text{CO})(\text{H})(\text{CH}_3)$



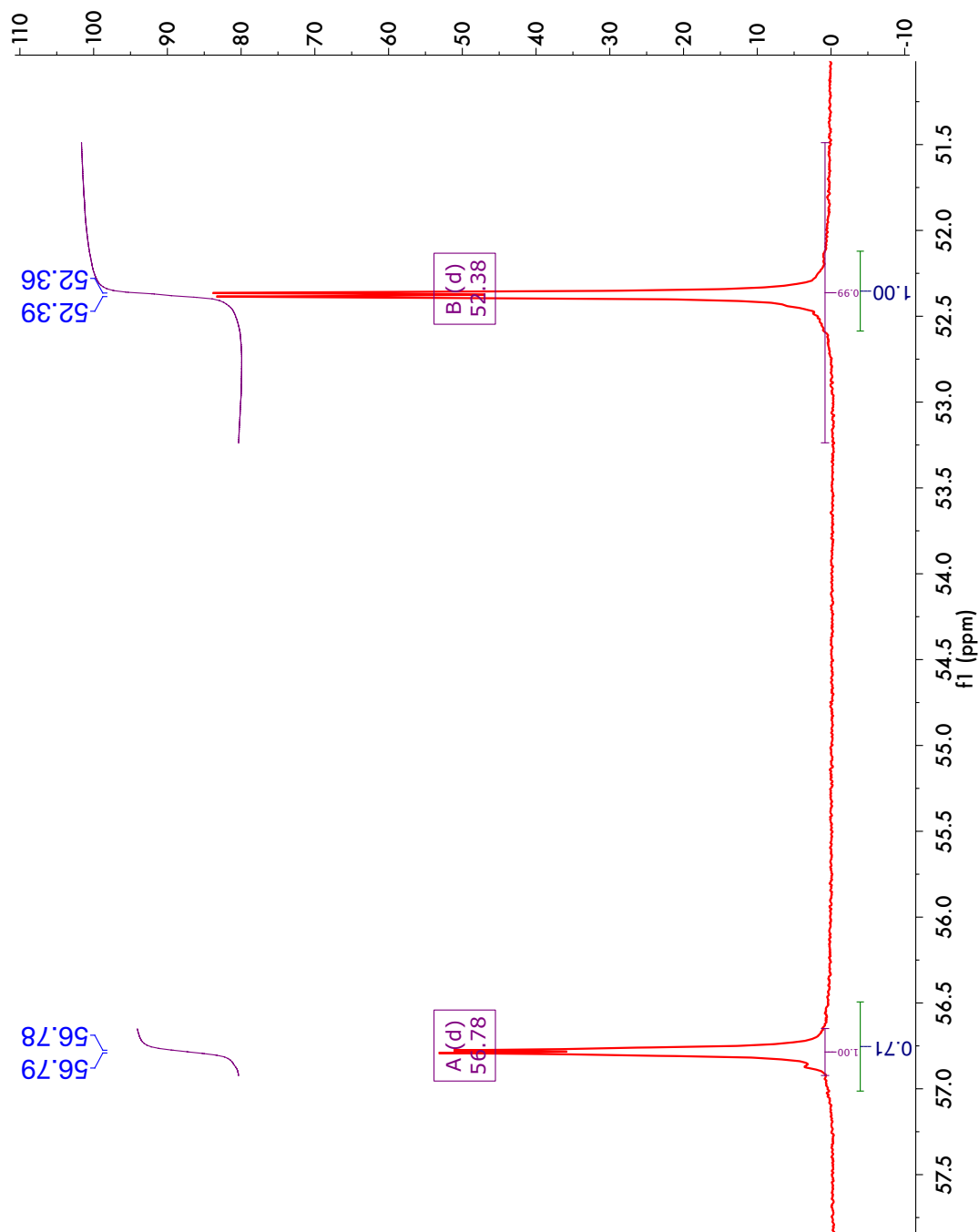
**Figure 5A.2.**  $^{31}\text{P}$  nmr spectrum of  $(^{\text{tBu}^4}\text{PCP})\text{Ir}(\text{CO})(\text{H})(\text{CH}_3)$



**Figure 5A.3.**  $^1\text{H}$  nmr spectrum of  $(^t\text{Bu}^4\text{PCP})\text{Ir}(\text{CO})(\text{H})(\text{CH}_2\text{CH}_3)$



**Figure 5A.4.**  $^{31}\text{P}$  nmr spectrum of  $(^{\text{tBu}}\text{PCP})\text{Ir}(\text{CO})(\text{H})(\text{CH}_2\text{CH}_3)$



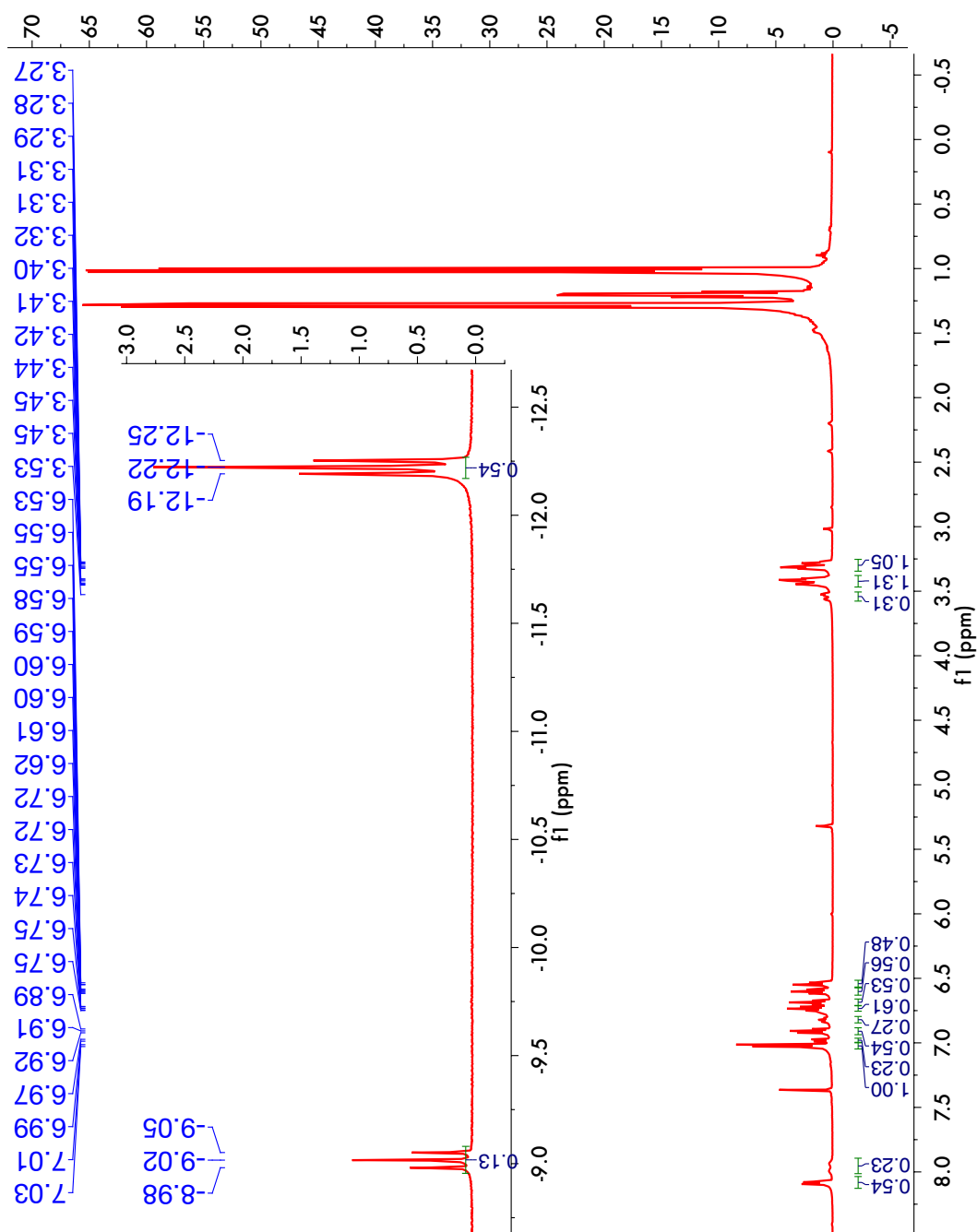
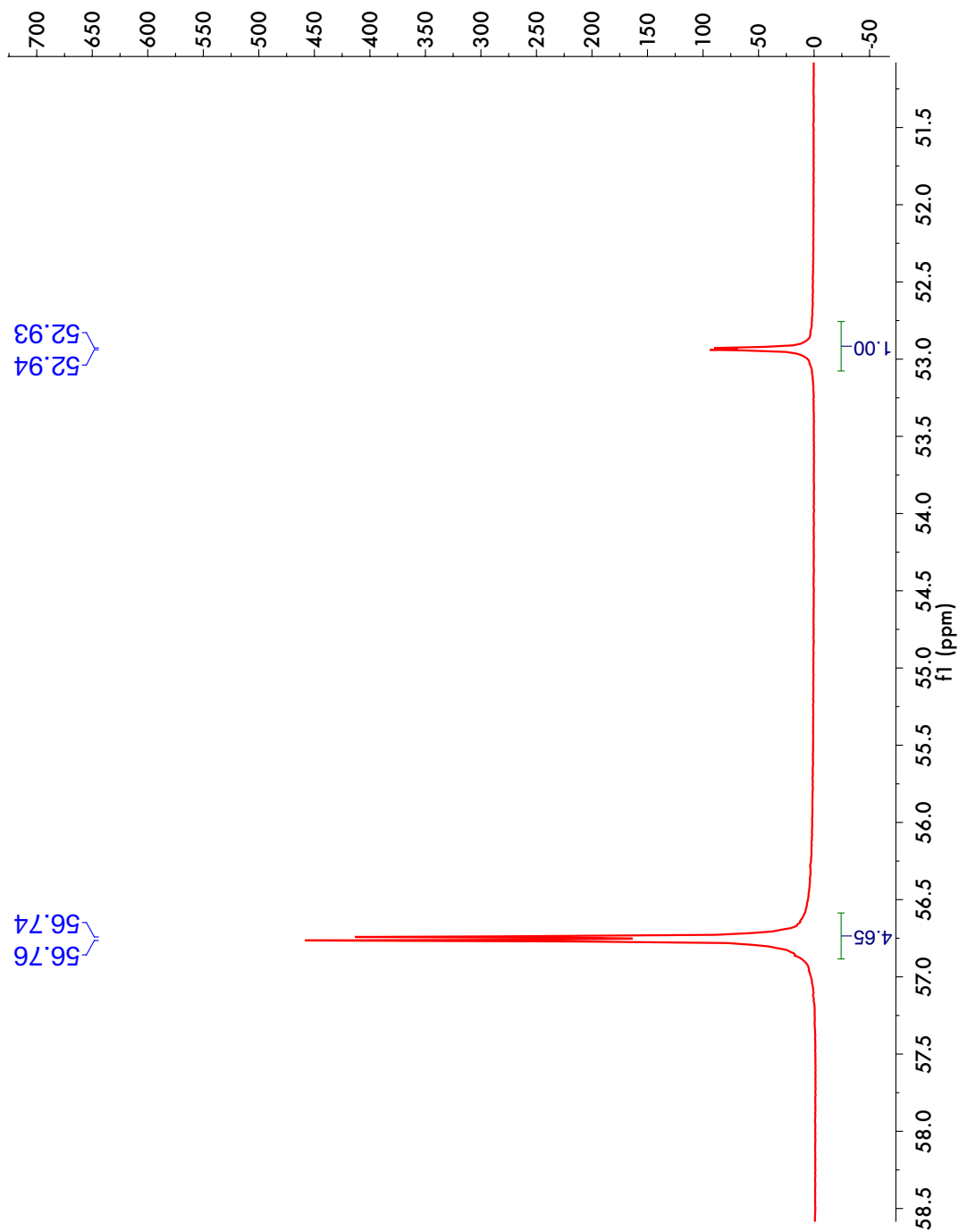


**Figure 5A.6.**  $^{31}\text{P}$  nmr spectrum of  $(^{\text{tBu}}\text{PCP})\text{Ir}(\text{CO})(\text{H})(\text{C}_6\text{H}_5)$





## 5.6 References

- (1) Hartwig, J. F. *Organotransition Metal Chemistry*; University Science Books: Sausalito, CA, 2010.
- (2) Bartlett, K. L.; Goldberg, K. I.; Borden, W. T. *Organometallics* **2001**, *20*, 2669.
- (3) Bartlett, K. L.; Goldberg, K. I.; Borden, W. T. *J. Am. Chem. Soc.* **2000**, *122*, 1456.
- (4) Kanzelberger, M.; Singh, B.; Czerw, M.; Krogh-Jespersen, K.; Goldman, A. S. *J. Am. Chem. Soc.* **2000**, *122*, 11017.
- (5) Krogh-Jespersen, K.; Czerw, M.; Zhu, K.; Singh, B.; Kanzelberger, M.; Darji, N.; Achord, P. D.; Renkema, K. B.; Goldman, A. S. *J. Am. Chem. Soc.* **2002**, *124*, 10797.
- (6) De Luca, N.; Wojcicki, A. *J. Organomet. Chem.* **1980**, *193*, 359.
- (7) Kanzelberger, M. Ph.D. Thesis, Rutgers University, 2004.
- (8) Anslyn, E. V.; Dougherty, D. A. *Modern Physical Organic Chemistry*; University Science Books: Sausalito, California, 2005.
- (9) Frisch, M. J. T., G. W.; Schlegel, H. B.; Scuseria, G. E.; Robb, M. A.; Cheeseman, J. R.; Scalmani, G.; Barone, V.; Mennucci, B.; Petersson, G. A.; Nakatsuji, H.; Caricato, M.; Li, X.; Hratchian, H. P.; Izmaylov, A. F.; Bloino, J.; Zheng, G.; Sonnenberg, J. L.; Hada, M.; Ehara, M.; Toyota, K.; Fukuda, R.; Hasegawa, J.; Ishida, M.; Nakajima, T.; Honda, Y.; Kitao, O.; Nakai, H.; Vreven, T.; Montgomery, Jr., J. A.; Peralta, J. E.; Ogliaro, F.; Bearpark, M.; Heyd, J. J.; Brothers, E.; Kudin, K. N.; Staroverov, V. N.; Kobayashi, R.; Normand, J.; Raghavachari, K.; Rendell, A.; Burant, J. C.; Iyengar, S. S.; Tomasi, J.; Cossi, M.; Rega, N.; Millam, N. J.; Klene, M.; Knox, J. E.; Cross, J. B.; Bakken, V.; Adamo, C.; Jaramillo, J.; Gomperts, R.; Stratmann, R. E.; Yazyev, O.; Austin, A. J.; Cammi, R.; Pomelli, C.; Ochterski, J. W.; Martin, R. L.; Morokuma, K.; Zakrzewski, V. G.; Voth, G. A.; Salvador, P.; Dannenberg, J. J.; Dapprich, S.; Daniels, A. D.; Farkas, Ö.; Foresman, J. B.; Ortiz, J. V.; Cioslowski, J.; Fox, D. J.; Gaussian 09, Revision A.02 ed.; Gaussian, Inc.: Wallingford, CT, 2009.
- (10) Parr, R. G.; Yang, W. *Density-Functional Theory of Atoms and Molecules*; University Press: Oxford, 1989.
- (11) Zhao, C. Y.; Truhlar, D. G. *Theo. Chem. Acc.* **2008**, *120*, 215.
- (12) Roy, L. E.; Hay, P. J.; Martin, R. L. *J. Chem. Theory Comput.* **2008**, *4*, 1029.
- (13) Krishnan, R.; Binkley, J. S.; Seeger, R.; Pople, J. A. *J. Chem. Phys.* **1980**, *72*, 650.
- (14) Barone, V.; Cossi, M. *J. Phys. Chem. A* **1998**, *102*, 1995.

## Chapter 6

### **Further experimental and theoretical explorations of acid-catalyzed oxidative addition and reductive elimination reactions involving (pincer)Ir(CO) complexes**

#### **Abstract**

In the preceding chapters, we reported surprising acid-catalyzed C-H bond breaking and forming reactions (oxidative addition and reductive elimination, respectively) involving (<sup>t</sup>Bu<sup>4</sup>PCP)Ir(CO) complexes. The scope of these reactions, however, was rather limited, particularly in the oxidative addition direction where only alkynes have been observed to add to (PCP)Ir(CO) complexes. This chapter concerns a fuller exploration of the scope of these acid-catalyzed process, specifically describing our attempts at implementing various strategies to favor the thermodynamics of C-H addition to four-coordinate square planar Ir(I) carbonyl complexes. These strategies include reducing the size of the substituents about the metal center, utilizing stronger  $\sigma$ -donors *trans* to the carbonyl ligand, and attempting addition of activated or functionalized substrates. Experimental and theoretical studies indicate that the oxidative addition of C-H bonds becomes more favorable by reducing the sterics on the (pincer)Ir(CO) complex and by incorporating a stronger  $\sigma$ -donor *trans* to the carbonyl ligand.

## 6.1 Introduction

In light of the surprising acid-catalyzed oxidative addition (Chapter 4) and reductive elimination (Chapter 5) of C-H bonds to and from (<sup>t</sup>Bu<sup>4</sup>PCP)Ir(CO) complexes, our interest turned toward expanding the scope of these rare transformations, particularly with regard to the oxidative addition of covalent bonds to (pincer)Ir(CO) complexes. The task of promoting oxidative addition is made difficult, however, as the reductive elimination of C-H bonds from transition metal complexes generally tends to be more favorable than the oxidative addition of those C-H bonds.<sup>1,2</sup> Consequently, the fact that alkyl and aryl C-H bonds rapidly undergo reductive elimination from six-coordinate (<sup>t</sup>Bu<sup>4</sup>PCP)Ir(CO)(H)(R) complexes in the presence of an acid catalyst suggests that oxidative addition of alkanes or arenes to (<sup>t</sup>Bu<sup>4</sup>PCP)Ir(CO) would be thermodynamically uphill. Even if the acid catalyst behaves as a true catalyst (*i.e.* the catalyst works in both directions, catalyzing both the reductive elimination and oxidative addition of C-H bonds), it can do nothing to overcome the unfavorable thermodynamics of addition. As a result, to expand the scope of these acid-catalyzed processes, we must devise new strategies to favor the thermodynamics of C-H oxidative addition.

There are multiple means of favoring the thermodynamics of addition of C-H bonds to transition metal complexes, with the most basic considerations involving alterations to the metal complex or to the substrate. With regards to altering the complex itself, a variety of stereoelectronic parameters could be tuned. The sterics about the metal center play a key role in determining not only the kinetics of C-H bond activation, but also the thermodynamic stability of the resulting oxidative addition adducts. For a crowded metal center like those found in iridium-pincer complexes, the thermodynamics

of addition might be greatly favored by altering the substituents on the phosphine groups, specifically by switching from the bulkier substituents (e.g. *tert*-butyl groups) examined in the previous chapters to less sterically demanding ones (e.g. *iso*-propyl or methyl). Such modification should give rise to purely steric differences, in contrast to changes to the ligand platform (for example, PCP versus POCOP), which beyond steric effects alone, might additionally give rise to unintended electronic differences that could adversely impact the favorability of the oxidative addition process. The resulting favorability gained by reducing the sterics is readily apparent from previous reports of H<sub>2</sub> oxidative addition to (PCP)Ir(CO) complexes: H<sub>2</sub> does not add to (<sup>tBu</sup><sub>4</sub>PCP)Ir(CO) even at elevated temperatures to form a stable six-coordinate species, while it readily adds at room temperature to the analogous (<sup>iPr</sup><sub>4</sub>PCP)Ir(CO) species.<sup>3</sup> In fact, the reduction in sterics need not be as dramatic as going from four *tert*-butyl substituents to four *iso*-propyl substituents, as even the (<sup>tBu</sup><sub>3</sub><sup>Me</sup>PCP)Ir(CO) complex (where only one *tert*-butyl group has been replaced by a methyl group) has been found to readily add H<sub>2</sub>, even at low temperatures.<sup>4</sup>

Beyond sterics, one may also alter the electronics of the transition metal complex to favor addition. Conventional wisdom has long held that the thermodynamics of oxidative addition to transition metal complexes is favored by metal centers bearing electron-donating ligands (*i.e.* strong  $\sigma$ -donors),<sup>5-7</sup> though theoretical work by former group member David Wang indicates that such generality is not true in most cases (where electron-*withdrawing* groups actually favor addition).<sup>4</sup> However, in the specific case of *trans* oxidative addition of C-H bonds to *four-coordinate* Ir(I) complexes (*i.e.* the process that occurs via the acid-catalyzed route reported in Chapter 4), DFT calculations indicate

that oxidative addition of C-H bonds actually *is favored* by strong  $\sigma$ -donors (specifically determined for the case where the  $\sigma$ -donor is *trans* to an ammonia ligand in the square planar structure  $(X)M(PH_3)_2(NH_3)$ ).<sup>4</sup> Extending this to isoelectronic (pincer)Ir(CO) complexes suggests that replacing the aryl-carbon with a stronger  $\sigma$ -donor (such as an aliphatic-carbon<sup>7</sup> or a silyl group) may promote the formation of stable six-coordinate oxidative addition adducts.

Finally, rather than, or perhaps in addition to, changing the catalyst, one could instead imagine promoting addition by selecting a substrate that is “activated” or otherwise more prone to undergo addition more readily. In this sense, substituents bearing electron-withdrawing groups<sup>8,9</sup> may be particularly apt to form stable oxidative addition adducts upon adding to square planar carbonyl complexes. This chapter will discuss our experimental and theoretical attempts to implement these different strategies for the more general addition of covalent bonds to (pincer)Ir(CO) complexes.

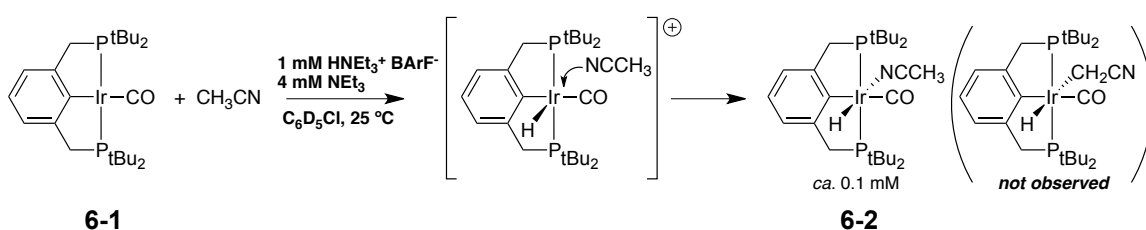
## 6.2 Results and Discussion

### 6.2.1. Reactions of $(^{tBu_4}PCP)Ir(CO)$ with non-alkynyl substrates.

Following the unprecedented success for oxidative addition of phenylacetylene, we attempted a variety of other substrates in the acid-catalyzed addition to  $(^{tBu_4}PCP)Ir(CO)$  (**6-1**). We started out with relatively simple substrates at room-temperature (identical conditions to the phenylacetylene addition described in chapter 4: 1 mM  $HNEt_3^+ BAr^F^-$  and 4 mM  $Et_3N$ ), before increasing the temperature to 80 °C and then 125 °C; however, no reaction was observed by NMR spectroscopy with unfunctionalized substrates such as benzene (2 M), n-hexane (2 M), 1-hexene (2 M), or

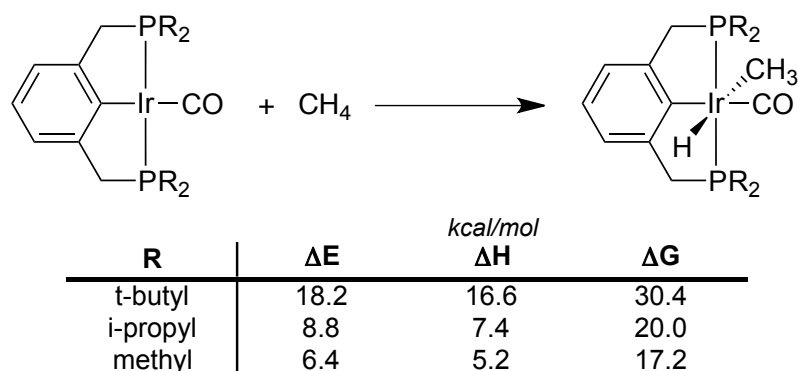
methane (1 atm), even after heating for several days. We next attempted functionalized substrates, particularly substrates with electron-withdrawing groups that generally favor the thermodynamics of addition product. However, no reaction was observed with 1,3-bis(trifluoromethyl)benzene (used as a solvent), pentafluorobenzene (used as a solvent), trifluoromethane (1 atm), or fluoromethane (1 atm). The addition of 500 mM acetonitrile (which Ittel and Tolman had observed to add to “Fe(dmpe)<sub>2</sub>”) <sup>10</sup> under standard conditions appeared to form a small amount (*ca.* 10 %) of a new product with a hydride signal in the <sup>1</sup>H nmr at −19.3 ppm (t, J = 12.8 Hz, 1H) and <sup>31</sup>P singlet with a chemical shift of 66.7 ppm (**6-2**). However, when excess acid was employed (10 mM), the amount of product grew larger (*ca.* 47 % new product), suggesting that the acid was behaving not as a catalyst but as a reactant that was subsequently incorporated into the product. The most likely explanation for this behavior is acetonitrile coordinating to (and thus trapping) the five-coordinate cationic intermediate (<sup>t</sup>Bu<sub>4</sub>PCP)Ir(CO)(H)<sup>+</sup> BAr<sup>F−</sup> through the nitrogen atom (**scheme 6.1**). This product would be expected to yield a hydride triplet (the methyl group is too remote to further split the hydride signal) in the vicinity of that observed for the product. This CH<sub>3</sub>CN-coordinated product was found to be highly thermally stable, as heating this product did not result in any conversion to the C-H addition product or loss of starting material. Given the fairly broad classes of substrates attempted, it appeared that the general ability to add substrates to (<sup>t</sup>Bu<sub>4</sub>PCP)Ir(CO) was beyond reach.

**Scheme 6.1.** Addition of CH<sub>3</sub>CN traps the cationic intermediate.



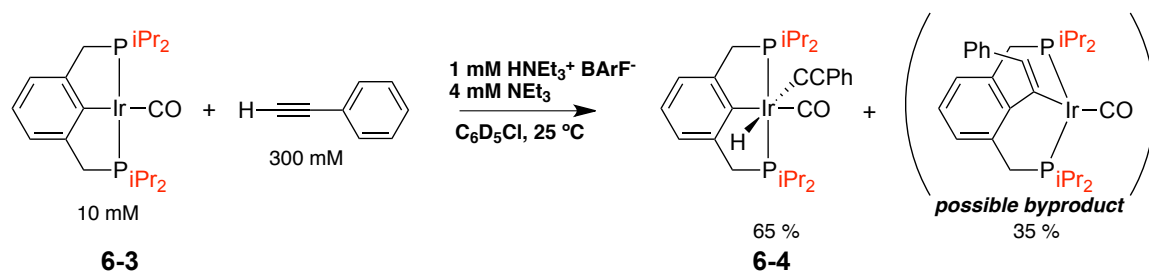
### 6.2.2 Reactivity of (<sup>i</sup>Pr<sup>4</sup>PCP)Ir(CO) complexes

We began further exploration of how best to promote C-H addition by following a route we have used to great effect in the past: pruning the sterics about the metal center. It has been previously observed that less sterically-crowded pincer complexes are generally more reactive than pincer complexes with bulky substituents on the phosphine ligands; for instance, in chapter 3 of this thesis, we reported a dramatic increase in catalytic activity toward *n*-hexane metathesis when switching from the (<sup>t</sup>Bu<sup>4</sup>PCOP)Ir catalyst to the (<sup>t</sup>Bu<sup>2</sup>PCOP<sup>i</sup>Pr<sup>2</sup>)Ir catalyst, a seemingly subtle change that produced the most active pincer-iridium co-catalyst employed to date for alkane metathesis. DFT calculations assessing the overall thermodynamics of methane addition to (<sup>R</sup><sup>4</sup>PCP)Ir(CO) complexes indicate that reducing the size of the R groups on phosphorous does in fact favor the thermodynamics of C-H oxidative addition to the (pincer)Ir(CO) complex (though in all cases, the thermodynamics remain significantly uphill): the six-coordinate methyl hydride carbonyl species is roughly 10 kcal/mol more favorable for the *iso*-propyl substituted complex versus the *tert*-butyl analogue (**table 6.1**). Interestingly, further reducing the size of the R group from *iso*-propyl to methyl has a much smaller effect on the thermodynamics of this addition. (<sup>Me</sup>PCP)Ir complexes are known to undergo facile decomposition (particularly dimerization), and since the additional benefit of methyl sterics is marginal at best, we instead pursued investigating the activity of the previously reported (<sup>i</sup>Pr<sup>4</sup>PCP)Ir(CO) complex (**6-3**) toward oxidative addition.<sup>3</sup>

**Table 6.1.** Calculated energies for *trans* oxidative addition of methane to (<sup>R4</sup>PCP)Ir(CO).

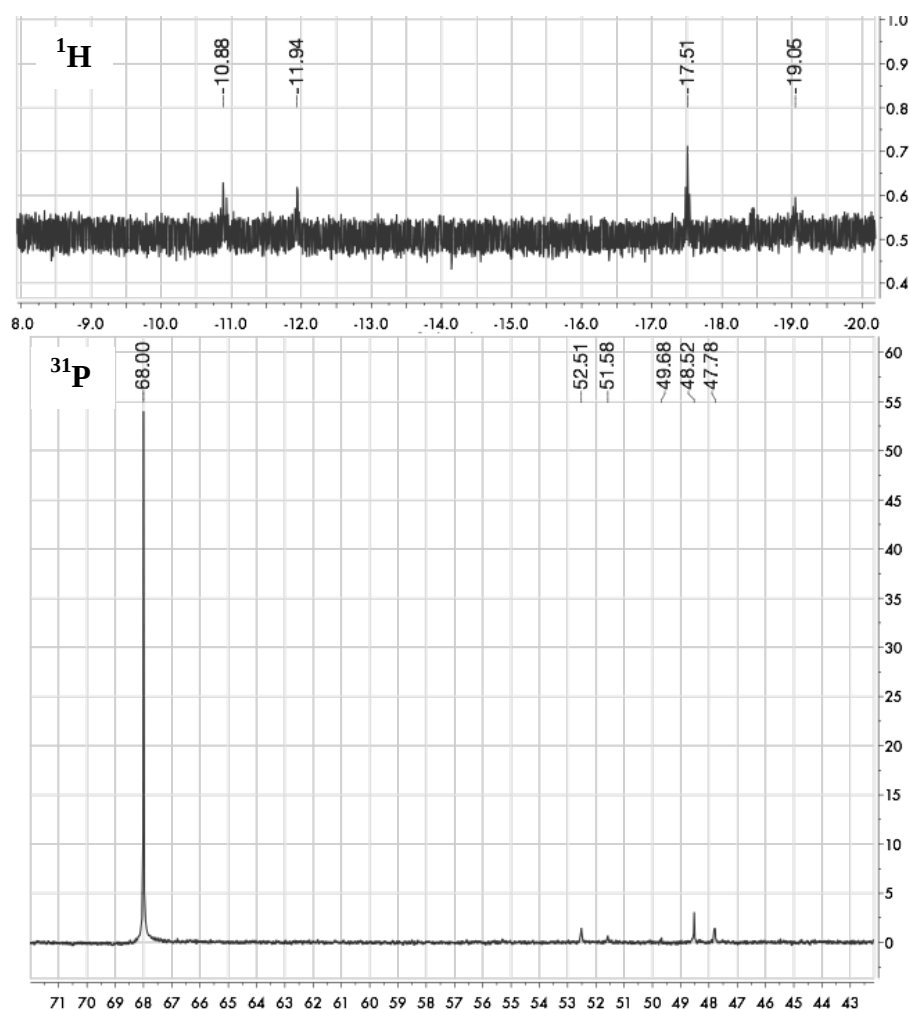
Prior to attempting other substrates, however, we returned to PhCCH as a substrate to provide a handle on (<sup>iPr4</sup>PCP)Ir(CO) reactivity and to aid in assessment of any other differences that may have resulted from changing to the less-hindered catalyst. As in the (<sup>tBu4</sup>PCP)Ir(CO) case, under our standard buffer-catalyzed conditions (1 mM HNEt<sub>3</sub><sup>+</sup> BAR<sup>F-</sup> and 4 mM Et<sub>3</sub>N), (<sup>iPr4</sup>PCP)Ir(CO) (10 mM) readily reacts with PhCCH (300 mM) at room temperature to yield the *trans* product (*ca.* 65 % by <sup>31</sup>P nmr) (**6-4**), which presents as a singlet at 49.6 ppm in <sup>31</sup>P nmr and as a triplet in the hydride region of the <sup>1</sup>H nmr (-11.9 ppm, *J* = 13.5 Hz); unlike the (<sup>tBu4</sup>PCP)Ir(CO) case, an additional unidentified byproduct (*ca.* 35 %) is present as well, as indicated by a singlet in the <sup>31</sup>P nmr at 35.5 ppm (no hydride signal is observed for this byproduct) (**scheme 6.2**). Use of excess base (20 mM) had no effect on mitigating this unknown byproduct, so, coupled with the absence of hydride signal, it is not likely that this byproduct is double-addition product (whose production in the case of (<sup>tBu4</sup>PCP)Ir(CO) is inhibited by base), but may possibly instead be the acetylide insertion product (formation of this species would likely be favored by the reduction in sterics).



**Scheme 6.2.** Acid-catalyzed addition of phenylacetylene to (<sup>i</sup>Pr<sup>4</sup>PCP)Ir(CO).

We then attempted the next two most basic types of unfunctionalized sp<sup>2</sup>- and sp<sup>3</sup>-hybridized C-H bonds: benzene (2 M) and methane (1 atm). Neither substrate, however, underwent addition at room temperature under the standard buffer reaction conditions. Heating the methane reaction to 125 °C did not yield any hint of product, but heating the benzene reaction to elevated temperature did appear to form small amounts of a number of new products, as evidenced by several new peaks in the <sup>31</sup>P nmr and some small hydride signals in <sup>1</sup>H nmr (roughly 18 % total conversion based on loss of (<sup>i</sup>Pr<sup>4</sup>PCP)Ir(CO)) (**figure 6.1**).

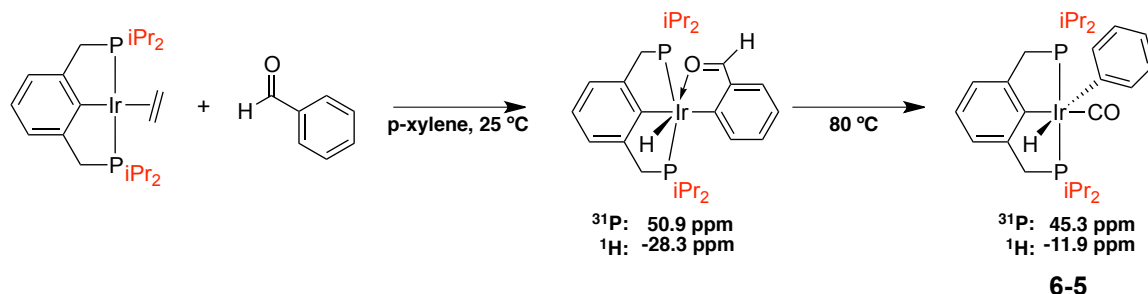
**Figure 6.1.**  $^{31}\text{P}$  (bottom) and  $^1\text{H}$  (top) NMR spectra of reaction of benzene and  $(^i\text{Pr}^4\text{PCP})\text{Ir}(\text{CO})$  in presence of buffer mixture at 125 °C after 96 hours.



If benzene did truly add to the  $(^i\text{Pr}^4\text{PCP})\text{Ir}(\text{CO})$  to form a small amount of products at elevated temperature as suggested by NMR spectroscopy, then acid-catalyzed elimination of benzene from  $(^i\text{Pr}^4\text{PCP})\text{Ir}(\text{CO})(\text{Ph})(\text{H})$  should be thermodynamically favorable.  $(^i\text{Pr}^4\text{PCP})\text{Ir}(\text{CO})(\text{Ph})(\text{H})$  (**6-5**) can be independently prepared by addition of benzaldehyde to  $(^i\text{Pr}^4\text{PCP})\text{Ir}(\text{ethylene})$  at 80 °C to give the *trans* phenyl hydride carbonyl as the major product (74 % yield), along with a small amount aryl hydride (17 % yield),

likely stabilized by dative Ir-O(=C) bonding (**scheme 6.3**). Of note, the *trans* phenyl hydride product **6-5** bears a hydride signal at -11.9 ppm, which matches one of the small hydride signals that results from the addition reaction. Subjecting this mixture to buffer solution and heating to 125 °C for 60 hours results in significant loss of benzene to afford the four-coordinate complex and some unknown byproducts, but even after 60 hours at 125 °C some six-coordinate product remains, suggesting that the forward reaction may indeed occur at elevated temperature to give small equilibrium amount of six-coordinate product.

**Scheme 6.3.** Synthesis of *trans*-(<sup>i</sup>Pr<sup>4</sup>PCP)Ir(CO)(Ph)(H).



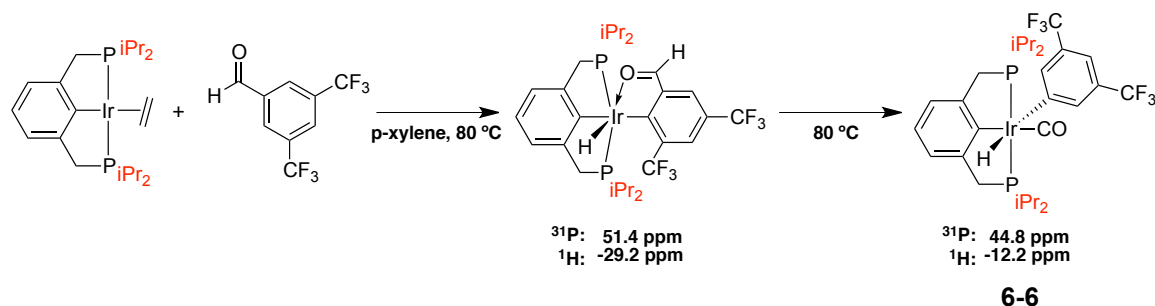
Encouraged by the results of acid-catalyzed benzene elimination from (<sup>i</sup>Pr<sup>4</sup>PCP)Ir(CO)(H)(C<sub>6</sub>H<sub>5</sub>), we postulated that a very electron-withdrawing arene could potentially form a more stable, readily observable product. Our first substrate, pentafluorobenzene, did not appear to form any significant product; however, to our surprise, we found that 1,3-bis(trifluoromethyl)benzene reacted rapidly at room-temperature to give a dark emerald green solution within 60 seconds of mixing. The product of this reaction appeared as a doublet in <sup>31</sup>P nmr at 51.5 ppm (*J* = 5.3 Hz) and as a hydride triplet at -19.3 ppm (*J*<sub>PH</sub> = 11.9 Hz) in the <sup>1</sup>H nmr. However, this relatively

high upfield shift was inconsistent with the typical six-coordinate (pincer)Ir(CO)(R)(H) complexes we have earlier reported, which normally present between -9 to -13 ppm. Curiously, both 1,4-bis(trifluoromethyl)benzene and trifluoromethylbenzene failed to undergo any type of reaction with (<sup>i</sup>Pr<sup>4</sup>PCP)Ir(CO). In the absence of buffer, no reaction between (<sup>i</sup>Pr<sup>4</sup>PCP)Ir(CO) and 1,3-bis(trifluoromethyl)benzene is observed, even at elevated temperature or after several weeks of reaction time.

The *trans*-(<sup>i</sup>Pr<sup>4</sup>PCP)Ir(CO)(H)(C<sub>8</sub>H<sub>3</sub>F<sub>6</sub>) (**6-6**) product was independently synthesized via addition of 3,5-bis(trifluoromethyl)benzaldehyde to (<sup>i</sup>Pr<sup>4</sup>PCP)Ir(ethylene), which, like the independently-synthesized phenyl hydride product (*vide supra*), gave two major products after heating for 6 hours at 80 °C (**scheme 6.4**). The minor product presents as a doublet in <sup>31</sup>P nmr at 51.4 ppm and has a high upfield hydride signal in <sup>1</sup>H nmr at -29.2 ppm (t, J = 14.0 Hz), consistent with a five-coordinate aryl hydride species where the hydride is *trans* to a coordination site that is datively occupied by the oxygen atom from the aldehyde moiety. The major product presents as a singlet in <sup>31</sup>P nmr at 44.8 ppm and has a hydride signal at -12.2 ppm (t, J<sub>PH</sub> = 14.2 Hz), which is expected for *trans*-(PCP)Ir(CO)(R)(H) complexes. This is notably different from the chemical shift that results from acid-catalyzed addition of 1,3-bis(trifluoromethyl)benzene, suggesting that that product is not the expected aryl hydride carbonyl. Treatment of the independently synthesized (<sup>i</sup>Pr<sup>4</sup>PCP)Ir(CO)(H)(C<sub>8</sub>H<sub>3</sub>F<sub>6</sub>) product with buffer at 125 °C, interestingly, did not result in loss of 1,3-bis(trifluoromethyl)benzene, but instead appears to undergo decomposition to multiple products, one of which is possibly the observed addition product based on signals in <sup>31</sup>P nmr and an upfield hydride signal near -19 ppm. Absent a crystal structure, we cannot at this point conclude that the addition product

arises from C-H oxidative addition of 1,3-bis(trifluoromethyl)benzene (and not some impurity), but can say with certainty that the transformation is acid-catalyzed and occurs only for the less sterically hindered *iso*-propyl-substituted analogue.

**Scheme 6.4.** Synthesis of *trans*-(<sup>i</sup>Pr<sup>4</sup>PCP)Ir(CO)(H)(C<sub>6</sub>H<sub>3</sub>F<sub>3</sub>).



### 6.2.3 Theoretical insights into factors favoring oxidative addition to square planar Ir(I) carbonyl complexes

At this point, it is clear that simply reducing the sterics of the (pincer)Ir(CO) complex alone is not sufficient to overcome the unfavorable thermodynamics of forming the six-coordinate product. To further our understanding of the factors influencing the favorability of C-H oxidative addition, we undertook a variety of DFT calculations to assess the role that sterics and electronics may play in improving the thermodynamics of addition. As Dave Wang had previously found that strong  $\sigma$ -donors promote *trans* oxidative addition to four-coordinate Ir(I) complexes, we first looked at analogous model complexes of the structure (X)(PH<sub>3</sub>)<sub>2</sub>Ir(CO) (X = CH<sub>3</sub>, SiH<sub>3</sub>, or GeH<sub>3</sub>—increasingly strong  $\sigma$ -donors) and their six-coordinate *trans* methyl hydride products. As shown in **table 6.2**, relative to carbon, stronger  $\sigma$ -donors like silicon and germanium do appear to slightly favor the thermodynamics of methane addition in these model complexes. The

difference between silicon and germanium donors is rather small (*ca.* 1 kcal/mol), but the differences between carbon and silicon or germanium are fairly significant (*ca.* 3-4 kcal/mol). Encouraged by these model studies, we next undertook a more thorough examination of known (pincer)Ir structures bearing this variety of  $\sigma$ -donor ligands.

**Table 6.2.** Calculated energies for methane oxidative addition to *trans*-(X)(PH<sub>3</sub>)<sub>2</sub>Ir(CO) (X = CH<sub>3</sub>, SiH<sub>3</sub>, or GeH<sub>3</sub>).

$  \begin{array}{c} \text{PH}_3 \\   \\ \text{X}-\text{Ir}-\text{CO} \\   \\ \text{PH}_3 \end{array} + \text{CH}_4 \longrightarrow \begin{array}{c} \text{PH}_3 \\   \\ \text{X}-\text{Ir}-\text{CO} \\   \quad \diagup \\ \text{H} \quad \text{CH}_3 \\   \\ \text{PH}_3 \end{array}  $			
		<i>kcal/mol</i>	
X	$\Delta E$	$\Delta H$	$\Delta G$
-CH <sub>3</sub>	11.5	10.4	22.8
-SiH <sub>3</sub>	6.9	5.4	19.5
-GeH <sub>3</sub>	7.6	6.8	18.4

Both Si and Ge pincer complexes of iridium (*i.e.* (PSiP)Ir and (PGeP)Ir) have been reported in the literature, though silyl pincer-iridium complexes are more common and are therefore the focus of these studies.<sup>11-13</sup> Both Turculet and Sola have reported systems utilizing different (PSiP)Ir complexes (**figure 6.2** (a) and (b), respectively). The Turculet pincer-iridium complexes have been reported with cyclohexyl substituents on the phosphine, capable of activating arene C-H bonds<sup>11,12</sup>, while Sola pincer-iridium complexes have been reported with phenyl substituents on the phosphine<sup>13</sup>; based upon the reported syntheses of these complexes, access to the hydrido chloride species with any traditional R groups (e.g. *tert*-butyl or *iso*-propyl) encountered in (pincer)Ir complexes should be fairly straightforward. With the hydrido chloride in hand, formation

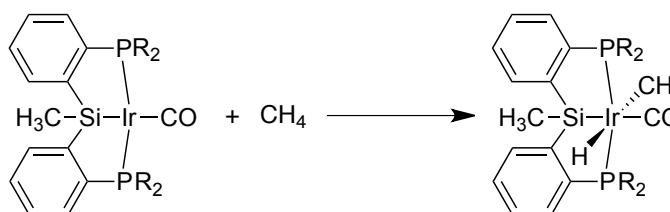
(a) C[Si](C1=CC=CC=C1)P(C2=CC=CC=C2)C3=CC=CC=C3Ir

(b) C[Si](C1=CC=CC=C1)P(C2=CC=CC=C2)C3=CC=CC=C3Ir

To explore the relative thermodynamics of methane addition to (PSiP)Ir(CO) complexes, we performed DFT calculations on a variety of (PSiP)-ligated iridium carbonyl complexes and their six-coordinate *trans* methyl hydride products. The “Turculet-type” (<sup>R4</sup>PSiP)Ir(CO) complexes were calculated with R groups of varying sizes (*t*-butyl, *i*-propyl, and methyl), and as would be expected, the thermodynamics of methane addition becomes more favorable as the size of R decreases (or, alternatively, as the sterics about the metal center decrease) (**table 6.3**). The difference is most prominent when going from *t*-butyl groups to *i*-propyl groups, whereupon addition of methane becomes roughly 15 kcal/mol more favorable; the difference between *i*-propyl and methyl substituents is essentially negligible in this case. Compared with the analogous (<sup>R4</sup>PCP)Ir(CO) complexes calculated earlier (**table 6.1**, *vide supra*), these Turculet-type (<sup>R4</sup>PSiP)Ir(CO) complexes do, in fact, appear to form more thermodynamically favored

adducts. For instance, the difference between (<sup>iPr4</sup>PCP)Ir(CO) and (<sup>iPr4</sup>PSiP)Ir(CO) regarding the change in Gibbs free energy upon *trans* oxidative addition of methane is *ca.* 8 kcal/mol, suggesting that a significant increase in favorability occurs when utilizing the stronger  $\sigma$ -donating silyl ligand. The calculated structures of (<sup>R4</sup>PSiP)Ir(CO) complexes are particularly interesting, as they feature distorted Si-Ir-C(O) and Ir-C-O bond angles, 162.7° and 171.6°, respectively. As Hoffmann has earlier reported, it is perhaps this deviation from square planarity that favors the thermodynamics of oxidative addition.

**Table 6.3.** Calculated energies for methane addition to Turculet-ligand (<sup>R4</sup>PSiP)Ir(CO).



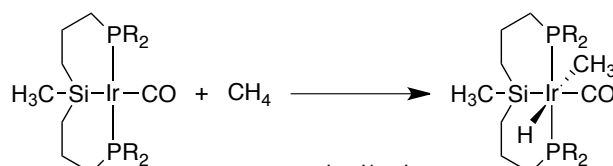
R	$\Delta E$	$\Delta H$ kcal/mol	$\Delta G$
t-butyl	14.2	12.6	26.3
i-propyl	1.5	0.6	11.1
methyl	0.2	-0.8	10.8

Calculations on “Sola-type” (<sup>R4</sup>PSiP)Ir(CO) complexes were also performed (**table 6.4**). These complexes exhibit similar trends as the Turculet-type complexes (more favorable thermodynamics compared to their respective (<sup>R4</sup>PCP)Ir(CO) analogues and increasing favorability with decreasing sterics), and have quite similar relative thermodynamics compared to their Turculet-pincer analogues. The largest difference in Gibbs free energy occurs between the Sola- and Turculet-type *iso*-propyl pincer complexes, where addition of methane to Turculet-(<sup>iPr4</sup>PSiP)Ir(CO) is about 5 kcal/mol more favorable than for the Sola-analogue. This difference may be engendered in the



geometry of the Sola-(<sup>i</sup>Pr<sup>4</sup>PSiP)Ir(CO) complex, which, unlike the Turculet analogue, does not exhibit a significant distortion from square planar geometry.

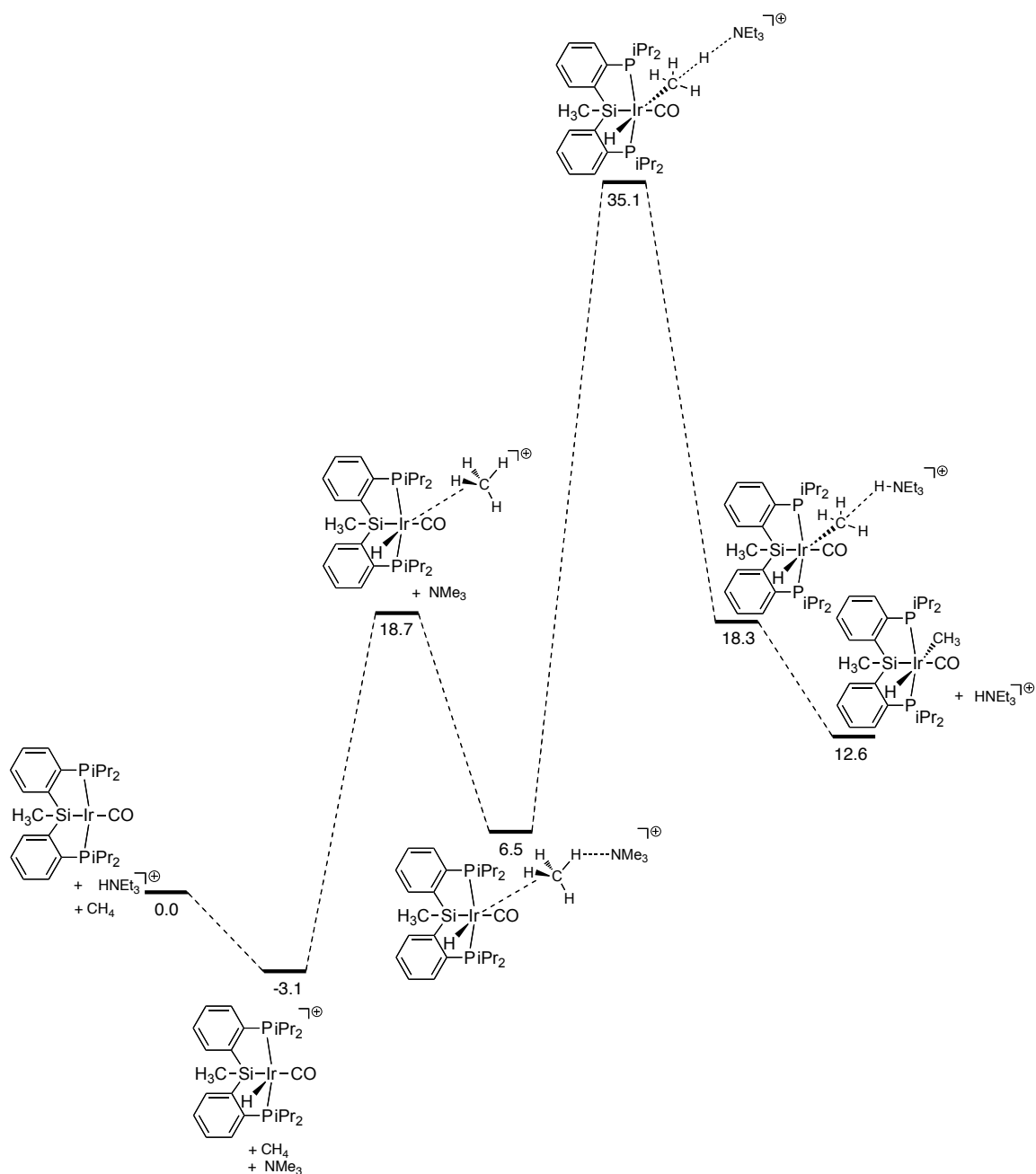
**Table 6.4.** Calculated energies for methane addition to Sola-ligand (<sup>R</sup>PSiP)Ir(CO).



R	ΔE	ΔH	ΔG
t-butyl	13.8	12.3	26.5
i-propyl	2.7	1.0	16.0
methyl	-0.5	-1.5	11.3

Based on these DFT calculations, the thermodynamics of methane addition generally seems most favorable for Turculet-type complexes (which have been reported to be catalytically active for C-H activation, unlike the Sola system), particularly when the R substituents on the phosphines are either methyl or *iso*-propyl groups. Since (<sup>i</sup>Pr<sup>4</sup>PSiP)Ir(CO) is likely easier to prepare experimentally compared to (<sup>Me</sup>PSiP)Ir(CO), a detailed examination of the potential mechanism for acid-catalyzed addition of methane to Turculet-(<sup>i</sup>Pr<sup>4</sup>PSiP)Ir(CO) was undertaken. As shown in **scheme 6.5**, if a mechanism analogous to that postulated for PhCCH addition to (<sup>t</sup>Bu<sup>4</sup>PCP)Ir(CO) is at play, formation of a methane  $\sigma$ -adduct with the catalytically-active cationic intermediate must occur. This intermediate is uphill by about 19 kcal/mol relative to free (<sup>i</sup>Pr<sup>4</sup>PSiP)Ir(CO), methane, and HNMe<sub>3</sub><sup>+</sup>, but is significantly stabilized by coordination of Me<sub>3</sub>N to the resulting adduct ( $\Delta G = 6.5$  kcal/mol). The methane adduct has geometric features consistent with an agostic complex, most notably evinced by the M-H distance of 2.2 Å and the M-H-C bond angle of 123°. <sup>14</sup> The rate-determining step is the transition state

**Scheme 6.5.** DFT-calculated pathway for the acid-catalyzed oxidative addition of methane to Turculet-ligand ( $i\text{Pr}^4\text{PSiP}$ )Ir(CO).



involving proton transfer from coordinated methane to base, having an activation energy of *ca.* 35 kcal/mol relative to free methane, acid, and ( $i\text{Pr}^4\text{PSiP}$ )Ir(CO); this is significantly lower than the calculated activation energy for the same step utilizing the

$(^t\text{Bu}^4\text{PCP})\text{Ir}(\text{CO})$  complex (*ca.* 51 kcal/mol, refer to the previous chapter), but more than double that of the activation energy for acid-catalyzed addition of PhCCH to  $(^t\text{Bu}^4\text{PCP})\text{Ir}(\text{CO})$  (*ca.* 16 kcal/mol), which might be expected as methane is significantly less prone to electrophilic addition compared to the alkynes.

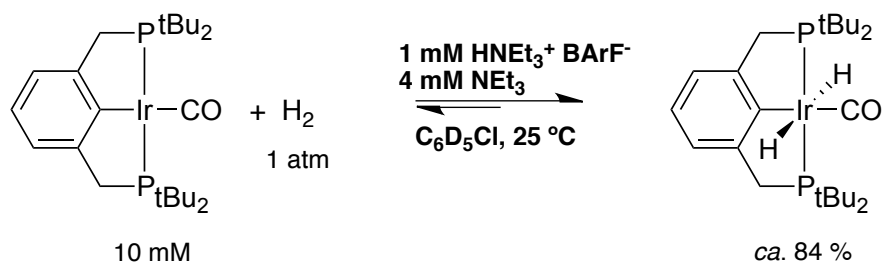
#### 6.2.4 Acid-catalyzed addition of $\text{H}_2$ to $(^t\text{Bu}^4\text{PCP})\text{Ir}(\text{CO})$

Although we are most interested in the oxidative addition of C-H bonds to (pincer)Ir(CO) complexes, catalyzing the addition of other bonds to these complexes is also of interest. As mentioned earlier, the addition of  $\text{H}_2$  to square planar carbonyl complexes is an iconic transformation, and yet  $\text{H}_2$  has not been reported to add to  $(^t\text{Bu}^4\text{PCP})\text{Ir}(\text{CO})$ .<sup>15</sup> Milstein has found that  $\text{H}_2$  readily adds to  $(^i\text{Pr}^4\text{PCP})\text{Ir}(\text{CO})$  to give a mixture of isomers (*cis* and *trans* dihydrides)<sup>3</sup>. More interestingly, Dave Wang had observed facile addition of  $\text{H}_2$  to the  $(^t\text{Bu}^3\text{MePCP})\text{Ir}(\text{CO})$  complex at room temperature, giving a complex mixture of dihydride stereoisomers.<sup>4</sup> We were intrigued by the apparent lack of reactivity of  $(^t\text{Bu}^4\text{PCP})\text{Ir}(\text{CO})$  toward  $\text{H}_2$  oxidative addition, and speculated that addition of  $\text{H}_2$  might be catalyzed by acid.

To this end,  $(^t\text{Bu}^4\text{PCP})\text{Ir}(\text{CO})$  (10 mM) in a  $\text{C}_6\text{D}_5\text{Cl}$  solution containing buffer (1 mM  $\text{HNEt}_3^+ \text{BAr}^{\text{F}-}$  and 4 mM  $\text{Et}_3\text{N}$ ) was subjected to 1 atmosphere of  $\text{H}_2$  gas (**scheme 6.6**). Upon thorough mixing for 5 minutes,  $^{31}\text{P}$  and  $^1\text{H}$  nmr spectroscopy revealed the presence of a single major new species (**6-7**) in solution in *ca.* 84 % yield, whose concentration was not observed to change over the ensuing 24 hour period. **6-7** presented as a singlet in  $^{31}\text{P}$  nmr at 75.7 ppm. In  $^1\text{H}$  nmr, the product displayed a hydride signal at -9.56 ppm (t,  $J_{\text{PH}} = 13.6$  Hz, 2H). These chemical shifts are fully consistent with

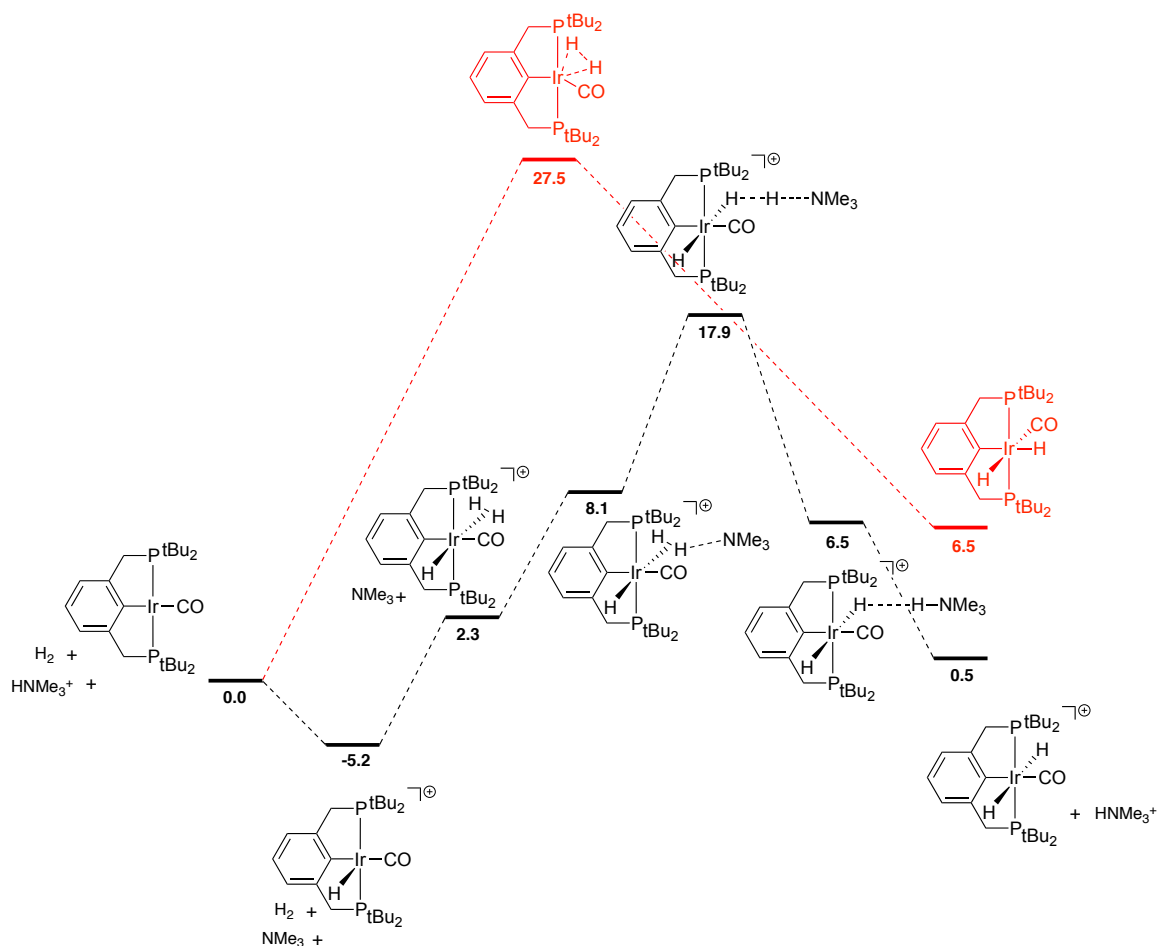
analogous signals reported by Dave Wang for the *trans*-dihydride product, (<sup>t</sup>Bu<sup>3</sup>MePCP)Ir(CO)(H)<sub>2</sub> (cf. <sup>31</sup>P nmr : 76.4 ppm, <sup>1</sup>H nmr: -9.58 ppm); thus we can conclude that the formation of *trans*-(<sup>t</sup>Bu<sup>4</sup>PCP)Ir(CO)(H)<sub>2</sub> (**6-7**) results from the acid-catalyzed oxidative addition of H<sub>2</sub>. That stable six-coordinate dihydride product forms in high yield suggests one of two scenarios: that the barrier to addition (to give *cis* or *trans* dihydride) is otherwise too high absent a catalyst or possibly that kinetic product formation (that is, formation of the *cis*-dihydride) is feasible but thermodynamically unfavorable and eliminates much more quickly than it isomerizes to the (presumably more thermodynamically stable) *trans*-dihydride.

**Scheme 6.6.** Acid-catalyzed addition of H<sub>2</sub> to (<sup>t</sup>Bu<sup>4</sup>PCP)Ir(CO).



To gain greater insight in the acid-catalyzed addition of H<sub>2</sub> as compared to the direct oxidative addition of H<sub>2</sub>, DFT calculations were performed on both the acid-catalyzed process and the direct *cis*-dihydride oxidative addition process (**scheme 6.7**). The activation barrier for direct H<sub>2</sub> oxidative addition to give the *cis*-dihydride is roughly 27.5 kcal/mol. Meanwhile, the activation barrier for the acid-catalyzed route is only 17.9 kcal/mol. Further, the *cis*-dihydride product is uphill by roughly 6.5 kcal/mol (relative to free H<sub>2</sub> and (<sup>t</sup>Bu<sup>4</sup>PCP)Ir(CO)), while the *trans*-dihydride product is only about 0.5 kcal/mol

**Scheme 6.7.** DFT-calculated pathways for the direct and acid-catalyzed oxidative addition of dihydrogen to  $(^t\text{Bu}^4\text{PCP})\text{Ir}(\text{CO})$ .



uphill (relative to free  $\text{H}_2$  and  $(^t\text{Bu}^4\text{PCP})\text{Ir}(\text{CO})$ ). The barrier to  $\text{H}_2$  reductive elimination from the *cis*-dihydride is ca. 21 kcal/mol. This implies that higher temperature is required for the non-catalyzed *cis* oxidative addition process to occur (to overcome the higher activation barrier), but at the same time, the reductive elimination of  $\text{H}_2$  from the resulting six-coordinate *cis*-dihydride adduct is both kinetically and thermodynamically favored (presumably even more so at the higher reaction temperature); consequently the observation of *cis*- $(^t\text{Bu}^4\text{PCP})\text{Ir}(\text{CO})(\text{H})_2$  is not likely (though its transient formation is

quite possible). The essentially thermoneutral thermodynamics of *trans*-dihydride product formation, coupled with the lower acid-catalyzed kinetic barrier, agrees well with experimental observation of *trans*-(<sup>t</sup>Bu<sup>4</sup>PCP)Ir(CO)(H)<sub>2</sub> (**6-7**) in equilibrium with free (<sup>t</sup>Bu<sup>4</sup>PCP)Ir(CO) under a hydrogen atmosphere.

### 6.3 Summary

The acid-catalyzed addition of C-H bonds to square planar carbonyl complexes represents an important advancement in the field of C-H activation chemistry, opening up the possibility of performing C-H bond activation catalysis under CO atmosphere leading to potential direct carbonylation of simple hydrocarbons. While we have discovered a few examples of this phenomenon, its generality needs to be further expanded. We have found that unfavorable thermodynamics of addition is a key impediment to achieving high reactivity, but that simply reducing the sterics of traditional (<sup>R</sup>PCP)Ir(CO) complexes is not sufficient enough to overcome these poor thermodynamics. DFT calculations support a strategy of favoring the addition to pincer complexes bearing stronger  $\sigma$ -donating ligands; the thermodynamics of the oxidative addition of methane to (<sup>i</sup>Pr<sup>4</sup>PSiP)Ir(CO), for example, is calculated to be roughly 20 kcal/mol more favorable than addition to (<sup>t</sup>Bu<sup>4</sup>PCP)Ir(CO).

### 6.4 Experimental

**General Considerations.** All reactions were conducted under an argon atmosphere in a drybox or using standard Schlenk techniques. 1,3-bis(trifluoromethyl)benzene, pentafluorobenzene, 3,5-bis(trifluoromethyl)benzaldehyde, and benzaldehyde were all

purchased from Sigma-Aldrich and vacuum-transferred to yield colorless liquids prior to bringing into the glovebox. Trifluoromethane and fluoromethane gases were purchased from Synquest Laboratories and used without further purification.  $\text{C}_6\text{D}_5\text{Cl}$  was purchased from Cambridge Isotope Labs, dried over  $\text{P}_2\text{O}_5$  and vacuum-transferred. Triethylammonium  $\text{B}(\text{C}_6\text{F}_5)_4^-$  was prepared as described in chapter 4.  $(^{\text{iPr}4}\text{PCP})\text{Ir}(\text{C}_2\text{H}_4)^{16}$  and  $(^{\text{iPr}4}\text{PCP})\text{Ir}(\text{CO})^3$  were prepared as previously described. All other reagents were purchased from commercial suppliers and used without further purification, other than freeze-pump-thaw degassing. NMR spectra were acquired on 400 or 500 MHz Varian VNMRs nmr spectrometers.  $^1\text{H}$  spectra are referenced to residual solvent peaks, while  $^{31}\text{P}$  spectra are referenced to an external  $\text{PMe}_3$  standard.

**Synthesis of  $(^{\text{tBu}4}\text{PCP})\text{Ir}(\text{CO})(\text{H})(\text{NCCH}_3)$  (6-2).** A solution consisting of 10 mM  $(^{\text{tBu}4}\text{PCP})\text{Ir}(\text{CO})$ , 1 mM  $\text{HNEt}_3^+ \text{BAR}^{\text{F}-}$ , 4 mM  $\text{Et}_3\text{N}$ , and 500 mM acetonitrile was prepared and transferred to a J. Young nmr tube. The solution was monitored periodically over a six-hour period. A new product with hydride signal appeared to have formed fairly rapidly and its concentration did not change over time. When the reaction was repeated with 10 mM  $\text{HNEt}_3^+ \text{BAR}^{\text{F}-}$  (all other conditions/concentrations remained the same) the concentration of the new product increased, indicating (non-catalytic) reaction with the acid.  $^{31}\text{P}\{^1\text{H}\}$  NMR ( $\text{C}_6\text{D}_5\text{Cl}$ , 200 MHz):  $\delta$  66.7 ppm (s).  $^1\text{H}$  NMR ( $\text{C}_6\text{D}_5\text{Cl}$ , 400 MHz):  $\delta$  7.17 (d,  $J = 7.5$  Hz, 2H), residual solvent signal overlaps with the other aryl proton signal, 3.32 (dvt,  $J = 16.8$  Hz,  $J = 3.4$  Hz, 2H), 3.21 (dvt,  $J = 16.8$  Hz,  $J = 4.1$  Hz, 2H), 1.80 (s, 3H, coordinated  $\text{CH}_3\text{CN}$ ), 1.09 (vt,  $J = 7.1$  Hz, 18H), 0.93 (vt,  $J = 7.1$  Hz, 18H), -19.1 (t,  $J = 12.6$  Hz, 1H).

**Synthesis of (<sup>i</sup>Pr<sup>4</sup>PCP)Ir(CO)(H)(CCPh) (6-4).** A solution consisting of 10 mM (<sup>i</sup>Pr<sup>4</sup>PCP)Ir(CO), 1 mM HNEt<sub>3</sub><sup>+</sup> BAr<sup>F-</sup>, 4 mM Et<sub>3</sub>N, and 300 mM phenylacetylene was prepared in a J. Young nmr tube. Upon addition of PhCCH, the solution rapidly turned a pale yellow color. <sup>31</sup>P and <sup>1</sup>H nmr indicated two new products, one in 65 % yield and the other in 35 % yield. The major product had spectroscopic features consistent with the six-coordinate *trans* phenylacetylide hydride complex, while the minor product lacked a hydride signal. *Major product* (<sup>i</sup>Pr<sup>4</sup>PCP)Ir(CO)(H)(CCPh): <sup>31</sup>P{<sup>1</sup>H} NMR: δ 49.6 ppm (s). <sup>1</sup>H NMR: *phenylacetylene signals cover aryl proton signals*, δ 3.59 (dvt, J = 16.0 Hz, J = 4.3 Hz, 2H), 3.18 (dvt, J = 16.1 Hz, J = 4.1 Hz, 2H), 2.65 (sept, J = 3.6 Hz, 2H), 1.84 (sept, J = 3.6 Hz, 2H), 1.28 (ddd, J = 19.3 Hz, J = 13.8 Hz, J = 7.6 Hz, 12H), 0.93 (q, J = 6.9 Hz, 12H), -11.9 (t, J = 13.5 Hz, 1H). *Minor product*: <sup>31</sup>P{<sup>1</sup>H} NMR: δ 35.5 ppm (s). <sup>1</sup>H NMR: *phenylacetylene signals cover aryl proton signals*, δ 3.72 (dvt, J = 15.4 Hz, J = 4.4 Hz, 2H), 3.38 (dvt, J = 15.4 Hz, J = 4.4 Hz, 2H), 2.84 (m), 2.51 (m), 1.04 (leaning dd, J = 15.7 Hz, J = 7.2 Hz, 12H), 0.84 (leaning dd, J = 14.4 Hz, J = 7.2 Hz, 12H).

**Synthesis of (<sup>i</sup>Pr<sup>4</sup>PCP)Ir(CO)(H)(C<sub>6</sub>H<sub>5</sub>) (6-5).** A solution consisting of 10 mM (<sup>i</sup>Pr<sup>4</sup>PCP)Ir(C<sub>2</sub>H<sub>4</sub>) and 20 mM benzaldehyde in p-xylene was heated to 80 °C in a J. Young nmr for six hours. After six hours, an equilibrium mixture of (<sup>i</sup>Pr<sup>4</sup>PCP)Ir(CO)(H)(Ph) (74 %), (<sup>i</sup>Pr<sup>4</sup>PCP)Ir(H)(C<sub>6</sub>H<sub>4</sub>CHO) (17 %) (<sup>31</sup>P: 50.9 ppm, <sup>1</sup>H: -28.3 ppm, t, J = 14.3 Hz), and an unknown byproduct (9 %) is observed (<sup>31</sup>P: 38.1 ppm). This mixture was subjected (without purification over than removal of solvent *in vacuo*) to buffer solution to observe acid-catalyzed benzene reductive elimination.



$(^{i\text{Pr}}_4\text{PCP})\text{Ir}(\text{CO})(\text{H})(\text{Ph})$ :  $^{31}\text{P}\{^1\text{H}\}$  NMR:  $\delta$  45.3 ppm (s).  $^1\text{H}$  NMR: *benzaldehyde and residual protio solvent signals obscure aryl proton signals*,  $\delta$  3.31 (dvt,  $J = 16.4$  Hz,  $J = 4.6$  Hz, 2H), 3.18 (dvt,  $J = 16.5$  Hz,  $J = 4.3$  Hz, 2H), 2.0 (m, 2H), 1.90 (m, 2H), 1.24 (dd,  $J = 15.9$  Hz,  $J = 6.9$  Hz, 6H), 1.17 (dd,  $J = 15.5$  Hz,  $J = 7.33$  Hz, 6H), 1.01 (dd,  $J = 14.8$  Hz,  $J = 7.0$  Hz, 6H), 0.92 (dd,  $J = 13.7$  Hz,  $J = 7.1$  Hz, 6H), -11.9 (t,  $J = 14.2$  Hz, 1H).

**Synthesis of  $(^{i\text{Pr}}_4\text{PCP})\text{Ir}(\text{CO})(\text{H})(\text{C}_8\text{H}_3\text{F}_6)$  (6-6).** A solution consisting of 10 mM  $(^{i\text{Pr}}_4\text{PCP})\text{Ir}(\text{C}_2\text{H}_4)$  and 15 mM 3,5-bis(trifluoromethyl)benzaldehyde in p-xylene was heated to 80 °C in a J. Young nmr for six hours. After six hours, an equilibrium mixture of  $(^{i\text{Pr}}_4\text{PCP})\text{Ir}(\text{CO})(\text{H})(\text{C}_8\text{H}_3\text{F}_6)$  (74 %),  $(^{i\text{Pr}}_4\text{PCP})\text{Ir}(\text{H})(\text{C}_8\text{H}_3\text{F}_6\text{CHO})$  (20 %) ( $^{31}\text{P}$ : 51.4 ppm,  $^1\text{H}$ : -29.2 ppm, t,  $J = 14.0$  Hz), and an unknown byproduct (6 %) is observed ( $^{31}\text{P}$ : 38.7 ppm). This mixture was subjected (without purification over than removal of solvent *in vacuo*) to buffer solution in attempt to observe acid-catalyzed arene reductive elimination.  $(^{i\text{Pr}}_4\text{PCP})\text{Ir}(\text{CO})(\text{H})(\text{C}_8\text{H}_3\text{F}_6)$  (6-6):  $^{31}\text{P}\{^1\text{H}\}$  NMR:  $\delta$  44.8 ppm (s).  $^1\text{H}$  NMR: *benzaldehyde and residual protio solvent signals obscure aryl proton signals*,  $\delta$  3.14 (vt,  $J = 4.4$  Hz, 4H), 1.76 (overlapping m, 4H), 1.14 (dd,  $J = 15.5$  Hz,  $J = 7.6$  Hz, 6H), 1.06 (dd,  $J = 15.8$  Hz,  $J = 7.30$  Hz, 6H), 0.92 (dd,  $J = 14.8$  Hz,  $J = 7.0$  Hz, 6H), 0.82 (dd,  $J = 13.9$  Hz,  $J = 7.1$  Hz, 6H), -12.2 (t,  $J = 14.2$  Hz, 1H).

**Synthesis of *trans*-( $^{\text{tBu}}_4\text{CP})\text{Ir}(\text{CO})(\text{H})_2$  (6-7).** A stock solution containing 10 mM  $(^{\text{tBu}}_4\text{PCP})\text{Ir}(\text{CO})$ , 1 mM  $\text{HNEt}_3^+ \text{BAR}^{\text{F}^-}$ , and 4 mM  $\text{Et}_3\text{N}$  in chlorobenzene- $d_5$  was prepared and 0.5 mL was transferred to a J. Young nmr tube. The sample was freeze-pump-thawed on the high vacuum line prior to addition of 1 atm of  $\text{H}_2$  gas. The sample

was allowed to equilibrate for 60 minutes prior to acquiring NMR data.  $^1\text{H}$  and  $^{31}\text{P}$  NMR spectroscopy indicated formation of a single new product in *ca.* 84 % yield based on  $^{31}\text{P}$  integration.  $^{31}\text{P}\{^1\text{H}\}$  NMR ( $\text{C}_6\text{D}_5\text{Cl}$ , 200 MHz):  $\delta$  74.7 ppm (s).  $^1\text{H}$  NMR ( $\text{C}_6\text{D}_5\text{Cl}$ , 400 MHz):  $\delta$  6.93 – 6.88 (overlapping multiplets, 3H), 3.30 (t,  $J$  = 3.6 Hz, 4H), 1.25 (vt,  $J$  = 6.11 Hz, 36 H), - 9.56 (t,  $J$  = 13.6 Hz, 2H).

**Computational Details.** All calculations were performed by the *Gaussian09* suite of molecular modeling software.<sup>17</sup> DFT calculations employing the M06L functional were used.<sup>18,19</sup> Ir atoms were described by a LANL2TZ basis set augmented by a diffuse d-type function (exponent = 0.07645) (value obtained as one-half times the exponent of the outermost d-type function in the LANL2TZ basis set for Ir).<sup>20</sup> All other atoms (C, H, O, N, P, Si, Ge) were described by 6-311G(d,p) basis sets.<sup>21</sup> Calculations on the complete mechanism of methane addition to ( $^{\text{iPr}}_4\text{PSiP}$ )Ir(CO) and  $\text{H}_2$  addition to ( $^{\text{tBu}}_4\text{PCP}$ )Ir(CO) made use of a conductor-like polarizable continuum model (c-PCM)<sup>22</sup> representing chlorobenzene (the solvent employed for all prior acid-catalyzed reactions) and were conducted at standard temperature and pressure. Calculations concerning the relative thermodynamics of methane addition were performed as routine gas-phase calculations.

## 6.5 Chapter 6 Appendix

### 6.5.1 NMR Spectra

**Figure 6A.1.**  $^1\text{H}$  nmr spectrum of the acid-catalyzed (10 mM) reaction of  $\text{CH}_3\text{CN}$  and  $(^t\text{Bu}^4\text{PCP})\text{Ir}(\text{CO})$  at room-temperature after five hours.

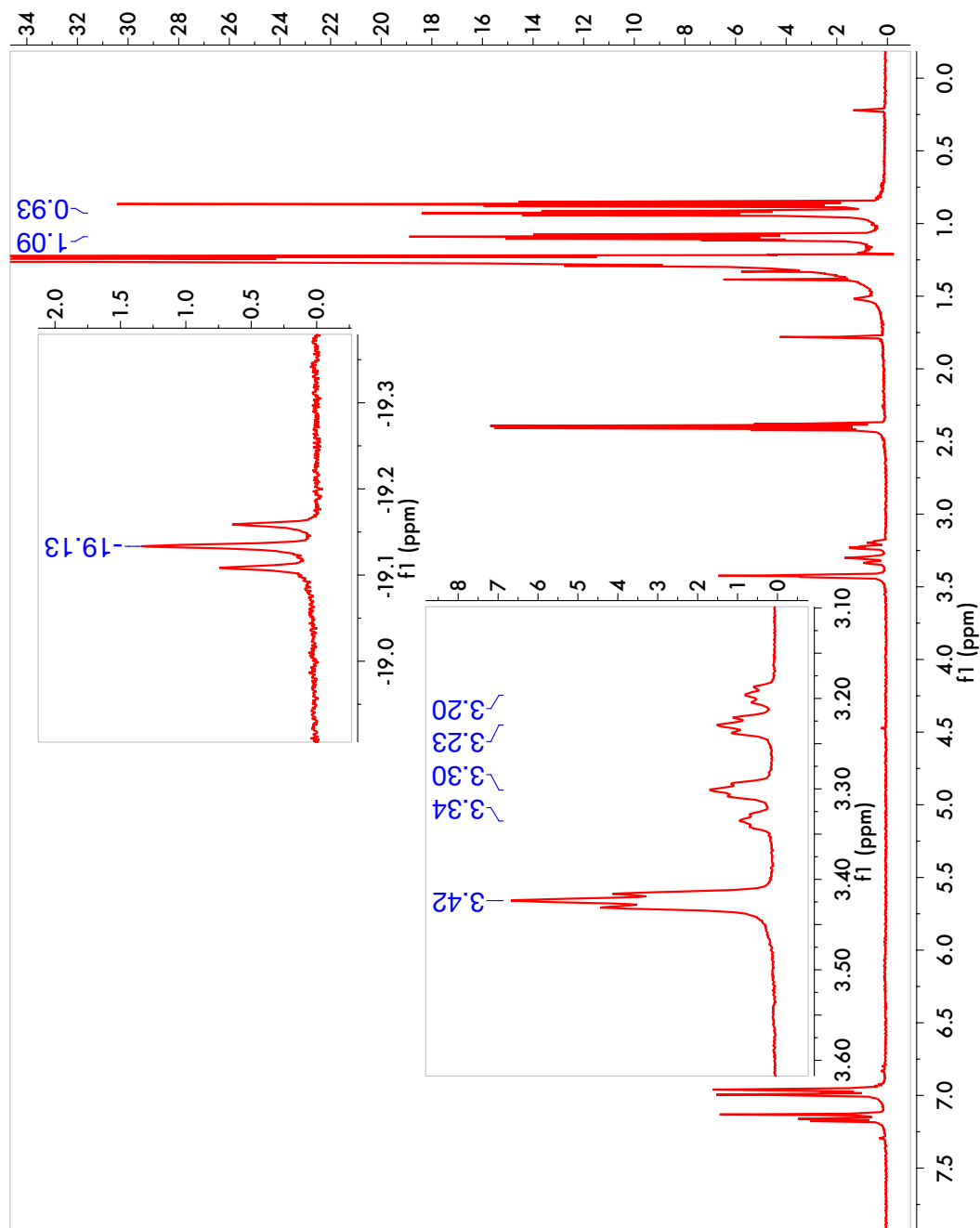


**Figure 6A.2.**  $^{31}\text{P}$  nmr spectrum of the acid-catalyzed (10 mM) reaction of  $\text{CH}_3\text{CN}$  and  $(^{\text{tBu}}_4\text{PCP})\text{Ir}(\text{CO})$  at room-temperature after five hours.

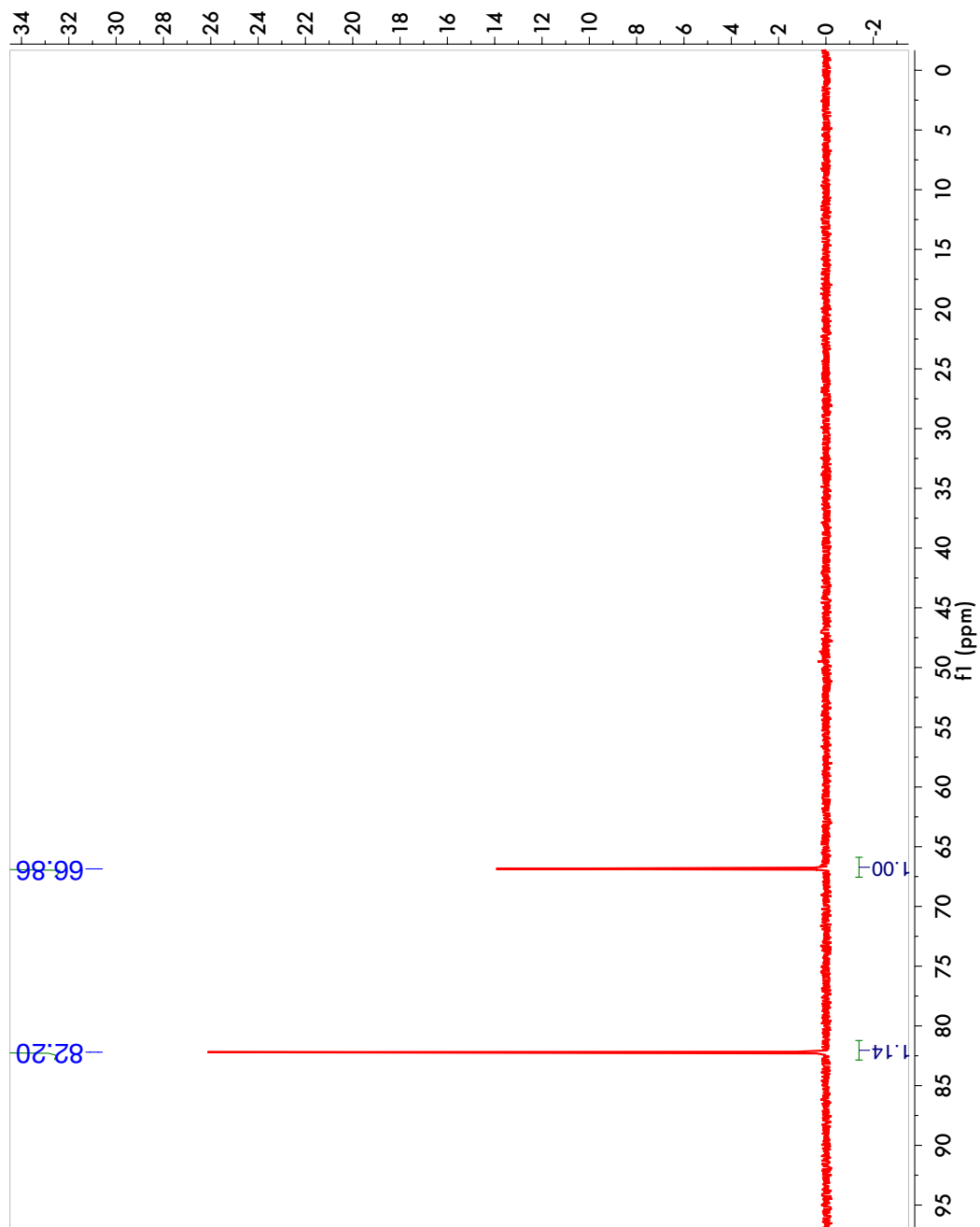


**Figure 6A.3.**  $^1\text{H}$  NMR spectrum of products from acid-catalyzed reaction of  $(^i\text{Pr}_4\text{PCP})\text{Ir}(\text{CO})$  (10 mM) and  $\text{PhCCH}$  (300 mM).

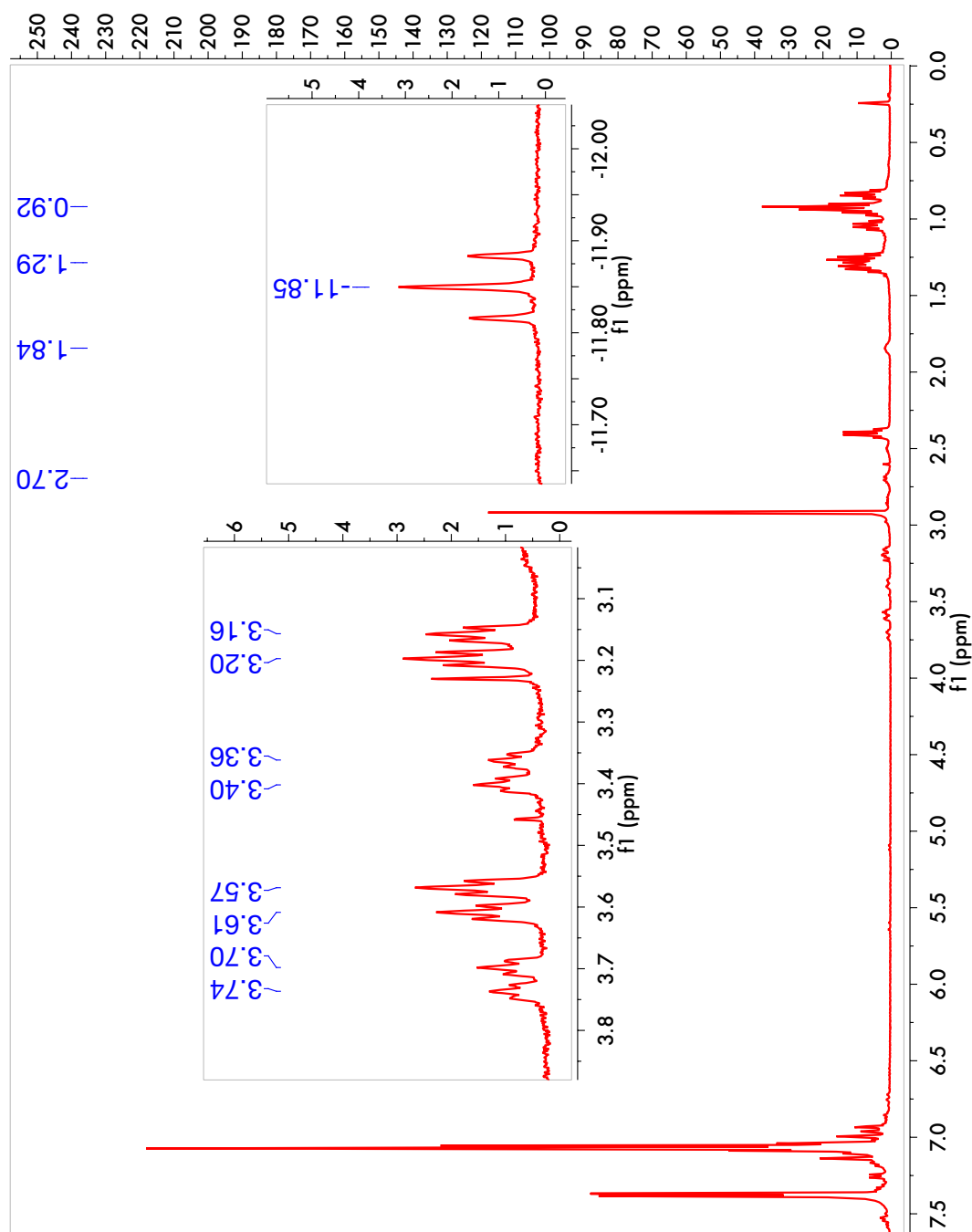


**Figure 6A.4.**  $^{31}\text{P}$  NMR spectrum of products from acid-catalyzed reaction of ( $^{\text{iPr}}_4\text{PCP}$ )Ir(CO) (10 mM) and PhCCH (300 mM).

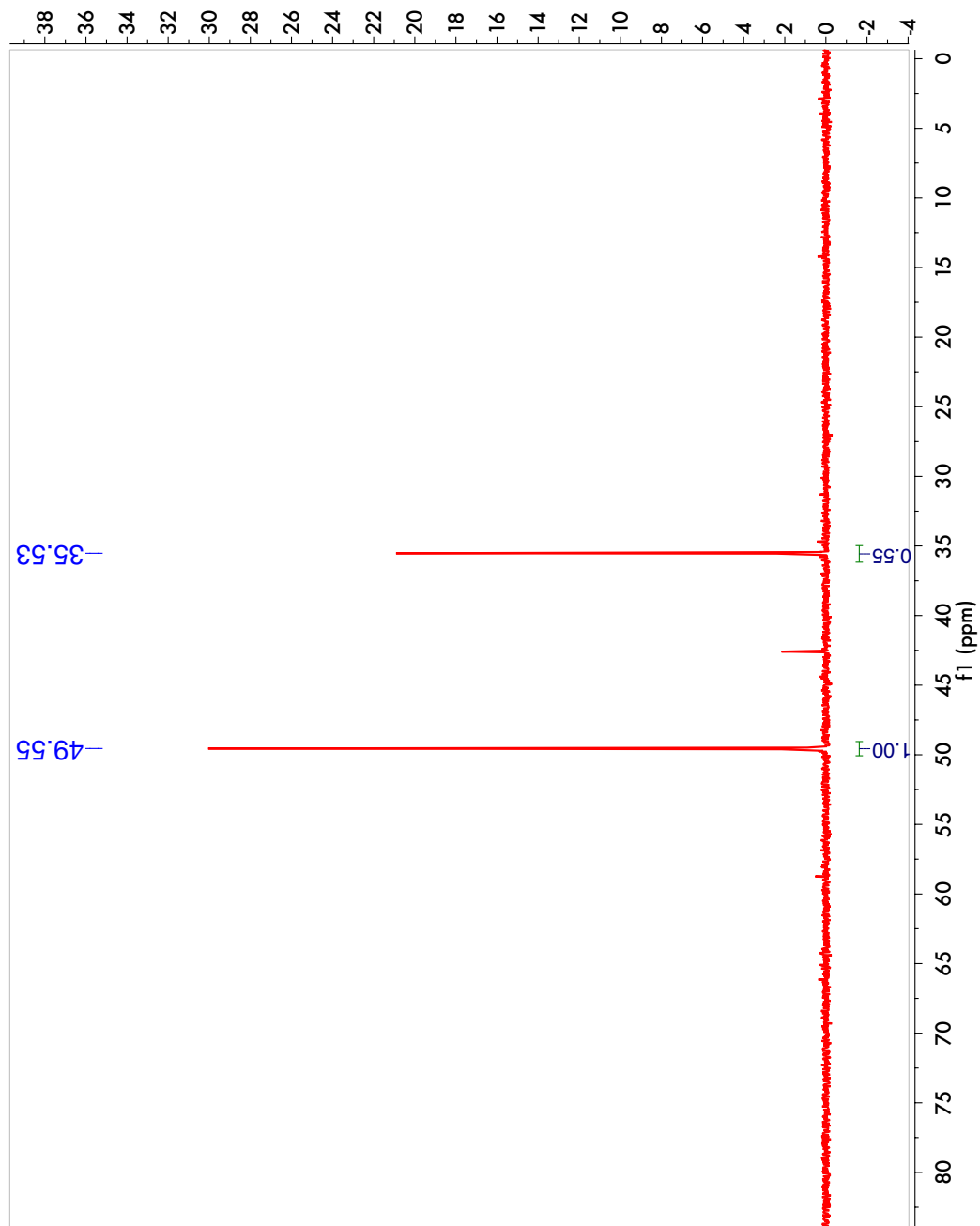


**Figure 6A.5.**  $^1\text{H}$  NMR spectrum of independently synthesized  $(^i\text{Pr}^4\text{PCP})\text{Ir}(\text{CO})(\text{H})(\text{Ph})$ .

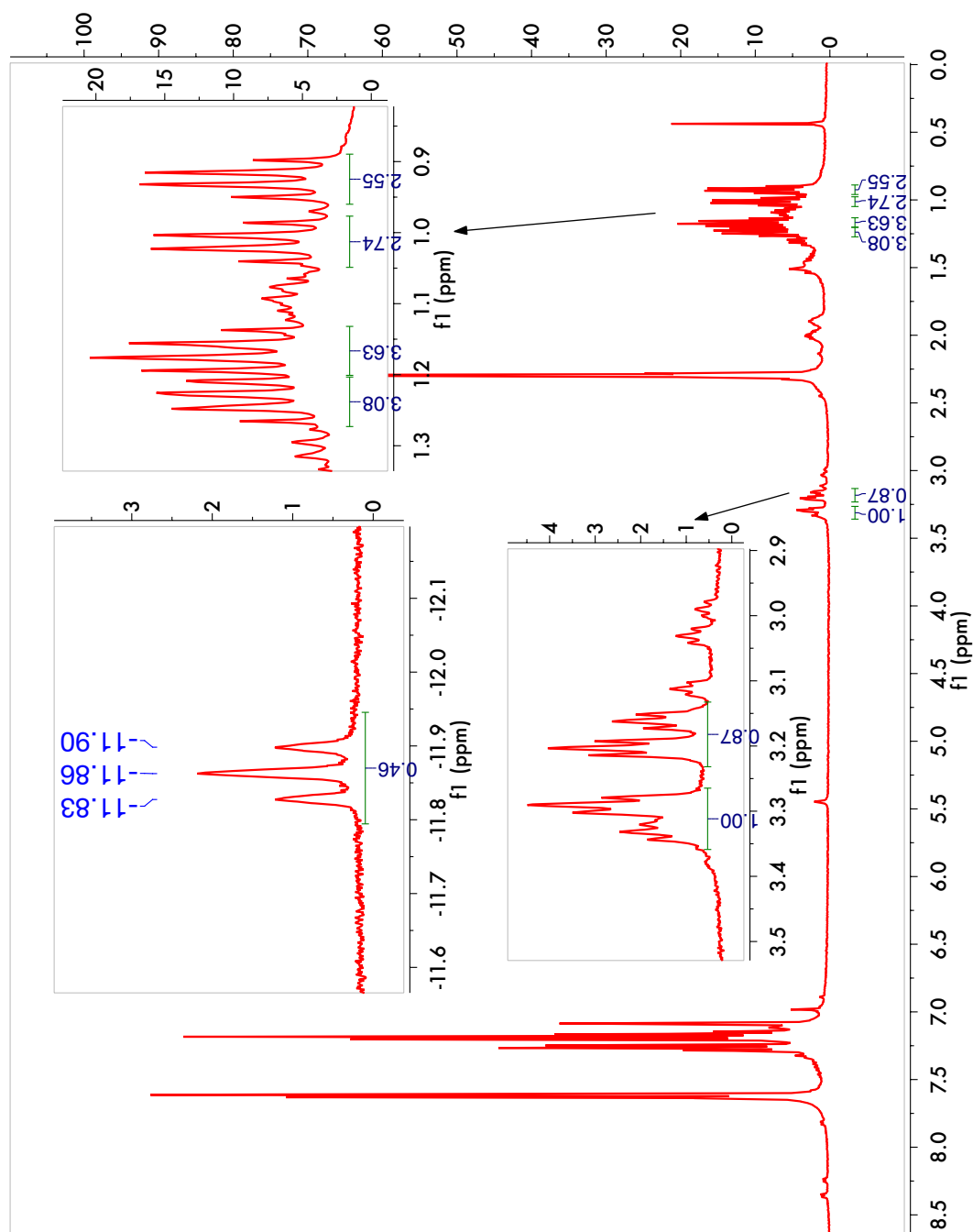


**Figure 6A.6.**  $^{31}\text{P}$  NMR spectrum of independently synthesized ( $i\text{Pr}^4\text{PCP}$ )Ir(CO)(H)(Ph).

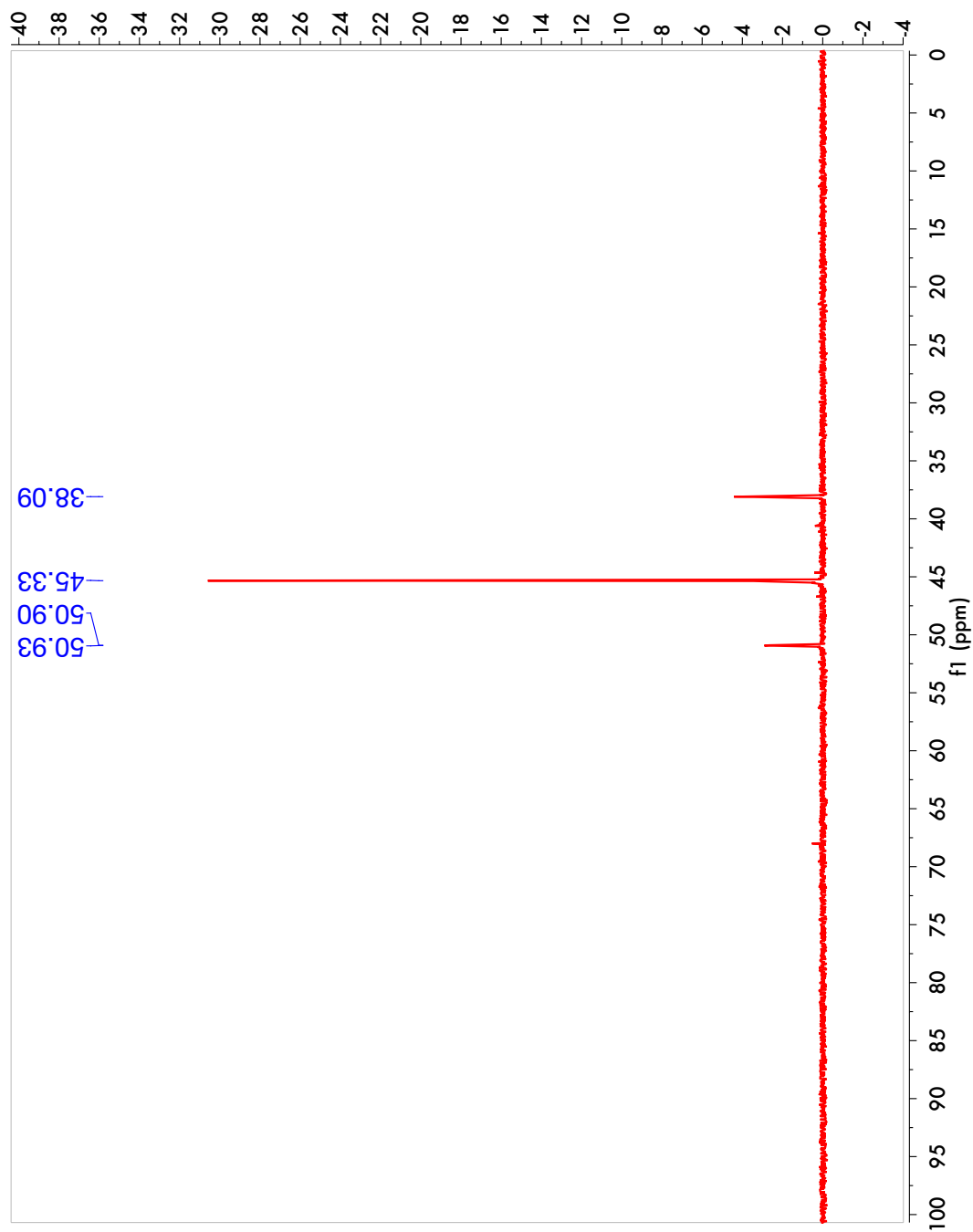




**Figure 6A.7.**  $^1\text{H}$  NMR spectrum of independently synthesized  $(^{\text{iPr}_4}\text{PCP})\text{Ir}(\text{CO})(\text{H})(\text{C}_8\text{H}_3\text{F}_6)$ .

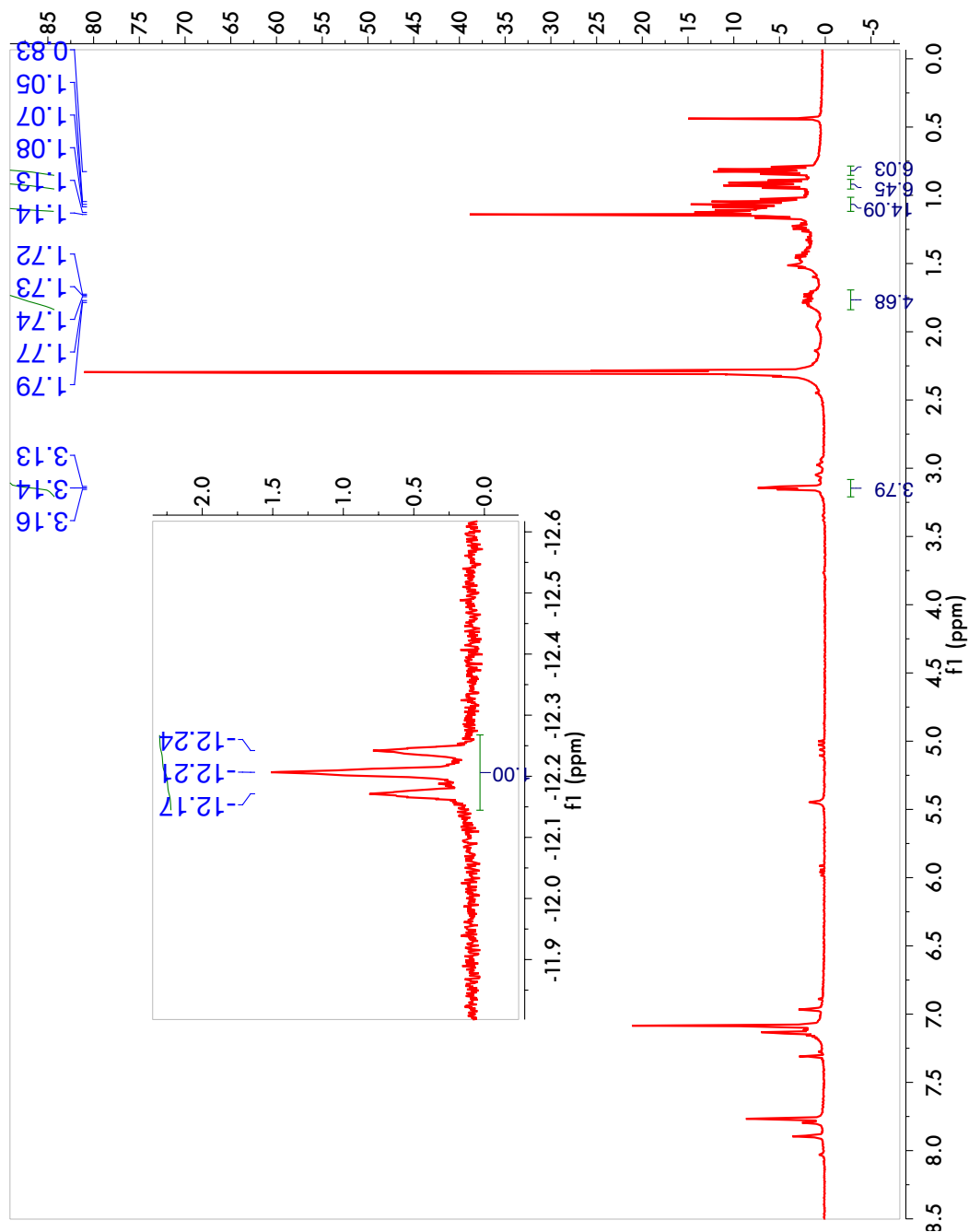


**Figure 6A.8.**  $^{31}\text{P}$  NMR spectrum of independently synthesized  $(^{\text{iPr}}_4\text{PCP})\text{Ir}(\text{CO})(\text{H})(\text{C}_8\text{H}_3\text{F}_6)$ .

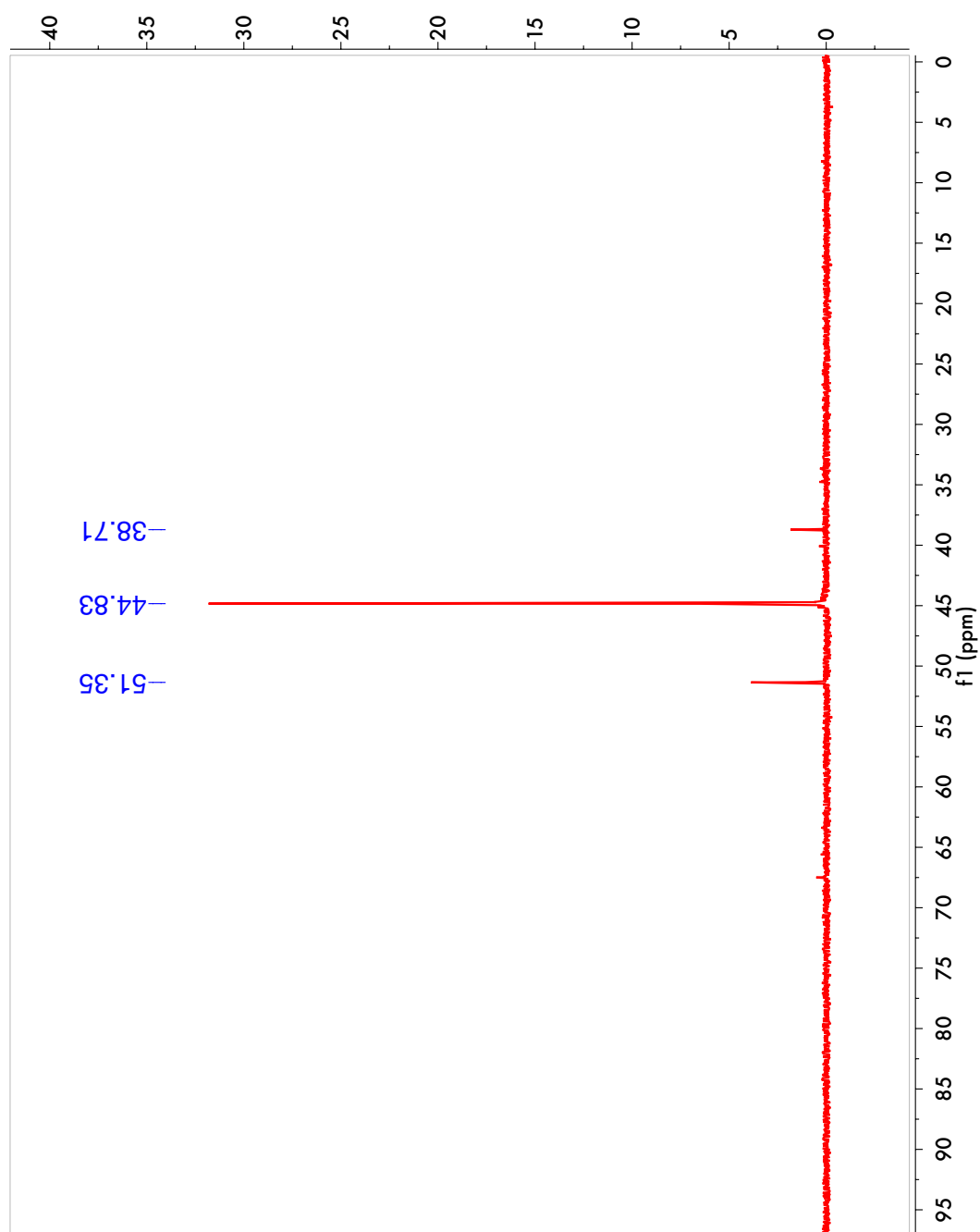


**Figure 6A.9.**  $^1\text{H}$  NMR spectrum of products from acid-catalyzed reaction of  $(^t\text{Bu}^4\text{PCP})\text{Ir}(\text{CO})$  (10 mM) and  $\text{H}_2$ .

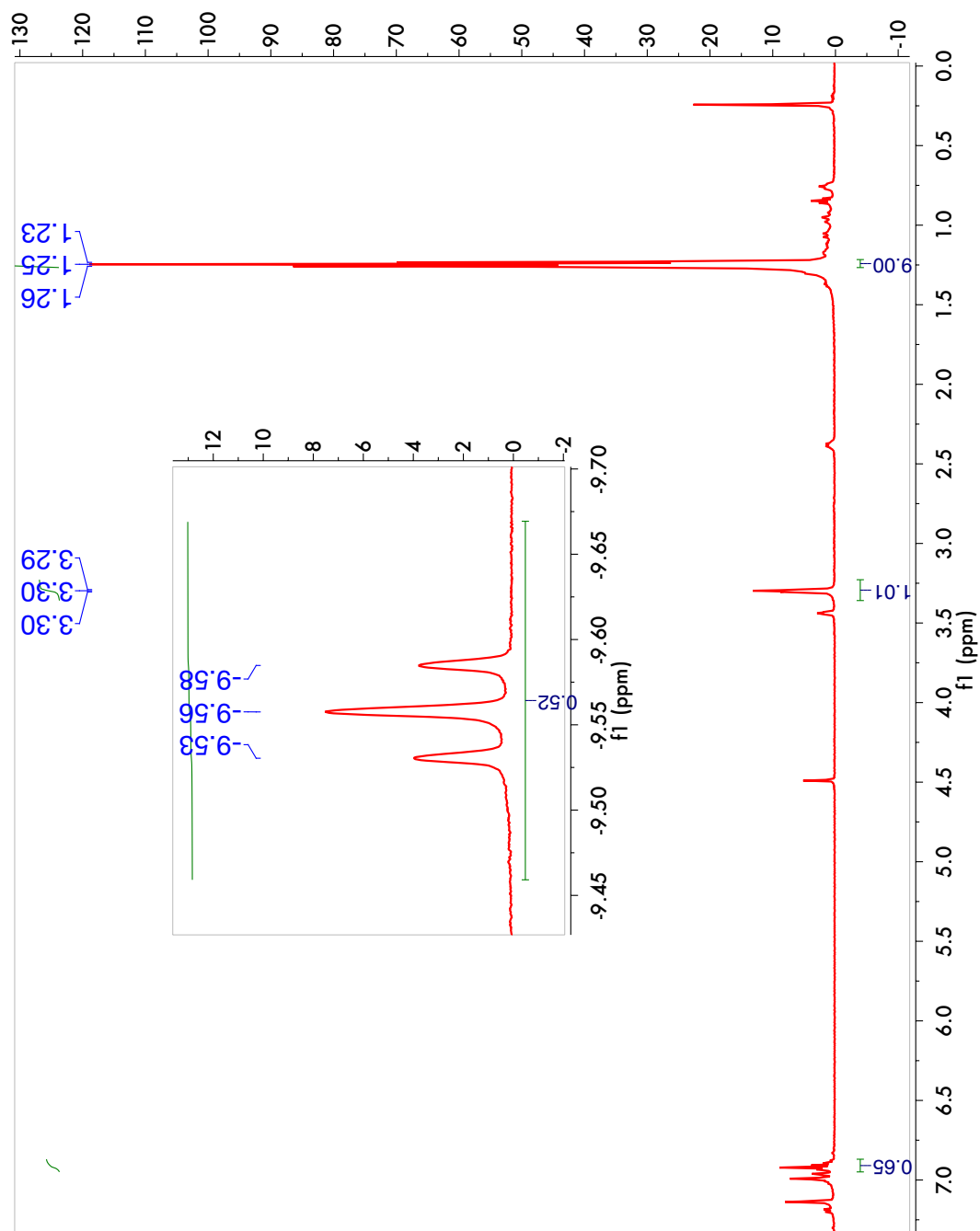
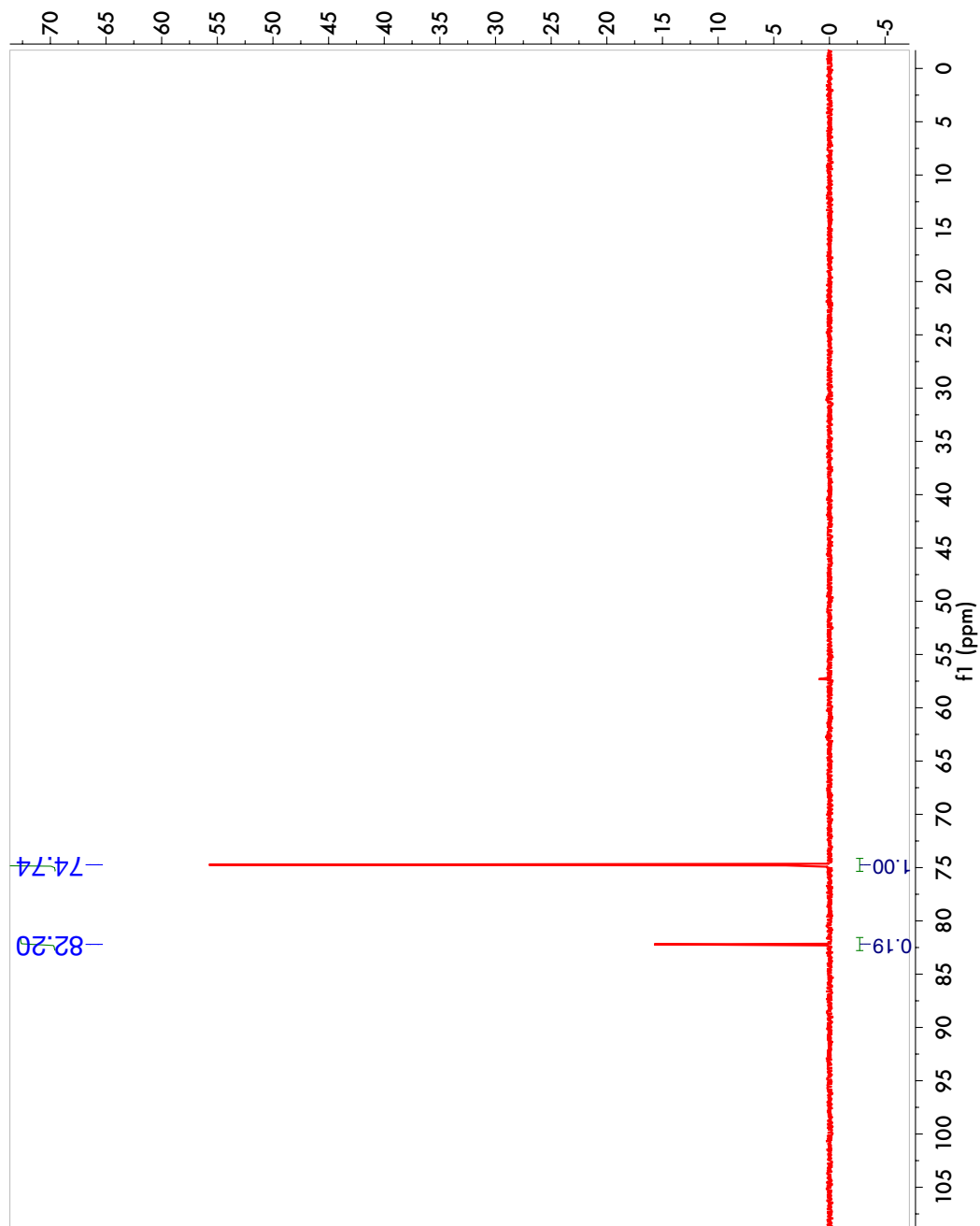


**Figure 6A.10.**  $^{31}\text{P}$  NMR spectrum of products from acid-catalyzed reaction of  $(^t\text{Bu}^4\text{PCP})\text{Ir}(\text{CO})$  (10 mM) and  $\text{H}_2$ .



## 6.6. References

- (1) Goldman, A. S.; Goldberg, K. I. In *Activation and Functionalization of C-H Bonds*; Goldberg, K. I., Goldman, A. S., Eds. 2004; Vol. ACS Symposium Series 885, p 1.
- (2) Halpern, J. *Inorg. Chim. Acta.* **1985**, *100*, 41.
- (3) Rybtchinski, B.; Ben-David, Y.; Milstein, D. *Organometallics* **1997**, *16*, 3786.
- (4) Wang, D. Ph. D. Thesis, Rutgers University, 2012.
- (5) Hartwig, J. F. *Organotransition Metal Chemistry*; University Science Books: Sausalito, CA, 2010.
- (6) Crabtree, R. H. *The Organometallic Chemistry of the Transition Metals*; 4th ed.; John Wiley & Sons, Inc.: Hoboken, NJ, 2005.
- (7) Zhao, J.; Goldman, A. S.; Hartwig, J. F. *Science* **2005**, *307*, 1080.
- (8) Choi, J.; Choliy, Y.; Zhang, X.; Emge, T. J.; Krogh-Jespersen, K.; Goldman, A. S. *J. Am. Chem. Soc.* **2009**, *131*, 15627.
- (9) Choi, J.; Wang, D. Y.; Kundu, S.; Choliy, Y.; Emge, T. J.; Krogh-Jespersen, K.; Goldman, A. S. *Science* **2011**, *332*, 1545.
- (10) Ittel, S. D.; Tolman, C. A.; English, A. D.; Jesson, J. P. *J. Am. Chem. Soc.* **1978**, *100*, 7577.
- (11) MacLean, D. F.; McDonald, R.; Ferguson, M. J.; Caddell, A. J.; Turculet, L. *Chem. Commun.* **2008**, 5146.
- (12) Morgan, E.; MacLean, D. F.; McDonald, R.; Turculet, L. *J. Am. Chem. Soc.* **2009**, *131*, 14234.
- (13) Sola, E.; Garcia-Camprubi, A.; Andres, J. L.; Martin, M.; Plou, P. *J. Am. Chem. Soc.* **2010**, *132*, 9111.
- (14) Brookhart, M.; Green, M. L. H.; Parkin, G. *Proc. Natl. Acad. Sci.* **2007**, *104*, 6908.
- (15) Liu, F.; Goldman, A. S. *Chem. Commun.* **1999**, 655.
- (16) Ahuja, R.; Punji, B.; Findlater, M.; Supplee, C.; Schinski, W.; Brookhart, M.; Goldman, A. S. *Nature Chem.* **2011**, *3*, 167.
- (17) Frisch, M. J. T., G. W.; Schlegel, H. B.; Scuseria, G. E.; Robb, M. A.; Cheeseman, J. R.; Scalmani, G.; Barone, V.; Mennucci, B.; Petersson, G. A.; Nakatsuji, H.; Caricato, M.; Li, X.; Hratchian, H. P.; Izmaylov, A. F.; Bloino, J.; Zheng, G.; Sonnenberg, J. L.; Hada, M.; Ehara, M.; Toyota, K.; Fukuda, R.; Hasegawa, J.; Ishida, M.; Nakajima, T.; Honda, Y.; Kitao, O.; Nakai, H.; Vreven, T.; Montgomery, Jr., J. A.; Peralta, J. E.; Ogliaro, F.; Bearpark, M.; Heyd, J. J.; Brothers, E.; Kudin, K. N.; Staroverov, V. N.; Kobayashi, R.; Normand, J.; Raghavachari, K.; Rendell, A.; Burant, J. C.; Iyengar, S. S.; Tomasi, J.; Cossi, M.; Rega, N.; Millam, N. J.; Klene, M.; Knox, J. E.; Cross, J. B.; Bakken, V.; Adamo, C.; Jaramillo, J.; Gomperts, R.; Stratmann, R. E.; Yazyev, O.; Austin, A. J.; Cammi, R.; Pomelli, C.; Ochterski, J. W.; Martin, R. L.; Morokuma, K.; Zakrzewski, V. G.; Voth, G. A.; Salvador, P.; Dannenberg, J. J.; Dapprich, S.; Daniels, A. D.; Farkas, Ö.; Foresman, J. B.; Ortiz, J. V.; Cioslowski, J.; Fox, D. J.; Gaussian 09, Revision A.02 ed.; Gaussian, Inc.: Wallingford, CT, 2009.
- (18) Zhao, C. Y.; Truhlar, D. G. *Theo. Chem. Acc.* **2008**, *120*, 215.

- (19) Parr, R. G.; Yang, W. *Density-Functional Theory of Atoms and Molecules*; University Press: Oxford, 1989.
- (20) Roy, L. E.; Hay, P. J.; Martin, R. L. *J. Chem. Theory Comput.* **2008**, 4, 1029.
- (21) Krishnan, R.; Binkley, J. S.; Seeger, R.; Pople, J. A. *J. Chem. Phys.* **1980**, 72, 650.
- (22) Barone, V.; Cossi, M. *J. Phys. Chem. A* **1998**, 102, 1995.